University of Alberta

Modulation of Spontaneous Neural Network Bursting in Newborn Rat Brain Slices by Extracellular Calcium, Methylxanthines and Opioids

by

Chase M. Kantor

A thesis submitted to the Faculty of Graduate Studies and Research
in partial fulfillment of the requirements for the degree of

Doctor of Philosophy

Department of Physiology

Fall, 2012
Edmonton, Alberta

For Alicia

Abstract

Spontaneous neuronal bursting appears to be pivotal for brain maturation. This thesis studied such synchronized neural network oscillations in immature newborn rat hippocampus, cortex, and *locus coeruleus*. For this, horizontal brain slices were generated for (simultaneous) suction electrode recording of extracellular population bursting in these structures and monitoring their electrical activity indirectly at cellular resolution via imaging of associated cytosolic Ca^{2+} rises. In a first project, it was found that all rhythms were robust and stable for several hours in superfusate with close-to-physiological content of the neuroactive cations Ca^{2+} (1 mM) and K^{+} (3-4 mM) and were depressed by superfusate with elevated (1.5-3 mM) Ca^{2+} content and this inhibition was countered by raising K^{+} to 5-7 mM ('Ca^{2+}/K^{+} antagonism').

This thesis studied how the above hippocampal and cortical rhythms are affected by two classes of drugs that are frequently administered to (preterm) human infants: (*i*) the methylxantines caffeine and theophylline which are the gold standard for treatment of apneas of prematurity, but can evoke seizures, and (*ii*) opioids that are used for analgesia, but can depress breathing by inhibiting medullary respiratory network bursting. It was found that submillimolar bath-applied methylxanthine tended to increase the rate and/or amplitude of hippocampal and cortical bursts. At low millimolar doses, they suppressed normal rhythm in both areas and evoked large amplitude rhythmic seizure-like discharges. Similar seizure-like discharges were evoked in the hippocampus, but not cortex, by bath-application of 1-10 µM of the µ-opioid receptor agonist [D-Ala2, N-MePhe4, Gly-ol]-enkephalin (DAMGO), which blocked *locus coeruleus* rhythm.

In summary, the findings indicate that hippocampal, cortical and *locus coeruleus* networks in newborn rat horizontal slices show robust bursting in solution with close-to-physiological extracellular Ca^{2+} and K^{+} levels. Methylxanthines cause seizure-like discharges at doses that are likely higher than in extracellular brain tissue *in vivo* during clinical application. Opioids exert their typical inhibitory action on *locus coeruleus* neurons; however, they do not suppress bursting in cortex and hippocampus, but rather evoke hyperexcitability in the latter area. Potential mechanisms of methylxantine- and opioid-evoked perturbation of network oscillations are discussed including potential consequences for maturation of these neural circuits.

Acknowledgments

I would first like to thank my supervisor, Dr. Klaus Ballanyi for his invaluable support and encouragement during my brief stay in his laboratory, as well as the members of the lab, Dr. Junya Kuribayashi, Bogdan Panaitescu, and various summer students for their help and dedication. I would especially like to thank Dr. Araya Ruangkittisakul for her unparalleled commitment to my training and research goals. Without her help and expertise, this thesis would be a lot shorter and probably written in crayon.

I would like to thank my committee members, Drs. Peter Nguyen and Simon Gosgnach, for their suggestions and guidance, both research oriented and personal, Drs. Peter Smith, Ed Karpinski, Tony Ho, and Enrico Cherubini for taking the time to be a part of my candidacy and thesis defense, and slipping me the questions ahead of time. To Dr. Steve Harvey, who not only chaired my thesis defense and made sure I wasn't picked apart, but was also tremendously supportive in my undergraduate degree when I needed it most: I owe my gratitude and sincerest thanks.

To my friends and family: you know who you are and thanks. You can stop reading here.

Table of Contents

List of Figures

List of Abbreviations

4^{th} V	fourth ventricle
AC	adenylyl cyclase
ADO	adenosine
AMPA	amino-3-hydroxy-5-methyl-4isoxazole-prprionic acid
ATP	adenosine triphosphate
Bic	bicuculline
CA(1-3)	cornu ammonis(1-3)
Caff	caffeine
cAMP	cyclic-adenosine monophosphate
CNQX	6-cyano-7-nitroquinoxaline-2,3-dione
DAMGO	[D-Ala2, N-MePhe4, Gly-ol]-enkephalin
DG	dentate gyrus
EC	entorhinal cortex
ENO	early network oscillation
FC	fornix commissure
FI	fluorescence intensity
GABA	γ-aminobutyric acid
Gbz	gabazine
GDP	giant depolarizing potential
GFAP	glial fibrillary acid protein
GIRK channel	g protein-coupled inward-rectifying K^+ channel
Glu	glutamate
IA	interictal activity

ILE	ictal-like event
KCC2	K^+/Cl^- cotransporter
LC	locus coeruleus
MAS	methylxanthine-associated seizure
MOR	μ-Opioid Receptor
NKCC1	$Na^+/K^+/Cl^-$ cotransporter
NMDA	N-methyl-D-aspartic acid
OF	orbifrontal cortex
PDE	phosphodiesterase
PFA	paraformaldehyde
PKA	protein kinase A
PR	perirhinal cortex
preBötC	preBötzinger complex
ROI	region of interest
RYR	ryanodine receptor
SD	sprague-dawley
SO	stratum oriens
SP	stratum pyramidale
SPA	spontaneous plateau assemblies
SR	stratum radiatum
SR-101	sulforhodamine-101
SSC	somatosensory cortex
Sub	subiculum
SWO	slow wave oscillation
tACPD	trans-1-amino-1,3-dicarboxycyclopentane

Theo	theophylline
TTX	tetrodotoxin
VRC	ventral Respiratory Column
W	wistar
XII	hypoglossal motonucleus/nerves

CHAPTER 1

General Introduction

1.1 Overview

At a given stage of brain development, nervous structures can differ substantially in their degree of maturation. For example, already at birth neural respiratory networks in the lower brainstem (‘*medulla oblongata*’) must provide a robust excitatory drive to muscles mediating breathing movements. At this stage, ‘higher’ brain circuits, such as the hippocampal formation and the entorhinal or perirhinal cortex, are yet immature and still have to develop characteristic features such as synaptic connectivity. For this maturation, neural networks typically show spontaneous activity evident from often synchronous electrical discharges due to neuromodulator-evoked membrane potential depolarization which causes action potential firing. Such rhythmic neuronal bursting leads to oscillatory rises of cytosolic Ca^{2+} which can subsequently initiate a variety of cellular processes. An important example for such processes is Ca^{2+}-dependent consolidation of the presynaptic and postsynaptic molecular components necessary for synapse formation. Perturbation of this dynamic and labile scenario during this phase may result in long-term impairment of the function of neural circuits. Clinical application of drugs, such as caffeine or opioids for countering ‘apneas of prematurity’ (i.e. arrest of breathing in preterm human infants) or managing pain, respectively, may evoke such impairment if they perturb spontaneous network activities in immature (cortical) structures in newborns. In fact, while these methylxanthines are the gold standard for stimulating immature respiratory networks they can also exert severe systemic effects including nausea, hyperglycemia, tachycardia, tachypnea and seizures. Thus, despite their therapeutic effects on breathing, methylxanthines can potentially evoke seizure-like hyperexcitability in developing cortical circuits. In contrast, clinical use of opioids for analgesia may inhibit spontaneous bursting in developing brain circuits similar to their established depressing effect on respiratory networks in both neonates and adults.

Biophysical, biochemical and molecular properties of developing neural circuits are being studied in a variety of *in vivo* and *in vitro* models from numerous animal species. In that regard, brain slices are instrumental for analyzing dynamic functional properties of neurons and neighboring glia that occur on a time scale of milliseconds to hours in such circuits. This widely used *in vitro* model enables electrophysiological analyses of membrane potential fluctuations or underlying ionic currents, often in combination with monitoring extracellular 'field' potentials and/or optical imaging of membrane potential or cellular signaling factors like cytosolic Ca^{2+}. In fact, studies using these approaches have established the above described view that spontaneous electrical activity and resulting Ca^{2+} rises are pivotal for proper brain maturation.

For these analyses, brain slices should optimally be studied in superfusate with an ionic content that mimics that of extracellular ('interstitial') brain fluid. This is because the interstitial concentrations of the cations Ca^{2+} and K^{+} especially influence neuronal excitability. Consequently, prior to testing effects of drugs like methylxanthines and opioids on developing brain circuits in slices, it is important to determine the optimal relation between a close-to-physiological superfusate Ca^{2+} and K^{+} content and robust endogenous bursting. Knowledge gained from these studies may be applicable to the development of a more efficient treatment of central nervous depression or sensory hyperexcitability as can be associated with apneas of prematurity and pain management, respectively. Likely, this will also lead to a better understanding of the cellular mechanisms underlying various other neurological diseases.

1.2 Rhythmic Brain Slices and *En Bloc* Models

The use of isolated brain tissues for studying mammalian brain functions was pioneered by Henry McIlwain. In the early 1950s, his group developed slice preparations for biochemical studies of brain energy metabolism (McIlwain et al., 1951). During the following 15 years, they showed, for example, that neurons in brain slices have a membrane potential of -60 to -90 mV and depolarize during tissue anoxia or hypoglycemia evoked by removal from the superfusate of oxygen or glucose, respectively (Li & McIlwain, 1957). They also noted in these studies that brain slices from adult mammals have a maximal allowable thickness of ~0.5 mm because of limited diffusion of the pivotal metabolites oxygen and glucose that are supplied via the circulating superfusate. Moreover, they established local drug application to slices and found that synaptic responses can be recorded following electrical stimulation of afferent axons (Gibson & McIlwain, 1965; Yamamoto & McIlwain, 1966).

This work kindled numerous slice studies that were devoted to the analysis of cellular properties in a large variety of brain areas. For exemplifying some of these 'classical' studies, excerpts are taken in the following from a comprehensive review, which may be consulted for individual citations (Jahnsen, 1986). Up to that time, neurons were typically studied in slices isolated from the following brain areas of (mostly) mature mammals: hippocampal CA_1 and CA_3 regions **(Fig. 1-1)**, neocortex, neostriatum, inferior olive and spinal dorsal horn or motor nuclei. In such slices, stimulation of afferent axons, or depolarization of neurons by current injection via the recording sharp microelectrode, revealed cell type- and area-specific active regenerative discharges resulting from transmembrane Na^+ and Ca^{2+} ion fluxes. For example, only ~1% of hippocampal neurons showed spontaneous discharge at regular intervals ('tonic firing') with rates of 20-80

action potentials/s. In silent cells, injection of positive current pulses into CA3 neurons elicited 'triangular shaped' depolarizations leading at their peak to bursts of 3-7 action potentials, also tagged as 'spikes'. Other CA3 neurons responded to such current injection with a fast spike train and were identified as inhibitory interneurons that release the inhibitory neurotransmitter γ-aminobutyric acid (GABA). Similar populations of silent 'fast spiking' GABAergic interneurons and (glutamatergic) spiking and bursting interneurons were found in neocortical slices.

In contrast to low numbers of spontaneously active neurons in the above structures, spontaneous activity was typical for neurons in slices from other brain regions studied during the 1980s (Jahnsen, 1986). For example, steady discharge of 1-5 spikes/s was characteristic for most neurons in *locus coeruleus* slices while 5% of cells, presumably interneurons, displayed no activity. Very similar 'tonic' activity was revealed for most neurons in brainstem slices containing the dorsal vagal nucleus and in midbrain slices containing the *substantia nigra* as one component of the basal ganglia. Moreover, tonic discharge at higher rates (mean 26 spikes/s) was characteristic for neurons of the deep cerebellar nuclei in guinea pig slices. When these cells were hyperpolarized with steady current and then stimulated below the threshold for fast action potentials with depolarizing current pulses, they responded with two types of potentials. One was a 'spikelet' with an amplitude of a few millivolts and a duration of 5-10 ms which often triggered action potentials. The other was a steady depolarization, which often produced prolonged firing that could include spike inactivation. Already at that time, it was assumed that non-inactivating Na^+ conductances, among others, contribute, to the latter 'plateau potentials'. Corresponding plateau potentials were found in cerebellar slices in Purkinje neurons as the most characteristic neurons of the cerebellar cortex that are ontogenetically related to the neurons in the deep

cerebellar nuclei. Since then, a role of such 'persistent' Na^+ channels has been suggested in the generation of endogenous bursting in neurons of diverse brain regions **(§1.4)**. Properties of Purkinje cells were thoroughly studied in guinea pig slices in two 'classical' papers in 1980. Specifically, Llinas and Sugimori were the first to record in these studies membrane potential responses under visual control and to obtain simultaneous recordings from both soma and dendrites. They studied how voltage-activated fast Na^+ channels and non-inactivating Na^+ channels cooperate with several types of voltage-activated Ca^{2+} channels to produce activities similar to those *in vivo*. Purkinje neurons in these studies showed also spontaneous rhythmic discharge of mixed Na^+ and Ca^{2+} action potentials. These bursts had a duration of 5-15 s and were interrupted by a period of silence with similar duration. Under their experimental conditions, the 'submerged' cerebellar slices were viable at 37 ^oC for extended time periods as indicated by the statement of the authors that the latter autonomous bursts did not change their properties during >24 h.

The thalamus was a further brain region referred to in the review by Jahnsen (1986). At that time, it appeared that thalamic neurons in brain slices were silent *in vitro* without stimulation and had surprisingly similar stimulus-evoked electroresponsive properties although their morphology could vary. If they were depolarized from rest with constant current injection, they began firing with a frequency at steady-state depending clearly on the magnitude of the injected current. When thalamic neurons in slices were hyperpolarized with constant current and then stimulated with current pulses insufficient to evoke firing at rest, the response pattern was completely different. Specifically, instead of tonic discharge, these cells respond with a burst of 2-7 action potentials riding on a depolarizing wave lasting ~25 ms. Based on these findings, Llinas and

Jahnsen hypothesized that these two electroresponsive properties, i.e., tonic firing *versus* bursting of thalamic neurons in guinea pig slices are causally related to Θ and α rhythms, respectively, in the electroencephalogram.

Most current studies on *ex vivo* brain tissues make use of newborn or juvenile animals, typically rats and mice, as evident from an array of examples mentioned in a recent book on 'Isolated Central Nervous System Circuits' (Ballanyi, 2012) and related publications (Konnerth, 1990; Ballanyi, 1999). The wide spread use of these animal models is due to several reasons: (*i*) patch-clamp recording in concert with imaging of cellular signaling factors like Ca^{2+} and pH, is principally possible under visual control from cells in acute brain slices and represents a technological milestone for cellular analyses of nervous functions. Contrary, in most brain regions neurons cannot be visualized in slices from mature mammals partially because of formation of myelin bubbles at the slice surface in the aftermath of the slicing procedure, (*ii*) since the development of genetically-engineered mouse models >20 years ago, mouse models are used in a steadily increasing number of studies. Because 'knock out' mice often die at birth or shortly afterwards, most slice studies on such mice make use of newborn or fetal animals, (*iii*) many brain structures are much smaller at birth compared to adults. Consequently, a slice from a newborn animal of 0.5 mm thickness, which is often the physical restriction for sufficient oxygen and glucose supply of mature brain tissue (see above), contains more intact circuitry of a given structure than a slice from a mature animal. Accordingly, some studies are more feasible using young mice *versus* rats because of smaller circuit dimensions. However, this is not always the case because specific mouse brain structures may be more vulnerable to some experimental procedures such as multiphoton imaging which can impose, e.g., a caloric challenge that causes

damage to the tissue, and (*iv*) metabolic rates are notably lower in most newborn brain regions compared to corresponding areas in adults, and neural network functions can thus be maintained by enhanced anaerobic metabolism. This is ultimately important for thick slices ('slabs') and *'en bloc'* preparations that have an anoxic core which utilize anaerobic glycolysis for survival *ex vivo* (Lutz, 1992; Haddad & Jiang, 1993; Ballanyi et al., 1999; Ballanyi, 1999, 2004a,b).

Based on the latter considerations, neural networks in 'adult' slices are often reduced below the minimal anatomical substrate for generating *in vivo*-like activity. Primarily due to smaller network dimensions and lower metabolic rates, slabs or *en bloc* models have been developed with the aim to combine preservation of spontaneous activities with the application of potent *in vitro* approaches such as live cell imaging and concomitant intracellular electrophysiological recording. In this regard, non-perfused perinatal rodent *en bloc* preparations were generated several decades ago for analysis of cortical development or motor behaviours, such as respiration and locomotion. Specifically, a large number of studies on the newborn rodent (brainstem) spinal cord preparation provided valuable information about properties of central pattern generators that initiate and control respiratory and locomotor behaviors (Suzue, 1984; Ballanyi et al., 1999; Clarac et al., 2004). As one prominent example, less than a decade after Suzue (1984) reported that a newborn rat brainstem-spinal cord preparation generates respiratory-related activities, this *en bloc* model was reduced to a <500 µm thick transversal brainstem slice that is capable of generating inspiratory-related motor output (Smith et al., 1991). Since then, various studies have used brainstem slices to analyze mechanisms of inspiratory rhythm generation by neural networks in the rhythmogenic pre-Bötzinger complex (preBötC) (Feldman & Del Negro, 2006; Ballanyi & Ruangkittisakul, 2009).

In a ‘bottom up’ approach, spontaneous giant depolarizing potentials (GDPs) were firstly discovered in 600 µm thick newborn rat hippocampal slices **(Figs. 1-1, 1-2)** (Ben-Ari et al., 1989) before the same group showed almost a decade later that these rhythmic events are also a feature of the *en bloc* newborn rat hippocampus (Khalilov et al., 1997). The latter isolated ‘intact hippocampal formation’ contains the entire circuitry of this brain area and enables the analysis of interactions between the ipsilateral and contralateral hippocampal aspects that are connected via the septum **(Fig. 1-1)**. Since their discovery, isolated rhythmic neural networks like locomotor central pattern generators, inspiratory rhythm-generating preBötC neurons and GDP-generating hippocampal networks are subject to intensive research. This research combines quantitative pharmacology with high-resolution electrophysiological approaches such as ‘patch-clamp’ or multi-electrode arrays and genetically engineered mouse models. A further pivotal tool for such analyses of (isolated) brain regions is Ca^{2+} imaging of their activity and morphology as dealt with in the following.

1.3 Imaging of Ca^{2+} Oscillations in Developing Neural Networks

Ca^{2+} regulates many physiological processes, starting at the act of fertilization, further acting as a universal intracellular second-messenger, and finally triggering pathological events and apoptosis (Takahashi et al., 1999). Ultimately, cytosolic Ca^{2+} is of utmost importance for subsequent developmental processes including the formation and differentiation of various brain cells. Specifically, early stages of neuronal development seem to be associated with fluctuations of the free cytosolic concentration of Ca^{2+} (Ca_i) which can be measured with optical imaging approaches using fluorescent Ca^{2+} dyes (Takahashi et al., 1999; Spitzer, 2006; Yuste et al.,

2006). These early neuronal Ca_i oscillations are mostly initiated by excitatory neurotransmitters which depolarize the plasmalemmal cell membrane to cause opening of voltage-activated Ca^{2+} channels. The resulting Ca^{2+} influx into the cytosol can be accompanied by a typically smaller Ca^{2+} influx through neurotransmitter receptor-activated ion channels such as Ca^{2+}-permeable α-amino-3-hydroxy-5-methyl-4isoxazole-proprionic acid (AMPA)/kainate-type 'ionotropic' glutamate receptors (Takahashi et al., 1999; Spitzer, 2006; Yuste et al., 2006). In addition, neurotransmitters like glutamate, or neuromodulators such as adenosine triphosphate, can activate 'metabotropic' receptors resulting in a Ca_i rise via Ca^{2+} release from intracellular stores. In glial cells, which neighbor neurons in all brain structures and typically lack voltage-activated Ca^{2+} channels, metabotropic 'Ca^{2+} excitability' moderates communication between each other and with neurons or other types of glia, specifically oligodendrocytres and immunoreactive microglia of non-neural origin (Agulhon et al., 2008; Wang & Bordey, 2008; Ballanyi et al., 2010).

In the mature brain, GABA and glycine comprise the 'classical' inhibitory neurotransmitters (Kaila, 1994). During early brain development, however, they exert a strong depolarizing action that is often the chief component of (rhythmic) neuronal excitation (Owens & Kriegstein, 2002; Spitzer, 2006). In the latter review articles, numerous examples are given for involvement of the resulting Ca_i oscillations in developmental processes such as termination of proliferation of neuronal progenitor cells, migration of neurons from the ventricular surface to their target brain areas, or subsequent outgrowth of their axons and dendrites. Finally, these rhythmic activities are involved in the initial formation and consolidation of synaptic processes. The cellular mechanisms underlying these processes downstream to the electrical and Ca_i oscillations are

mostly unknown. For neuronal migration and axonal pathfinding, there is evidence that the ratio of cellular adenosine-monophosphate and cyclic-guanosine monophosphate is pivotal (Spitzer, 2006).

In several well-studied systems, Ca_i imaging is an effective analytical tool for studying neuronal development. The zebrafish embryo is an excellent model in that regard because development occurs within days while its translucence enables Ca_i imaging in the brain of the intact animal (Kettunen, 2012). The spinal cord is a further established model system. Though initially studied in chicks, its emphasis has since transitioned to rodent embryos, thought to be more closely related to humans and also affording comprehensive genetic engineering techniques. These spinal cord models are mostly used to investigate the maturation of both central pattern generators and motoneuronal networks involved in locomotor behaviors (O'Donovan et al., 2008). Similarly, developmental aspects of respiratory central pattern generators and related motor circuits are intensively studied with Ca_i imaging techniques in fetal rodent models (Bouvier et al. 2010; Ruangkittisakul et al., 2009).

With regards to the newborn hippocampus and cortex, which are primarily investigated in this thesis, various studies performed Ca_i imaging, mostly *in vitro* on acute brain slices (Fig. 1-1). Analysis of Ca_i rises associated with hippocampal GDPs commenced almost a decade after these events were detected using electrophysiological approaches **(Fig. 1-2)** (Ben-Ari et al., 1989). These Ca_i measurements were conducted at around the same time primarily by the groups of Ben-Ari and Cherubini (Khalilov et al., 1997; Leinekugel et al., 1997; Canepari et al., 2000), who discovered GDPs in the latter pioneering study, and by the group of Konnerth **(Fig. 1-3)**

(Garaschuk et al., 1998, 2000). Although technically easier than Ca_i imaging in most slices of adult mammalian brain areas (see above), these studies were done 10 years after the initial reports on neuronal Ca_i dynamics were performed on slices of the mature cerebellum (Ross & Werman, 1987; Tank et al., 1988) and hippocampus (Regehr et al., 1989). This was mainly due to the fact that only few groups studied developing mammalian brain circuits at that time.

As one major outcome, the above Ca_i imaging studies on hippocampal slices from newborn rats consolidated the previous electrophysiological findings that GDPs rely greatly on activation of $GABA_A$ receptors as outlined in detail below **(§1.4)**. One of these reports demonstrated by simultaneous multiphoton Ca_i measurements in the hippocampus and entorhinal cortex **(Figs. 1-1, 1-3)** that rhythmic events in the latter area occur at notably slower rates and propagate at a speed of 2.1 mm/s starting in the posterior cortex in contrast to synchronous and faster (10-20 events/min) hippocampal bursting (Garaschuk et al., 2000). They also showed in that study that the cortical rhythm persisted after blockade of $GABA_A$ receptors with bicuculline **(Fig. 1-3)**. Contrary, blockade of AMPA/kainate-type glutamate receptors with 6-cyano-7-nitroquinoxaline-2,3-dione (CNQX) abolished cortical bursting, whereas hippocampal GDPs persisted **(Fig. 1-3)**. These findings exemplified that neural network oscillations can differ substantially between neonatal brain regions regarding both cellular mechanisms and spatiotemporal patterns.

Further examples for differences between spatiotemporal patterns of developmentally related neural network oscillations were obtained in the somatosensory cortex and neocortex. Much of that work is based on studies by the group of Yuste (Mao et al., 2001; Froemke et al., 2002; Cossart et al., 2005; Nikolenko et al., 2007). Using newborn rodent slices for Ca_i imaging in

arrays of up to several hundred dye-loaded cells, they demonstrated with sophisticated online signal analysis that apparently random neuronal activity originates from 'microcircuits' of 5-13 neurons that are repetitively active at an average rate of 0.02-0.06 Hz. They also showed that these neonatal (neo)cortical neuron clusters are coupled via gap junctions rather than chemical synapses, which are mostly formed later during postnatal development to constitute the predominant interface for neural network connectivity. Yuste and colleagues pointed out in the above studies that the identification of apparently random correlated activities is very much facilitated by the interpretation of dynamic maps of neuronal activities obtained from Ca_i imaging. In fact, they argue that such analysis is barely possible with conventional electrophysiological techniques using single or few microelectrodes because of the low spatiotemporal resolution. Microelectrode arrays are a powerful electrophysiological tool in that regard, but their spatial resolution is yet limited by the size of the individual microchips comprising the array (Jones et al., 2011). Using similar optical and statistical analytical tools as Yuste's group, Ben-Ari and colleague have recently detected with Ca_i imaging in neonatal rat slices GABAergic 'hub' neurons that orchestrate synchrony in developing hippocampal networks (Bonifazi et al., 2009).

While (population) Ca_i imaging is undoubtedly an important tool for analyzing connectivity patterns and other functional and cellular properties of developing brain circuits, this method has some limitations. Firstly, confocal and multiphoton microscopes, which are mostly used for such imaging, operate by exciting the intracellularly loaded fluorescent Ca^{2+} dyes with high energy lasers for confocal imaging that is potentially toxic, whereas the (near) infrared laser used in multiphoton microscopy can constitute a caloric challenge to the studied tissue (Takahashi et al.,

1999; Yuste et al., 2006; Ruangkittisakul & Ballanyi, 2009). Nevertheless, continuous multiphoton/confocal imaging from rhythmically active neurons is possible for time periods of up to several hours as our group has demonstrated for the isolated preBötC in newborn rat brainstem slices (Ruangkittisakul et al., 2006, 2008, 2009). For such imaging, preBötC cells are loaded with the fluorescent Ca^{2+} dye Fluo-4-AM by focal injection via a broken patch electrode following the approach that was reported by Konnerth's group (Stosiek et al., 2003). In our hands, this loading procedure is much more effective compared to incubating slices with Fluo-4-AM or similar membrane permeable Ca^{2+} dyes such as Fluo-8L AM, Calcium-Green or Oregon-Green AM. On the one hand, bath-applied Ca^{2+} dyes only stain cells within the superficial slice layers, up to a depth of ~60 µm, whereas dye injection labels cells located in depths >100 µm. On the other hand, injection stains a higher proportion of (inspiratory active) preBötC neurons compared to neighboring glial cells which include mostly astrocytes, but may also comprise oligodendrocytes and microglia (Ruangkittisakul et al., 2009; Ballanyi et al., 2010). Accordingly, when using population Ca_i imaging for neuronal network analyses, it needs to be considered that glial Ca_i rises may contribute to the overall mapped signals. Based on our preliminary evidence, we assume that astrocytes in the newborn rat brainstem slices are not spontaneously rhythmically active and can be discriminated from preBötC neurons by their characteristic sporadic Ca_i rises and larger Ca_i responses to some neuromodulators such as adenosine-triphosphate, norepinephrine, or 1-amino-1,3-dicarboxycyclopentane (tACPD) which activate metabotropic glutamate receptors (Ruangkittisakul et al., 2009; Ballanyi et al., 2010).

Also for other brain areas, these and further pharmacological agents have been elucidated for identifying Ca^{2+} dye-loaded neurons *versus* glia (Agulhon et al., 2008; Halassa & Haydon, 2010;

Ballanyi et al., 2010). A further tool in that regard is the red fluorescence dye sulforhodamine-101 (SR-101) which is currently considered to selectively stain astrocytes both *in vivo* (Nimmerjahn et al., 2004) and *in vitro* (Kafitz et al., 2008). However, previous studies have instead proposed that SR-101 selectively labels (active) neurons (Keifer et al., 1992; Mandal & Anderson, 2009). We have reported preliminary evidence that the capability of SR-101 to stain either astrocytes or neurons in the hippocampus and cortex of newborn rat slices depends on the loading protocol **(§2.2.3)** (Kantor et al., 2012). Although the fact that neurons and glia in various types of brain slices from (neonatal) mammals are both stained by Ca^{2+} dyes poses a limitation for neuron-glia discrimination, it provides a means to study functional interactions between these two cell types. Indeed, there is steadily increasing evidence that neurons and glial cells interact in a way that can even influence behaviors, such as sleep (Halassa & Haydon, 2010) or the (chemical) control of breathing (Ballanyi et al., 2010; Gourine et al., 2010). In that regard, Yuste's group recently showed with Ca_i imaging in newborn mouse slices that astrocytes regulate 'up states' in the developing neocortex (Pozkanzer & Yuste, 2011).

1.4 Hippocampal and Cortical GDPs and ENOs

The development of viable acute slices and *en bloc* preparations described above **(§1.2)** has led to the discovery that endogenous electrical activity is a hallmark of fetal development of numerous mammalian central nervous structures (Maffei & Galli-Resta, 1990; Ho & Waite, 1999; Kudo et al., 2004; Champagnat et al., 2011; Owens & Kriegstein, 2002; Spitzer, 2006; O'Donovan et al., 2008). Related research using such *in vitro* models has revealed that spontaneous rhythmic discharges continue into the early postnatal period for various brain

structures that are immature at this developmental stage. This holds true for different aspects of the mammalian cortex including the hippocampus. Hippocampal activities in acute slices or *en bloc* models from neonatal rodents are extensively studied since several decades by the groups of Ben-Ari, Cherubini, Kaila and Konnerth **(Figs. 1-1, 1-2, 1-3, 1-4)**. Correspondingly, neonatal cortical rhythms are being investigated particularly by the groups of Yuste, Kriegstein and Luhmann. According to Kaila's group (Palva et al., 2000), the major presumptive role of these neonatal neural network oscillations is as follows: 'Spontaneous neural activity is crucial for the formation of the intricate patterns of cortical connectivity during development. In particular, temporal correlations in presynaptic and postsynaptic activity have been hypothesized to be a critical determinant in the selection of neurons that are to become wired together.' A thorough review of the work of these groups and related studies by others is beyond the scope of this thesis. Accordingly, the aim of this section is to outline basic properties of spontaneous synchronized bursting in these isolated brain regions with regards to the primary aim of this thesis, which is to analyze effects of methylxanthines and opioids on these rhythms.

As dealt with above **(§1.3)**, Ca_i imaging is a crucial tool for studying neuronal (population) bursting. However, the majority of findings regarding the underlying mechanisms were, and are still, based on electrophysiological analyses of biophysical membrane properties and synaptic interactions. These analyses make use of various techniques such as fine-tipped microelectrodes for either field potential recording or analysis of membrane potential fluctuations and underlying ionic currents. About 20 years ago, whole-cell patch-clamp recording has been adapted to brain slices for this purpose, in which neurons (or glial cells) are either targeted under visual control in superficial layers up to a depth of 100 µm (Konnerth, 1990) or 'blind patch-clamped' in deeper

tissue layers (Blanton et al., 1989). These techniques are referred to in more detail in the Methods chapter **(§2.1.5)**.

For analyzing hippocampal GDPs, it is imperative to consider that the mechanisms may differ for bursting in individual neurons compared to network-based rhythmic extracellular field potentials **(Fig. 1-4)** (Khazipov et al., 2004; Sipilä et al., 2005; Sipilä & Kaila, 2007). In this regard, it is important to use an appropriate terminology for cellular and network activities. Thus, in the following individual bursts in hippocampal neurons will be labeled 'hGDPs', whereas field potentials will be coined hippocampal early network oscillations ('hENOs') according to the study by Garaschuk et al. (2000).

Regarding the role of GABA in these events, there is a general agreement between groups. Specifically, it was shown that GABA acts on $GABA_A$ receptors to cause a major depolarization of neonatal hippocampal neurons. In physiological interstitial fluid, $GABA_A$ receptors are permeable to both Cl^- and HCO_3^- (Kaila, 1994; Sipilä & Kaila, 2007). However, the relative contribution of either conductance to a particular $GABA_A$ receptor-mediated membrane potential or current response can differ notably between (developing) neurons (Kaila 1994; Kaila et al., 1993; Kulik et al., 2000). In many developing neurons, the magnitude of the effective $GABA_A$ receptor-mediated depolarizations depends greatly on an inwardly-directed 'Cl^- pump'. Since three decades, it is known that such a Cl^- pump promotes depolarizing GABA actions not only in immature neurons (Obata et al., 1978), but also in some neurons in the adult mammalian nervous system, such as dorsal root and sympathetic ganglion neurons (Deschenes et al., 1976; Ballanyi & Grafe, 1985). Since then, evidence is steadily accumulating on the roles of depolarizing

GABA in brain development and the molecular entity of the inwardly-directed Cl^- pump which is comprised of a $Na^+/K^+/Cl^-$ cotransporter as one member of a family of cation-chloride cotransporters (Rivera et al., 1999; Owens & Kriegstein, 2002; Li et al., 2002; Payne et al., 2003; Spitzer, 2006). This 'NKCC1' is predominantly expressed early in brain development and serves to establish a relatively high (25-50 mM) intracellular free Cl^- concentration in both fetal neurons and glia (Kettenmann et al., 1991; LoTurco et al., 1995; Ho & Waite, 1999; Kudo et al., 2004; Owens & Kriegstein, 2002; Spitzer, 2006; O'Donovan et al., 2008). Compared to the prominent role of NKCC1 during early brain development, expression of its major functional counterpart, the Cl^- extruder KCC2, lags behind notably (Plotkin et al., 1997; Rivera et al., 1999; Payne et al., 2003). In the hippocampus, this developmental 'ontogenetic shift' shift from dominant NKCC1 expression to a major role of KCC2 occurs during the second to third postnatal week (Rivera et al., 1999; Payne et al., 2003; Khazipov et al., 2004). As stated in the latter reports, this time course coincides with the reversal of depolarizing into hyperpolarizing $GABA_A$ receptor responses and disappearance of hGDPs in the third postnatal week.

Based on these considerations on the role of depolarizing GABA, a possible scenario for cellular and network mechanisms involved in hGDPs and hENOs is as follows. The initial view that hGDPs are primarily triggered ('paced') by phasic GABAergic responses residing in the interneuronal network does not explain how depolarizing GABA contributes to hENOs, i.e. the network behavior (Sipilä et al., 2005; Sipilä & Kaila, 2007). Blockade of the *N*-Methyl-D-aspartic acid (NMDA) type of ionotropic glutamate receptors was found to reduce the frequency of hGDPs, while they were abolished by combined administration of NMDA-receptor blockers and AMPA/kainate receptor antagonists (Ben-Ari et al., 1989; Bolea et al., 1999; Khazipov et al.,

2001; Sipilä et al., 2005). This suggests that glutamatergic synaptic transmission, particularly involving AMPA/kainate receptors, is critical for their generation. In line with this view, a pronounced glutamatergic component in the response was unmasked upon blockade of GABAergic conductances (Khazipov et al., 1997; Bolea et al., 1999). This glutamatergic conductance of immature pyramidal neurons peaks at the beginning of the hGDP, whereas postsynaptic GABAergic currents last over a notably longer time window (Ben-Ari et al., 1989, 2001; Sipilä et al., 2005). While $GABA_A$ receptor blockers such as bicuculline inhibit hGDPs, hENOs are restored upon elevation of K^+ content in the superfusate (Sipilä et al., 2005). It was thus suggested that a non-patterned mode of GABA transmission was sufficient to pace hGDPs and that GABAergic transmission is, instead, 'permissive' and provides a depolarizing stimulus to intrinsically pace-making pyramidal neurons **(Fig. 1-4)** (Sipilä & Kaila, 2007).

Several candidates are being discussed regarding voltage-activated conductances that mediate intrinsic bursting of hippocampal pyramidal neurons. One candidate is a hyperpolarization-activated cyclic nucleotide-gated current ('h-current'), which is known to mediate cellular bursting in various (mature) neural networks (Lüthi & McCormick, 1998). The h-current may be responsible for, at least, the initiation of GDPs in immature networks (O'Donovan, 1999) and its pharmacological blockade was shown to disrupt the generation of hGDPs (Bender & Baram, 2008). In addition, the h-current is functional at postnatal day (P) 2, peaks during the first postnatal week and then declines, in line with the above described time window for the occurrence of hGDPs (Vasilyev & Barish, 2002). However, blockade of the h-current had little effect on immature CA_3 bursts in a different study (Sipilä et al., 2006). Other work proposed that transiently activated ('T-type') Ca^{2+} channels contribute to slow depolarizations in CA3

pyramidal neurons (Avery & Johnston, 1996). However, T-type Ca^{2+} channel blockers did not inhibit the hGDPs themselves, but rather act through the associated slow after-hyperpolarization (sAHP) and this disrupted the refractory period of the burst (Sipilä et al., 2006). The latter effect was mimicked by the cholinergic agonist carbachol, pointing to a role of a slow Ca^{2+}-activated K^+ currents in burst termination (Sah, 1996; Sipilä et al., 2006). The latter study (Sipilä et al., 2006) also showed that blockade of persistent Na^+ channels (**1.1**) abolished hGDPs. Taken together, intrinsic bursts in hGDPs seem to be generated by persistent Na^+ channels which depolarizes the membrane to spike threshold until the specific Ca^{2+}-activated K^+ current hyperpolarizes the cell and terminates the burst **(Fig. 1-4)**.

Regarding their requirements for network activity, hippocampal pyramidal neurons have three essential properties. Specifically they (*i*) respond with voltage-dependent intrinsic bursts when depolarized **(§1.1)** (Menendez de la Prida & Sanchez-Andres, 2000), (*ii*) receive both tonic and phasic GABAergic conductances leading to depolarization (Ben-Ari et al., 1989), and (*iii*) are interconnected by excitatory recurrent collaterals (Bolea et al., 1999). During the developmental period when synaptic connections are starting to be established, hGDPs are the main type of network activity in pyramidal cells and interneurons before the second postnatal week (Ben-Ari et al., 1989; Khazipov et al., 1997). It is important to note that network activity is not limited to the CA_3 subfield where they have been discovered and mostly studied (Ben-Ari et al., 1989; Sipilä & Kaila, 2007). In fact, hGDPs and resulting hENOs originate mainly in the CA_3 region and are then transmitted to the CA_1 area, but not through the typical Schaffer-collateral pathway for which glutamatergic projection afferents are not yet established **(Fig. 1-1)**. Slices containing an isolated CA_3 and surrounding layers generate spontaneous network activity in the absence of

inputs from the mossy fibre pathway or the hilus (Khazipov et al., 1997; Bolea et al., 1999). Additionally, hGDPs in the CA_1 area can back-propagate via axon collaterals from a class of GABAergic interneurons to the CA_3 subfield and drive hGDPs there **(Fig. 1-1)** (Menendez de la Prida et al., 1998). In non-intact slices containing either the isolated CA_1 subfield or the dentate gyrus, spontaneous network events with a frequency similar to CA_3-derived hGDPs are still present (Menendez de la Prida et al., 1998; Ben-Ari, 2001). This suggests that cellular elements required for generation of hGDPs are contained in all hippocampal subfields.

Unlike the hippocampus, work on rodent brain slices that display spontaneous electrical activities shortly after birth was first shown as Ca^{2+} oscillations in a network of neighbouring neocortical neurons (Garaschuk et al., 2000). Since then, the list of spontaneous activities that occur in the perinatal, postnatal, and embryonic period in cortical networks and on a cellular level have expanded to include cortical GDPs (cGDPs), gap-junction-mediated synchronous plateau assemblies ('SPAs'), briefly described in the previous section, in addition to *in vivo* recorded spindle-bursts and gamma oscillations (Garaschuk et al., 1998; Khazipov et al., 2004; Allene et al., 2008; Yang et al., 2009). Such variety may principally reflect a requirement for multiple patterns to moderate normal maturation, perhaps concurrently or at different stages of development, but also the variability in experimental approaches used to study these activities (Allene & Cossart, 2010). As such, the wide range of spontaneous cortical bursts described may in fact refer to the same phenomenon. Portions of this section are summarized from the above cited review on NMDA-driven activity waves in the neocortex (Allene & Cossart, 2010).

cENOs are large-scale and low frequency Ca^{2+} oscillations which propagate longitudinally across the brain in waves of activity and occur immediately after birth **(Fig. 1-3)** (Garaschuk et

al., 2000). Such network activity in the neocortex was thought to depend critically on NMDA recptor activation and tonic extracellular glutamate, whereas hGDP generation relies on the early depolarizing action of GABA (Ben-Ari, 1989; Garaschuk et al., 2000; Allene et al., 2008). Thus, a distinction arose that divided emerging network patterns into glutamate-driven cortical oscillations and GABAergic hippocampal activity, representing intrinsic difference between neighbouring structures. However, the fact that GABA also excites immature cortical neurons in a similar fashion to hGDPs suggested that endogenous GABAergic transmission is also important in modulating cortical networks, though not necessary in generating them (Yuste and Katz, 1991; Garaschuk et al., 2000). Moreover, blocking the depolarizing action of GABA with bumetanide seems to impair at least one form of cortical bursts (Rheims et al., 2008). Due to these apparent similarities, cENOs were originally thought to be the cortical counterpart to hGDPs, although this view has since fallen out of favour with the emergence of cGDPs that synchronize local network assemblies and appear later than cENOs (Allene et al., 2008).

It was suggested that cENOs (in concurrence with SPAs) represent the dominant network pattern in the cortex shortly after birth, which is subsequently replaced by cGDPs after the first postnatal week (Allene et al., 2008). However, cENOs continue to persist in neocortex from rodent slices until at least P12 (Garaschuk et al., 2000), suggesting that network activity in the cortex diversifies over the first few postnatal weeks rather than transitioning from one state to another. Regardless of the time course of activity, ENOs are primarily NMDA receptor-driven events, implying a crucial role for these receptors early in development. As already mentioned, GABAergic synapses are formed prior to glutamatergic synapses in the hippocampus. Whether the sequence of synapse formation in the neocortex differs from the hippocampus is not clear.

GABAergic transmission, which modulates neocortical activity, is apparent as early as P2 (Rheims et al., 2008). Furthermore, functional GABAergic and NMDA receptor-mediated currents jointly contribute to the development of AMPA receptor-mediated transmission (Wang & Kriegstein, 2008). Thus, as hENOs have been proposed to be jointly mediated by GABAergic and glutamatergic conductances (Sipilä et al., 2005), there appears to exist a similar synergistic action of these two transmitters governing spontaneous activities in the (neo)cortex.

The above described GDPs/ENOs are not an exclusive feature of isolated rodent brains tissues because they have also been found in slices of rabbits (Menendez de la Prida et al., 1996), ferrets (Brumberg et al., 2000; Sanchez-Vives et al., 2000) and primates (Khazipov et al. 2001).

1.5 Correlation of ENOs with Hippocampal and Cortical Activities *In Vivo*

In intact animals, the hippocampus displays a variety of neural network oscillations that are correlated to different functional states, such as wakefulness, sleep or exploration in neonatal and adult states (Maier et al., 2003). One of these oscillatory patterns in the rat hippocampus are sharp waves which appear during slow-wave sleep, immobility and consumatory behavior (Silipä & Kaila, 2007) and are typically characterized as slow, irregular bursts that occur maximally during sleep states (1 Hz) and last between ~30-120 ms (Buzsaki et al., 1986; Leinekugel et al., 2002). These events persist through development and are accompanied by fast (typically 140-200 Hz) 'ripples' in the adult hippocampus (O'Keefe & Nadel, 1978; Sipilä & Kaila, 2007). The latter activity is thought to be strongly correlated with memory consolidation during sleep states (Wilson & McNaughton, 1994; Kudrimoti et al., 1999; Ego-Stengel & Wilson, 2010), and can

reactivate spatial maps during awake states (Dupret et al., 2010). Like any spontaneous electrical neural activity, there must be an endogenous origin of these sharp waves, which is supported by the findings that surgical ablation of afferents to the hippocampus rather increases than decreases occurrence of these events (Sipilä & Kaila, 2007). It was suggested that sharp waves are generated via endogenously bursting CA3 pyramidal neurons that are interconnected through excitatory collaterals, much in the same way that network-driven events are generated *in vitro* in the neonate (Sipilä et al., 2005). Additionally, if sharp waves are indeed the *in vivo* correlate to GDPs/ENOs, they must share other properties essential for network activity. Both sharp waves and hGDP/ENOs are associated with glutamatergic and GABAergic currents (Ben-Ari, 2001; Sipilä et al., 2005) and are both blocked upon NKCC1 inhibition with bumetanide **(§1.4)** (Sipilä et al., 2006). Furthermore, sharp waves are the first detected activity that is endogenously generated in the hippocampus (Karlsson & Blumberg, 2003; Leinekugel et al., 2002), thus fitting temporally with occurrence of hGDPs. All this suggests that occurrence of network events early in development, e.g. sharp waves and GDP/ENOs, is dependent on intrinsically bursting neurons with reduced efficacy of GABAergic inhibition or during overall enhancement of excitation.

In vivo studies have revealed a pattern of synchronous cortical activity that occurs in tandem with fast recurrent cortical oscillations *in vitro* (Khazipov et al., 2004). The so called 'spindle bursts' most likely correspond to human premature delta brushes recorded in EEG (Milh et al., 2007). With similar bursting behavior, e.g. frequency and duration, limited spatial connectivity, and developmental profile (Khazipov et al., 2004), spindle-bursts are likely the *in vivo* expression of cGDPs in slices. The recession of both spindle bursts and delta brushes tightly

parallels the maturation of inhibitory GABAergic currents, implicating a necessity of this neurotransmitter in their generation (Allene et al., 2008).

Spreading Ca_i rises at rates similar to those of cENOs and reflecting the correlated activity of thousands of neurons were detected in neocortex of unanesthetized mice during sleep-like resting states (Adelsberger et al., 2005). These *in vivo* Ca^{2+} waves propagate along the entire cortical mantle, in contrast to localized sharp waves or spindle bursts recorded in anesthetized rats (Leinekugel et al., 2002; Khazipov et al., 2004). Novel direct-coupled electroencephalogram recordings in human neonates further revealed the presence of slow activity patterns in the neocortex not seen with conventional approaches (Vanhatalo et al., 2002). The authors of that study noted that the slow activity recorded in their study was intriguingly similar to synchronous activity observed in neocortical brain slices.

1.6 ENO-like Bursting in *Locus Coeruleus*

In the first project for this thesis, the effects of variation of the Ca^{2+} and K^+ content of the superfusate were investigated not only on hENOs and cENOs, but also on spontaneous bursting of *locus coeruleus* networks that are contained in the same novel type of horizontal newborn rat brain slice developed for this thesis **(Fig. 1-1)**. Accordingly, this section serves to provide background information on basic functions of this brain structure and its developmental state plus activities in newborns.

The *locus coeruleus* represents a cluster of noradrenergic neurons that are located in the dorsal pons adjacent to the fourth ventricle. It was first described by Reil in 1809, and was named *locus coeruleus* in 1812 (Maeda, 2000). The *locus coeruleus* is associated with arousal and sleep-wake cycles and is the major noradrenergic nucleus in the brain that projects to a vast number of structures including cortex, hippocampus, cerebellum, brainstem and spinal cord (Berridge & Waterhouse, 2003; Samuels & Szabadi, 2008). Norepinephrine (i.e. noradrenaline) is synthesized by *locus coeruleus* neurons from the amino-acid L-tyrosine by the rate-limiting enzyme dopamine-hydroxylase and stimulates different signaling pathways via α_1, α_2 and β adrenergic receptors (Smythies, 2005; Hein, 2006). α_1 and α_2 receptors are coupled to the inhibitory G_i/cyclic-adenosine monophosphate (cAMP) second-messenger system while β adrenergic receptors are coupled to the stimulatory G_s/cAMP system. The *locus coeruleus* has long been considered as an exclusively noradrenergic nucleus, though there is now evidence that noradrenaline is co-released with other neuromodulators such as brain-derived-neurotrophic factor, enkephalins, neuropeptide-Y or somatostatin which likely serve to fine tune its actions (Olpe & Steinmann, 1991; Berridge & Waterhouse, 2003). Axons from *locus coeruleus* neurons are characterized by profuse branching to innervate wide areas, mainly ipsilaterally (Mason & Fibiger, 1979). Axon terminals in *locus coeruleus* neurons have the 'classical' structure of a chemical synapse, but varicosities are present along the axon and serve to promote noradrenaline release at various spots of their passage through different brain areas. This 'volume transmission release' affects not only neurons, but also glia and blood vessels (Paspalas & Papadopoulos, 1996; Fuxe et al., 2010).

Previous studies have shown that the noradrenergic *locus coeruleus* system is already functional at birth, but continues to develop postnatally (Dreyfus et al., 1983; Nakamura et al., 1987; Maubecin & Williams, 1999; Murrin et al., 2007). In rats, *locus coeruleus* neurons differentiate at embryonic day 12 (E12) while noradrenaline appears at E14 (Lauder & Bloom, 1974). At ~P10, the *locus coeruleus* appears to have matured to an almost adult-like neural circuit (Moriceau et al., 2010). Noradrenaline from the *locus coeruleus* also regulates the development of Cajal-Retzius cells, the first type of cortical neurons (Naqui et al., 1999), and is thus crucial for normal brain maturation. In the neonatal period, noradrenaline is also implicated in olfactory learning, maternal recognition and infant survival (Moriceau et al., 2010).

Regarding their electrical activities, *locus coeruleus* neurons in the adult brain fire in both tonic and phasic modes (Hobson et al., 1975; Aston-Jones & Cohen, 2005). The tonic mode is characterized by a low-frequency regular pattern with a higher discharge during wakefulness, lower discharge during non-REM sleep and no activity during REM sleep. Additionally, *locus coeruleus* neurons display spontaneous electrical activities that are synchronized during development. Nakamura and colleagues (1987) showed that *locus coeruleus* neurons in anesthetized rats *in vivo* display a spontaneous firing rate (0.2-3 Hz) which is significantly greater in P7-18 rats compared to P1-6, similar to frequencies recorded in brain slices. Early studies on rats revealed that *locus coeruleus* neuronal excitability depends on various conductances, including a persistent Ca^{2+} current, a tetrodotoxin (TTX) -sensitive persistent Na^{+} current and Ca^{2+}-activated K^{+} currents (Williams et al., 1984). More recent studies indicate the additional involvement of an inwardly-directed non-specific cation current carried primarily by Na^{+} (Nestler et al., 1999; Murai & Akaike, 2005). In contrast, Ca^{2+} currents are seemingly not

involved in pacemaker activity of mouse *locus coeruleus* neurons, while the strengths of Na^+ and K^+ currents increase during development (De Oliveira et al., 2011). However, this may be a species-specific phenomenon because the incidence of spontaneous firing in mouse *locus coeruleus* neurons rather decreases during development.

In vitro studies showed that early postnatal *locus coeruleus* neurons display Ca^{2+}-dependent subthreshold membrane potential oscillations which become less pronounced during maturation, contrary to their increasing (tonic) discharge rate (Williams et al., 1984; Williams & Marshall, 1987; Christie et al., 1989). Synchronous activity of the *locus coeruleus* neurons is apparently mediated by electrotonic coupling through gap junctions (Maubecin & Williams, 1999; Bennett & Zukin, 2004). This was also demonstrated by electrical and dye-coupling experiments between pairs of neurons (Christie et al., 1989; Christie & Jelinek, 1993; Oyamada et al., 1999; Ballantyne et al., 2004). It was further suggested that electrotonic coupling decreases with age similar to neurons in other brain regions, as discharge synchrony between *locus coeruleus* neurons in adult rats become reduced (Bennet & Zukin, 2004). In the adult rat, spontaneous membrane potential oscillations are rarely seen, but can be induced by bath application of barium or tetraethylamonium (Ishimatsu & Williams, 1996).

Besides the role in arousal and control of performance, the *locus coeruleus* is implicated in homeostatic functions including cardiovascular regulation (Guyenet, 1991) and breathing (Oyamada et al., 1998, 1999; Hilaire et al., 2004; Viemari et al., 2004; Hilaire, 2006; Gargaglioni et al., 2010). It is not considered part of respiratory rhythm-generating networks, but noradrenaline released by pontine structures is involved in their modulation. Noradrenaline

exerts a combination of α_1 facilitatory and α_2 inhibitory effects on medullary inspiratory networks with apparent species differences between rats and mice (Errchidi et al., 1991; Hilaire et al., 2004; Adachi et al., 2005). *Locus coeruleus* neurons send information and receive feedback from medullary respiratory networks, which allows them to exhibit central respiratory-modulated firing (Guyenet et al., 1993; Oyamada et al., 1998, 1999). Oyamada and colleagues (1998) demonstrated that spontaneous activity of *locus coeruleus* neurons in the newborn rat *en bloc* model is related to inspiratory rhythm. Previous transneuronal tracing studies demonstrated an anatomical pathway between *locus coeruleus* and medullary respiratory networks. Neurotrophic viruses applied to phrenic motoneurons were localized in some *locus coeruleus* neurons in adult rats and mice (Dobbins & Feldman, 1994; Burnet et al., 2001; Feldman et al., 2007) and even in neonatal mice (Hilaire et al., 2004).

1.7 Ca^{2+}/K^{+} Antagonism of Rhythmic Neural Circuits

Much attention has been paid to Ca^{2+} entry into neurons and its regulation of Ca^{2+}-dependent channels and enzymes as well as its contribution to various forms of synaptic plasticity including long-term potentiation (Bliss & Collingridge, 1993). The ionic composition of the interstitial brain fluid, particularly regarding the cations K^{+}, Ca^{2+} and Mg^{2+}, greatly affect neuronal excitability (Hille, 2001; Somjen, 2002). For example, exposure of neuronal tissues to low (<0.5 mM) extracellular Ca^{2+}, or high (> 7 mM) extracellular K^{+} is a common model for epilepsy **(Fig. 1-7)** (Konnerth et al., 1986; Jefferys, 1995; Kilb et al., 2007). Hypocalcaemia and associated seizures can also occur in intact animals, specifically as a result of vitamin D deficiency, hypothyroidism or renal failure (Riggs, 2002; Castilla-Guerra et al., 2006). In contrast, abnormally high levels of Ca^{2+} in the interstitial spaces cause a general depression of brain

function (Riggs, 2002). In support of this, other studies have shown that focal injection of Ca^{2+} depressed the spontaneous activity of neural respiratory networks in the lower brainstem (Leusen, 1972). The resulting Ca^{2+}-mediated depression of breathing was reversed when K^+ was simultaneously injected (Leusen, 1972). Such a 'Ca^{2+}/K^+ antagonism' that also determines rhythmic bursting of isolated respiratory networks (Ruangkittisakul et al., 2007) may also influence the excitability in other (isolated) brain structures.

This depressing action of raised extracellular Ca^{2+} seems counterintuitive at first glance. According to the Goldman equation (Hille, 2001), raising Ca^{2+} in the extracellular space should increase the driving force for Ca^{2+} influx and thus increase membrane excitability. That depression can occur nevertheless, is at least partly explained by the surface charge theory proposed by Huxley >50 years ago. He hypothesized that Ca^{2+} ions may be sequestered to the outside of the plasma membrane, creating an electric field which would not only add to the resting membrane potential, but may bias voltage sensors within the membrane (Hille, 2001). Actual binding of Ca^{2+} to the membrane or to sensors of ionic channels is not required since the screening of Ca^{2+} hovering near the membrane would effectively neutralize its negative charge. Lowering extracellular Ca^{2+} content has the opposite effect of reduced shielding (Hille, 2001). Consequently, voltage-dependent currents, e.g. an unspecified Ca^{2+}-sensing cation channel in hippocampal neurons, can become activated to directly affect postsynaptic membrane excitability (Xiong et al., 1997). In an extreme example, reducing Ca^{2+} to the nanomolar range has been shown to alter the specificity of Na^+ channel permeability to favor Ca^{2+} fluxes (Hess & Tsien, 1984) and similar results on Ca^{2+}-induced hyperexcitability have already been shown during seizure activities (Köhr & Heinemann, 1989; Heinemann et al., 1990). Such phenomena

do not represent a physiological action, but may occur during some pathological conditions, e.g. hyperparathyroidism-evoked hypercalcaemia (Somjen et al., 1987; Riggs, 2002; Castilla-Guerra et al., 2006).

Alternatively, Ca^{2+}-induced neuronal depression may be caused by a stimulatory effect on tonically active inhibitory neurons. Influx of Ca^{2+} into presynaptic cells is essential for normal synaptic transmission and increasing this divalent cation in the superfusate should enhance release of neurotransmitters (Hille, 2001). In hippocampal slices, raising superfusate Ca^{2+} to 1.2 and 1.8 mM exaggerated synaptic transmission which was depressed when Ca^{2+} was lowered to 0.8 mM (Balestrino et al., 1986; Rausche et al., 1990). Though Ca^{2+}-induced inhibition of inhibitory neurons seems unlikely considering that not only are the majority of functional synapses GABAergic early in development, but also that GABAergic transmission is excitatory, thus increasing synaptic transmission should augment bursting (Jefferys, 1995; Ruangkittisakul et al., 2007). In a hippocampal slice, Xiong et al. (1997) demonstrated that decreasing extracellular Ca^{2+} activated a postsynaptic non-selective cation channel and depolarized the membrane, though this theory hinged on the surface-screening effects of Ca^{2+} modulating the activation of the sensor. In cortical slices, however, reducing Ca^{2+} to 1 mM increased the tendency of immature entorhinal cortical neurons to generate bursts and this was thought to be mediated through increasing persistent Na^{+} currents (Sheroziya et al., 2009). Other studies in diverse brain regions have documented the same phenomenon, however. Spontaneous rhythmic activities in slices obtained from the ferret visual and prefrontal cortex were unmasked when extracellular Ca^{2+} was reduced from 2 to 1.2 mM (Sanchez-Vives & McCormick, 2000). Additional high-frequency (300-750 Hz) bursting neurons in the neocortex with interburst

frequencies of 10-80 Hz, so-called 'chattering cells' and corresponding with gamma frequencies *in vivo*, were also uncovered with more physiological ionic superfusate composition (Brumberg et al., 2000). Regarding stimulation of spontaneous supramedullary neural network bursting by raised extracellular K^+, it was shown that this reinstated bicuculline-evoked depression of hGDPs (Sipilä et al., 2005) as well as cortical bursting that was inhibited by blockade of ionotropic glutamate receptors (McCabe et al., 2007). It is not clear, however, whether an increased excitatory drive can recover Ca^{2+}-induced depression of cortical network-driven activities as demonstrated with a Ca^{2+}/K^+ antagonism on respiratory networks (Leusen, 1972; Ruangkittisakul et al., 2007).

1.8 Neural Network Modulation by Methylxanthines

The Ballanyi laboratory has recently studied effects of methylxanthines on respiratory and *locus coeruleus* networks in newborn rat *in vitro* slices. Thus, this topic has been reviewed in previous studies and a recent PhD thesis **(Fig. 1-5)** (Ruangkittisakul & Ballanyi, 2006, 2010; Panaitescu et al., unpublished). Below is a brief summary of methylxanthine action and emphasis on its relevance to immature cortical circuits.

Methylxanthines like caffeine, theophylline, aminophylline, theobromine are common ingredients in commercial products, such as coffee, soda, energy drinks, and are also used in combination with non-prescriptive analgesics and cold remedies. Caffeine consumed from dietary sources is rapidly absorbed from the gastrointestinal tract (Arnaud, 2011), is metabolized by the liver through demethylation (Kennedy et al., 1987; Berthou et al., 1992) and can easily

cross the blood-brain barrier where it can be further metabolized locally (Johansson et al., 1996). Methylxanthines have many therapeutic actions. They are known to be a potent bronchodilators, to increase arousal (Barry et al., 2005) and locomotor activity (Nehlig et al., 1992), improve performance on learning and memory tasks (Angelucci et al., 1999), cognitive performance (Smit & Rogers, 2000), auditory vigilance and reaction time (Lieberman et al., 1987), and enhance feelings of well being (Garrett & Griffiths, 1997). In addition to these multiple actions, methylxanthines have been administered as a respiratory stimulant for more than 30 years (Martin et al., 2005) and are the current gold standard in the treatment of apneas of prematurity (Comer et al., 2001; Schmidt et al., 2006; Henderson-Smart & Steer, 2010).

At serum concentrations of 0.2-2 mg/l (i.e. 0.001-0.01 mM), about the typical daily intake, caffeine blocks adenosine A_1 and A_2 receptors **(Fig. 1-6)** (Fredholm et al., 1999). A_1 receptor activation can inhibit adenylyl cyclase, thereby decreasing cAMP availability while A_2 receptors typically stimulate adenylyl cyclase and possibly some voltage-gated Ca^{2+} channels (Fredholm et al., 1999). Additionally, at low millimolar doses caffeine and theophylline can inhibit cyclic nucleotide-dependent phosphodiesterases (PDEs) which serve to break down cAMP or other cyclic nucleotides **(Fig. 1-6)** (Francis et al., 2011). cAMP is a major stimulus to rhythmogenic respiratory networks (Ballanyi et al., 1997, 1999; Richter et al., 1997; Manzke et al., 2003; Ballanyi, 2004). Accordingly, various recent studies from our group have explored the potential of specific PDE blockers like rolipram for stimulation of breathing (Ballanyi et al., 1999; Ballanyi, 2004; Ruangkittisakul & Ballanyi, 2006, 2010; Ruangkittisakul et al., 2006, 2007, 2008). Also at low millimolar doses, methylxanthines stimulate Ca^{2+} release from stores by

increasing the Ca^{2+} sensitivity of ryanodine-senstive Ca^{2+} release channels **(Fig. 1-6)** (Magkos & Kavouras, 2005).

As mentioned above, methylxanthines (more commonly caffeine) are administered to preterm human infants for reversing severe apneas of prematurity (Comer et al., 2001; Schmidt et al., 2006; Henderson-Smart & Steer, 2010). However, caffeine doses >10 times higher than those that typically block adenosine receptors are generally used in clinical settings and this therapy can last for several weeks until the (preterm) neonate has matured (Aden, 2011). In a case series, three premature neonates received overdoses of theophylline for apnea of prematurity with maximum serum levels of the drug ranging from 55-123 mg/l resulting in varied adverse effects ranging from emesis and tachycardia to seizures (Lowry et al., 2001). Of utmost concern regarding so-called 'theophylline-associated seizures' is that there is no readily available reversing agent, thus these seizures are usually intractable (Nakada et al., 1983; El-Bitar & Boustany, 2009). Pharmacological intervention with diazepam is mostly ineffective in controlling theses seizures, suggesting that theophylline might interact with benzodiazepines (Nakada et al., 1983; Yoshikawa, 2007). As such, how methylxanthines exert their proconvulsive role remains mostly undetermined.

Theophylline-associated seizures (Nakada et al., 1983; Dunn & Parekh, 1991; Korematsu et al., 2008; El-Bitar & Boustany, 2009) are presumably due to the following mechanisms (Boison, 2011): (*i*) decrease of seizure threshold through inhibition of adenosine receptors, (*ii*) inhibition of blood flow through adenosine antagonism (Puiroud et al., 1988), (*iii*) inhibition of pyridoxal

5'-phosphate, which may decrease GABA synthesis, or (*iv*) direct inhibition of $GABA_A$ receptors **(Fig. 1-6)** (Sugimoto et al., 2001). In a critical window during which early excitatory GABAergic function is crucial for proper brain development by regulating the balance between cortical excitation and inhibition, the blockade of these processes by caffeine or other methylxanthines has potential deleterious consequences. In a study in which GABAergic excitation was blocked by bumetanide, the authors found permanent alterations in cortical circuits such as reduced arborization of dendrites and spine density, and impairment in sensorimotor gating (Wang & Kriegstein, 2011). In a different study, different types of seizure-like bursts, namely ictal activities (IAs) and interictal-like events (ILEs) were evoked by bumetanide **(Fig. 1-7)** (Kilb et al., 2007). Other studies have shown that caffeine alters adenosine receptor expression and distribution (Montandon et al., 2008), causes neuronal apoptosis (Kang et al., 2002; Black et al., 2008) and transiently prevents astrocytogenesis (Desfrere et al., 2007) or cerebral vasoconstriction (Hoecker et al., 2002).

Proconvulsive effects of caffeine *in vitro* are produced in hippocampal slices from newborn rats. During brief periods of anoxia, caffeine induces ILEs in immature CA_3 hippocampal neurons (Dzhala et al., 1999). As an explanation, adenosine levels in extracellular brain tissue are known to increase during brain anoxia leading to depression of neuronal activity and hereby preventing seizures in the neonatal hippocampus. Through antagonism of A_1 adenosine receptors **(Fig. 1-6)** caffeine presumably blocks this neuroprotective effect of adenosine, which might disturb development of neonatal networks resulting in neurological sequelae in adults (Holmes & Ben-Ari, 1998). Based on the above, there is an ongoing debate whether or not methylxanthines are safe for preterm infants (Millar & Schmidt, 2004).

1.9 Neural Network Modulation by Opioids

Preterm infants are frequently treated with opioids for pain management, overdoses of which can be fatal due to their depressing action on brainstem respiratory networks (Durrmeyer et al., 2010; Walter-Nicolet et al., 2010). There are several classes of plant-derived, synthetic, and endogenous opioids, some of which include: endorphins, endomorphins, dynorphines, and nociceptin-orphanin. Endogenous opioids are involved in (mostly inhibitory) modulation of central nervous signaling pathways, such as presynaptic inhibition of pain sensation, while others can induce euphoria, e.g. a 'runner's high' during sustained physical exercise (Waldhoer et al., 2004). Opioids act on seven transmembrane-spanning G protein-coupled opioid receptors of various types. Specifically, they act on either μ-, κ-, δ-, or NOR-type, named for their respective ligands or areas in which they were discovered, some of which coupled to pertussis toxin-sensitive G_i/G_o proteins **(Fig. 1-6)** (Waldhoer et al., 2004). Activation of this complex leads to the uncoupling of G proteins from the receptor to inhibit adenylyl cyclase, resulting in the fall of cellular cAMP. This leads to subsequent blockade of the protein kinase-A signaling system and modulation of various receptor-coupled and voltage-gated ion channels **(Fig. 1-6)** (Santiago & Edelman, 1985; Richter et al., 1997; Connor & Christie, 1999). The mechanisms of action of opioids involve blockade of voltage-activated Ca^{2+} channels at the presynaptic terminal thereby limiting vesicle release or, alternatively, activation of postsynaptic G protein-coupled inward-rectifying K^+ (GIRK) channels **(Fig. 1-6)**. Whether opioid targets are located pre- or postsynaptically ultimately depends on the cell type (Christie, 1991; Nestler et al., 1999; Williams et al., 2001).

Opioid use is at time associated with side effects, such as nausea, vomiting, constipation, sedation and, as already mentioned, respiratory depression. Systemic effects of opioids include slowed rate of breathing, reduction of upper airway patency, rigidity of abdominal and chest walls, and reduction of respiratory responses to hypoxia (Santiago & Edelman, 1985; Pattinson, 2008; Dahan et al., 2010). Opioid-induced respiratory depression occurs in ~17% of surgeries, the outcome of which can be fatal if measures to rapidly and selectively counter this depression are not taken (Cashman & Dolin, 2004). In preterm or young infants, opioids such as morphine provide relief for pain associated with intubation and mechanical ventilation which can last for many weeks (Du et al., 2006). These infants have a high susceptibility for apneas and respiratory depression due to decreased elimination of the drug and a more permeable blood-brain-barrier (Lynn & Slattery, 1987). Thus, concentrations of opioids in brain regions are usually several-fold higher than those seen in adults and have a longer duration of action. However, few studies have examined the adverse neurological effects these drugs might have on the developing brain.

In contrast, the role of opioids has been extensively studied in *locus coeruleus* networks, both *in vivo* and *in vitro*, which has provided a basis for the classical pharmacological pathways of opioids. In *locus coeruleus* neurons, all three classes of opioid receptors are functional, with prevalence of μ-receptors on postsynaptic neurons (Christie, 1991). Specifically, opioids suppress *locus coeruleus* neuronal activity through activation of μ-receptors and exert their actions through stimulation of inhibitory G proteins resulting in inhibition of adenylyl cyclase and GIRK channel activation, which in turn leads to membrane hyperpolarization and prevention of action potential firing **(Fig. 1-6)** (Williams et al., 1982, 1984; Christie, 1991; Law et al., 2000). Inhibition of adenylyl cyclase is usually followed by a reduction of cellular cAMP and

consequent reduction of phosphorylation of the nonspecific cation current implicated in *locus coeruleus* neuron bursting (Alreja & Aghajanian, 1991, 1993; Nestler et al., 1999). Thus studies on opioid effects on the *locus coeruleus* network have provided a stereotypic case of postsynaptic inhibition of spontaneously active neurons. Whether μ-receptor activation in cortical/hippocampal networks leads to a similar depression is still under vigorous debate.

Experiments in rats established that μ-, κ-, and δ-opioid receptors are functional in the adult hippocampus and cortex (Goodman et al., 1980; Stengaard-Pedersen, 1983; Lewis et al., 1983; Mansour et al., 1987). It was also shown in both *in vivo* and *in vitro* studies that these receptor types are already active in newborn rodents, with μ- and κ-receptors predominating in the early postnatal period (Leslie et al., 1982; Pickel, 1982; Meilandt et al., 2004). However, expression of opioid receptor subtypes is heterogeneous in the mammalian hippocampus, with μ-receptor expression limited almost exclusively to inhibitory (GABAergic) interneurons in the CA_1 subfield (Arvidsson et al., 1995; Mansour et al., 1995; Bausch & Chavkin, 1995; Drake & Milner, 1999, 2002; Stumm et al., 2004). The primary effect of opioids is the inhibition of interneuronal firing (Zieglgänsberger et al., 1979; Madison & Nicoll, 1988; Cohen et al., 1992; Kouvaras et al., 2008). In the mature brain, opioid-evoked inhibition of (inhibitory) interneurons plays a key role in the generation and propagation of certain epilepsies (Siggins et al., 1986). However, several studies have also proposed that opioids act directly on pyramidal CA_3 neurons (Bloom, 1983; Moore et al., 1994) to both inhibit signaling through presynaptic K^+ conductance activation (Wimpey & Chavkin, 1991) and stimulate bursting behavior by either augmenting an m-current during prolonged depolarizations (Moore et al., 1994) or NMDA-receptor mediated responses (Przewlocki et al., 1999). The above mechanisms all describe activation of μ-receptors

in the mature state, when GABAergic conductance are primarily hyperpolarizing. It is not clear what effect, if any, activation of these receptors has on GABAergic interneurons which provide a depolarizing input to pyramidal intrinsic bursters.

1.10 Objectives and Hypotheses

The major aim of this thesis was to investigate how spontaneous electrical bursting and associated Ca_i oscillations in neonatal hippocampal and cortical neural networks that function at birth to support their maturation are affected by drugs that are clinically administered to (preterm) infants. Newborn rats were used for this work because previous findings from others (Ben-Ari et al., 2007; Sipilä & Kaila, 2007) and our group (Kantor et al., 2012) have shown that activity remains stable for several hours in brain slices from that species. In these slices, suction electrodes were used for recording of spontaneous electrical hippocampal and cortical neuronal population activities while multiphoton/confocal imaging was performed for monitoring associated Ca_i oscillations at the cellular level. For an initial project, these approaches were applied to determine the optimal concentrations of superfusate Ca^{2+} and K^+ for robust network bursting in these cortical areas. For that project, electrophysiological recordings were also performed on the spontaneously rhythmic *locus coeruleus* that was contained in the same slice type developed for this thesis, which thus enables simultaneous recording of population activities from all three rhythmic brain areas. One of the remaining two result chapters was dedicated to the analysis of methylxanthines on the hippocampal and cortical oscillations, whereas the second chapter studied modulation of these events by opioids. In the following, aims and hypotheses for these three projects are summarized.

1.10.1 Project-1: Ca^{2+}/K^{+} Antagonism of ENOs and ENO-like Locus Coeruleus rhythm

Findings that Ca^{2+} injection into respiratory brainstem areas depresses breathing, and that this inhibition is reversed by concomitant K^{+} injection, led to the hypothesis that the activity of neural networks controlling this behavior is determined by a Ca^{2+}/K^{+} antagonism (Leusen, 1972). This hypothesis is strongly supported by findings from our group (Ruangkittisakul et al., 2007, 2010; Ballanyi & Ruangkittisakul, 2009) in that the isolated preBötC is highly sensitive to these cations, which greatly affect neuronal excitability (Hille, 2001, Somjen, 2002). While most studies on cortical slice use artificially-raised superfusate Ca^{2+} and K^{+} concentrations to boost synaptic transmission, some studies presented evidence that spontaneous activity may occur in (cortical) brain slice areas in superfusate with close-to-physiological Ca^{2+} (1-1.2 mM) and K^{+} (3-4 mM) concentrations (Sanchez-Vives & McCormick, 2000, Sheroziya et al., 2009). It was the aim of this project to perform a quantitative analysis for determining the optimal superfusate concentrations for these cations to provide robust hENOs, cENOs and ENO-like *locus coeruleus* bursts.

I hypothesize for *Project-1:*

I) Superfusate with close-to-physiological Ca^{2+} and K^{+} content provides most robust hENOs, cENOs and ENO-like *locus coeruleus* bursting.

II) hENOs, cENOs and ENO-like *locus coeruleus* bursts are similarly sensitive to Ca^{2+} and K^{+} as the isolated preBötC, meaning that a Ca^{2+}/K^{+} antagonism is typical for active neural networks in neonates.

III) The Ca^{2+}/K^{+} dependence of neuronal population bursting is reflected by a corresponding dependence of cytosolic Ca^{2+} oscillations, as to be determined for the hippocampal and cortical networks.

1.10.2 Project-2: Methylxanthine-evoked Perturbation of ENOs

Methylxanthine administration to preterm infants for stabilization of breathing can evoke seizures (Delanty et al., 1998; Comer et al., 2001; Korematsu et al., 2008; El-Bitar & Boustany, 2009). Unpublished findings from our group indicate that methylxanthine-evoked seizure-like spinal hyperexcitability perturbs inspiratory rhythms in newborn rat brainstem-spinal cords with a contribution of blockade of $GABA_A$ receptors. One major aim of this thesis was to determine if methylxanthines also perturb spontaneous rhythms in other neural networks during the early postnatal time period. For this purpose, the same horizontal brain slice model developed for *Project-1* was used for bath-application of the clinically commonly used methylxanthines caffeine and theophylline (Comer et al., 2001; Schmidt et al., 2006; Henderson-Smart & Steer, 2010). In a parallel approach, multiphoton/confocal Ca^{2+} imaging in the hippocampus and entorhinal/perirhinal cortex was done using these slices. One major rationale for such imaging was to reveal whether potential methylxanthine-evoked hyperexcitability is due to deregulation of neuronal Ca^{2+} homeostasis (Dzhala et al., 1999; Cherubini et al., 1991). As a further aim, it was intended to study involvement of $GABA_A$ receptors in case methylxanthines evoke indeed hippocampal and cortical hyperexcitability.

I hypothesize for Project-2:

I) Methylxanthines can transform hENOs and cENOs into seizure-like events

II) This reconfiguration of spontaneous bursting is mimicked by the $GABA_A$ receptor antagonist gabazine

III) Methylxanthine-evoked perturbations of hENOs and cENOs is due to deregulation of their neuronal Ca^{2+} homeostasis

1.10.3 Project-3: Opioid Effects on ENOs

Opioids depress breathing and spontaneous activity in *locus coeruleus* neurons from neonates via μ-receptors (Christie, 1991; Alvarez-Maubecin et al., 2000; Montadon et al., 2008; Ballanyi et al., 2009; Panaitescu et al., unpublished). Corresponding research on ENOs is needed because opioid treatment for neonatal pain can continue for extended time periods and may thus affect developing cortical circuits. It is also not clear whether glial cells respond in a different way to opioids than neurons. Suction electrode recordings from the CA_3 region and neocortex were performed in newborn horizontal brain slices in addition to multiphoton/confocal Ca^{2+} imaging of hENOs. A novel method for the visual discrimination between neurons and glial cell in the hippocampus will also be used to further unravel neuron-glia interactions during opioid administration.

I hypothesize for Project-3:

I) Opioids block hENOs and cENOs in similar fashion as isolated preBötC and *locus coeruleus* bursting

II) Opioid depression of ENOs is due to μ-opioid receptor activation and thus reversed by the antagonist naloxone

III) Cai in (astrocytic) glial cells is changed by opioids as a reflection of their possible activation by opioids.

Figures

Fig. 1-1

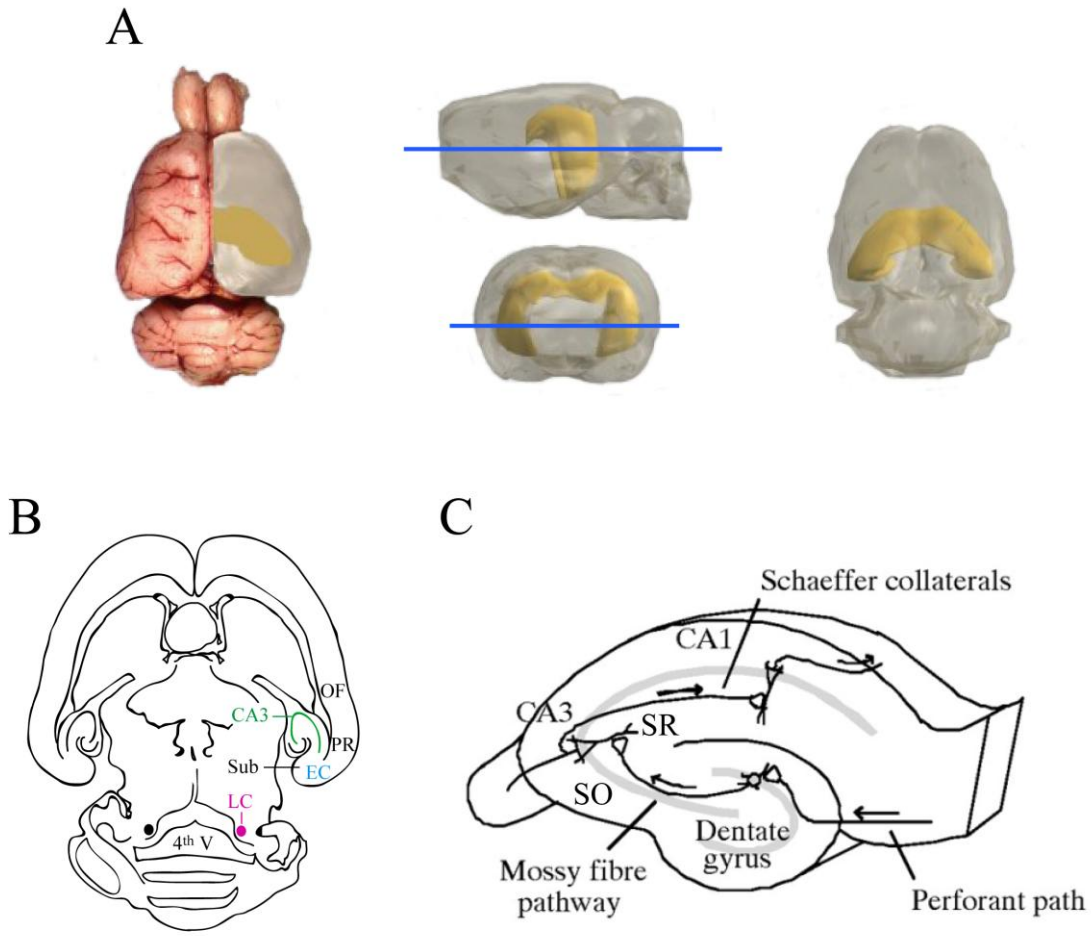

Fig. 1-1: Schematic of newborn rat/mouse hippocampal slice. A, dorsal view of a rat brain with cerebellum and olfactory bulbs intact with 3-D renderings (grey) showcasing the hippocampal formation (yellow). Blue lines indicate depth at which horizontal slices were cut. **B**, schema of a horizontal brain section at a level that enables simultaneous recording of ENOs in both entorhinal cortex (EC) and the CA_3 hippocampal area (CA_3) plus ENO-like bursting in the brainstem area of the *locus coeruleus* (LC). **C**, Circuitry and anatomical subregions within a hippocampal slice. Other abbreviations: OF, orbifrontal cortex; PR, perirhinal cortex, Sub, subiculum; 4^{th} V, fourth ventricle; SR, stratum radiatum; SO, stratum oriens. Modified from **A**: http://synapses.clm.utexas.edu/anatomy/hippo/hippo.stm; **B:** Kantor et al., 2012; **C**: Nguyen et al., 2006.

Fig. 1-2

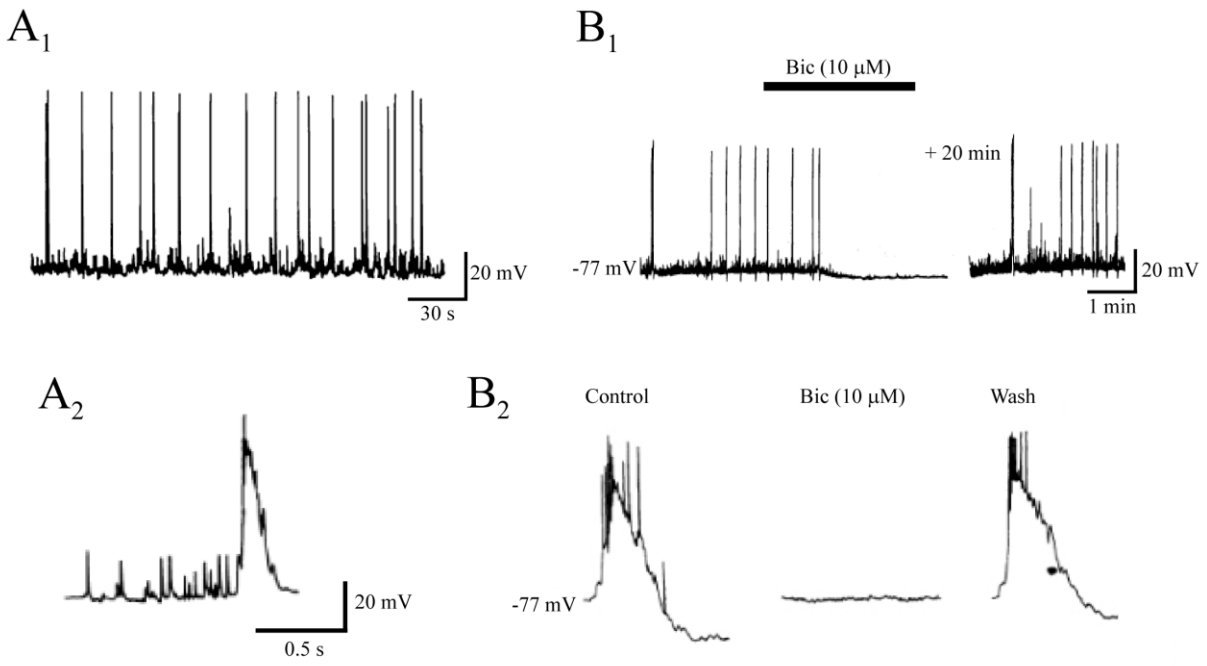

Fig. 1-2: Electrically-recorded giant depolarizing potentials (GDPs) in the newborn rat hippocampal slice. GDPs are synchronous neuronal population discharges, consisting of recurrent long lasting depolarizing potentials, with amplitudes up to 50 mV and lasting several hundreds of milliseconds. **A_1**, GDPs recorded from a CA_3 pyramidal neuron at P3. GDPs are typically preceded by a number of spontaneously occurring synaptic events. **A_2**, A GDP preceded by spontaneous synaptic activity shown in an expanded time scale. **B_1**, continuous trace in a P4 slice showing spontaneous GDPs. Bath application of bicuculline (Bic) induced membrane hyperpolarization, reduced the spontaneous synaptic noise and blocked GDPs. The effect of Bic washed out after 20 min. **B_2**, the three panels show faster recordings of the events indicated in **B_1**. Figures and legends modified from, **A**: Cherubini et al., 2010; **B**: Ben-Ari et al., 1989.

Fig. 1-3

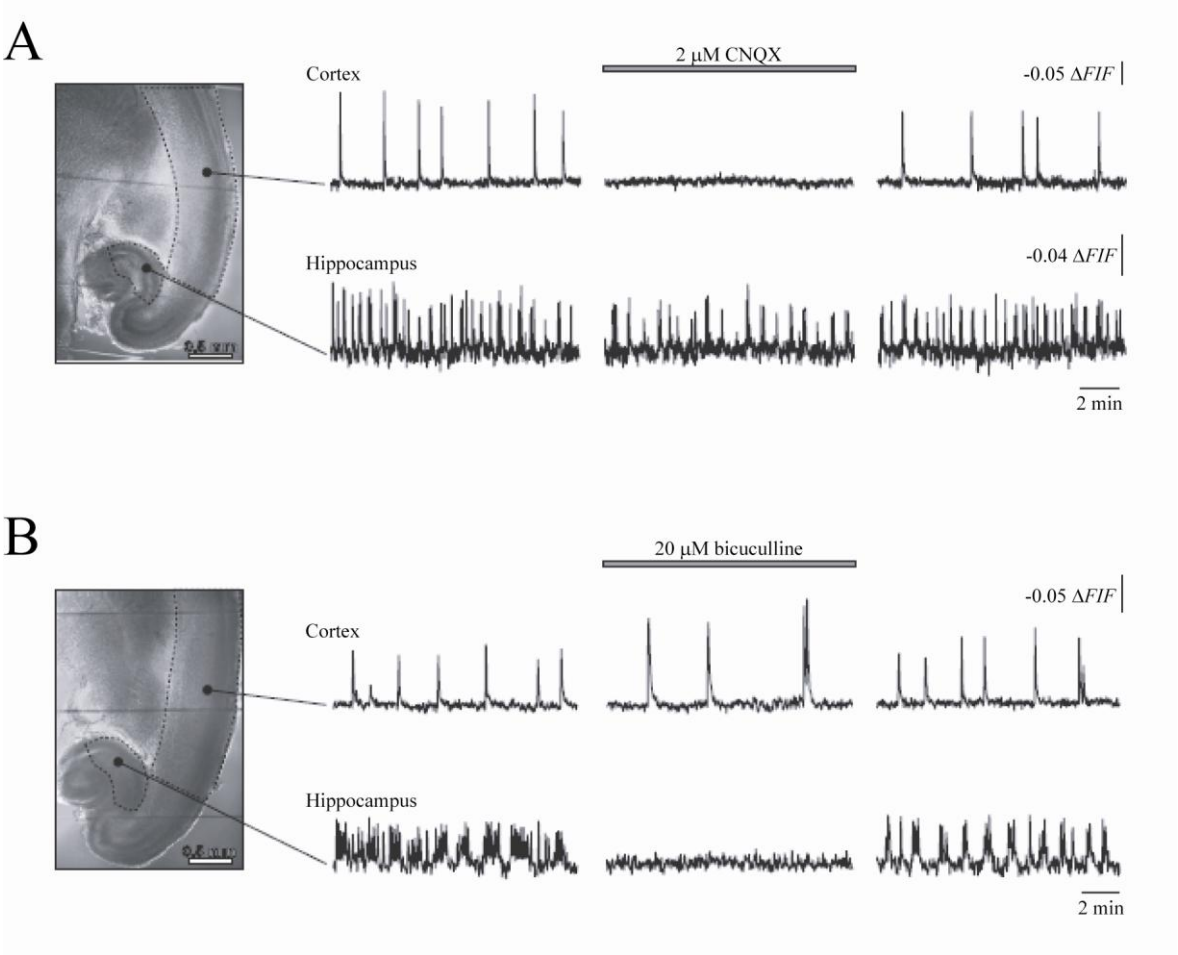

Fig. 1-3: Calcium-related early network oscillations (ENOs) in newborn rat horizontal slice. A, Microphotograph of a horizontal brain slice from a P1 rat taken at low magnification (4x objective). Black dots indicate the position of nonoverlapping regions of interest (covering about 1 mm^2) from which the activity dependent fluorescence was recorded (right). Fluorescence data are expressed as –ΔF/F (defined as background subtracted bycorrected decrease in fluorescence, divided by the resting fluorescence). Simultaneous fluorometric recordings from cortical (upper panel) and hippocampal (lower panel) regions in a control (left), in the presence of 2 mM 6-cyano-7-nitroquinoxaline- 2,3-dione (CNQX, middle) and after washout of CNQX (right). **B**, Experiment similar to the one shown in A illustrating the effect of 20 μM Bic. Here, bicuculline exaggerates spontaneously occurring cENOs, while blocking hENOs. The slice was obtained from a P1 rat. Figures and legends modified from Garaschuk et al., 2000.

Fig. 1-4

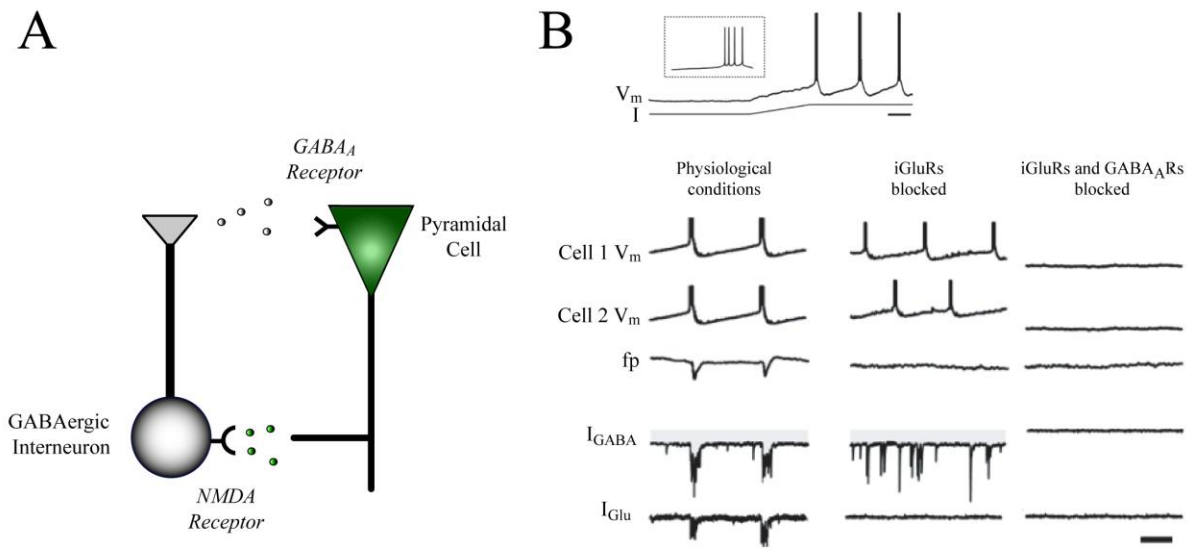

Fig. 1-4: Cellular and synaptic mechanisms of GDP generation. A, cartoon schematic demonstrating a simple circuit between an excitatory γ-aminobutyric acid (GABA) -ergic interneuron forming synapses with a (glutamatergic) pyramidal cell. GABA acts on A-type GABA receptors to drive GDPs in pyramidal neurons. Oscillations in interneurons are reciprocally activated by NMDA-R activation. **B**, Immature CA_3 pyramidal neurons generate voltage-dependent intrinsic bursts in the absence of synaptic transmission. The slow change in V_m is induced by current injection. (left), Under physiological conditions, GDPs are seen as synchronous bursts of action potentials in intracellular recordings in immature CA_3 pyramidal cells (Cell 1 and Cell 2), paralleled by a slow negative deflection in the field potential (fp). GDPs are associated with ionotropic GABAergic (I_{GABA}) and glutamatergic currents (I_{Glu}). **B** (centre), Blockade of ionotropic glutamatergic transmission desynchronizes pyramidal cell bursting and abolishes fp deflections as well as bursts of GABAergic currents that reflect interneuronal activity. **B** (right), Blockade of tonic and synaptic $GABA_A$ receptor currents hyperpolarizes immature CA3 pyramidal neurons and, consequently, abolishes intrinsic bursting (the effect of membrane potential on intrinsic bursting is illustrated in part **A**). The traces are semi schematic. *Time calibration bars:* 2 s in **A** and **B**, 200 ms in the inset in **A**. For voltage and current amplitudes, see original references cited in the text. Figures and legends modified from, Sipilä & Kaila, 2007.

Fig. 1-5

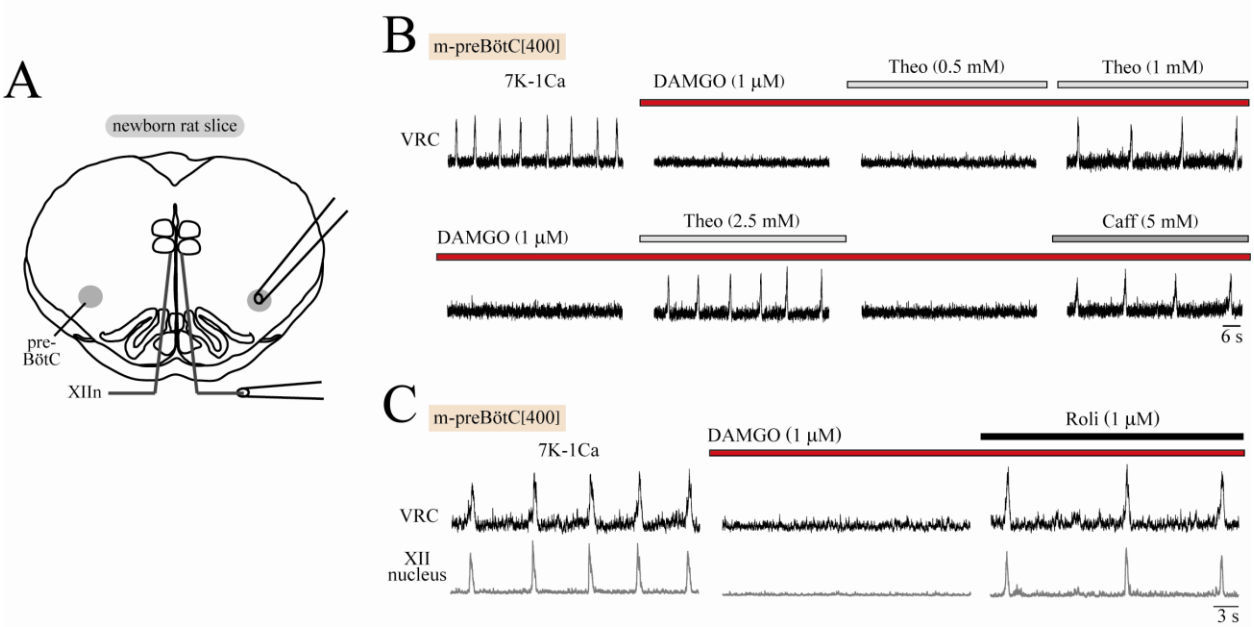

Fig. 1-5: Opioids abolish inspiratory-related bursting in preBötC slices and is stimulated by methylxanthines. The pre-Bötzinger complex (preBötC) is a brainstem region located in the ventral respiratory column (VRC) that generate respiratory rhythm in mammals and remains active in a transversal newborn rat brainstem slice. **A**, Rhythmic preBötC and XII motor output is monitored with suction electrodes from XII nerve roots (XIIn). **B**, Reversal by methylxanthines of depression by the μ-opioid receptor agonist DAMGO of inspiratoryVRC rhythm in a 400 μm brainstem slice. Bath-application of 0.5 mM theophylline (Theo) in 7K–1Ca superfusate did not reverse block of VRC rhythm by DAMGO (1 μM), whereas 1 and 2.5 mM Theo restored rhythm, though at slightly lower rate than in control. Also, bath-application of 5 mM caffeine (Caff) was capable of reactivating VRC rhythm to a rate similar to control. Note that the agents were applied consecutively to the same slice with an interval of at least 15 min of wash between each drug application to allow sufficient time to reverse their action. **C**, Reversal by the PDE4 blocker rolipram of depression by DAMGO of VRC rhythm in a 400 μm brainstem slice. Rolipram reactivated VRC rhythm within 7 min after start of bath-application, VRC rhythm that had been blocked by DAMGO. Figures and legends modified from Ruangkittisakul et al., 2010.

Fig. 1-6

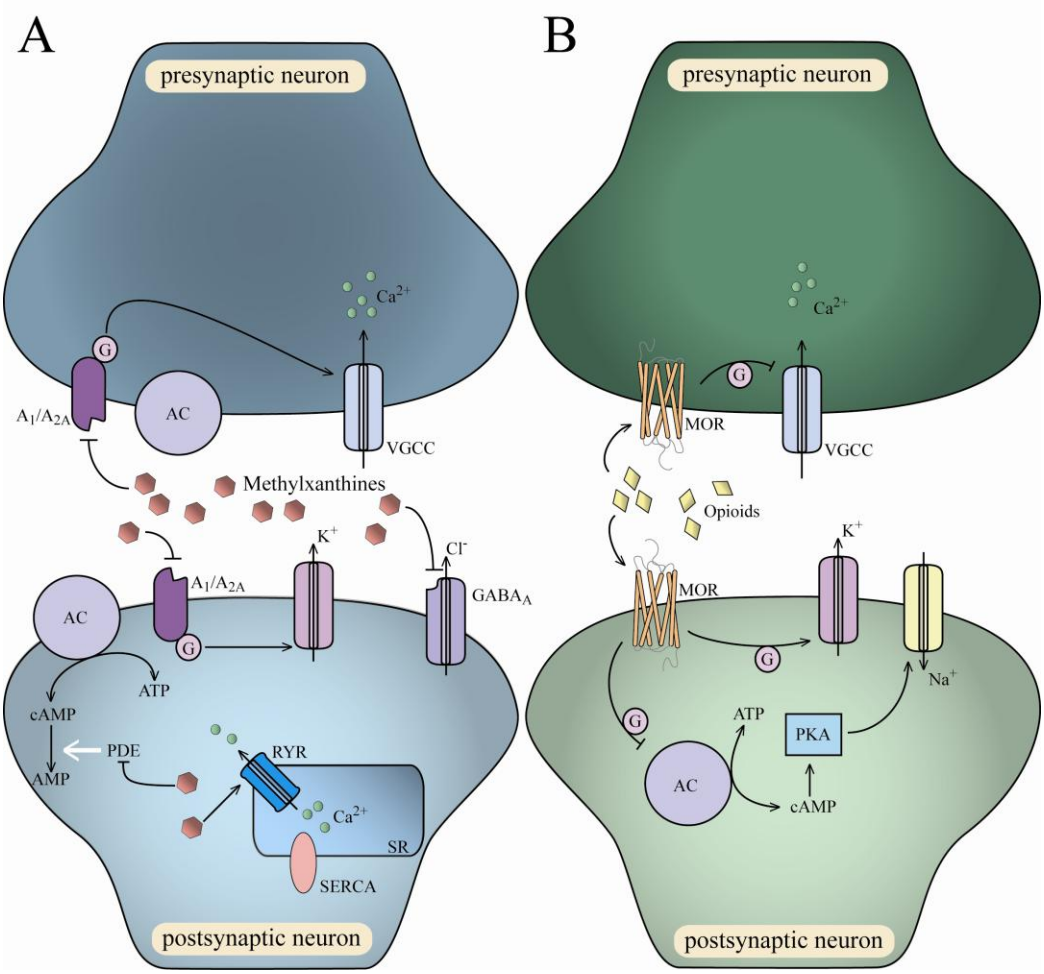

Fig. 1-6: **Possible mechanisms of methylxanthines and opioids. A**, Methylxanthines are known to act by (i) pre- or postsynaptic G protein-coupled adenosine receptors (mainly A_1, A_{2A}), (ii) inhibition of cAMP-dependent PDEs, (iii) activation of ryanodine (RYR) receptors to release Ca^{2+} from intracellular stores, or (iv) antagonizing A-type GABA receptors. Abbreviations: AC, adenylyl cyclase; Ca^{2+}, calcium ions; $G_{s/i}$, stimulatory/inhibitory G proteins; cAMP, cyclic adenosine monophosphate; K^+, potassium ions; Na^+ sodium ions; PKA, protein kinase A; VGCC, voltage-gated calcium channels. **B**, Opioids can act presynaptically through G protein-coupled opioid receptors, causing inhibition of voltage gated calcium channels or postsynaptic activation of a G protein-coupled inward-rectifying K^+ (GIRK) channels through μ-opioid receptor (MOR) activation. MOR activation can also inhibit adenylyl cyclase.

Fig. 1-7

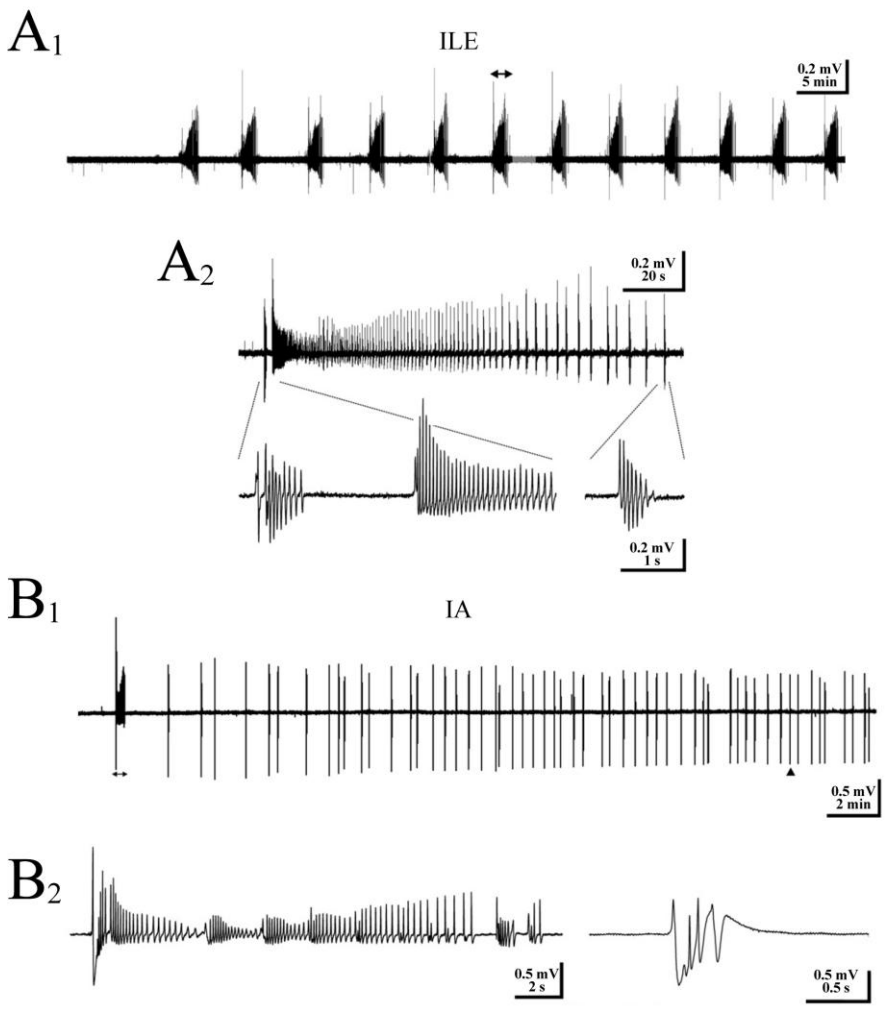

Fig. 1-7: Epileptiform activity induced by elevated K^+ and $GABA_A$/Glycine Receptor blockade. A_1, Field-potential recording in the CA_3 region of an intact hippocampal preparation from a P6 mouse. Application of 8.5 mM K^+ solution induced repetitive ictal-like events (ILE). **A_2**, One ILE, as marked in **A_1**, displayed at higher temporal resolution. Initial burst and one of the bursts in the clonic phase are displayed at higher temporal resolution below the trace. **B_1**, Field-potential recording in the CA_3 region of an intact hippocampal preparation from a P4 mouse. Combined application of 10 μM gabazine and 30 μM strychnine induced one initial ictal-like event (ILE) and subsequent repetitive interictal activity (IA). **B_2**, The initial ILE shown in higher temporal resolution. (left), One interictal burst, as marked (black triangle) in **B_1**, displayed in higher temporal resolution. Figures and legends modified from **A**-**B**: Kilb et al., 2007.

1.11 References

Adelsberger H, Garaschuk O, Konnerth A (2005) Cortical calcium waves in resting newborn mice. Nat Neurosci 8, 988-990

Aden U (2011) Methylxanthines during pregnancy and early postnatal life. Handb Exp Pharmacol 200, 373-389

Adachi T, Robinson DM, Miles GB, Funk GD (2005) Noradrenergic modulation of XII motoneuron inspiratory activity does not involve alpha2-receptor inhibition of the Ih current or presynaptic glutamate release. J Appl Physiol 98, 1297-1308

Agulhon C, Petravicz J, McMullen AB, Sweger EJ, Minton SK, Taves SR, Casper KB, Fiacco TA, and McCarthy KD (2008) What is the role of astrocyte calcium in neurophysiology? Neuron 59, 932-946

Allene C, Cattani A, Ackman JB, Bonifazi P, Aniksztejn L, Ben-Ari Y, Cossart R (2008) Sequential generation of two distinct synapse-driven network patterns in developing neocortex. J Neurosci 28, 12851-63

Allene C, Cossart R (2010) Early NMDA receptor-driven waves of activity in the developing neocortex: physiological or pathological network oscillations? J Physiol 588, 83-91

Alreja M, Aghajanian GK (1991) Pacemaker activity of locus coeruleus neurons: whole-cell recordings in brain slices show dependence on cAMP and protein kinase A. Brain Res 556, 339-343

Alreja M, Aghajanian GK (1993) Opiates suppress a resting sodium-dependent inward current and activate an outward potassium current in locus coeruleus neurons. J Neurosci 13, 3525-3532

Alvarez-Maubecin V, Garcia-Hernandez F, Williams JT, Van Bockstaele EJ (2000) Functional coupling between neurons and glia. J Neurosci 20, 4091-4098

Angelucci ME, Vital MA, Cesario C, Zadusky ZR, Rosalen PL, Da Cunha C (1999) The effect of caffeine in animal models of learning and memory. Eur J Pharmacol 373, 135-140

Arnaud MJ (2011) Pharmacokinetics and metabolism of natural methylxanthines in animal and man. Handbook Exp Pharmacol 200, 33-91

Arvidsson U, Riedl M, Chakrabarti S, Lee J, Nakano A, Dado R, Loh H, Law P, Wessendorf M, Elde R (1995) Distribution and targeting of a μ-opioid receptor (MOR1) in brain and spinal cord. J Neurosci 15, 3328 –3341

Aston-Jones G, Cohen JD (2005) An integrative theory of locus coeruleus-norepinephrine function: adaptive gain and optimal performance. Ann Rev Neurosci 28, 403-450

Avery RB, Johnston D (1996) Multiple channel types contribute to the low-voltage-activated calcium current in hippocampal CA3 pyramidal neurons. J Neurosci 16, 5567-5582

Balestrino M, Aitken PG, Somjen GG (1986) The effects of moderate changes of extracellular K+ and Ca2+ on synaptic and neural function in the CA1 region of the hippocampal slice. Brain Res 377, 229-239

Ballantyne D, Andrzejewski M, Muckenhoff K, Scheid P (2004) Rhythms, synchrony and electrical coupling in the locus coeruleus. Resp Physiol Neurobiol 143, 199-214

Ballanyi K (1999) Isolated tissues: In Vitro Preparations. In: Modern Techniques in Neuroscience Research. Windhorst U, Johansson H (eds). Springer, Heidelberg, pp 307-326

Ballanyi K (2004a) Neuromodulation of the perinatal respiratory network. Curr Neuropharmacol 2, 221-243

Ballanyi K (2004b) Protective role of neuronal KATP channels in brain hypoxia. J Exp Biol 207, 3201-3212

Ballanyi K, Grafe P (1985) An intracellular analysis of gamma-aminobutyric-acid-associated ion movements in rat sympathetic neurones. J Physiol 365, 41-58

Ballanyi K, Lalley PM, Hoch B, Richter DW (1997) cAMP-dependent reversal of opioid- and prostaglandin-mediated depression of the isolated respiratory network in newborn rats. J Physiol 504, 127-134

Ballanyi K, Onimaru H, Homma I (1999) Respiratory network function in the isolated brainstem-spinal cord of newborn rats. Progr Neurobiol 59, 583-634

Ballanyi K, Panaitescu B, and Ruangkittisakul A (2010) Control of breathing by nerve glue. Sci Signal 3, pe41

Ballanyi K, Ruangkittiskul (2009) Structure-function analysis of rhythmogenic inspiratory pre-Botzinger complex networks in "calibrated" newborn rat brainstem slices. Respir Physiol Neurobiol 168, 158-178

Barry RJ, Rushby JA, Wallace MJ, Clarke AR, Jonstone SJ, Zlojutro I (2005) Caffeine effects on resting-state arousal. Clin Neurophysiol 116, 2693-2700

Bausch SB, Chavkin C (1995) Colocalization of mu and delta opioid receptors with GABA, parvalbumin, and a G-protein-coupled inwardly rectifying potassium channel (GIRK1) in the rodent brain. Analgesia 1, 282-285

Ben-Ari Y (2001) Developing networks play a similar melody. TRENDS Neurosci 24, 353-360

Ben-Ari Y, Gaiarsa JL, Tyzio R, Khazipov R (2007) GABA: a pioneer transmitter that excites immature neurons and generates primitive oscillations. Physiol Rev 87, 1215-1284

Ben-Ari Y, Cherubini E, Corradetti R, Caiarsa JL (1989) Giant synaptic potentials in immature rat CA3 hippocampal neurones. J Physiol 416, 303-325

Bennett MV, Zukin RS (2004) Electrical coupling and neuronal synchronization in the mammalian brain. Neuron 41, 495-511

Bender, R.A., Baram, T.Z. (2008) HCN channels in developing neuronal network. Prog Neurobiol 86, 129-140.

Berridge CW, Waterhouse BD (2003) The locus coeruleus-noradrenergic system: modulation of behavioral state and state-dependent cognitive processes. Brain Res Rev 42, 33-84

Berthou F, Guillois B, Riche C, Dreano Y, Jacqz-Aigrain E, Beaune PH (1992) Interspecies variations in caffeine metabolism related to cytochrome P4501A enzymes. Xenobiotica 22, 671-680

Black AM, Pandya S, Clark D, Armstrong EA, Yager JY (2008) Effect of caffeine and morphine on the developing pre-mature brain. Brain Res 1219, 136-142

Blanton MG, Lo Turco JJ, Kriegstein AR (1989) Whole cell recording from neurons in slices of reptilian and mammalian cerebral cortex. J Neurosci Methods 30, 203-210

Bliss TV, Collingridge GL (1993) A synaptic model of memory: long-term potentiation in the hippocampus. Nature 361, 31-39

Bloom FE (1983) The endorphins: a growing family of pharmacologically pertinent peptides. Ann Rev Pharmacol Toxicol 23, 151-170

Bonifazi P, Goldin M, Picardo MA, Jorquera I, Cattani A, Bianconi G, Represa A, Ben-Ari Y, and Cossart R (2009) GABAergic hub neurons orchestrate synchrony in developing hippocampal networks. Science 326, 1419-1424

Boison D (2011) Methylxanthines, seizures, and excitotoxicity. Handbook Exp Pharmacol 200, 251-266

Bolea S, Avignone E, Berretta N, Sanchez-Andres JV, Cherubini E (1999) Glutamate controls the induction of GABA-mediated giant depolarizing potentials through AMPA receptors in neonatal rat hippocampal slices. J Neurophysiol 81, 2095-2102

Bouvier J, Thoby-Brisson M, Renier N, Dubreuil V, Ericson J, Champagnat J, Pierani A, Chédotal A, Fortin G (2010) Hindbrain interneurons and axon guidance signaling critical for breathing. Nat Neurosci 13, 1066-1074

Burnet H, Bevengut M, Chakri F, Bou-Flores C, Coulon P, Gaytan S, Pasaro R, Hilaire G (2001) Altered respiratory activity and respiratory regulations in adult monoamine oxidase A-deficient mice. J Neurosci 21, 5212-5221

Buzsaki G (1986) Hippocampal sharp waves: their origin and significance. Brain Res 398, 242-252

Canepari M, Mammano F, Kachalsky SG, Rahamimoff R, Cherubini E (2000) GABA- and glutamate-mediated network activity in the hippocampus of neonatal and juvenile rats revealed by fast calcium imaging. Cell Calcium 27, 25-33

Cashman JN, Dolin SJ (2004) Respiratory and haemodynamic effects of acute postoperative pain management: evidence from published data. Br J Aneaesth 93, 212-223

Castilla-Guerra L, del Carmen Fernandez-Moreno M, Lopez-Chozas JM, Fernandez-Bolanos R (2006) electrolytes disturbances and seizures. Epilepsia 47, 1990-1998

Champagnat J, Morin-Surun MP, Bouvier J, Thoby-Brisson M, Fortin G (2011) Prenatal development of central rhythm generation. Respir Physiol Neurobiol 178, 146-155

Cherubini E, Ben-Ari Y, Ito S, Kmjevic K (1991) Persistent pulsatile release of glutamate induced by N-methyl-D-aspartate in neonatal rat hippocampal neurons. J Physiol 436, 531-547

Clarac F, Pearlstein E, Pflieger JF, Vinay L (2004) The in vitro neonatal rat spinal cord preparation: a new insight into mammalian locomotor mechanisms. J Comp Physiol A Neuroethol Sens Neural Behav Physiol 190, 343-357

Cohen GA, Doze VA, Madison DV (1992) Opioid inhibition of GABA release from presynaptic terminals of rat hippocampal interneurons. Neuron 9, 325-335

Comer AM, Perry CM, Figgitt DP (2001) Caffeine citrate: a review of its use in apnoea of prematurity. Paediatr Drugs 3, 61-79

Conner-Kerr TA, Simmons DR, Peterson GM, Terrian DM (1993) Evidence for the corelease of dynorphin and glutamate from rat hippocampal mossy fiber terminals. J Neurochemistry 61, 627–636

Connor M, Christie MD (1999) Opioid receptor signaling mechanisms. Clin Exp Pharmacol Physiol 26, 493-499

Cossart R, Ikegaya Y, Yuste R (2005) Calcium imaging of cortical networks dynamics. Cell Calcium 37, 451-457

Christie MJ (1991) Mechanisms of opioid action son neurons of the locus coeruleus. Progr Brain Res 88, 197-205

Christie, M.J., Jelinek, H.F. (1993) Dye-coupling among neurons of the rat locus coeruleus during postnatal development. Neuroscience. 56, 129-137.

Christie MJ, Williams JT, North RA (1989) Electrical coupling synchronizes subthreshold activity in locus coeruleus neurons in vitro from neonatal rats. J Neurosci 9, 3584-3589

Dahan A, Aarts L, Smith TW (2010) Incidence, reversal, and prevention of opioid-induced respiratory depression. Anesthesiology 112, 226-238

Delanty N, Vaughan CJ, French JA (1998) Medical causes of seizures. Lancet 352, 382-390

De Oliveira RB, Howlett MC, Gravina FS, Imtiaz MS, Callister RJ, Van Helden DF (2011) Developmental changes in pacemaker currents in mouse locus coeruleus neurons. Brain research 1425, 27-36

Deschenes M, Feltz P, Lamour Y (1976) A model for an estimate in vivo of the ionic basis of presynaptic inhibition: an intracellular analysis of the GABA-induced depolarization in rat dorsal root ganglia. Brain Res 118, 486-493

Desfrere L, Olivier P, Schwendimann L, Verney C, Gressens P (2007) Transient inhibition of astrocytogensis is developing mouse brain following postnatal caffeine exposure. Ped Res 62, 604-609

Drake CT, Milner TA (1999) Mu opioid receptors are in somatodendritic and axonal compartments of GABAergic neurons in rat hippocampal formation. Brain Res 849, 203-215

Drake CT, Milner TA (2002) Mu opioid receptors are in discrete hippocampal interneuron subpopulations. Hippocampus 12, 119-136

Dreyfus CF, Markey KA, Goldstein M, Black IB (1983) Development of catecholaminergic phenotypic characters in the mouse locus coeruleus in vivo and in culture. Dev Biol 97, 48-58

Dobbins EG, Feldman JL (1994) Brainstem network controlling descending drive to phrenic motoneurons in rat. J Comp Neurol 347, 64-68

Du W, Warrier I, Tutaq Lehr V, Salari V, Ostrea E, Aranda JV (2006) Changing patterns of drug utilization in a neonatal intensive care population. Am J Perinatol 23, 279-285

Dunn DW, Parekh HU (1991) Theophylline and status epilepticus in children. Neuropediatrics 22, 24-26

Dupret D, O'Neill J, Pleydell-Bouverie B, Csicsvari J (2010) The reorganization and reactivation of hippocampal maps predict spatial memory performance. Nat. Neurosci 13, 995-U122

Durrmeyer X, Vutskits L, Anand KJ, Rimensberger PC (2010) Use of analgesic and sedative drugs in the NICU: integrating clinical trials and laboratory data. Pediatr Res 67, 117-127

Dzhala V, Desfreres L, Melyan Z, Ben-Ari Y, Khazipov R (1999) Epileptogenic action of caffeine during anoxia in the neonatal rat hippocampus. Ann Neurol 46, 95-102

Ego-Stengel V, Wilson MA (2010) Disruption of ripple-associated hippocampal activity during rest impairs spatial learning in the rat. Hippocampus 20, 1-10

El-Bitar MK, Boustany RM (2009) Common causes of uncommon seizures. Ped Neurol 41, 83-87

Errchidi S, Monteau R, Hilaire G (1991) Noradrenergic modulation of the medullary respiratory rhythm generator in the newborn rat: an in vitro study. J Physiol 443, 477-498

Feldman JL, Del Negro CA (2006) Looking for inspiration: new perspectives on respiratory rhythm. Nat Rev Neurosci 7, 232-242

Feldman JL, Geimer S, Marshall WF (2007) The mother centriole plays an instructive role in defining cell geometry. PLoS Biol 5, e149

Francis SH, Sekhar KR, Ke H, Corbin JD (2011) Inhibition of cyclic nucleotide phosphodiesterases by methylxanthines and related compounds. Handbook Exp Pharmacol 200, 93-133

Fredholm BB, Battig K, Holmen J, Nehlig A, Zvartau EE (1999) Actions of caffeine in the brain with special reference to factors that contribute to its widespread use. Pharmacol Rev 51, 83-133

Froemke RC, Kumar VS, Czkwianianc P, Yuste R (2002) Analysis of multineuronal activation patterns from calcium-imaging experiments in brain slices. Trends Cardiovasc Med 12, 247-252

Fuxe K, Dahlstrom AB, Jonsson G, Marcellino D, Guescini M, Dam M, Manger P, Agnati L (2010) The discovery of central monoamine neurons gave volume transmission to the wired brain. Progr Neurobiol 90, 82-100

Garaschuk O, Hanse E, Konnerth A (1998) Developmental profile and synaptic origin of early network oscillations in the CA1 region of rat neonatal hippocampus. J Physiol Lond 507, 219-236

Garaschuk O, Linn J, Eilers J, Konnerth A (2000) Large-scale oscillatory calcium waves in the immature cortex. Nature 3, 452-459

Gargaglioni LH, Hartzler LK, Putnam RW (2010) The locus coeruleus and central chemosensitivity. Resp Physiol Neurobiol 173, 264-273

Garrett BE, Griffiths RR (1997) The role of dopamine in the behavioral effects of caffeine in animals and humans. Pharmacol Biochem Behaviors 57, 533-541

Gibson IM, McIlwain H (1965) Continuous recordings of changes in membrane potential in mammalian cerebral tissues in vitro: recovery after depolarization by added substances. J Physiol 176, 261-283

Goodman RR, Snyders SH, Kuhar MJ, Young WS III (1980) Differentiation of delta and mu opiate receptor localization by light microscopic autoradiography. Proe Nutl Acad Sci USA. 77, 6239-6243

Gourine AV, Kasymov V, Marina N, Tang F, Figueiredo MF, Lane S, Teschemacher AG, Spyer KM, Deisseroth K, Kasparov S (2010) Astrocytes control breathing through pH-dependent release of ATP. Science 329, 571-575

Guyenet PG (1991) Central noradrenergic neurons: the autonomic connection. Progr Brain Res 88, 365-380

Guyenet PG, Koshiya N, Huangfu D, Verberne AJ, Riley TA (1993) Central respiratory control of A5 and A6 pontine noradrenergic neurons. Am J Physiol 264, R1035-R1044

Haddad GG, Jiang C (1993) O_2 deprivation in the central nervous system: on mechanisms of neuronal response, differential sensitivity and injury. Prog Neurobiol 40, 277-318

Halassa MM, Haydon PG (2010) Integrated brain circuits: astrocytic networks modulate neuronal activity and behavior. Annu Rev Physiol 72, 335-355

Hein L (2006) Adrenoceptors and signal transduction in neurons. Cell Tiss Res 326, 541-551

Heinemann U, Stabel J, Rausche G (1990) Activity-dependent ionic changes and neuronal plasticity in rat hippocampus. Progr Brain Res 83, 197-214

Henderson-Smart DJ, Steer PA (2010) Caffeine versus theophylline for apnea in preterm infants. Cochrane Database Syst Rev, CD000273

Hess P, Tsien RW (1984) Mechanism of ion permeation through calcium channels. Nature 309, 453-456

Hilaire G (2006) Endogenous noradrenaline affects the maturation and function of the respiratory network: possible implication for SIDS. Auton Neurosci 126, 320-331

Hilaire G, Viemari JC, Coulon P, Simonneau M, Bevengut M (2004) Modulation of the respiratory rhythm-generator by the pontine noradrenergic A5 and A6 groups in rodents. Resp. Physiol Neurobiol 143, 187-197

Hille B (2001) Ion channels of excitable membranes. Sunderland, MA: Sinauer Associates.

Ho SM, Waite PME (1999) Spontaneous activity in the perinatal trigeminal nucleus of the rat. NeuroReport 10, 659–664

Hobson JA, McCarley RW, Wyzinski PW (1975) Sleep cycle oscillation: reciprocal discharge by two brainstem neuronal groups. Science 189, 55-58

Hoecker C, Nelle M, Poeschl J, Beedgen B, Linderkamp O (2002) Caffeine impairs cerebral and intestinal blood flow velocity in preterm infants. Pediatrics 109, 784-787

Holmes GL, Ben-Ari Y, (1998) Seizures in the developing brain: perhaps not so benign after all. Neuron 21, 1231-1234

Ishimatsu M, Williams JT (1996) Synchronous activity in locus coeruleus results from dendritic interactions in pericoerulear regions. J Neurosci 16, 5196-5204

Jahnsen H (1986) Responses of neurons in isolated preparations of the mammalian central nervous system. Prog Neurobiol 2, 351-372

Jefferys JG (1995) Nonsynaptic modulation of neuronal activity in the brain: electric currents and extracellular ions. Physiol Rev 75, 689-723

Johansson B, Georgiev V, Kuosmanen T, Fredholm BB (1996) Long-term treatment with some methylxanthines decreases susceptibility to bicuculline- and pentylenetetrazol-induced seizures in mice. Relationship to c-fos expression and receptor binding. Eur J Neurosci 8, 2447-2458

Jones IL, Livi P, Lewandowska MK, Fiscella M, Roscic B, Hierlemann A (2011) The potential of microelectrode arrays and microelectronics for biomedical research and diagnostics. Anal Bioanal Chem 399, 2313-2329

Kafitz KW, Meier SD, Stephan J, Rose CR (2008) Developmental profile and properties of sulforhodamine 101-Labeled glial cells in acute brain slices of rat hippocampus. J Neurosci Methods 169, 84-92

Kaila K (1994) Ionic basis of GABAA receptor channel function in the nervous system. Prog Neurobiol 42, 489–537

Kaila K, Voipio J, Paalasmaa P, Pasternack M, Deisz RA (1993) The role of bicarbonate in GABAA receptor-mediated IPSPs of rat neocortical neurones. J Physiol Lond 464, 273–289

Karlsson KA, Blumberg MS (2003) Hippocampal theta in the newborn rat is revealed under conditions that promote REM sleep. J Neurosci 23, 1114-1118

Kang SH, Lee YA, Won SJ, Rhee KH, Gwag BJ (2002) Caffine-induced neuronal death in neonatal rat brain and cortical cell cultures. Neruoreport 13, 1945-1950

Kantor CM, Panaitescu B, Kuribayashi J, Ruangkittisakul A, Jovanovic I, Leung V, Lee TF, MacTavish D, Jhamandas JH, Cheung PY, Ballanyi K (2012) Spontaneous neural network oscillations in hippocampus, cortex, and locus coeruleus of newborn rat and piglet brain slices. In: Isolated CNS circuits. (Ballanyi K, ed.) Humana-Springer (in press)

Keifer J, Vyas D, Houk JC (1992) Sulforhodamine labeling of neural circuits engaged in motor pattern generation in the in vitro turtle brainstem-cerebellum. J Neurosci 12, 3187-3199

Kennedy JS, Leduc BW, Scavone JM, Harmatz JS, Shader RI, Greenblatt DJ (1987) Pharmacokinetics of intravenous caffeine: comparison of high-performance liquid chromatographic and gas chromatographic methods. J Chromatogr 422, 274-280

Kettenmann H, Blankenfeld GV, Trotter J (1991) Physiological properties of oligodendrocytes during development. Ann NY Acad Sci 633, 64-77

Kettunen P (2012) Calcium imaging in the zebrafish. Adv Exp Med Biol 740, 1039-1071

Khalilov I, Esclapez M, Medina I, Aggoun D, Lamsa K, Leinekugel X, Khazipov R, Ben-Ari Y (1997) A novel in vitro preparation: the intact hippocampal formation. Neuron 19, 743-749

Khazipov R, Escalpez M, Caillard O, Bernard C, Khalilov I, Tyzio R, Hirsch J, Dzhala V, Berger B, Ben-Ari Y (2001) Early development of neuronal activity in the primate hippocampus in utero. J Neurosci 21(24), 9770-9781

Khazipov R, Khalilov I, Tyzio R, Morozova E, Ben-Ari Y, Holmes GL (2004) Developmental changes in GABAergic actions and seizure susceptibility in the rat hippocampus. Eur J Neurosci 19, 590-600

Khazipov R, Leinekugel X, Khalilov I, Gaiarsa JL, Ben-Ari Y (1997) Synchronization of GABAergic interneuronal network in CA3 subfield of neonatal rat hippocampal slices. J Physiol Lond 498, 763-772

Köhr G, Heinemann U (1989) Effects of NMDA antagonists on pictrotoxin-induced, low Mg2+-induced and low Ca2+-induced epileptogenesis and on evoked changes in extracellular Na+ and Ca2+ concentrations in rat hippocampal slices. Epilepsy Res 4, 187-200

Konnerth A (1990) Patch-clamping in slices of mammalian CNS. Trends Neurosci 13, 321-323

Konnerth A, Heinemann U, Yaari Y (1986) Nonsynaptic epileptogenesis in the mammalian hippocampus in vitro. I. Development of seizurelike activity in low extracellular calcium. J Neurophysiol 56, 409-423

Korematsu S, Miyahara H, Nagakura T, Suenobu S, Izumi T (2008) Theophylline-associated seizures and their clinical characterizations. Pediatr Int 50, 95-98

Kouvaras E, Asprodini EK, Asouchidou I,Vasilaki A, Kilindris T, Michaloudis D, Koukoutianou I, Papatheodoropoulos C, Kostopoulos G(2008) Fentanyl treatment reduces GABAergic inhibition in the CA1 area of the hippocampus 24 h after acute exposure to the drug. Neuropharmacology 55, 1172-1182

Kudo N, Nishimaru H, Nakayama K (2004) Developmental changes in rhythmic spinal neuronal activity in the rat fetus. Prog Brain Res 143, 49-55

Kudrimoti HS, Barnes CA, McNaughton BL (1999) Reactivation of hippocampal cell assemblies: effects of behavioral state, experience, and EEG dynamics. J Neurosci 19, 4090-4101

Kulik A, Nishimaru H, Ballanyi K (2000) Role of bicarbonate and chloride in GABA- and glycine-induced depolarization and $[Ca^{2+}]_i$ rise in fetal rat motoneurons in situ. J Neurosci 20, 7905-7913

Lauder JM, Bloom FE (1974) Ontogeny of monoamine neurons in the locus coeruleus, raphe nuclei and substantia nigra of the rat. I. Cell differentiation. J Comp Neurol 155, 469-481

Law PY, Wong YH, Loh HH (2000) Molecular mechanisms and regulation of opioid receptor signaling. Ann Rev Pharmacol Toxicol 40, 389-430

Leinekugel X, Khazipov R, Cannon R, Hirase H, Ben-Ari Y, Buzsaki G (2002) Correlated bursts of activity in the neonatal hippocampus in vivo. Science 296, 2049-2052

Leinekugel X, Medina I, Khalilov I, Ben-Ari Y, Khazipov R (1997) Ca^{2+} oscillations mediated by the synergistic excitatory actions of GABA(A) and NMDA receptors in the neonatal hippocampus. Neuron 18, 243-255

Leslie FM, Tso S, Hurlbut E (1982) Differential appearance of opiate receptors subtypes in neonatal rat brain. Life Sciences 31, 1393-1396

Leusen I (1972) Regulation of cerebrospinal fluid composition with reference to breathing. Physiol Rev 52, 1-56

Lewis ME, Pert A, Pert CB, Herkenham M (1983) Opiate receptor localization in rat cerebral cortex. J Comp Neurol 216, 339-58

Li CL, McIlwain H (1956) Maintenance of resting membrane potentials in slices of mammalian cerebral cortex and other tissues in vitro. J Physiol 139, 178-190

Li H, Tornberg J, Kaila K, Airaksinen MS, Rivera C (2002) Patterns of cation-chloride cotransporter expression during embryonic rodent CNS development. Eur J Neurosci 16, 2358–2370

Lieberman HR, Wurtman RJ, Emde GG, Roberta C, Coviella IL (1987) The effects of low doses of caffeine on human performance and mood. Psychopharmacol 92, 308-312

LoTurco JJ, Owens DF, Heath MJS, Davis MBE, Kriegstein AR (1995) GABA and glutamate depolarize cortical progenitor cells and inhibit DNA synthesis. Neuron 15, 1287-1298

Lowry JA, Jarret RV, Wasserman G, Pettett G, Kauffman RE (2001) Theophylline toxicokinetics in premature newborns. Arch Pediatr Adolesc Med 155, 934-939

Lüthi A, McCormick DA (1998) H-current: properties of a neuronal and network pacemaker. Neuron 21, 9-12

Lutz PL (1992) Mechanisms for anoxic survival in the vertebrate brain. Annu Rev Physio 54, 601-618

Lynn AM, Slattery JT (1987) Morphine pharmacokinetics in early infancy. Anesthesiol 66, 136-139

Madison DV, Nicoll RA (1988) Enkephalin hyperpolarizes interneurones in the rat hippocampus. J Physiol 398, 123-130

Maeda T (2000) The locus coeruleus: history. J Chem Neuroanat 18, 57-64

Maffei L, Galli-Resta L (1990) Correlation in the discharges of neighboring rat retinal ganglion cells during prenatal life. Proc Natl Acad Sci USA 87, 2861–2864

Magkos F, Kavouras SA (2005) Caffeine use in sports, pharmacokinetics in man, and cellular mechanisms of action. Crit. Rev Food Sci Nutr 45, 535-562

Maier N, Nimmrich V, Draguhn A (2003) Cellular and network mechanisms underlying spontaneous sharp wave-ripple complexes in mouse hippocampal slices. J Physiol Lond 550, 873–887

Mandal R, Anderson CW (2009) Anatomical organization of brainstem circuits mediating feeding motor programs in the marine toad, Bufo marinus. Brain Res 1298, 99-110

Mansour A, Fox CA, Burke S, Akil H,Watson SJ (1995) Immunohistochemical localization of the cloned mu-opioid receptor in the rat CNS. J Chem Neuroanat 8, 283-305

Mansour A, Khachaturian H, Lewis ME, Akil H, Watson SJ (1987) Autoradiographic differentiation of mu, delta and kappa opioid receptors in the rat forebrain and midbrain. J Neurosci 7, 2445-2464

Manzke T, Guenther U, Ponimaskin EG, Haller M, Dutschmann M, Schwarzacher S, Richter DW (2003) 5-$HT_{4(a)}$ receptors avert opioid-induced breathing depression without loss of analgesia. Science 301, 226-229

Mao BQ, Hamzei-Sichani F, Aronov D, Froemke RC, Yuste R (2001) Dynamics of spontaneous activity in neocortical slices. Neuron 35, 883-898

Martin RJ, Abu-Shaweesh JM (2005) Control of breathing and neonatal apnea. Biol Neonate 87, 288-295

Marty S, Wehrle R, Sotelo C (2000) Neuronal activity and brain-derived neurotrophic factor regulate the density of inhibitory synapses in organotypic slice cultures of postnatal hippocampus. J Neurosci 20, 8087–8095

Mason ST, Fibiger HC (1979) Regional topography within noradrenergic locus coeruleus as revealed by retrograde transport of horseradish peroxidase. J Comp Neurol 187, 703-724

Maubecin VA, Williams JT (1999) Developmental changes mediated by purinergic signaling in the pathophysiology of CNS disorders. Semin. Cell Dev Biol 22, 252-259

McCabe AK, Easton CR, Lischalk JW, Moody WJ (2007) Roles of glutamate and GABA receptors in setting the developmental timing of spontaneous synchronized activity in the developing mouse cortex. Dev Neurobiol 67, 1574-1588

McIlwain H, Buchel L, Cheshire JD (1951) The inorganic phosphate and phosphocreatine of Brain especially during metabolism in vitro. Biochem J 48, 12-20

Meilandt WJ, Barea-Rodriguez E, Harvey SAK, Martinez JL Jr (2004) Role of hippocampal CA3 μ-opioid receptors in spatial learning and memory. J Neurosci 24, 2953-2962

Menendez de la Prida L, Bolea S, Sanchez-Andres JV (1996) Analytical characterization of spontaneous activity evolution during hippocampal development in the rabbit. Neurosci Lett 218, 185-187

Menendez de la Prida L, Bolea S, Sanchez-Andres JV (1998) Origin of the synchronized network activity in the rabbit developing hippocampus. Eur J Neurosci 10, 899–906

Menendez de la Prida L, Sanchez-Andres JV (2000) Heterogeneous populations of cells mediate spontaneous synchronous bursting in the developing hippocampus through a frequency-dependent mechanism. Neuroscience 97, 227–241

McPherson PS, Kim YK, Valdivia H, Knudson CM, Takekura H, Franzini-Armstrong C, Corondado R, Campbell KP (1991) The brain ryanodine receptor: a caffeine-sensitive calcium release channel. Neuron 7, 17-25

Milh M, Kaminska A, Huon C, Lapillonne A, Ben-Ari Y, Khazipov R (2007) Rapid cortical oscillations and early motor activity in premature human neonate. Cereb Cortex 17, 1582-1594

Millar D, Schmidt B (2004) Controversies surrounding xanthine therapy. Semin. Neonatal. 9, 239-244

Montadon G, Kinkead R, Bairam A (2008) Adenosinergic modulation of respiratory activity: developmental plasticity induced by perinatal caffeine administration. Respir Physiol Neurobiol 164, 87-95

Moore SD, Madamba SG, Schweitzer P, Siggins GR (1994) Voltage dependent effects of opioid peptides on hippocampal CA3 pyramidal neurons in vitro. J Neurosci 14, 809-820

Moriceau S, Roth TL, Sullivan RM (2010) Rodent model of infant attachment learning and stress. Dev Psychobiol 52, 651-660

Murai Y, Akaike T (2005) Orexins cause depolarization via nonselective cationic and K^+ channels in isolated locus coeruleus neurons. Neurosci Res 51, 55-65

Murrin LC, Sanders JD, Bylund DB (2007) Comparison of the maturation of the adrenergic and serotonergic neurotransmitter systems in the brain: implications for differential drug effects on juveniles and adults. Biochem Pharmacol 73, 1225-1236

Nakada T, Kwee IL, Lerner AM, Remler MP (1983) Theophylline-induced seizures: clinical and pathophysiologic aspects. Western J Med 138, 371-374

Nakamura S, Kimura F, Sakaguchi T (1987) Postnatal development of electrical activity in the locus coeruleus. J Neurophysiol 58, 510-524

Naqui SZ, Harris BS, Thomaidou D, Parnavelas JG (1999) The noradrenergic system influences the fate of Cajal-Retzius cells in the developing cerebral cortex. Dev Brain Res 113, 75-82

Nehlig A, Daval JL, Debry G (1992) Caffeine and the central nervous system: mechanisms of action, biochemical, metabolic and psychostimulant effects. Brain Res Rev 17, 139-170

Nestler EJ, Alreja M, Aghajanian GK (1999) Molecular control of locus coeruleus neurotransmission. Biol Psychiatry 46, 1131-1139

Nguyen PV (2006) Comparative plasticity of brain synapses in inbred mouse strains. J Exp Biol 209, 2293-2303

Nikolenko V, Poskanzer KE, Yuste R (2007) Two-photon photostimulation and imaging of neural circuits. Nat Methods 4, 943-950

Nimmerjahn A, Kirchhoff F, Kerr JN, Helmchen F (2004) Sulforhodamine 101 as a specific marker of astroglia in the neocortex in vivo. Nat Methods 1, 31-37

O'Donovan MJ (1999) The origin of spontaneous activity in developing networks of the vertebrate nervous system. Curr Opin Neurobiol 9, 94-104

O'Donovan MJ, Bonnot A, Mentis G Z, Arai Y, Chub N, Shneider NA, and Wenner P (2008) Imaging the spatiotemporal organization of neural activity in the developing spinal cord. Dev Neurobiol 68, 788-803

Obata K, Oide M, Tanaka H (1978) Excitatory and inhibitory actions of GABA and glycine on embryonic chick spinal neurons in culture. Brain Res 144, 179-184

O'Keefe J, Nadel L (1978) The hippocampus as a cognitive map. Oxford Uni Press, Oxford

Olpe HR, Steinmann M (1991) Responses of locus coeruleus neurons to neuropeptides. Progr Brain Res 88, 241-248

Owens DF, Kriegstein AR (2002) Is there more to GABA than synaptic inhibition? Nat Rev Neurosci 3, 715-727

Oyamada Y, Ballantyne D, Muckenhogg K, Scheid P (1998) Respiration-modulated membrane potential and chemosensitivity of locus coeruleus neurones in the in vitro brainstem-spinal cord of the neonatal rat. J Physiol 513, 381-398

Oyamada Y, Andrzejewski M, Muckenhoff K, Scheid P, Ballantyne D (1999) Locus coeruleus neurones in vitro: pH-sensitive oscillations of membrane potential in an electrically coupled network. Resp Physiol Neurobiol 118, 131-147

Palva JM, Lamsa K, Lauri SE, Rauvala H, Kaila K, Taira T (2000) Fast network oscillations in the newborn rat hippocampus in vitro. J Neurosci 20, 1170-1178

Panaitescu B (2010) Antagonistic modulation of spontaneous neural network activities in isolated newborn rat brainstem preparations by opioids and methylxanthines. Doctoral Thesis, University of Alberta, Edmonton. p???

Paspalas CD, Papadopoulos GC (1996) Ultrastructural relationships between noradrenergic nerve fibers and non-neuronal elements in the rat cerebral cortex. Glia 17, 133-146

Pattinson KT (2008) Opioids and the control of respiration. Br J Anaesth 100, 747-758

Payne JA, Rivera C, Voipio J, Kaila K (2003) Cation-chloride co-transporters in neuronal communication, development and trauma. Trends Neurosci 26, 199-206

Pickel V (1982) Central noradrenergic neurons: Identification, distribution, and synaptic interactions with axons containing morphine-like peptides. J Clin Psychiatry 43, 13-16

Plotkin MD, Snyder EY, Hebert SC, Delpire E (1997) Expression of the Na-K-2Cl cotransporter is developmentally regulated in postnatal rat brains: a possible mechanism underlying GABA's excitatory role in immature brain. J Neurobiol 33(6), 781-795

Poskanzer KE, Yuste R (2011) Astrocytic regulation of cortical UP states. Proc Natl Acad Sci USA 108, 18453-8

Przewlocki R, Parsons KL, Sweeney DD, Trotter C, Netzeband JG, Siggins GR, Gruol DL (1999) Opioid enhancement of calcium oscillations and burst events involving NMDA receptors and L-type calcium channels in cultured hippocampal neurons. J Neurosci 19, 9705-9715

Rausche G, Ingelmund P, Heinemann U (1990) Effects of changes in extracellular potassium, magnesium, and calcium concentration on synaptic transmission in are CA1 and the dentate gyrus of rat hippocampal slices. Pflugers Arch 415, 588-593

Regehr WG, Connor JA, Tank DW (1989) Optical imaging of calcium accumulation in hippocampal pyramidal cells during synaptic activation. Nature 341, 533-536

Richter DW, Lalley PM, Pierrefiche O, Haji A, Bischoff AM, Wilken B, Hanefeld F (1997) Intracellular signal pathways controlling respiratory neurons. Resp Physiol Neurobiol 110, 113-123

Riggs JE (2002) Neurologic manifestations of electrolyte disturbances. Neurol Clin 20, 227-239

Rivera C, Voipio J, Payne JA, Ruusuvuori E, Lahtinen H, Lamsa K, Pirvola U, Saarma M, Kaila K (1999) The K^+/Cl^- co-transporter KCC2 renders GABA hyperpolarizing during neuronal maturation. Nature 397, 251-255

Rheims S, Represa A, Ben-Ari Y, Zilberter Y (2008) Layer-specific generation and propagation of seizures in slices of developing neocortex: role of excitatory GABAergic synapses. J Neurophys 100, 620-628

Rivera C, Voipio J, Payne JA, Ruusuvuori E, Lahtinen H, Lamsa K, Pirvola U, Saarma M, Kaila K (1999) The K^+/Cl^- co-transporter KCC2 renders GABA hyperpolarizing during neuronal maturation. Nature 397, 251–255

Ross WN, Werman R (1987) Mapping calcium transients in the dendrites of Purkinje cells from the guinea-pig cerebellum in vitro. J Physiol 389, 319-336

Ruangkittisakul A, Ballanyi K (2006) Reversal by phosphodiesterase-4 blockers of in vitro apnea in the isolated brainstem-spinal cord preparation from newborn rats. Neurosci Lett 401, 194-198

Ruangkittisakul A, Ballanyi K (2010) Methylxanthine reversal of opioid-evoked inspiratory depression via phosphodiesterase-4 blockade. Resp Physiol Neurobiol 172, 94-105

Ruangkittisakul A, Okada Y, Oku Y, Koshiya N, Ballanyi K (2009) Fluorescence imaging of active respiratory networks. Respir Physiol Neurobiol 168, 26-38

Ruangkittisakul A, Schwarzacher SW, Ma Y, Poon B, Secchia L, Funk GD, Ballanyi K (2006) High sensitivity to neuromodulators-activated signaling pathways at physiological $[K^+]$ of confocal-imaged respiratory centre neurons in online-calibrated newborn rat brainstem slices. J Neurosci 26, 11870-11880

Ruangkittisakul A, Schwarzacher SW, Secchia L, Ma Y, Bobocea N, Poon BY, Funk GD, Ballanyi K (2008) Generation of eupnea and sighs by a spatiochemically organized inspiratory network. J Neurosci 28, 2447-2458

Ruangkittisakul A, Secchia L, Bornes TD, Palathinkal DM, Ballanyi K (2007) Dependence on extracellular Ca^{2+}/K^+ antagonism of inspiratory centre rhythms in slices and en bloc preparations of newborn rat brainstem. J Physiol 584, 489-508

Sah P (1996) Ca(2+)-activated K+ currents in neurones: types, physiological roles and modulations. TINS 19, 150-154

Samuels ER, Szabadi E (2008) Functional neuroanatomy of the noradrenergic locus coeruleus: its roles in the regulation of arousal and autonomic function part II: physiological and pharmacological manipulations and pathological alterations of locus coeruleus activity in humans. Curr Neuropharmacl. 6, 254-285

Sanchez-Vives MV, McCormick DA (2000) Cellular and network mechanisms of rhythmic recurrent activity in neocortex. Nat Neurosci 3, 1027-1034

Santiago TV, Edelman NH (1985) Opioids and breathing. J. Appl Physiol 59, 1675-1685

Schmidt B, Roberts RS, Davis P, Doyle LW, Barrington KJ, Ohlsson A, Solimano A, Tin W (2006) Caffeine therapy for apnea of prematurity. N Engl J Med 354, 2112-2121

Sheroziya MG, von Bohlen und Halbach O, Unsicker K, Egorov AV (2009) Spontaneous bursting activity in the developing entorhinal cortex. J Neurosci 29, 12131-12144

Sipilä S T, Huttu K, Soltesz I, Voipio J, and Kaila K (2005) Depolarizing GABA acts on intrinsically bursting pyramidal neurons to drive giant depolarizing potentials in the immature hippocampus. J Neurosci 25, 5280-5289

Sipilä ST, Huttu K, Voipio J, Kaila K (2006) Intrinsic bursting of immature CA3 pyramidal neurons and consequent giant depolarizing potentials are driven by a persistent Na current and terminated by a slow Ca-activated K current. Eur J Neurosci 23, 2330-2338

Sipilä ST, Kaila K (2007) GABAergic control of CA3-driven network events in the developing hippocampus. Results Probl. Cell Differ 44, 99-121

Siggins GR, Henriksen SJ, Chavkin C, Gruol D (1986) Opioid peptides and epileptogenesis in the limbic system: cellular mechanisms. Adv Neurol 44, 501-512

Smit HJ, Rogers PJ (2000) Effects of low doses of caffeine on cognitive performance, mood and thirst in low and higher caffeine consumers. Psychopharmacol 152, 167-173

Smith JC, Ellenberger HH, Ballanyi K, Richter DW, Feldman JL (1991) Pre-Botzinger complex: a brainstem region that may generate respiratory rhythm in mammals. Science 254, 726-729

Smythies J (2005) Section III. The norepinephrine system. Interntl Rev Neurobiol 64, 173-211

Somjen GG (2002) Ion regulation in the brain: implications for pathophysiology. Neuroscientist 8, 254-267

Somjen GG, Allen BW, Balestrino M, Aitken PG (1987) Pathophysiology of pH and Ca^{2+} in bloodstream and brain. Can J Physiol Pharmacol 65, 1078-85

Spitzer N C (2006) Electrical activity in early neuronal development. Nature. 444, 707-712

Stengaard-Pedersen K (1983) Comparative mapping of opioid receptors and enkephalin immunoreactive nerve terminals in the rat hippocampus. A Radiohistochem and Immuno Study Histochem 79, 311-333

Stosiek C, Garaschuk O, Holthoff K, Konnerth A (2003) In vivo two-photon calcium imaging of neuronal networks. Proc Natl Acad Sci USA 100, 7319-7324

Stumm RK, Zhou C, Schultz S, Holit V (2004) Neuronal types expressing μ- and δ-opioid receptor mRNA in the rat hippocampal formation. J Compar Neurol 469, 107-118

Sugimoto T, Sugimoto M, Uchida I, Mashimoto T, Okada S (2001) Inhibitory effects of theophylline on recombinant $GABA_A$ receptor. Neuroreport 12, 489-493

Suzue T (1984) Respiratory rhythm generation in the in vitro brain stem-spinal cord preparation of the neonatal rat. J Physiol 354, 173-183

Takahashi A, Camacho P, Lechleiter JD, Herman B (1999) Measurement of intracellular calcium. Physiol Rev 79, 1089-1125

Tank DW, Sugimori M, Connor JA, Llinás RR (1988) Spatially resolved calcium dynamics of mammalian Purkinje cells in cerebellar slice. Science 242, 773-777

Vanhatalo S, Tallgren P, Andersson S, Sainio K, Voipio J, Kaila K (2002) DC-EEG discloses prominent, very slow activity patterns during sleep in preterm infants. Clin Neurophys 113, 1822-1825

Vasilyev DV, Barish ME (2002) Postnatal development of the hyperpolarization-activated excitatory current Ih in mouse hippocampal pyramidal neurons. J Neurosci 22, 8992-9004

Viemari JC, Bevengut M, Burnet J, Coulon P, Pequignot JM, Tiveron MC, Hilaire G (2004) Phox2a gene, A6 neurons, and noradrenaline are essential for development of normal respiratory rhythm in mice. J Neurosci 24, 928-937

Wang DD, and Bordey A (2008) The astrocyte odyssey. Prog Neurobiol 86, 342-367

Wang DD, Kriegstein AR (2008) GABA regulates expiratory synapse formation in the neocortex via NMDA receptor activation. J Neurosci 28, 5547-5558

Wang DD, Kriegstein AR (2011) Blocking early GABA depolarization with bumetanide results in permanent alterations in cortical circuits and sensorimotor gating deficits. Cereb Cortex 21, 574-587

Waldhoer M, Bartlett SE, Whistler JL (2004) Opioid receptors. Ann Rev Biochem 73, 953-990

Walter-Nicolet E, Annequin D, Biran V, Mitanchez D, Tourniaire B (2010) Pain management in newborns: from prevention to treatment. Paediatr Drugs 12, 353-365

Williams JT, Egan TM, North RA (1982) Enkephalin opens potassium channels on mammalian central neurones. Nature 299, 74-77

Williams JT, Marshall KC (1987) Membrane properties and adrenergic responses in locus coeruleus neurons of young rats. J Neurosci 7, 3687-3694

Williams JT, North RA, Shefner SA, Nishi S, Egan TM (1984) Membrane properties of rat locus coeruleus neurones. Neuroscience 13, 137-156

Williams JT, Christie MJ, Manzoni O (2001) Cellular and synaptic adaptations mediating opioid dependence. Physiol Rev 81, 299-343

Wilson MA, McNaughton BL (1994) Reactivation of hippocampal ensemble memories during sleep. Science 265, 676-679

Wimpey TL, Chavkin C (1991) Opioids activate both an inward rectifier and a novel voltage-gated potassium conductance in the hippocampal formation. Neuron 6, 281-289

Xiong Z, Lu W, MacDonald JF (1997) Extracellular calcium sensed by a novel cation channel in hippocampal neurons. Proc Natl Acad Sci USA 94, 7012-7017

Yamamoto C, McIlwain H (1966) Electrical activities in thin sections from the mammalian brain maintained in chemically-defined media in vitro. J Neurochem 13, 1333-1343

Yang JW, Hanganu-Opatz IL, Sun JJ, Luhmann HJ (2009) Three patterns of oscillatory activity differentially synchronize developing neocortical networks in vivo. J Neurosci 29, 9011-9025

Yoshikawa H (2007) First-line therapy for theophylline-associated seizures. Acta Neurol Scand Suppl. 186, 57-61

Yuste R, Konnerth A, and Masters B (2006) Imaging in neuroscience and development, a laboratory manual. J Biomed Opt 11, 19902

Yuste R, Peinado A, Katz LC (1992) Neuronal domains in developing neocortex. Science 257, 665-669

Zieglgansberger W, French ED, Siggins GR, Bloom FE (1979) Opioid peptides may excite hippocampal pyramidal neurons by inhibiting adjacent inhibitory interneurons. Science 205, 415-417

CHAPTER 2

Methods

This chapter is mostly based on a book article that is in press:

Kantor C[1#], Panaitescu B[1#], Kuribayashi J[1], Ruangkittisakul A[1], Jovanovic I[1], Leung V[1], Lee TF[2], MacTavish D[3], Jhamandas J[3], Cheung PY[2], Ballanyi K[1*] (2012) Spontaneous Neural Network Oscillations in Hippocampus, Cortex and *Locus Coeruleus* of Newborn Rat and Piglet Brain Slices. In: In: Isolated Central Nervous System Circuits (Ed K Ballanyi), Neuromethods Series (Ed W Walz). Springer Science+Business Media, LLC, New York, NY.

The authors are from the following institutions:

[1]Centre for Neuroscience and Department of Physiology; [2]Departments of Pediatrics, Pharmacology & Surgery; [3]Department of Medicine, University of Alberta, Edmonton, AB, Canada T6G 2S2

The authors contributed as follows:

I developed horizontal slices for studying rhythmic bursting in 3 brain areas, did the vast majority of experiments and corresponding analyses on hippocampus and cortex in these slices, and contributed to writing of the manuscript. B. Panaitescu performed a majority of recordings and analyses on *locus coeruleus* oscillations. V. Leung and I. Jovanovic were supervised by me during some experiments for their PHYSL-467 reading and lab course. A. Ruangkittisakul and J. Kuribayashi participated in some analysis and experiments, respectively. T.F. Lee from Dr. P.Y. Cheung's group provided piglet brains. D. MacTavish from Dr. J.H. Jhamandas's group introduced our group to immunohistochemical labeling of slices with GFAP antibody.

Note that the Introduction of this book article is not inserted here because all aspects are mentioned in more detail in the Introduction for this thesis.

2.1 Materials

Some materials used by us for studying ENOs in brain slices are identical with those for analyzing dorsal vagal neurons or respiratory neurons in isolated brainstem models. We refer to them here in abbreviated form because these materials, and rationales for their use, are described in the original papers on these systems and in corresponding chapters of this book [chapters 1-Trapp & Ballanyi and 2-Ruangkittisakul et al.].

2.1.1 Animal Models

ENOs, also called GDPs (Ben-Ari et al., 1989, 2007; Sipilä & Kaila, 2008), are typically analyzed in brain slices from early postnatal rats and mice. Our group has so far only studied ENOs in slices from Sprague-Dawley or Wistar rats of postnatal day (P) 0-12 obtained from Charles River Laboratory Inc. (Wilmington, MA, USA; www.criver.com) and with P1-4 Yorkshire-Landrace piglets weighing 1.4-2.2 kg (Jantzie et al., 2010) obtained from the Swine Research Technology Centre of University of Alberta.

2.1.2 Solutions

In the following, we refer to compositions of solutions for (*i*) superfusing brain slices, (*ii*) filling patch electrodes 'whole-cell' recording (from *locus coeruleus* neurons) and (*iii*) histology.

2.1.2.1 Superfusates

ENOs in hippocampus, cortical regions and *locus coeruleus* **(Fig. 2-1)** are principally stable in superfusate that we also recommend for studying preBötC slices with a rostrocaudal thickness >600 µm [see also chapter 2-Ruangkittisakul et al.]. Because the frequently used term 'artificial cerebrospinal fluid' ('ACSF') is not fully appropriate for reasons outlined in the latter chapter, we prefer to use the terms '(standard) superfusate' or 'standard/control solution'. Standard superfusate has the following ionic composition (in mM): 120 NaCl, 3 KCl, 1 $CaCl_2$, 2 $MgSO_4$, 1.25 NaH_2PO_4, 26 $NaHCO_3$. The pH of this solution is adjusted to 7.4 by on-going gassing with carbogen, which is a mixture of 95% O_2 and 5% carbon dioxide (CO_2). Such 'carbogenation' is, for example, achieved with a gas dispersion tube, also termed 'micro filter candle' (Fisher Scientific, Canada; wwwfisher.ca or Robu, Hattert, Germany; www.robuglas.com). Standard superfusate also contains typically 10 or 20 mM D-glucose ('dextrose') **(§2.2.1**, **2.3.1)**.

For studying ENO-like bursting in *locus coeruleus*, horizontal newborn rat slices can be cut at room temperature in standard superfusate and directly transferred to the recording chamber. The other slice types are cut in ice-cold 'sucrose' solution containing (in mM) 234 sucrose, 4 KCl, 8 $MgSO_4$, 26 $NaCO_3$, 1 NaH_2PO_4, and 10-20 glucose to prevent excitotoxicity and preserve spontaneous neuronal activity later during recording in standard solution (Ballanyi, 1999; Garaschuk et al., 2000) [see also chapters 1-Trapp & Ballanyi and 2-Ruangkittisakul et al.]. Following cutting, slices were directly transferred to the recording chamber in a limited series of experiments.

For the majority of experiments, slices were stored on a nylon net in a 150 ml beaker filled with 'recovery' solution to allow on-going superfusion and subfusion of carbogenated solution and kept at 25-27 ˚C by placing the beaker in a water bath (Isotemp102S, Fisher). Recovery solution is identical to standard solution, except K^+ varies between 3-4 mM and Ca^{2+} between 1-1.2 mM. For investigating Ca^{2+}/K^+ antagonism of ENOs (**§1**), superfusate Ca^{2+} was varied between 0 and 5 mM and K^+ between 3-8 mM (**§2.3**) **(Fig. 2-2)**.

2.1.2.2 Electrode Solutions

The Ballanyi laboratory currently uses two types of patch electrode solutions for whole-cell patch-clamp recording (**§3.2.2**), i.e. (*i*) standard ('low Cl^-') pipette solution containing (in mM) 120 K-gluconate, 1 NaCl, 1 $CaCl_2$, 1 $MgCl_2$, 11 K_4-BAPTA, 0.5 Na_2-ATP and 10 Hepes; pH adjusted to 7.4 with KOH, (*ii*) 'high Cl^-' solution of identical composition except that 120 mM KCl replaces 120 mM K-gluconate. Properties of *locus coeruleus* neurons were studied using low Cl^- patch solution (**§3.2.2**, **4.1.1**). Rationales for particular compositions of patch electrode solutions are given elsewhere (Neher & Sakmann, 2009; Walz, 2009) [see also chapters 1-Trapp & Ballanyi, 2-Ruangkittisakul et al. and 3-Moore et al.].

2.1.2.3 Histological solutions

For histological analysis based on thionin staining of nervous structures such as layers or nuclei of neuron somata **(Fig. 2-1)** (Ruangkittisakul et al., 2006, 2007, 2008) [see also chapter 2-Ruangittisakul et al.], slices are fixed in 4% paraformaldehyde (Sigma) in phosphate buffer,

which is a ~1:2 mixture of 0.1 M NaH_2PO_4 + 0.1 M Na_2HPO_4 in H_2O, resulting pH 7.2. Thionin staining solution consists of 0.1 M Na^+-acetate trihydrate + 0.1 M acetic acid + 1% thionin acetate dissolved in distilled water. For live cell labeling of neurons and glia **(Fig. 2-3)**, slices are incubated for 1-1.5 h in carbogenated standard solution with SR-101 (Sigma) at 165 µM 20-23 ^oC or 1 µM at 34 ^oC, respectively. Immunohistochemical identification of GFAP in astrocytes of horizontal newborn rat brain slices (**1.**) was performed on slices fixed with 4% paraformaldehyde for at least 2 h. Subsequently, phosphate buffer solution is used with either 4% paraformaldehyde or 0.5% Triton X (Sigma) added. As described under (**§2.2.3**), slices are ultimately exposed via incubation to a rabbit GFAP primary antibody and, 1 day later, to an Alexa-488 goat anti-rabbit secondary antibody both from Invitrogen (Carlsbad, CA, USA; www.invitrogen.com) (**§2.2.3**). SR-101 and/or GFAP labeled slices are inspected using the multiphoton/confocal imaging stations (**§2.1.8**).

2.1.3 Devices for Generating Brain Slices

Under anesthesia using isoflurane (Baxter Corp., Deerfield, IL, USA; www.baxter.com) (**§2.2.1**), the brain of newborn rats is dissected with fine forceps (e.g. Dumont #5, straight tip [0.05 x 0.02 mm] or Dumont #5SF [0.025 x 0.005 mm]) and (iris) scissors (e.g. Vannas-style, straight tip angle [length 80 mm, 2.5 mm blade] or Vannas Tübingen [length 85 mm, 5 mm blade]), supplied e.g. by Fine Science Tools Inc. (Vancouver, BC, Canada; www.finescience.com).

For isolating the piglet brain (**§2.2.1.2**), an animal is anesthetized with 2-5% isoflurane (Benson Medical Industries Inc., Markham, ON, Canada; www.bensonmedical.com) through a gas mask.

A catheter (5 Fr Argyle TM, Sherwood Medical Co., St. Louis, MO, USA; www.epa.gov) is placed at the femoral artery for systemic pressure measurement and medication administration. Using a pulse oximeter (Nellcor, Hayward, CA, USA; www.respiratorysolution.covidien.com) and a HP78833B monitor (Hewlett Packard Co., Palo Alto, CA, USA; www.hp.com), O_2 saturation, heart rate and blood pressure are continuously monitored. Following surgical instrumentation, the piglet is allowed to stabilize for 30 min before euthanization using an intra-arterial bolus of 120 mg/kg sodium pentobarbital (Bimeda-MTC, Cambridge, ON, Canada; www.bimeda.com). The skull is opened with an electric saw (e.g. Dremel Mini Mite Cordless Rotary Tool, Racine, WI, USA; www.dremel.com) and then dissected with fine forceps (see above), large scissors (e.g. Student Surgical Scissors [length 14.5 cm, 4.5 cm blade], Fine Science Tools Inc.) or a razor blade (Double Edge Stainless Steel Razor Blade [1.0 mm thickness], Electron Microscopy Sciences, Hatfield, PA, USA; www.emsdiasum.com) and a pair of large forceps/tongs (e.g. Multi-Use Tongs FSE [length 20 cm, 2.5 cm stirrup jaws], Fisher Scientific) for stability.

The entire newborn rat brain or a piglet brain block (**§2.2.1**) is transferred to the vise of a vibratome such as the VT1000S (Leica Biosystems, Nussloch, Germany; www.leica-microsystems.com) or the 5000mz (Campden Instruments Ltd, Loughborough, UK; www.campdeninstruments.com). A less expensive device, such as the 'McIlwain' tissue chopper (Warner Instruments, Hamden, CT, USA; www.warneronline.com), may cause more damage to superficial slice layers, but can be used if recording approaches are restricted to extracellular or 'blind' patch-clamp techniques in thicker slices (**§2.2.2**).

2.1.4 Recording Chamber and Superfusion System

As reviewed in (Ballanyi, 1999; Ballanyi & Ruangkittisakul, 2009a,b) and outlined and exemplified with figures elsewhere in this book [see chapters 1-Trapp & Ballanyi and 2-Ruangkittisakul et al.], a commercial submerged-type acrylic recording chamber with glass bottom, e.g. from Warner Instruments, is used by us for experiments involving visualization of cells using an upright microscope. A custom-made acrylic chamber is used for 'blind' recording experiments, in which basic slice structures and electrode positions are recognizable using a low magnification stereomicroscope (**§2.1.8**). The latter type of chamber requires a cold-light source with flexible glass fiber guides, e.g. from World Precision Instruments (WPI, Sarasota, FL, USA; www.wpiinc.com) or Zeiss (Oberkochen, Germany; www.zeiss.com). The recording chambers are continuously perfused with carbogenated standard solution (**§2.1.2**) that is pre-warmed in a water bath (DC-10, Thermo Haake, Sigma-Aldrich, Canada; www.sigmaaldrich.com) and administered via a peristaltic ('roller') pump such as the Watson-Marlow Alitea (Sin-Can, Calgary, AB, Canada; www.sincaninc.com). Superfusate passes through an acrylic custom-made bubble trap before entering the recording chamber that is kept at 26-28 °C via a temperature control system such as the TC-324B (Harvard Apparatus, Saint-Laurent, QC, Canada; www.sincaninc.com). Superfusate is removed from the recording chamber via a hypodermic needle (gauge 18G1½'') connected to either (another channel of) the peristaltic pump or a vacuum system, e.g. an aquarium pump. Tygon® or stainless steel tubing (e.g. Fisher Scientific, Canada; www.fishersci.ca) should be used for the superfusion system because they are impermeable to O_2 and CO_2 thus preventing the loss of these or other gases such as nitrogen for eliciting hypoxia during transport of fluid to the recording chamber. Optimal flow rates are at least 5 ml/min for recording chambers with a volume of ~1 ml and should be adapted

correspondingly to provide similar fluid exchange rates if chambers of different volumes need to be used [for rationales, see chapters 1-Trapp & Ballanyi and 2-Ruangkittisakul et al.]. In the majority of our published studies, we applied drugs by addition to the superfusate ('bath-application').

For imaging experiments or patch-clamp recording from visualized superficial cells (Ballanyi, 1999; Garaschuk et al., 2000; Ballanyi & Ruangkittisakul, 2009a,b), a brain slice is transferred to the recording chamber and held in place with nylon strings. The strings are fixed to a frame made from platinum, or tantalum as a cheaper alternative, that are both supplied by Goodfellow (Huntington, United Kingdom; www.goodfellow.com) [see Fig. 1.4 in chapter 1-Trapp & Ballanyi]. In recording chambers with sylgard-184® ('Kwik-Gard', WPI) added, slices can alternatively be fixed with insect pins ('minutien pins', stainless steel, length 10 mm, tip diameter 0.02 mm, base diameter 0.2 mm; Fine Science Tools Inc.). Suction electrode(s) for electrophysiological recording (**§2.1.5**) provide further mechanical stability. Depending on the angle of the light guide from the cold-light source, carbon powder may be added while preparing the initially fluid sylgard-184® for better visualization of electrode positions or slice details.

2.1.5 Patch and Suction Electrodes

For electrophysiological recording of extracellular neural population activity and biophysical membrane properties of single cells, we use suction electrodes and patch electrodes, respectively [see also chapters 1-Trapp & Ballanyi and 2-Ruangkittisakul et al.]. Both types of electrodes are pulled from borosilicate glass capillaries (GC-150TF-10; 1.5 mm outer diameter x 1.17 mm

inner diameter, Harvard Apparatus). The tip of suction electrodes can be grinded down ('bevelled') to a desired size (50-250 μm) with sand paper or whetstone ('True hard Arkansas whetstone', Fine Science Tools). Then they are fire-polished using a commercial lighter while blowing air through the electrode to avoid closure by melting. To minimize tissue damage particularly for recording under visual control using a short distance high magnification objective (Ballanyi, 1999; Garaschuk et al., 2000; Ballanyi & Ruangkittisakul, 2009a,b), electrodes are beveled at an angle (30-45^{o}) to produce a cut tip surface that is parallel to the slice surface. Alternatively, a straight tip electrode is heated and bent down ~45^{o} at its shank to obtain a parallel tip surface and allow manoeuvring under the objective. Suction and patch electrodes are inserted into a holder system (ESP-M15-P and MHH-25, Warner Instrument Corp.) with an outlet for connecting a Tygon® tube that is attached for suction to a 5 ml standard medical syringe. Fine-tuning of suction is achieved with a manually tuneable syringe (e.g. Gilmont micrometer syringe; www.vwrsp.com). Suction electrodes and patch electrodes are fabricated using microelectrode pullers such as the P-1000 (Sutter Instrument Company, Novato, CA, USA; www.sutter.com) or the DMZ (Dagan Corporation, Minneapolis, MI, USA; www.dagan.com). The PC-10 (Narishige International Inc, East Meadow, NY, USA; usa.narishige-group.com) is a less expensive alternative, but is not designed for pulling sharp microelectrodes.

2.1.6 Micromanipulators and Antivibration Tables

As illustrated in Fig. 2-3 in chapter 2-Ruangkittisakul et al., patch electrodes are positioned with either a MP-285 (Sutter Instrument Company) or a MX7600 stepmotor, both (potentially) equipped with digital display of recording depth (Siskiyou Corporation, Grants Pass, OR, USA;

www.siskiyou.com). Cheaper non-electronic manipulators, such as the MM33 (Märzhäuser, Wetzlar, Germany; www.marzhauser.com) or the MMN-1 (Narishige International Inc., East Meadow, NY, USA; www.narishige.co.jp) are sufficient for positioning extracellular electrodes. For positioning electrodes on the xy-stage of an upright microscope (**§2.1.8**), You-2 (Narishige) or Kleindiek-Nanotechnik (Reutlingen, Germany; www.nanotechnik.com) miniature manipulators are well suited. Manual or motorized xy-stages can, e.g., be obtained from Siskiyou Design Inc. or Luigs-Neumann (Ratingen, Germany; www.Luigs-neumann.com). Mechanically unstable and electrically noisy laboratories require use of an antivibration table in combination with a Faraday cage both e.g., provided by Newport (Irvine, CA, USA; www.newport.com) or Kinetic Systems (Boston, MA, USA; www.kineticsystems.com). The Faraday cage is mounted on the antivibration table and thus electrically shields the microscope, experimental chamber and manipulators that are positioned on this table. A simple and less expensive (but often sufficient) system uses a stone or metal plate resting on rubber or silicone dampers while a metal (tool) cabinet serves as a Faraday cage.

2.1.7 Amplifiers, Stimulators and Computer-Based Data Acquisition

For intracellular electrophysiological recording, we use patch-clamp amplifiers from HEKA (Lambrecht, Germany, www.heka.com) or 'sample-and-hold' SEC amplifiers from npi electronic (Tamm, Germany; www.npielectronic.com). For suction electrode recording, AC-coupled differential amplifiers (gain 1-10k, band-pass filtering 0.3-3 kHz) are needed such as the Model-1700 from AM-Systems (Sequim, WA, USA; www.am-systems.com) or the DAM-50 from WPI. For better resolution particularly of signals with an amplitude <100 µV, integration of

the output signal at a time constant of 20-50 ms is recommended using, e.g., the MA-821/RSP 'Moving Averager' (CWE; www.cwe-inc.com) [see Fig. 2-4 in chapter 2-Ruangkittisakul et al.]. Signals are sampled into a computer via an interface and acquisition software at rates of 1-10 kHz for suction electrode signals and 4-20 kHz for membrane potential (or current) recordings. Convenient hardware/software packages are supplied by HEKA, npi or Axon Instruments (Molecular Devices; Sunny Vale, CA, USA; www.moleculardevices.com). Commonly used multichannel electrophysiological recording systems are 'Powerlab' (ADInstruments, Colorado Springs, CO, USA; www.adinstruments.com) or 'Spike-2' (Cambridge Electronic Design Ltd, Cambridge, UK; www.ced.co.uk). In most of these systems, software options are implemented for electrical stimulation in combination with an isolation unit, e.g. from WPI, AM-Systems or A.M.P.I. (Jerusalem, Israel; www.ampi.co.il).

2.1.8 Microscopes, Imaging Devices and Fluorescent Dyes

For optic control or mechanic fixation of a preparation and subsequent microelectrode positioning for blind recording, a stereomicroscope is used such as the Stemi-2000 (Zeiss), SZXZ (Olympus, Center Valley, PA, USA; www.olympusamerica.com) or the ELZ (Scienscope, Chino, CA, USA; www.scienscope.com). Visualization is facilitated by attaching a simple video camera, e.g. from WPI, to the stereomicroscope which can also be fully substituted by a video system equipped with zoom optics. The video signal is displayed on a separate monitor or, using a frame grabber, as an inset on the computer monitor used for controling the (intracellular) recording [see also chapter 3-Moore et al.]. Recording under visual control from superficial neurons in slices (Ballanyi, 1999; Garaschuk et al., 2000; Ballanyi & Ruangkittisakul, 2009a,b)

is done using an upright microscope such as the Zeiss Axioskop-2FS (or successor) or the Olympus BX61WI equipped with a water immersion lens (usually 40x or 60x magnification) with a working distance of at least ~2 mm to facilitate electrode positioning. The microscope should be equipped with differential interference contrast (DIC) optics for approaching individual cells which then appear almost in 3D-like fashion (Yuste et al., 2006) [see also chapters 1-Trapp/Ballanyi, 4-Fish et al., 5-Nakamura et al. and 9-Broicher & Speckmann]. Cells located up to 80 µm below the slice surface can be visualized for targeted patch-clamp recording by attaching a charge-coupled device (CCD) camera with infrared (IR) sensitivity to the microscope and displaying the resulting IR-DIC image on a monitor. Convenient CCD cameras are the ImageM or Orca-R2 (Hamamatsu, Bridgewater, NJ, USA; www.hamamatsu.com) or Coolsnap (Röper, Ottobrunn, Germany; www.roperscientific.de). For patch-clamping cells that are fluorescence-tagged, e.g. with green fluorescent protein, an epifluorescence system is required. Details of such systems using a CCD camera or photomultiplier are described elsewhere (Yuste et al., 2006) [see also chapters 1-Trapp/Ballanyi, 3-Moore et al., 4-Fish et al., 5-Nakamura et al. and 9-Broicher & Speckmann].

The Ballanyi laboratory is equipped with confocal and multiphoton microscopes for imaging the activity and morphology of neurons showing ENOs and neighboring (astrocytic) glia. Similar to our approaches for loading respiratory neurons and glia in preBötC slices (Ruangkittisakul et al., 2006, 2007, 2008) [see also chapter 2-Ruangkittisakul et al.], we load rhythmically active neurons and glia in horizontal brain slices with the membrane-permeant acetoxymethyl (AM) forms of the fluorescent Ca^{2+}-sensitive dyes Fluo-4 or Fluo-8L (TEF Labs, Austin, TX, USA; www.teflabs.com or Invitrogen) **(Fig. 2-3)**. These dyes are firstly dissolved at 5 mM in dimethyl

sulfoxide, containing 20% pluronic acid (Invitrogen) and then further diluted with standard superfusate (**§2.2.1**) to 0.5 mM for tissue injection or to 10 µM for loading via incubation (**§2.2.3**). For dye incubation, a slice is transferred to a 1.8 ml cryotube (Nunc A/S, Roskilde, Denmark; www.nuncbrand.com) with a hole in the lid for insertion of a Tygon® tube used for carbogenation of dye-containing standard superfusate (**§2.1.4**). Direct contact of the tube inlet with the solution needs to be avoided to prevent mechanic stress of the slice by perturbation of the fluid due to bubble/foam formation originating from pluronic acid. The cryotube is inserted into a heating unit (Isotemp-125D, Fisher) and the slice is exposed to the dye for 30 min at 30 ^{o}C. After entering the cells, AM component of the Ca^{2+} dyes is dissociated by esterases thus enabling Fluo-4 or Fluo-8L molecules to interact with Ca_i (Garaschuk et al., 2000; Stosiek et al., 2003; Yuste et al., 2006; Ruangkittisakul & Ballanyi, 2009; Ruangkittisakul et al., 2009). These and other fluorescent dyes should not be exposed for time periods of several hours or more to room light.

Fluorescence signals are monitored using either a FV300 laser scanning confocal microscope and software (488 nm argon laser, 20x XLUMPlanF1-NA-0.95 objective; Olympus FV300, Fluoview software) or a FV300 connected with an infrared titanium-sapphire laser (10W Mira/Verdi, Coherent, Santa Clara, California, USA; www.coherent.com) for multiphoton imaging (Stosiek et al., 2003; Yuste et al., 2006; Ballanyi & Ruangkittisakul, 2009a,b; Ruangkittisakul et al., 2006, 2007, 2008. The latter microscopes and software are also used by us for imaging of fluorescent SR-101 and Alexa-Fluo-488 tagged to GFAP (**§1**) using techniques that we have adapted to further improve the resolution of morphological features of both neurons and glia in slice regions showing ENOs (**§2.2.3**, **2.3**). For histological analysis of thionin stained

morphological structures **(Fig. 2-1)**, slices are either transferred on a 'hanging drop' glass slide (Fisher Scientific) to an upright microscope (Zeiss Standard 16, magnification x32) connected to a PL-A642-1.3-Megapixel CCD camera (PixeLINK, Ottawa, ON, Canada; www.pixelink.com) or to a Petri dish under a stereo microscope (Zeiss-SR15, magnification x32) connected to a PL-A686-6.6-Megapixel CCD camera (PixeLINK).

2.1.9 Agents

Most agents for our studies on ENOs are obtained from Sigma-Aldrich except salts for superfusate, Na^+ acetate trihydrate or acetic acid (Fisher Scientific). Most other agents, such as neurotransmitters and corresponding (ant)agonists, are purchased from Tocris Biosciences (Ellisville, Missouri, USA; www.tocris.com), MP Biomedicals (www.mpbio.com), TEF Labs Inc. (Austin, Texas, USA; www.teflabs.com) or Alomone Labs Ltd. (Jerusalem, Israel; www.alomone.com). Fluorescence dyes and immunohistochemical agents are purchased from Invitrogen, ATT Bioquest (Sunnyvale, CA, USA; www.attbio.com), and TEF Labs Inc.

2.2 Methods

In this section, techniques are described for generating newborn rat and piglet brain slices in which ENOs are generated spontaneously by different neural networks for several hours in superfusate with close-to-physiological ion content. Reference is made here also to microelectrode-based recording of extracellular neuronal population activity, membrane

potential fluctuations or Ca_i rises at cellular resolution. Finally, histological approaches are mentioned for discriminating neurons from glia in these slices.

2.2.1 Generation of Brain Slices

Initially, we used horizontal brain slices from newborn rats **(Fig. 2-1)** to establish recording of ENOs from hippocampus and cortex (studied in P0-P12 animals) and/or *locus coeruleus* (studied in P0-P4 pups). After conditions were determined for obtaining long-term recording of ENOs in rat slices, horizontal and coronal slices were generated from the brains of newborn piglets that are used in the Cheung laboratory as an *in vivo* model for systemic effects of asphyxia in human infants (Lingwood et al., 2008; Jantzie et al., 2010). Basically the same procedures are used for slicing, except that the piglet brain is substantially larger that the newborn rat brain, and therefore needs to be cut into smaller blocks prior to starting the slicing procedure.

2.2.1.1 Horizontal Slices From Newborn Rats

All procedures were approved by the University of Alberta Animal Care and Use Committee and carried out in compliance with guidelines of the Canadian Council for Animal Care. Animals are anesthetized with 100-200 µl isoflurane until the paw withdrawal reflex disappears and then decapitated above the shoulder. To visualize the skull, the cranium is pinched with fine forceps and the skin plus nasal cavity is cut away with small scissors (**§2.1.3**). The preparation is then transferred to a customized acrylic chamber with sylgard-184® (WPI) at its base and secured in place with two 21-Gauge ‘Precision Glide’ needle tips (Becton Dickinson, Franklin Lakes, NJ,

www.bd.com). The chamber is quickly filled with 0-4˚C cold continuously carbogenated sucrose solution (**§2.2.1**). For initial experiments, horizontal brain sectioning was performed at 19-22˚C in standard superfusate (**§2.2.1**) similar to preparation of newborn rat preBötC slices (Ruangkittisakul et al., 2006, 2007, 2008; Ballanyi & Ruangkittisakul, 2009a). In our hands, slices generated with that approach only show minor spontaneous hippocampal and cortical activities, whereas stable ENOs in these areas are revealed following sectioning in ice-cold sucrose solution (**§2.2.1**). With the preparation kept submerged, a sagittal incision is made down the midline of the skull starting from the nasal cavity and terminating immediately posterior to the cerebellum with spring-scissors (**§2.1.3**). Next, two lateral incisions are made to the left and right of the posterior end of this opening. Two additional lateral cuts are made just anterior to the olfactory bulb. To expose the brain, the skull is removed by connecting longitudinal incisions that are made between the anterior and posterior lateral cuts. The brain is isolated from the spinal cord with a coronal section through the pons, immediately posterior to the cerebellum and another section through the olfactory bulbs. Using a small spatulum, the brain is lifted slightly to enable cutting of remaining arteries and cranial nerves on the ventral surface with microscissors (**§2.1.3**) followed by removal of the brain including cerebellum from the cranial cavity.

Next, the brain is glued with cyanoacrylate glue on its ventral surface to a metal cutting plate that is then inserted into the vise of the Leica vibratome (**§2.1.3**). Subsequently, the vise is filled with ice-cold carbogenated sucrose solution. The brain is sectioned horizontally at maximal frequency of lateral blade movement, initially in 0.5-1 mm steps in posterior-to-anterior direction until the fornix commissure appears thin and elongated. Once the desired anatomical section level is reached **(Fig. 2-1)**, the speed for forward movement of the blade is reduced to achieve a smooth

slice surface with minimized damage of superficial cell layers. Depending on the size of the recording chamber (**§2.1.4**) as well as the age of the animal and slice thickness (typically 200-500 µm), horizontal slices may be hemisected along the midline, potentially generating 2-10 rhythmic preparations **(Fig. 2-1)**. With practice, the entire procedure takes 20-25 min. Complete or hemisected horizontal slices are placed on a net in a bath incubator and stored at 27 ˚C for at least 1 h in continuously carbogenated recovery solution (**§2.2.1**, **2.1.3**). A single slice is then transferred to the recording chamber and fixed with insect pins to the sylgard-184® layer on the bottom of the recording chamber and the superfusion system is activated (**§2.1.4**).

Generation of horizontal rat brain slices containing the *locus coeruleus* is technically very similar to generating slices for recording of ENOs in hippocampus and cortex, except as follows. For one, caudal separation of the brain from the rest of the brainstem/spinal cord must be further posterior to the cerebellum, eventually including some anterior portion of the spinal cord, thus preserving a complete fourth ventricle. It is not necessary to isolate and slice the brain in sucrose solution because spontaneous bursting in *locus coeruleus* is very similar regardless of whether dissection is done with ice-cold sucrose solution or in standard superfusate at 19-22˚C (**§2.2.1**). However, if simultaneous recording in cortex, hippocampus and *locus coeruleus* in a single slice is intended for direct comparison of drug effects on these events **(Fig. 2-1)**, ice-cold sucrose solution needs to be used to increase the probability for recording stable hippocampal and cortical ENOs. As described above, the brain is glued on its ventral surface and transferred to the Leica vibratome. Unlike the previous method described, it is sectioned in anterior-to-posterior direction to avoid tearing of the fourth ventricle. Serial sections are cut at maximal frequency for lateral blade movement, initially at 400-600 µm steps until the apex of the fourth ventricle

appears. At this point, slice thickness is reduced to 100 µm when approaching the *locus coeruleus* with forward cutting speed reduced. Each slice is inspected 'online' using a microscope (**§2.1.8**). Once the *locus coeruleus* starts to appear in the 100 µm thin section as a dark oval area close to the lateral border of the fourth ventricle and the fornix commissure appears extremely thin and elongated if not altogether absent, one (typically 400 µm thick) brain slice is cut. Hemisection of this slice provides two independently rhythmic *locus coeruleus* aspects with each a diameter of 200-400 µm in all dimensions **(Fig. 2-1)**. These procedures take 25-30 min.

2.2.1.2 Horizontal and Coronal Slices from Newborn Piglets

After instrumentation, a newborn piglet is stabilized for 30 min before harvesting the brain with tools described above (**§2.1.3**). Immediately after euthanization, the skin above the cranium is removed to allow access to the skull. An electric, rotating circular saw is used to cut away the dorsal portion of skull covering the cortex. It is essential that the window is laterally wide enough for easy removal of the brain, which takes between 1-3 min. A large spatulum is used for cutting through the olfactory bulb and isolating the brain from the rest of the spinal cord by cutting anterior to the cerebellum as well as removing the whole brain from the intracranial space. Extra care must be taken at this step to ensure that the spatulum does not penetrate brain tissue and potentially destroys areas to be studied. The isolated brain is immediately placed in a 100 ml Pyrex beaker (Corning Life Sciences, Wilkes Barre, PA, USA; www.corning.com) containing 50 ml of 0-4˚C cold carbogenated sucrose solution. With a pair of large forceps/tongs holding the brain in place, a pair of large scissors is used to vertically hemisect the brain. An

additional coronal cut is made to separate the frontal lobes from the rest of the brain and yielding 4 similarly sized tissue blocks, which can cool down more quickly than the whole brain. One posterior tissue block containing the somatosensory cortex is then transferred to the dissecting chamber used for generating rat slices and filled with ice-cold continuously carbogenated sucrose solution. A coronal ~5-10 mm thick slab containing the somatosensory cortex is cut (Craner & Ray, 1991) and the ventral half of the slab, which contains most of the caudate and putamen, is removed manually with a razor blade. Next, the tissue is glued either on its posterior or anterior surface with cyanoacrylate glue to the vibratome vise. Using a fine-tipped forceps (**§2.1.3**), extra care should be given when removing the arachnoid membrane covering the cortex to ensure complete sectioning of slices. Coronal slices, 250-500 µm thick, are cut using Leica vibratome in the inferior-to-superior direction, and stored as described above.

The ventral half of the posterior brain quarter contains the hippocampus and most of the limbic system. The tissue block is glued with dorsal cut surface down to the vibratome vise as described above. The arachnoid membrane surrounding the gyri is then carefully removed with fine-tip forcepses to facilitate smooth sectioning of tissue. Horizontal slices are cut in posterior-to-anterior direction. Roughly 1-1.5 mm of tissue must be sectioned relatively quickly before the hippocampal formation can be identified and 6-8 slices of 250-500 µm thickness can be generated which are stored as described above (**§2.2.1**).

2.2.2 Electrophysiological Recording

We found that suction electrodes used for electrophysiological recording of extracellular activity in isolated respiratory networks [see also chapter 2-Ruangkittisakul et al.] are also very useful for recording ENOs and ENO-like bursting in the *locus coeruleus* (**§3.2.1, 2.3**). Our experience with patch recording in the slices of the present study is restricted to *locus coeruleus* neurons. For this, we use the same electrodes as for recording from medullary dorsal vagal neurons or respiratory neurons [see also chapters 1-Trapp & Ballanyi, 2-Ruangkittisakul et al. and 3-Moore et al.].

2.2.2.1 Suction Electrode Recording

Extracellular population activity recorded with a suction electrode that is connected to a differential amplifier for AC-coupled recording typically has an amplitude in the low millivolt range, but is quite often as small as 10-100 µV (**§2.1.5**). These signals are very sensitive to electrical noise, which may require use of a Faraday cage. It is also recommended to record and display them as a moving average (integrated) trace for better signal-to-noise ratio (**§2.7**) **(Fig. 2-1)**. Suction electrodes of apparently identical shape can differ notably in the capability of recording small signals. Prior to starting a series of experiments, it is thus beneficial to prepare a set of about ten such electrodes and record ENOs in a test slice for choosing the most responsive electrodes. These electrodes can be used for up to several months, provided that they are cleaned with distilled water after each experiment.

Following positioning of these electrodes on the slice surface, the initial (modest) suction may be relieved by disconnecting the syringe from the suction tube (**§2.1.5**). The electrode should only make contact with the superficial tissue layer, particularly in <300 µm thin slices. Though, when placed on the slice surface, gentle suction using a micrometer syringe (**§2.1.5**) may improve the signal notably. In case of a 'leaky' recording with steadily decreasing signal amplitude, it may be necessary to re-establish modest suction every 10-20 min. In particular in hippocampal slice areas, suction electrodes record tonic neuronal population discharge in addition to phasic ENO bursting. This is most evident in the integrated signal (**2.1.7**) when blockade of such activity with opioids or high superfusate Ca^{2+} cause a sometimes pronounced decrease of the baseline of this signal (Panaitescu et al., 2009; Ballanyi & Ruangkittisakul, 2009a) [see also chapter 2-Ruangkittisakul et al.].

2.2.2.2 Patch-Clamp Recording

Similar to our experience with dorsal vagal or respiratory brainstem neurons [see chapters 1-Trapp & Ballanyi and 2-Ruangkittisakul et al.], blind whole-cell recordings from *locus coeruleus* neurons are stable for up to several hours (mostly 30-60 min) (**Fig. 2-4)**. For such recordings, the electrode is advanced perpendicularly using a MX7600 motor-driven micromanipulator with an added display of recording depth (**§2.1.6**). While advancing the electrode through the tissue, positive pressure (~30 mmHg) is applied to avoid clogging which is evident from an increase in electrical resistance (Smith et al., 1991; Panaitescu et al., 2009). Augmentation by up to 300% of a voltage signal in response to repetitive (~25 Hz) injection of negative DC current pulses (-1 nA, 10 ms) indicates that the electrode is close to a neuronal cell membrane. The probability for

a GΩ seal, which is necessary for every mode of patch recording (Neher & Sakman, 2009; Walz, 2009), correlates with the occurrence of electrode potential oscillations that resemble sine waves. At this instance, the patch electrode is moved upward and downward by 1-5 µm for several times until both the amplitude and speed of such electrode potential oscillations becomes maximal. At this point, the amplitude of the stimulation pulse is decreased to 0.1 nA and positive pipette pressure is released. In ~30% of cases, a GΩ seal develops spontaneously within <3 s as evident from an increase in the amplitude of the current-induced electrode potential change. If electrode potential does not start to continuously increase upon removal of positive pressure during this time period, negative pressure of up to -50 mmHg is applied. After formation of a seal >1 GΩ, the whole-cell configuration is established by abrupt and brief suction (~100 mmHg). If patch electrodes are not 'perfect', e.g., due to use-related corrosion of the electrode puller filament (**§2.1.5**), suction may have to be substituted by (or combined with) 1 ms 500-1000 nA pulse using the 'ZAP' function of the amplifier/software, if implemented. We do not correct membrane potential values for liquid-junction potentials that presumably range from 10-20 mV (Neher & Sakman, 2009; Walz, 2009) [for rationale, see chapter 2-Ruangkittisakul et al.]. Once membrane potential stabilizes within several minutes after establishing whole-cell recording, membrane resistance is monitored via injection of hyperpolarizing DC current pulses (40–250 pA, 0.5–0.7 s) at intervals of 5-15 s **(Fig. 2-4)**.

2.2.3 Multiphoton/Confocal Imaging

Because neural activity is associated with cytosolic Ca_i rises (**1.**), fluorescence imaging using Ca^{2+}-sensitive dyes is widely used for monitoring both activity and morphology of brain cells

(Garaschuk et al., 2000; Yuste et al., 2006; Ruangkittisakul et al., 2006, 2008; Ballanyi & Ruangkittisakul, 2009a; Ruangkittisakul & Ballanyi, 2009; Agulhon et al., 2008; Wang & Bordey, 2008; O'Donovan et al., 2008; Ballanyi et al., 2010). As exemplified in the latter (review) articles, imaging technologies changed over the past ten years from primarily CCD camera to multiphoton/confocal approaches, with a concomitant increase in the number of optical studies on *in vivo* neural systems. One major drawback of Ca_i imaging is related to the fact that fluorescent Ca^{2+} dyes non-differentially stain neurons, astrocytes and oligodendrocytes (plus microglia of non-neural origin) particularly in immature or cultured neural structures (Ruangkittisakul & Ballanyi, 2009; Ruangkittisakul et al., 2009; Ballanyi et al., 2010). For discriminating between neurons and glia, it has been proposed based on both *in vivo* (Nimmerjahn et al., 2004) and *in vitro* findings (Kafitz et al., 2008) that the fluorescence dye SR-101 selectively stains glia. However, according to other reports the same dye selectively stains neurons (Keifer et al., 1992; Mandal & Anderson, 2009).

In the following, we describe our approach for Ca_i imaging in bursting neurons and adjacent (astrocytic) glia in brain slices and also refer to our novel distinct protocols for loading either primarily neurons or astrocytes with SR-101. Moreover, we outline an established immunohistochemical approach for fluorescence labeling with GFAP in fixed slices for ultimately attributing Ca_i recordings to astrocytes (Nimmerjahn et al., 2004; Wang & Bordey, 2008; Agulhon et al., 2008; Kafitz et al., 2008). For our multiphoton/confocal Ca^{2+} imaging approach of ENOs in brain slices, we use two procedures for loading cells with either Fluo-4 or Fluo-8L via injection into a specific target area or incubation of the entire slice, respectively (**§2.1.8**). For incubation with dye at 30 ^{o}C, a slice is transferred for 30 min to a cryotube

containing continuously carbogenated standard superfusate with 10 µM Fluo-8L-AM added (**§2.1.8**). This results in almost equal loading of neurons and glial cells in rat slices whereas primarily glial cells are loaded in hippocampus of piglet slices (**§2.3.2.1**). For focal dye application **(Fig. 2-3)**, 0.5 mM Fluo-4-AM is backfilled into a broken patch pipette with an outer diameter of 5-10 µm (**§2.1.8**) and subsequently pressure-injected (25-50 mmHg) for 10 min (Stosiek et al., 2003; Ruangkittisakul et al., 2006, 2008) at 30-100 µm depth into the spontaneously active slice area of interest. This leads to staining of cells located between the surface and a depth of at least 100 µm. While imaging, rhythmic neuronal population activity can principally be recorded with a suction electrode (**§2.1.5**, **3.2.1**) from a spot in the vicinity of the area to which Ca^{2+} dye has been applied (**§2.5**).

Fluorescence signals in tissue depths of up to 60 µm and 90 µm are measured using either an Olympus FV-300-based laser scanning confocal microscope or a custom made multiphoton system based on a further FV-300 system connected to an IR titanium-sapphire laser (**§2.1.8**) **(Fig. 2-3)**. The Ca^{2+} dye stained region is mostly monitored using a 20x objective with 2-3x digital zoom at reduced settings for y-axis scanning. Compared to full frame acquisition at a resolution of 512 x 512 pixels, such 'clipped mode' imaging samples an area of 512 x 80-220 pixels thus enabling scan rates of 1.25-3 Hz which are normally sufficient to detect 70-100% of the peak of spontaneous Ca_i rises. An exception are ENO-like rhythms in *locus coeruleus* which occur at a rate of 1-4 Hz and are thus normally too fast to be resolved with our imaging approach (**§2.5**). However, oscillations can be slowed down pharmacologically in *locus coeruleus* for Ca_i imaging (**§2.3.1.1**) **(Fig. 2-3)**. The morphology of cell bodies and primary dendrites is best revealed by combining 'z-stack' image series, using single z-steps sizes of

0.05-1 µm, with 3D-animation using Fluoview software (**§2.1.8**). Fluo-4 or Fluo-8 fluorescence emission is weak at low cytosolic Ca^{2+} levels (Stosiek et al., 2003; Yuste et al., 2006; Ruangkittisakul & Ballanyi, 2009; Ruangkittisakul et al., 2009). Therefore, to improve morphological reconstruction, slices are exposed at the end of Ca_i imaging experiments to glutamate (0.25-1 mM, 5-10 min) for generation of z-stacks **(Fig. 2-3)**. Glutamate-induced fluorescence signals are 3-10 times larger than those associated with spontaneous activities.

For visualizing cell layers or nuclei in newborn rat and piglet brain slices with thionin **(Fig. 2-1)**, slices are fixed after experiments in 4% paraformaldehyde for at least 15 min, typically overnight. For subsequent staining with thionin, slices are 'washed' in phosphate buffer for 2 min, then immersed for 90 s in thionin solution (**§2.1.2.3**) and sequentially washed in phosphate buffer (2 min), 50% ethanol (4 min) and finally in phosphate buffer (2 min). The following procedures are used for immunohistochemical identification of GFAP in astrocytes of horizontal newborn rat brain slices [see also (Kafitz et al., 2008)].

After electrophysiological recording, the (mostly 400 µm thick) slices are fixed and stored at 4 ^{o}C in in phosphate buffer with 4% paraformaldehyde for at least 2 h, optimally > 1 day. Fixed slices are then washed 3 times for 10 min each in phosphate buffered solution. Slices are subsequently incubated in methanol for 10 min followed immediately wash with 3% hydrogen peroxide in phosphate buffer for 10 min and washed 3 times in this solution each time for 10 min. They are then incubated over night at 4 ^{o}C in rabbit GFAP antibody diluted 1:500 in phosphate buffer with 0.5% Triton X. The following day, slices are washed 3 times for 10 min

each in phosphate buffer and then incubated at room temperature for 2 h in Alexa-488 goat anti-rabbit diluted 1:500 in phosphate buffer with 0.5% Triton X. Finally, sections are washed 3 times each for 10 min in phosphate buffer and then stored in this solution with 4% paraformaldehyde added until visual inspection using the confocal/multiphoton microscopes (**§2.1.8**).

2.2.4 Data Analysis

No quantitative data are provided in the examples for this article. However, the following sections describe methods used for quantification of data. ENOs are continuously recorded at a sampling rate of 1-10 kHz (**§2.1.7**). Burst rate is averaged over 2 min time windows. Burst duration is defined using ClampFit software (Molecular Devices Corporation, Chicago, Il, USA; www.moleculardevices.com) as the time interval from when the signal increases above and decreases below a threshold set at 10% of the peak amplitude for that burst. Pharmacologically altered rhythms are described by averaging burst rates over a 2 min time period at steady state. Values are means ± SEM. Significance ($P< 0.05$) is assessed by Student's t-test or one-way ANOVA using Prism (GraphPad Software Inc., La Jolla, CA, USA; www.graphpad.com).

Imaging analysis is performed by drawing with Fluoview software (Olympus) regions of interest (ROIs) around cell somata and obtaining a time-series analysis of fluorescent intensity changes for each region of interest (**§2.1.8**). Fluorescence intensity data are transferred to Excel for further computation and plotting of graphs. 3D reconstruction is obtained from z-stack series (**§2.1.8**). As typical 3D settings, we use a x-y plane with rotation in x and y axes to give a 3D

impression of cell morphology, and x-z plane with y axis rotation to reveal the depth of fluorescence signal. For generating figures for publication, fluorescence intensities are plotted in graphs using both Excel (Microsoft office) and Illustrator (Adobe; www.adobe.com). For generation of movies, large files are compressed using Premiere Pro CS3 software (Adobe).

2.3 Results

In the following, some of our electrophysiological imaging findings are exemplified for ENOs in horizontal newborn rat slices and horizontal plus coronal newborn piglet slices. A detailed description will follow in original reports that are currently being prepared for publication.

2.3.1 ENO(-like) Rhythms in Horizontal Newborn Rat Brain Slices

Here, properties of robust ENO-like activity in *locus coeruleus* are compared with those of developmentally related ENOs (**§1**) in entorhinal cortex and hippocampus in the same slice type.

2.3.1.1 ENO-like Bursting in Locus Coeruleus

ENO-like bursting in *locus coeruleus* consists of particularly robust bursts with very good signal-to-noise ratio, which do thus not require use of 'quiet' suction electrodes (**§2.2.2.1**) **(Figs. 2-1-2-3)**. Because both *locus coeruleus* aspects are not coupled, bilateral bursting is asynchronous **(Fig. 2-3)**. Accordingly, a horizontal slice can be sectioned in the midline for studying both *locus coeruleus* aspects separately. In both complete and split slices, ENO-like rhythms are revealed

right at the start of recording at normal rate while burst amplitude may take 0.5-1 h to reach steady state. Bursting in *locus coeruleus* is stable for >5 h in standard superfusate with physiological Ca^{2+} (1-1.2 mM) and K^+ content (3 mM).

Similar to bursting of the isolated preBötC (**§1**) (Ruangkittisakul et al., 2007, 2011; Ballanyi & Ruangkittisakul, 2009), *locus coeruleus* activity is determined by a Ca^{2+}/K^+ antagonism. Specifically, supraphysiological superfusate Ca^{2+} levels depress the rate (and amplitude) of ENO-like rhythm which ceases upon raising Ca^{2+} to >3 mM. This Ca^{2+} depression of *locus coeruleus* rhythm is reversed by raising K^+ to 6-8 mM **(Fig. 2-2)**. The blocker of voltage-activated Na^+ channels tetrodotoxin (TTX) abolishes bursting within <10 min at concentrations >10 nM. Riluzole, which is an inhibitor of the 'persistent' subtype of such channels that mediate intrinsic bursting (Feldman & Del Negro, 2006; Ballanyi & Ruangkittisakul, 2009a; Sipilä & Kaila, 2008), does not fully block rhythm within 20 min at 50 µM which is already beyond the level at which the drug is specific **(Fig. 2-5)**. Bursting in *locus coeruleus* is also depressed following activation of ionotropic $GABA_A$ and glycine receptors with muscimol (2.5 µM) and glycine (1 mM), respectively. This depression is countered by the $GABA_A$ and glycine receptor antagonists gabazine (1-5 µM) and strychnine (5 µM), respectively. Moreover, >50 nM DAMGO inhibits *locus coeruleu*s rhythm via a pronounced hyperpolarization and this depression is antagonized by either >250 nM of the opioid receptor antagonist naloxone **(Fig. 2-4)** or >1 mM methylxanthine. The latter observations are in line with our findings on the isolated preBötC (Ruangkittisakul & Ballanyi, 2010). Also chemical anoxia evoked by bath-application of cyanide (1 mM) blocks these bursts after more than 5 min, whereas rhythm persists, albeit with a transformed pattern, in response to 0.01-5 mM adenosine **(Fig. 2-6)**. Neither gabazine

(Fig. 2-6), strychnine nor methylxanthines disrupted *locus coeruleus* bursting when added to standard superfusate.

In control, Ca_i fluctuations are detectable in most *locus coeruleus* cells although their amplitudes are often rather small (**§2.5**). Injection of Ca^{2+} dye or SR-101 into the *locus coeruleus* reveals basic morphological features of several cell classes (**§2.2.3**) **(Fig. 2-3)**. Presumptive neurons have a soma diameter of 20-35 µm, whereas most cells with a soma diameter of ~10 µm most likely represent astrocytes (Wang & Bordey, 2008; Algulhon et al., 2008; Ballanyi et al., 2010). In response to either lowering Ca^{2+} to 0.5 mM, or raising K^+ to 7-9 mM in the superfusate, the rate of ENOs decreases to <0.3 bursts/s while single burst duration increases, often to >1 s. In this situation, larger cells show synchronous Ca_i rises, whereas presumptive astrocytes remain silent **(Fig. 2-3)**. Bath-application of glutamate (0.5-1 mM) evokes a prominent Ca_i rise that persists in both cell types for >5 min. Therefore, this feature can be used for z-stack imaging of their morphology (**§2.2.3**) **(Fig. 2-3)**. In contrast, the metabotropic glutamate receptor agonist trans-1-aminocyclopentane-1,3-dicarboxylic acid (t-ACPD, 25 µM) causes primarily (oscillatory) Ca_i rises in presumptive astrocytes. This is in line with the view that their excitability is primarily comprised of store-mediated Ca^{2+} release (**§1**) (Wang & Bordey, 2008; Algulhon et al., 2008; Ballanyi et al., 2010). Bath-application at 20-23 ^oC of 165 µM of the morphological dye SR-101 improves the resolution of morphological details in *locus coeruleus*, but does not appear to primarily stain mainly neurons as in hippocampus (**§2.3.1.2**) **(Fig. 2-3)**. Conversely, 1 µM SR-101 at 34 ^oC results in (fainter) staining of all cell types contrary to astrocyte labeling in newborn rat hippocampus (Kafitz et al., 2008) (**§2.3.1.2**).

2.3.1.2 ENOs in Hippocampus

The capability of hippocampal networks in the CA_3 area or neighbouring regions **(Fig. 2-1)** for generating long-term stable ENOs appears to depend critically on a recovery period of at least 1 h (**§2.1.2.1**, **2.2.1**). The rate of these ENOs ranges between 4-30 bursts/min (mostly 10-20 bursts/min) and single burst duration is typically 0.5-2 s. In ~20% of slices, ENOs of slightly higher rate and shorter single burst duration ('spikes') can occur in addition to the typical ENOs. Slices that have been stored in recovery solution for several hours can mostly generate robust ENOs in the recording chamber for further several hours. In our initial experiments performed in spring/summer of 2010, we used 20 mM glucose as in other studies (Garaschuk et al., 2000) [see also chapter 2-Ruangkittisakul et al.]. Changing to 10 mM glucose later did not seem to influence the probability for occurrence (or basic properties) of stable hippocampal ENOs. However, success rates of obtaining stable ENOs decreased in the following fall/winter. We have resumed using 20 mM glucose in spring/summer of 2011 and currently (summer/fall 2011) have a success rate of >70% for simultaneous recording of robust persistent hippocampal and cortical rhythms.

Regardless of whether analysis is done on slices from a single pup or across multiple litters, hippocampal ENOs that persist for >3 h are seen in ~40% of slices. Similar to ENO-like bursting in *locus coeruleus* (**§2.3.1.1**), hippocampal ENOs typically show a good signal-to-noise ratio **(Figs. 2-1, 2-2, 2-5, 2-6)**. In our hands, they are rarely seen in slices from <P3 rats and their amplitude seems to be larger at more regular rate in slices from >P5 animals. Hippocampal ENOs depend presumably on a depolarizing GABA action that switches to a hyperpolarization

during the second postnatal week (**§1**) (Ben-Ari et al., 2007; Sipilä & Kaila, 2008; Blaesse et al., 2009). However, in our hands hippocampal ENOs are also typical for slices from P12 rats which are the oldest animals tested so far by us. We have not studied yet whether hippocampal ENOs depend on $GABA_A$ receptors at that age.

Hippocampal ENOs in newborn rats show a pronounced Ca^{2+}/K^+ antagonism **(Fig. 2-2)**. In ~50% of slices, raising Ca^{2+} to 2 mM abolishes the typical type of bursting which is restored by raising K^+ from 3 mM to 6-8 mM while spike-like ENOs are less sensitive to high Ca^{2+} similar to ENO-like *locus coeruleus* rhythm (**§2.3.1.1**). Raising K^+ to >6 mM in 1 mM Ca^{2+} hyperexcites the hippocampal circuits which can profoundly perturb hippocampal ENOs **(Fig. 2-2)**. In ~50% of slices, ENOs are not robust in 3K/1Ca, but bursting is enhanced and stabilized by raising K^+ to 4-5 mM. TTX (at >10 nM) and riluzole (5-20 µM) **(Fig. 2-5)** abolish both types of ENOs within <20 min. Bursting is also abolished during 5-10 min time periods of chemical anoxia or bath-applied adenosine (10-250 µM) **(Fig. 2-6)**. Gabazine (1-5 µM) often transforms hippocampal ENOs into large amplitude seizure-like events that occur at a rate of 0.5-5 bursts/min **(Fig. 2-6)**. Occasionally, a similar transformation of burst pattern is seen in one population of slices upon application of >100 nM DAMGO. In other slices, DAMGO transforms ENOs into rhythmic events with a rate of 0.2-1 bursts/min and a single burst duration of up to 1 min.

Suction electrode recorded hippocampal ENOs are principally well reflected by Ca_i oscillations in CA_3 pyramidal layer neurons with a soma diameter of 15-25 µm **(Fig. 2-7)**. Because incubation of slices with Fluo-8L-AM stains both neurons and glia, injection of dye is not

necessary for loading neurons as in isolated newborn rodent respiratory networks in our hands (**§2.2.3**) (Ruangkittisakul et al., 2006, 2008) [see also chapter 2-Ruangkittisakul et al.]. Synchronized bursting seems to be more prominent in slice layers deeper than 60 µm as evident in ~50% of cases from 'diffuse' Ca_i increases originating from cells that cannot be visualized at sufficient resolution at such depths. Ca_i rises in a notable portion of superficial neurons are synchronized with the 'background' Ca_i oscillations while neighboring neurons may show out-of-phase oscillations. Sparsely distributed cells with a soma diameter of ~10 µm in the pyramidal CA_3 or CA_1 cell layer (*stratum pyramidale*) and numerous cells of similarly small size in the adjacent (dendritic) areas of the *stratum radiatum* and *stratum oriens*, both most likely representing mostly astrocytes, do not show synchronized spontaneous Ca_i rises. Glutamate notably increases Ca_i in both types of cells and enables their morphological characterization (**§2.2.3**) **(Fig. 2-7)**, whereas t-ACPD and adenosine triphosphate (ATP) often induce Ca_i oscillations in presumptive astrocytes with minor effects on Ca_i in neurons.

The latter finding shows that profiling of neuromodulator-evoked Ca_i responses is one tool for discriminating small neurons from astrocytes as we have described for the isolated preBötC in brainstem slices (Ruangkittisakul et al., 2009a) [see also chapter 2-Ruangkittisakul et al.]. A further approach in this regard involves fluorescence imaging using SR-101. In initial experiments, we found that incubation of living horizontal newborn rat brain slices at room temperature with 165 µM of the dye (**§2.2.3**) primarily stains neuronal cell bodies in the CA_3 pyramidal cell layer **(Fig. 2-7)**. These findings are similar to previous reports on selective neuronal staining in other isolated nervous tissues (Keifer et al., 1992; Mandal & Anderson, 2009). More recently, we have incubated such slices at 34 ^oC with 1 µM SR-101 which appears

to primarily label astrocytes **(Fig. 2-7)**. This is similar to what was observed in newborn rat hippocampal slices (Kafitz et al., 2008), and similar to selective astrocyte staining by this dye *in vivo* (Nimmerjahn et al., 2004). It thus seems that these different parameters used for loading cells with SR-101 are suitable to discriminate neurons from glia. For unknown reasons, it seems unfeasible to incubate slices with Fluo-8L-AM plus high SR-101 doses for simultaneous Ca_i imaging and neuron labeling, respectively. Contrary, dual Ca_i imaging and morphological labeling is possible in glia of slices exposed to 10 µM Fluo-8L-AM and subsequent loading of 1 µM SR-101 at high temperature **(Fig. 2-7)**. It should be considered that SR-101 may induce hyperexcitability of neural networks as suggested by findings in a recent study (Kang et al., 2010.

Our very recent findings indicate that it is possible to stain slices that were chemically fixed after optical Ca_i recording with SR-101 for morphological analysis. Also in chemically fixed slices, we have applied an established immunohistochemical approach (Kafitz et al., 2008) for staining astrocytes with GFAP. While staining can be very pronounced in slices that have only been used in standard superfusate for time periods <1.5 h **(Fig. 2-7)**, it is not clear yet whether double-labeling of GFAP with Fluo-8L [as shown by Kafitz and colleagues (2008)] or triple labeling with Fluo-8L and SR-101 can be done routinely in our hands in slices used for electrophysiological imaging for several hours.

2.3.1.3 ENOs in (Entorhinal) Cortex

Similar to hippocampal ENOs, spontaneous synchronized bursting for several hours in (entorhinal) cortex is primarily observed in slices that have been stored in recovery solution for 1 to >5 h (**§2.1.2.1**). In spring/summer of 2010, 'simple' ENOs in entorhinal cortex were revealed in almost all slices studied in superfusate with either 10 or 20 mM glucose. These cortical ENOs consisted mostly of a 0.3-1.5 s lasting events that occurred at a rate of 0.2-2 bursts/min and thus resemble very much ENOs shown in the original paper on these rhythms (Garaschuk et al., 2000). In ~50% of slices, the signal-to-noise ratio was very good as for hippocampal ENOs or ENO-like bursting in *locus coeruleus*, whereas in the other cases amplitudes of signals could be <100 µV thus requiring selected suction electrodes (**§2.2.2.1**). Since winter 2010, we observe also other patterns of cortical ENOs in a majority of slices. In addition to slow single peak events described above, multipeak bursts can occur at either slow (<1 burst/min) or faster rates (>4 bursts/min). Moreover, (multipeak) events lasting several seconds are observed that either represent the only type of rhythm in a given slice or can be intermingled with one or several of the other patterns. Independent on the types of ENO pattern in enthorhinal cortex, rhythmic bursting in this region and neighboring areas **(Fig. 2-1)** shows pronounced Ca^{2+}/K^{+} antagonism and is abolished by TTX, riluzole, adenosine and anoxia with a sensitivity similar to that of hippocampal ENOs **(Figs. 2-2, 2-5, 2-6)**. Also gabazine evokes large amplitude seizure-like rhythmic bursting in (entorhinal) cortex, similar to that seen in hippocampus **(Fig. 2-6)**.

So far, we have not systematically studied Ca_i dynamics in cortical areas. But, preliminary findings indicate that our multiphoton/confocal imaging approach using loading of cells via

incubation of slices with Fluo-8L-AM is feasible for Ca_i imaging in both neurons and glia **(Fig. 2-8)**. Similarly, morphological imaging with high or low SR-101 doses (plus GFAP staining) seems principally possible for identifying cortical neurons *versus* astrocytes **(Fig. 2-8)**.

2.3.2 ENOs in Newborn Piglet Brain Slices

In the past decade, piglets are increasingly used as an experimental model in neuroscience (Lind et al., 2007; Lingwood et al., 2008; Jantzie et al., 2010). These studies employ various techniques such as behavioral testing, electro encephalogram recording, functional *in vivo* imaging such as positron emission tomography, and also molecular biology, for studying brain development and establishing models for various brain disorders. However, we are not aware of previous electrophysiological (imaging) studies to identify functional neural circuits in newborn piglet brain slices. In summer 2010, we have established techniques corresponding to those applied to newborn rat slices to detect and characterize for the first time ENOs in piglet slices.

2.3.2.1 ENOs in Hippocampus and Cortex of Horizontal Slices

Following recovery of slices for 1 to >5 h (**§2.1.2.1**), suction electrode recording in both hippocampus and (entorhinal) cortex reveals spontaneous activity in >80% of cases that can last for several hours. Contrary to ENOs in rat slices, very regular large amplitude bursting is detected in only <20% of cases in the CA_3 area of hippocampus. Instead, this area exhibits sharp activity peaks with a duration of 0.1-0.5 s. Such bursting occurs at a rate of 2-20 bursts/min with intermittent periods of up to 30 s during which the baseline of the integrated signals shows fast

low amplitude fluctuations **(Fig. 2-9)**. Both, large peaks and baseline fluctuations reflect synchronized neural bursting because they disappear in response to >0.1 µM TTX plus >50 µM of the voltage-activated Ca^{2+} channel blocker Cd^{2+}. In ~60% of slices, spontaneous activity is depressed by raising Ca^{2+} from 1 mM to 2-3 mM or by addition of adenosine (10-250 µM) **(Fig. 2-9)**. Chemical anoxia abolishes bursting in all cases whereas gabazine (1-5 µM) evokes mostly large amplitude seizure-like bursting in ~40% of slices. Principally similar spontaneous activity and effects of the above drugs are revealed in entorhinal cortex of horizontal slices **(Fig. 2-9)**.

Incubation of slices with Fluo-8L-AM seems to be less effective compared to injection of Fluo-4-AM which stains both neurons and presumptive astrocytes in entorhinal cortex **(Fig. 2-10)**. In only few cases, spontaneous Ca_i rises occur primarily in astrocytes while glutamate evokes a notable Ca_i increase in both cell types. In hippocampal regions, only astrocytes appear to respond to either glutamate or t-ACPD with a Ca_i rise. Neurons in that area do not show a change in fluorescence intensity in response to glutamate although the dye can enter the cells and reveal their morphology quite well in some cases. Upon staining with 165 µM SR-101, morphological features of neurons in both hippocampus and cortex can be resolved well **(Fig. 2-10)**.

2.3.2.2 ENOs in Somatosensory Cortex of Coronal Slices

Newborn pigs show great similarities to human infants in regards to gross anatomy and brain development (Lind et al., 2007) making them suited as models for neurological diseases. Of particular interest to us is the somatosensory cortex because significant histological and biochemical injuries have been demonstrated in this area of newborn pig after hypoxic-ischemic

insult (Martin et al., 1997). We therefore started to investigate ENOs in this region using coronal slice and to develop this model for future electrophysiological imaging study of hypoxic-ischemic effect in newborn brain (**§1**). Similar to horizontal piglet slices, coronal somatosensory cortical slices were stored for 1 to >5 h in recovery solution. In >70% of cases, we observed robust ENOs occurring at a regular rate of 0.2-1 Hz and having a single burst duration of 0.1-0.3 s **(Fig. 2-9)**. These ENOs are depressed by TTX (plus Cd^{2+}), and (mostly) also by raised Ca^{2+} or adenosine **(Fig. 2-9)** at concentrations similar to those used in horizontal piglet or rat slices. Chemical anoxia seems to abolish these events while gabazine can evoke seizure-like bursting. Upon loading cells in these slices with Fluo-4 via focal injection, multiphoton/confocal Ca^{2+} imaging is feasible in neurons and glia and reveals glutamate-evoked Ca_i rises in both types of cells. Also SR-101 imaging can be applied successfully for characterizing the morphology of neurons in somatosensorty cortex while glial labeling has not been tested yet.

2.4 Discussion

Findings from *in vitro* studies suggest that ENOs are pivotal for development of neural structures (Spitzer, 2006; Khazipov & Luhmann, 2006; O'Donovan et al., 2008;; Allene & Cossart, 2010) (**1**). There is steadily increasing evidence that ENOs in isolated hippocampal and cortical circuits are similar to spontaneous activities in these brain regions *in vivo* (Leinekugel et al., 2002; Khazipov & Luhmann, 2006; Ben-Ari et al., 2007; Milh et al., 2007; Sipilä & Kaila, 2008; Allene & Cossart, 2010; Brockmann et al., 2011). Contrary, so far only one study assessed *in vivo* activity in neonatal *locus coeruleus* (Nakamura et al., 1987). Specifically, the authors found that synchronized tonic activity is typical for the majority of *locus coeruleus* neurons in newborn

rat pups *in vivo* several days after birth, whereas such discharges occurs only sporadically in some of these cells immediately after birth. However, the animals in that study were anesthetized, and it is established that this can notably depress spontaneous bursting (Teppema & Baby, 2011). In contrast to these *in vivo* findings, tonic activity seems to be typical for *locus coeruleus* neurons in slices from newborn and juvenile rodents (Christie et al., 1989). In line with this, synchronized *locus coeruleus* neural networks in newborn rat brainstem-spinal cords are either tonically active or show rhythmic bursts of activity while some cells in both classes receive additional phasic synaptic input from respiratory networks (Ballantyne et al., 2004). Besides this discrepancy between *in vivo* and *in vitro* findings, it is not clear whether *locus coeruleus* networks in newborn rats are immature as cortical structures or rather (almost) mature as the preBötC. There is though evidence from studies in newborn rats that noradrenergic neurons are already functional in the early postnatal period and can support other developing networks (Felten et al., 1982; Moriceau et al., 2010). Based on these considerations, we hypothesized (**§1**) that *locus coeruleus* circuits in the newborn rat slices are functional, yet still developing, and thus generate non-developmentally related ENOs that are likely also present in intact unanesthetized animals.

ENOs in hippocampus, cortex and *locus coeruleus* rhythms share several common features. Firstly, a Ca^{2+}/K^{+} antagonism determines bursting in these isolated brain regions, in both rats and newborn piglets, in a fashion resembling that in the isolated preBötC and respiratory networks *in vivo* (Ruangkittisakul et al., 2007) [see also chapter 2-Ruangkittisakul et al.]. In the latter studies, we hypothesized that depression of preBötC bursting by modestly elevated extracellular Ca^{2+} is primarily of presynaptic origin and stated that the underlying molecular mechanism is yet

unknown (Ballanyi & Ruangkittisakul, 2009a; Panaitescu e tal., 2009; Ruangkittisakul et al., 2011). It should be noted that raised Ca^{2+} also depresses spontaneous activity in cortical slices from mature mammals (Sanchez-Vives, 2012). All this indicates that Ca^{2+}/K^{+} antagonism is a general characteristic feature of spontaneously active neural networks. As a further common feature of these networks, chemical anoxia abolishes all three types of spontaneous bursting in newborn rats plus hippocampal and cortical ENOs in piglets. The finding that this effect is stable for time periods >10 min without occurrence of a major tonic discharge indicates lack of profound perturbation of ion homeostasis. This is similar to our findings on a high tolerance to anoxia of neonatal respiratory neurons and adult dorsal vagal neurons, which is contrary to the fact that most adult central neurons respond to anoxia within few minutes with irreversible depolarization and Ca^{2+} deregulation (Ballanyi et al., 1999; Ballanyi, 2004a,b; Trapp & Ballanyi, 2012; De Curtis et al., 2012). Also adenosine, which accumulates in the extracellular space of (isolated) brain tissues during normal activity and particularly during hypoxia/anoxia (Ballanyi, 1999; Ballanyi et al., 1999; Ballanyi, 2004a,b; Ruangkittisakul & Ballanyi, 2010), depresses ENOs in neonatal hippocampus as previously reported (Safiulina et al., 2005), and also in cortex. In contrast, ENO-like rhythm in *locus coeruleus* seems to be resistant to this neuromodulator similar to minor effects on the isolated preBötC at least in our hands (Ballanyi, 1999; Ballanyi et al., 1999; Ballanyi, 2004a,b; Ruangkittisakul & Ballanyi, 2010). Also similar to the preBötC (Ballanyi, 1999; Ballanyi et al., 1999; Ballanyi, 2004a,b; Ruangkittisakul & Ballanyi, 2010), neural networks in *locus coeruleus* are depressed by μ-opioid receptor activation, which is intensely studied since several decades in *locus coeruleus* slices, e.g. (Christie et al., 1989). In contrast, μ-opioids either transform burst patterns or have minor effects on ENOs generated by hippocampal and cortical networks, respectively. Furthermore, seizure-like activity associated

with blockade of $GABA_A$ receptors can severely perturb ENOs in hippocampus and cortex, whereas rhythmogenic circuits in *locus coeruleus* are resistant to this manipulation. Finally, our findings on riluzole support observations by others (Sipilä et al., 2005, 2006; Sipilä & Kaila, 2008) suggesting that generation of hippocampal and cortical ENOs depends on persistent Na^+ channels. While these channels also contribute to intrinsic bursting in newborn rat respiratory networks (Ballanyi et al., 1999; Feldman & Del Negro, 2006), ENOs in *locus coeruleus* seem to be quite independent on these ion channels based on lack of effect of riluzole at doses <50 µM as shown by us here.

In summary, these (preliminary) results show that rhythmic bursting in isolated neural networks of the preBötC, hippocampus, cortex, and *locus coeruleus* shares various common properties albeit their varying degree of network maturation. Nevertheless, each of these structures has also characteristic features enabling their pharmacological discrimination, e.g. based on different responses to riluzole or adenosine. This indicates that the activity of each of these neural networks can potentially be targeted by specific novel clinically relevant agents that may not have an adverse effect on the other structures. We also found that electrophysiological imaging by complementing suction electrode or patch-clamp based observations with those revealed upon fluorescent Ca_i and morphological imaging is a potent tool to analyse the role of both neurons and neighboring astrocytes in the generation of these spontaneous activities and their modulation by pharmacological agents or experimental strategies that mimic neurological diseases or are candidates for their treatment.

2.5 Limitations and Perspectives

In the following, we refer to (potential) limitations of studying ENOs in newborn rat and piglet brain slices. We focus this discussion on factors that may be important for long-term stable ENOs in hippocampus and cortex and the feasibility of (combined) electrophysiological imaging.

2.5.1 Stability and Variability of ENOs

Spontaneous hippocampal and cortical ENOs are studied since >20 and >10 years, respectively (Ben-Ari et al., 1989, 2007; Garaschuk et al., 2000; Khazipov & Luhmann, 2006; Sipilä et al., 2005, 2006; Sipilä & Kaila, 2008; Kafitz et al., 2008; Bonifazi et al., 2009; Allene & Cossart, 2010; Ruusuvuori et al., 2010; Tyzio et al., 2010; Zilberter et al., 2010). References in the latter articles document the notably different experimental conditions among research groups. Major factors in this respect are the immediate use of slices after cutting *versus* storing them (on a net) in 'recovery solution' of particular composition and use of different types of 'cerebrospinal' superfusates (**§2.1.2.1**). Most relevant for the latter aspect are differing concentrations for superfusate Ca^{2+}, K^+ and glucose. Both, Ca^{2+} and K^+ have a major influence on neuronal excitability (Somjen, 2002; Ballanyi & Ruangkittisakul, 2009a,b; Zilberter et al., 2010) and our findings of pronounced Ca^{2+}/K^+ antagonism for all three types of ENOs strongly support this view. While hippocampal and cortical ENOs can be stable in our hands for at least 5 h in 3K/1Ca solution, elevation of K^+ to 4-5 mM can have a stabilizing effect on weak bursting in these areas. In contrast, ENO-like bursting in *locus coeruleus* is extremely robust and long lasting in 3K/1Ca. *Locus coeruleus* rhythms seem to be similar regardless of whether slices are directly used for

recording or firstly stored in recovery solution. Contrary, both hippocampal and cortical ENOs apparently depend greatly on such pre-incubation for recovery in our hands.

Important for the practicability of experiments, slices from both rats and piglets that have been stored for several hours can still generate all types of ENOs in the recording chamber for several more hours. This indicates that neural circuits in slices from newborn mammals remain functional for >10 h contrary to the view that (adult) brain slices should not be used for >5 h because of limited viability of neurons (Ballanyi, 1999; Ballanyi & Ruangkittisakul, 2009b). In fact, it is possible that the neonatal ENOs persist for >24 h in acute slices similar to inspiratory rhythm in preBötC slices [chapter 2-Ruangkittisakul et al.] and spontaneous diurnally related activity in slices from the suprachiasmatic nucleus [chapter 5-Nakamura et al.]. If this were the case, effects could be studied of 'slow' neuromodulators such as neurotrophic factors or responses of these networks to long-lasting application of opioids or methylxanthines to test whether this clinical scenario affects their bursting. However, it needs to be considered that some properties of neural circuits in slices may reconfigure within several hours after their isolation (Ballanyi, 1999). One obvious example for this is the 'wash-out' of preBötC rhythm in transversal medullary slices after several hours in 3K/1Ca solution. preBötC rhythm can be reactivated for multiple hours by raising of K^+ to 6-9 mM. However, high K^+ changes the sensitivity of the isolated inspiratory center to neuromodulators such as opioids or to anoxia (Ballanyi & Ruangkittisakul, 2009a).

Regarding superfusate glucose, hippocampal ENOs are possibly more robust in 20 *versus* 10 mM glucose. But, we did not test this systematically, and other experimental factors may also have changed at the same time. Regarding the most appropriate superfusate glucose content, it needs to be considered that glucose in brain interstitial space ranges between 0.1-2 mM, mostly depending on methods used for its determination (Zilberter et al., 2010) [for other references, see chapter 1-Trapp & Ballanyi]. Accordingly, it has been proposed that brain slices of newborn mammals should be studied in close-to-physiological glucose, i.e. ~1-2 mM, and/or in solution in which glucose is supplemented or fully substituted by energy substrates that are more relevant for newborns, specifically ketone bodies, lactate and pyruvate (Zilberter et al., 2010). In the latter review article, the authors refer to their related work showing that hippocampal and cortical ENOs are inhibited using close-to-physiological energy substrate levels in the superfusate. However, findings from other recent studies suggest that (10 mM) glucose provides an appropriate metabolic fuel for (newborn rodent) slices (Ruusuvuori et al., 2010; Tyzio et al., 2010). Obviously, this deserves further investigation.

2.5.2 Feasibility of Electrophysiological Imaging

One limitation that is common to the analysis of ENOs in all regions and slice types described above refers to simultaneous electrophysiological imaging. This approach is particularly feasible for studying inspiratory networks in newborn rodent brainstem slices because population activity can be recorded with suction electrodes in one lateral aspect of the bilaterally organized networks. Concurrently, the contralateral preBötC aspect or inspiratory active XII motor nucleus can be loaded with Ca^{2+} and/or morphological dyes for imaging which can be combined with

patch-clamp recording (Ballanyi & Ruangkittisakul, 2009a; Ruangkittisakul & Ballanyi, 2009; Ruangkittisakul et al., 2009) [see also chapter 2-Ruangkittisakul et al.].

Simultaneous electrophysiological imaging is principally also applicable for analyzing ENOs. For *locus coeruleus*, however, this bilaterally organized network does not generate synchronized activity, at least not *in vitro* under our experimental conditions. This does not allow activity phase analyses between extracellular recording via suction electrode in one aspect and imaging and/or intracellular patch-clamp recording in the contralateral aspect. Nevertheless, (pharmacological) imaging findings in one *locus coeruleus* aspect can be supported by results from electrophysiological recording in the contralateral aspect **(Fig. 2-3.)**. As a major limiting factor, Ca_i imaging in *locus coeruleus* is mostly not feasible in superfusate of close-to-physiological ion content. This is because ENOs occur at a rate of ~1 Hz while recovery from a single burst-related Ca_i increase in cortical structures or the isolated preBötC lasts typically >1 s using conventional Ca^{2+} dyes like Fluo-4 or Fluo-8L (Leinekugel et al., 1992; Garaschuk et al., 2000; Ballanyi & Ruangkittisakul, 2009a; Ruangkittisakul & Ballanyi, 2009; Ruangkittisakul et al., 2009) [see also chapter 2-Ruangkittisakul et al.]. Accordingly, *locus coeruleus* rhythm needs to be slowed down for Ca_i imaging, e.g. by raising superfusate K^+ or Ca^{2+} (**§2.3.1.1**). As a further limitation, SR-101 imaging using either low or high concentrations of this dye does not seem to discriminate between neurons and astrocytes in *locus coeruleus*, whereas Ca_i imaging of responses to particular 'gliomodulators' such as t-ACPD or ATP seems to be useful. Also, there is some evidence that SR-101 induces hyperexcitability in isolated (hippocampal) neural networks (Kang et al., 2010) while it is established that loading of cell with Ca^{2+}-sensitive dyes affects their intrinsic buffering capability (Yuste et al., 2000).

In contrast to *locus coeruleus*, the entire set of Ca_i and morphological imaging tools described above (**§2.2.3**, **2.1.3**) can be used for analyzing hippocampal ENOs. This will likely allow distinguishing different contributions of neuron (subtypes) and neighboring glia to processes involved in generation of ENOs. Moreover, it may be possible to study whether hampered interactions between these brain cell types are causally-related to perturbation of ENOs by anoxia and opioids (and possibly also methylxanthines), which is a primary research interest for our group (**1.**). To elucidate the roles of glia, further optical tools need to be applied for specifically discriminating astrocytes from oligodendrocytic glia and similarly small microglia of non-neural origin (Agulhon et al., 2008; Wang & Bordey, 2008; Ruangkittisakul et al., 2009; Ballanyi et al., 2010). Our established Ca_i and morphological imaging approaches are likely also suitable for analyzing neuron *versus* glia roles in cortical ENOs in newborn rat and piglet slices although we have not explored this in detail yet. For simultaneous electrophysiological imaging in different areas of (entorhinal) cortex, it needs to be considered that these ENOs propagate in a wave-like fashion (Garaschuk et al., 2000). In hippocampus, ENOs are typically most stable in the CA_3 area, which covers an area that extends for <500 µm. However, sometimes ENOs and related Ca_i oscilations are more prominent (and stable) in CA_1 regions. Consequently, it is difficult to position in hippocampus, cortex and *locus coeruleus* suction electrodes that have a short shank and outer diameters of 50-250 µm (**§2.1.5**, **2.2.2.1**) next to a patch electrode or a fluorescent dye-loaded area. While we found that suction electrode recording provides signals with excellent signal-to-noise ratio, much finer microelectrodes or slightly broken patch electrodes are traditionally used to record 'field' potentials provide a suitable alternative to record population activity next to imaged or patch-clamped cells (Ben-Ari et al., 1989, 2007;

Leinekugel et al., 1997, 2002; Khazipov & Luhmann, 2006; Sipilä et al., 2005, 2006; Sipilä & Kaila, 2008; Kafitz et al., 2008; Allene & Cossart, 2010).

Our preliminary findings indicate that whole-cell patch-clamp recording is feasible for time periods of up to several hours (mostly 0.5-1.5 h) from bursting *locus coeruleus* neurons as has also been reported by others (Christie et al., 1989; Ballantyne et al., 2004). It seems to be easier to initiate a whole-cell recording compared to neonatal respiratory neurons or dorsal vagal neurons *in vitro* [see chapters 1-Trapp & Ballanyi and 2-Ruangkittisakul et al.], but >50% of recordings are stable for only <10 min. Nevertheless, the success rate for >1 h whole-cell recording in *locus coeruleus* neurons is quite high overall. We have not yet established intracellular sharp microelectrode, whole-cell or perforated patch-clamp recording for analyzing hippocampal and cortical ENOs in the slices. However, all these approaches are feasible as indicated by extensive literature in that regard (Ben-Ari et al., 1989, 2007; Leinekugel et al., 1997, 2002; Khazipov & Luhmann, 2006; Sipilä et al., 2005, 2006; Sipilä & Kaila, 2008; Kafitz et al., 2008; Allene & Cossart, 2010).

2.5.3 Species Differences for Hippocampal and Cortical ENOs

We found that ENOs are less robust in hippocampus and entorhinal cortex of brain slices from newborn piglets compared to newborn rats. However, it needs to be considered that our data are based on preliminary findings from <10 animals and it took some effort to optimize all procedures between anesthetizing the animals and putting the cut slices into recovery solution. Accordingly, it is likely that with new series of experiments, a higher percentage of horizontal

slices would show more robust ENOs in the hippocampus and cortex. However, it is possible that ENOs in newborn piglets, which are more mature at birth and thus more resemble human newborns regarding brain development (Lind et al., 2007), are principally less regular than corresponding events in newborn rats. There may also be differences between brain regions regarding stability of ENOs because regular bursting was revealed in most somatosensory cortex slices. Moreover, Ca_i and morphological imaging seems feasible in somatosensory cortex, whereas we have yet no explanation why neuronal Ca_i imaging seems more difficult in hippocampus of piglet slices. Possibly, also this may improve with further technical refinement.

Figures

Fig. 2-1

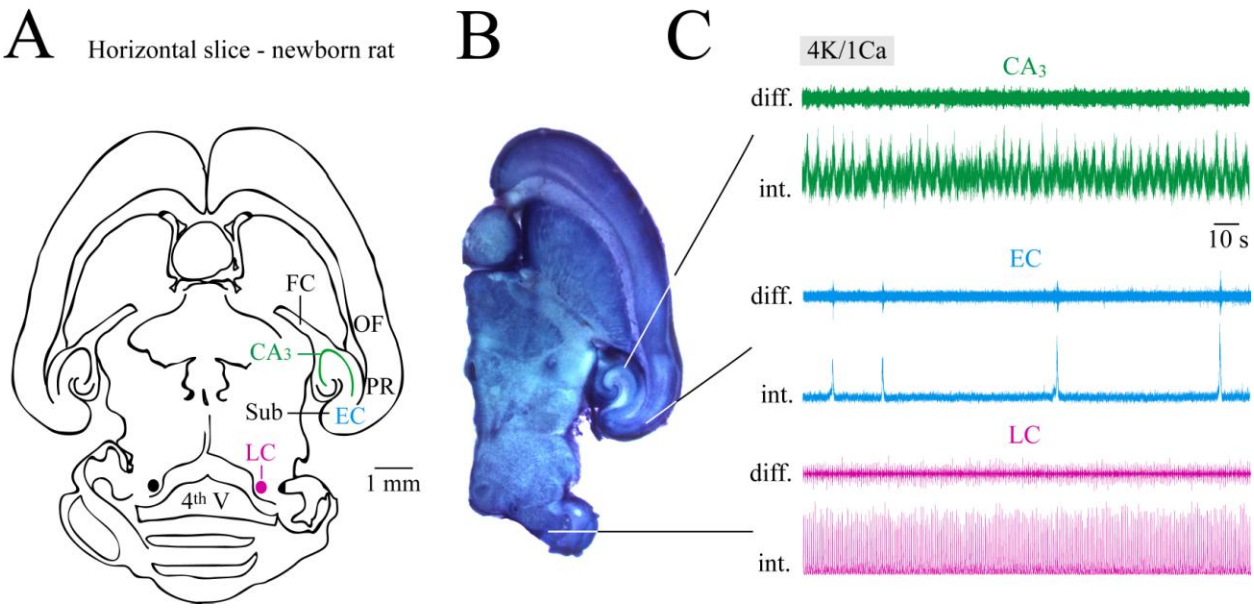

Fig. 2-1: Simultaneous suction electrode recording of spontaneous early network oscillations (ENOs) in horizontal newborn rat brain slices. A, schema of a horizontal brain section at a level that enables simultaneous recording of ENOs in both entorhinal cortex (EC) and the CA_3 hippocampal area (CA_3) plus ENO-like bursting in the brainstem area of the *locus coeruleus* (LC). Other abbreviations: FC, fornix commissure; OF, orbifrontal cortex; PR, perirhinal cortex, Sub, subiculum; 4^{th} V, fourth ventricle. **B**, detail from a paraformaldehyde-fixed and thionin-stained horizontal slice from a postnatal day (P) 1 Wistar rat old rat including the LC, EC and CA_3 regions. **C**, simultaneous suction electrode recordings from a 400 µm thick P1 Sprague-Dawley rat slice kept in superfusate containing (among other components) 4 mM K^+ and 1 mM Ca^{2+} (4K/1Ca) plus 20 mM glucose. Recordings of ENO (-like) bursting in the CA_3, EC and LC regions show the "raw" differentially amplified (x10k) and band-pass filtered (0.3-3 kHz) extracellular neural population signal before (upper traces) and after (lower traces) integration at a time constant of 20 ms using a "moving averager". Note that ENOs in the EC are typically the slowest events with a rate of 1-4 bursts/min whereas ENOs in the CA_3 area occur at 10-40 bursts/min and ENO-like bursting in the LC has a frequency of 0.5-3 Hz.

Fig. 2-2

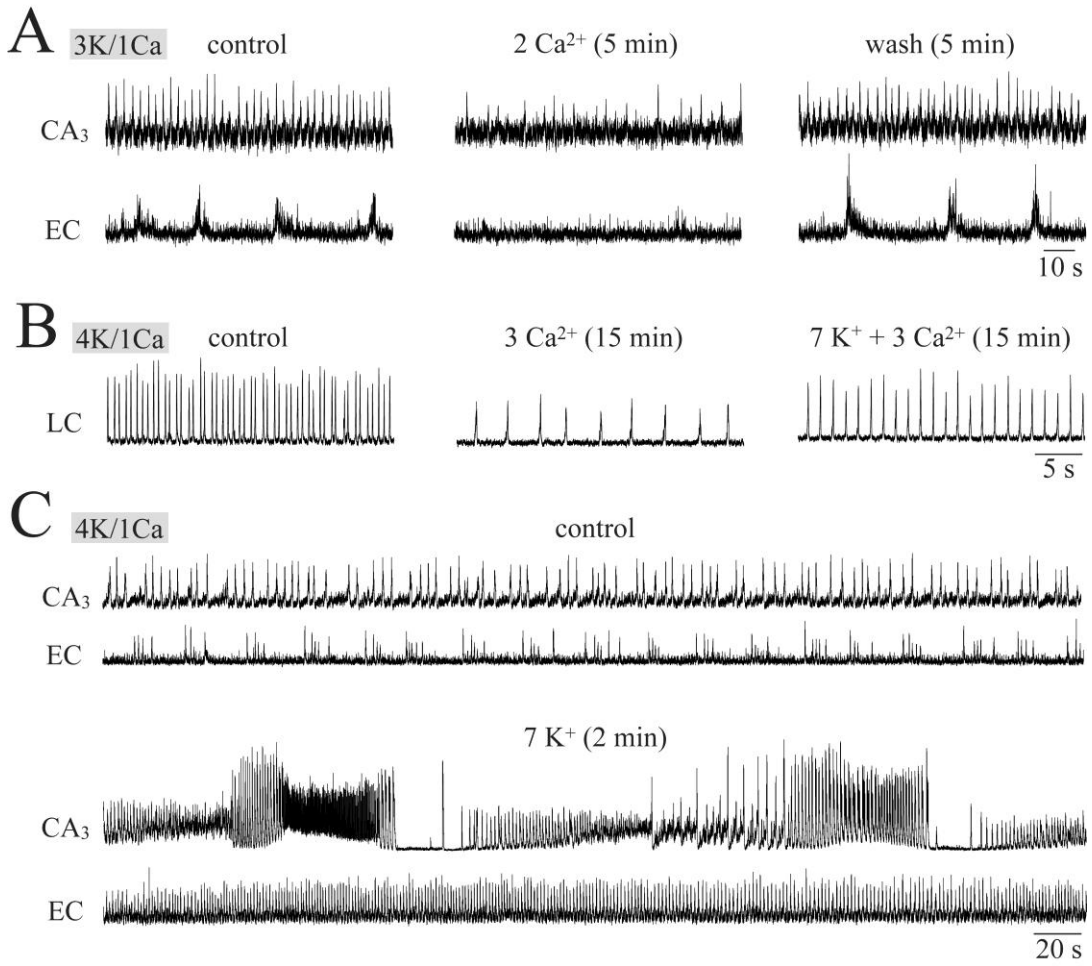

Fig. 2-2: Ca^{2+}/K^{+} antagonism of ENOs in horizontal newborn rat brain slices. A, simultaneous recording of ENOs in CA_3 and EC areas of a 500 µm thick P6 Wistar rat slice shows regular bursting in 3K/1Ca solution with 10 mM glucose. Within 5 min after start of bath-application of 2 mM Ca^{2+} in solution of otherwise identical composition, both types of ENOs were greatly depressed after 5 min, but recovered within 5 min after start of return to control superfusate. **B**, ENO-like LC bursting in a 400 µm thick slice from a P1 Wistar rat was inhibited by increasing the Ca^{2+} content of 4K/1Ca superfusate with 10 mM glucose to a total of 3 mM. This depression was partially reversed by also raising K^{+} to a total of 7 mM. **C**, in a 400 µm thick P10 Sprague-Dawley rat slice in 4K/1Ca solution with 20 mM glucose raising K^{+} to a total of 7 mM transformed the regular ENO pattern in the CA_3 region to large amplitude, seizure-like bursts interrupted by silent periods while ENOs in EC became faster and more uniform in amplitude.

Fig. 2-3

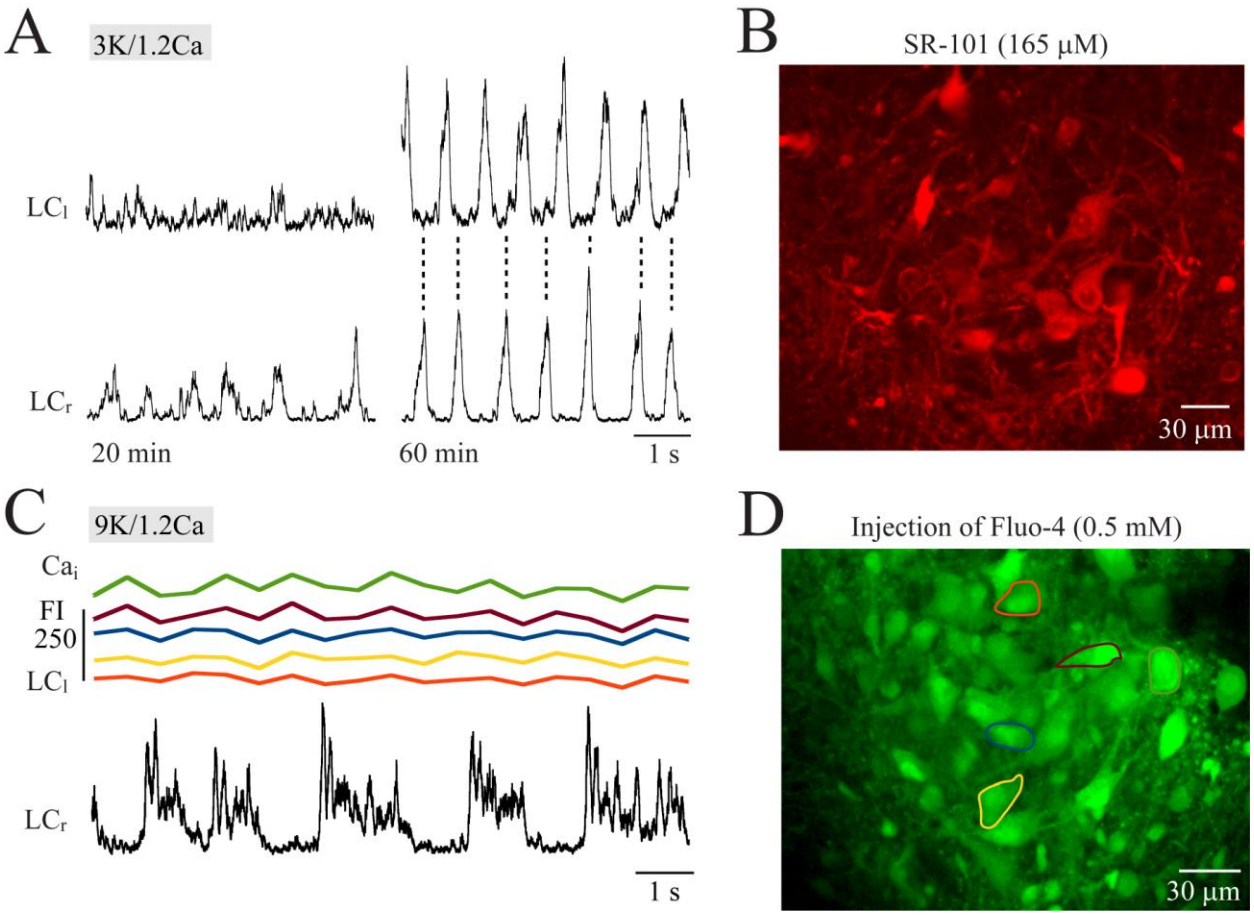

Fig. 2-3: Imaging of ENO-like bursts in the bilaterally organized LC of horizontal newborn rat slices. A, simultaneous suction electrode recording of rhythms in both LC aspects of a 400 µm thick P2 Wistar rat slice in 3K/1.2Ca solution with 10 mM glucose. As indicated here, it can last up to 1 h until the amplitudes of the asynchronous bursts reach steady-state. **B**, morphology of the neuron-glia network in one LC aspect as revealed upon loading of a 400 µm thick P2 Wistar rat slice that was incubated for 1 h at 22 ^{o}C in standard superfusate containing 165 µM of the red fluorescent dye sulforhodamine-101 (SR-101). Cells with a soma diameter of 20-35 µm likely represent neurons, whereas cells with a soma diameter of ~10 µm are presumably astrocytic glial cells. Thus, note that SR-101 does not show preferential staining in neurons *vs* glia in LC. **C**, LC bursting often occurs at rates of >1 Hz, which is beyond the binding/unbinding kinetics of commonly used Ca^{2+}-sensitive dyes such as Fluo-8L-AM (see also **Figs. 11.7, 11.8, 11.10**). Therefore, burst-related rises of the free cytosolic Ca^{2+} concentration (Ca_i) are typically

of small amplitude in standard 3K/1.2Ca solution. Lowering superfusate Ca^{2+} to 0.5 mM or raising K^+ to 7-9 mM may transform the pattern of the ENO-like rhythm to longer lasting bursts that can be reflected by periodic Ca_i increases as labeled in relative units of fluorescence intensity (FI) here. Each Ca_i trace was measured in neuronal soma regions that are outlined in the image in **D** by regions of interest (ROIs) using Fluoview software of the FV-300 Olympus confocal laser scan imaging system. Cells were loaded with the membrane-permeant (AM) form of Ca^{2+}-sensitive Fluo-4 via pressure injection into the LC using a broken patch electrode. The 'sharp' shape of the Ca_i peaks is due to the slow scan rate of 0.58 s/frame. Note that this or slower scan rates are sufficient to resolve the peak of rhythmic Ca_i rises in the EC or CA_3 areas (see **Figs. 11.7, 11.8, 11.10**). **D**, shows the imaged area from which the traces in **C** were derived. The image represents the tissue level of ~30 µm and is part of a 'z-stack' between slice surface and 50 µm obtained after bath-application of 0.5 mM glutamate for 10 min using the confocal laser scan Olympus system for a better visualization of neuronal morphology. Movies for **B**, **C** and **D** are shown in the *Supplemental Web Material*.

Fig. 2-4

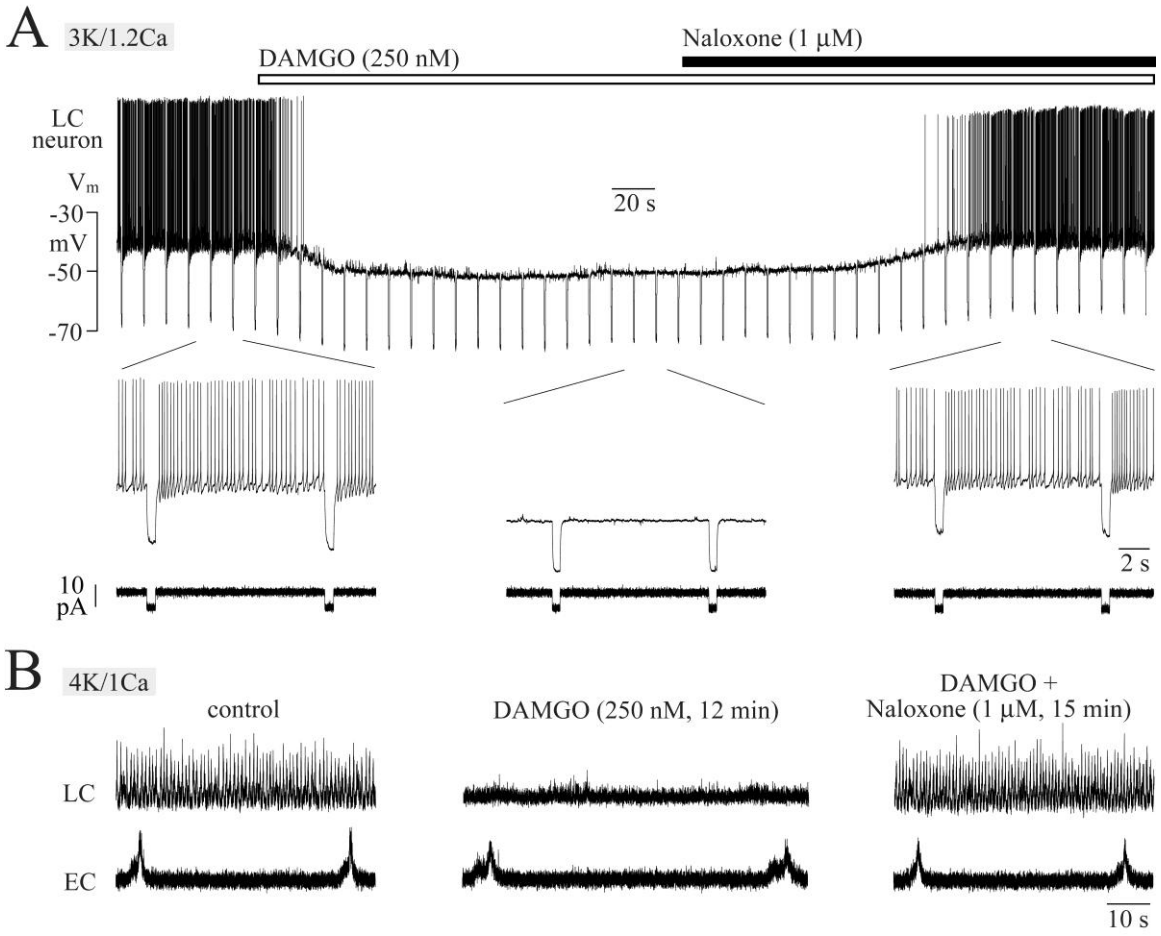

Fig. 2-4: Differential effects of opioids on cortical ENOs and ENO-like bursting in LC of horizontal newborn rat slices. A, 'blind' whole-cell patch-clamp recording from a LC neuron in a 400 µm thick brain P2 Wistar rat slice in 3K/1.2Ca superfusate with 10 mM glucose. A persistent membrane potential (V_m) hyperpolarization in response to bath-application of the µ-opioid receptor agonist [D-Ala2, N-MePhe4, Gly-ol]-enkephalin (DAMGO) was not accompanied by a major change in membrane resistance measured upon repetitive injection of a 8 pA hyperpolarizing DC current pulse (see lower trace of insets at higher time resolution). The DAMGO-evoked hyperpolarization and resulting inhibition of spontaneous 'tonic' action potential discharge were reversed by adding the opioid receptor antagonist naloxone. **B**, ENO-like LC bursting in 4K/1Ca solution with 20 mM glucose in a 400 µm thick P2 Sprague-Dawley rat slice was abolished in naloxone-sensitive fashion by DAMGO whereas simultaneously recorded ENOs in the EC of the same slice were not profoundly affected.

Fig. 2-5

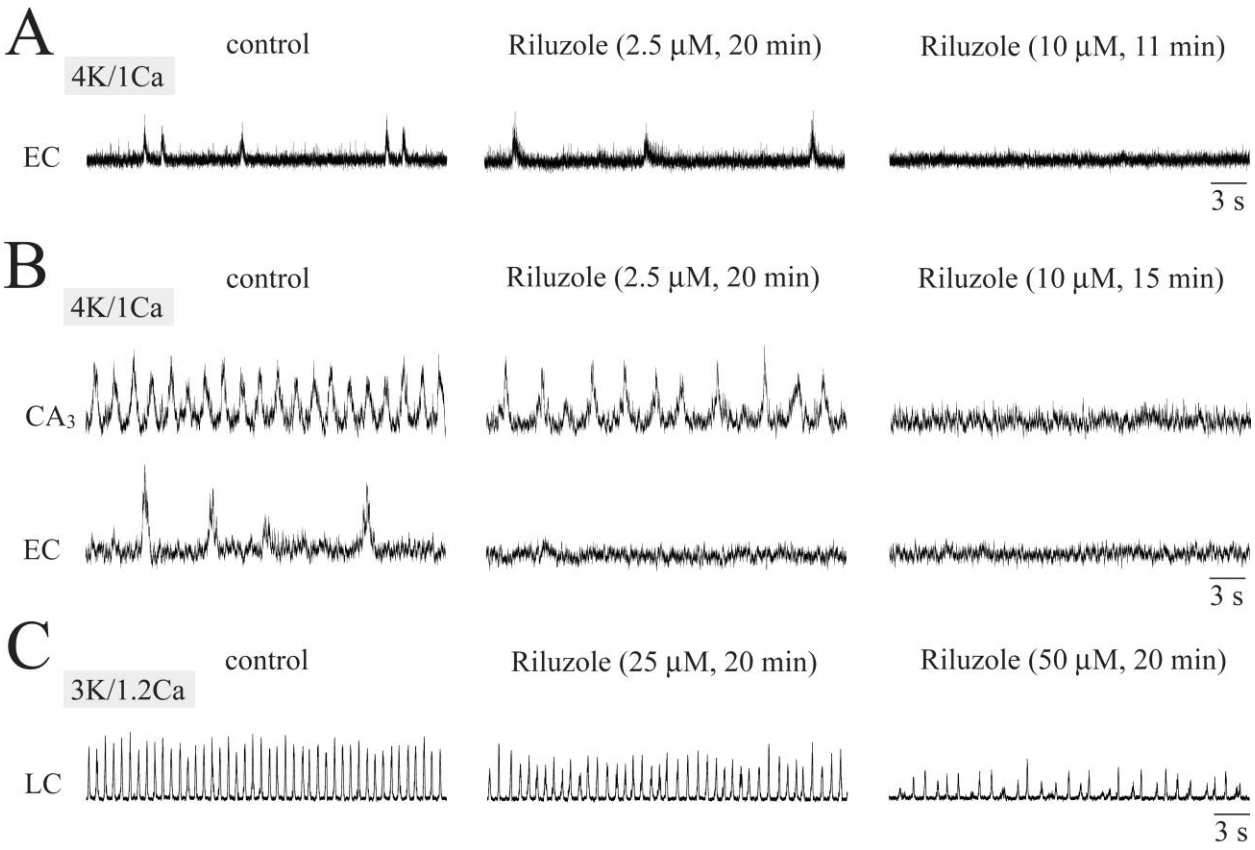

Fig. 2-5: Involvement of persistent Na^+ channels in ENOs of horizontal newborn rat brain slices. A, ENOs were recorded in 4K/1Ca superfusate with 10 mM glucose in the EC region of a 500 µm thick P0 Wistar rat slice. These events were not affected by bath-application of 2.5 µM of riluzole, a blocker of the 'persistent' sub-type of voltage-activated Na^+ channels, but were abolished within 11 min following bath-application of the agent at 10 µM. **B**, in a 500 µm thick slice from a P7 Wistar rat ENOs in 4K/1Ca superfusate with 20 mM glucose in the EC region were abolished within 20 min by application of 2.5 µM riluzole whereas 10 µM of the drug were necessary to block ENOs in the CA_3 region of the same slice. **C**, rhythmic bursting in 3K/1.2Ca superfusate with 10 mM glucose in the LC region of a 400 µm thick P1 Wistar rat slice were not affected by 25 µM riluzole while bursting was notably depressed 20 min after bath-application of 50 µM of the agent. Note that riluzole effects were typically irreversible.

Fig. 2-6

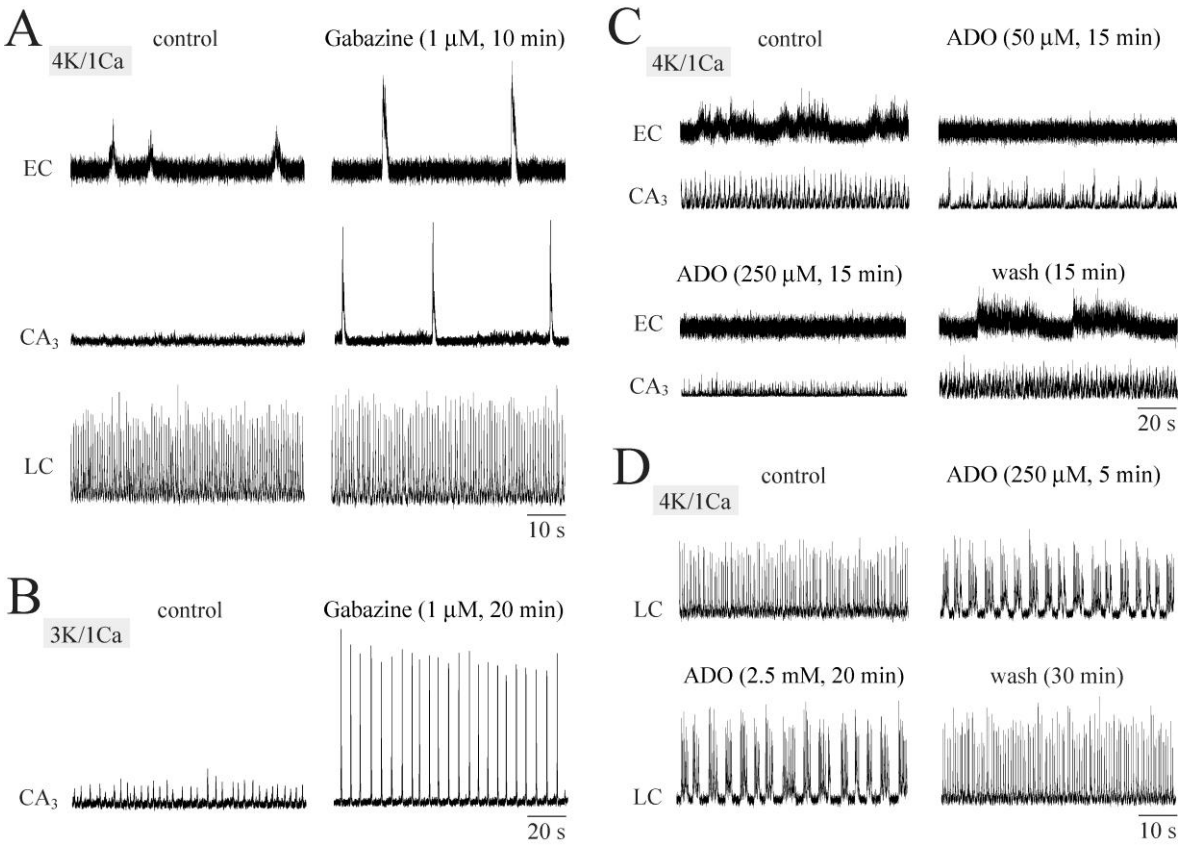

Fig. 2-6: Differential modulation by (anti)convulsant agents of bursting in CA_3, EC and LC regions of horizontal newborn rat slices. A, bath-application in 4K/1Ca solution with 10 mM glucose of the pharmacological 'seizure model' gabazine, an antagonist of A-type γ-aminobutyric acid ($GABA_A$) receptors, caused large amplitude bursting in both CA_3 and EC areas of a 400 µm thick P4 Wistar rat slice. Contrary, LC bursting in the same slice was not affected. **B**, in the CA_3 region of a 500 µm thick P6 Wistar rat slice in 3K/1Ca superfusate with 10 mM glucose, ENOs were transformed by gabazine into seizure-like large amplitude bursts of similar rate. **C**, ENOs in both the CA_3 and EC area of a 400 µm thick P8 Wistar rat slice in 4K/1Ca superfusate with 20 mM glucose were reversibly abolished upon bath-application of the 'endogenous anticonvulsant' adenosine (ADO). Note that hippocampal ENOs were more resistant to ADO than ENOs in the EC region in this experiment. **D**, in a 400 µm thick P1 Wistar rat slice in 4K/1Ca superfusate with 20 mM glucose LC bursting was not abolished even by 2.5 mM ADO while the agent notably transformed burst pattern already at 250 µM.

Fig. 2-7

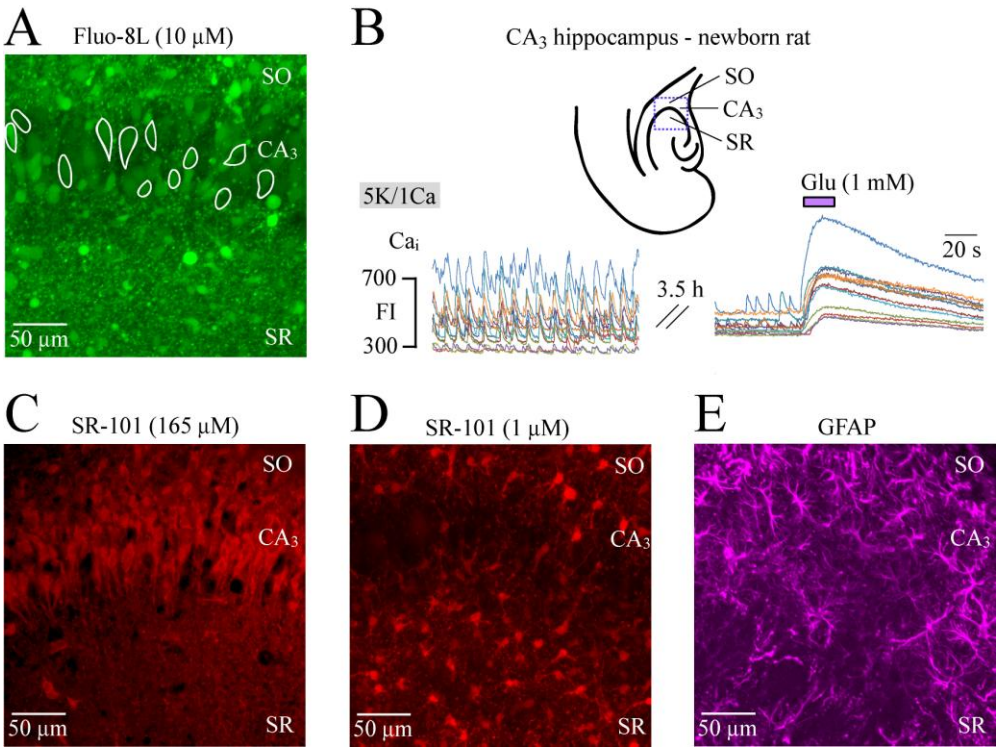

Fig. 2-7: Neuron-glia imaging in CA_3 hippocampal area of horizontal newborn rat slices. A, incubation of a 400 µm thick P3 Wistar rat slice with 10 µM of the membrane-permeant, AM form of the Ca^{2+}-sensitive dye Fluo-8L resulting in loading of neurons in the CA_3 layer and (astrocytic) glia that are densely packed particularly in *stratum radiatum* (SR) and *stratum oriens* (SO) (see also **C**-**E**). The image represents a summated z-stack of images at 0.5 µm steps in a tissue depth between 0-50 µm below the slice surface (see also **Fig. 11.3**). **B**, colored traces show the kinetics of spontaneous, mostly synchronous Ca_i rises in 4K/1Ca solution 10 mM glucose in somatic areas of CA_3 neurons indicated by the ROIs in **A**. Traces in the right part illustrate that Ca_i baseline is still low after 3.5 h of (non-continuous) imaging and that the amplitude of a Ca_i rise associated with bath-application of glutamate (Glu) for 20 s is notably larger than spontaneous Ca_i increases. **C**, morphology of CA_3 neurons revealed following incubation of a 400 µm thick P3 Wistar rat slice for 1 h at 20-23 ^oC with 165 µM of SR-101. **D**, incubation for 0.5 h with 1 µM SR-101 at 34 ^oC resulted in staining of presumptive astrocytes in a 400 µm thick P4 Wistar rat slice. **E**, in a 400 µm thick P10 Wistar rat slice, immunohistochemical staining (details in Methods) for glial fibrillary acidic protein (GFAP) to identify astrocytes. Movies for **A**,**C**-**E** are provided in *Supplemental Web Material*.

Fig. 2-8

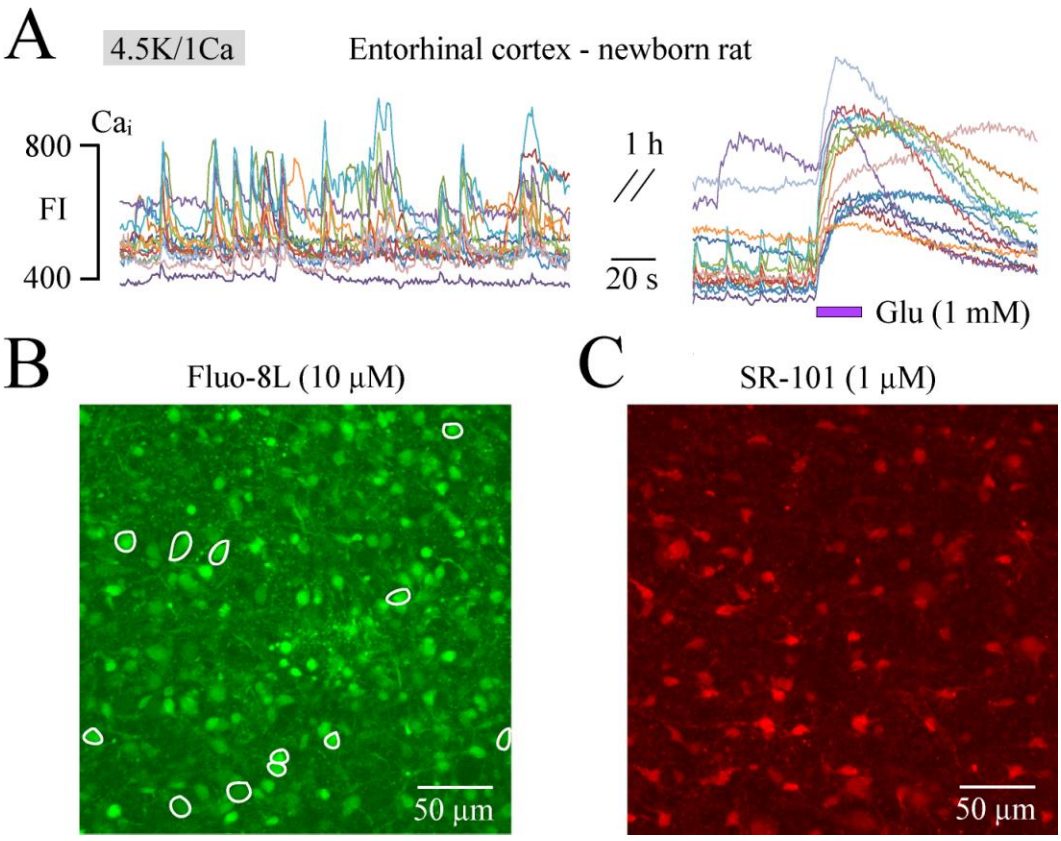

Fig. 2-8: Neuron-Glia imaging in EC of horizontal newborn rat slices. A, colored traces show the kinetics of spontaneous Ca_i rises in 4.5K/1Ca solution with 20 mM glucose in the soma regions (indicated by ROIs in the image of **B**) of neurons and glial cells located 15 µm below the slice surface of a 400 µm thick P1 Wistar rat slice loaded with Fluo-8L by incubation. As is more evident from the movie in *Supplemental web material*, these Ca^{2+} rises occur (synchronously) in small clusters of up to several dozens of cells. Traces in the right show that cells are still active and responsive to bath-applied Glu after long term (non-continuous) recording. The movie in the *Supplemental Web Material* illustrates that almost all cells in the imaged area respond to Glu. **B**, shows the area imaged in **A** at the peak of the Glu response, with ROIs around the somata of cells whose Cai responses are shown in **A** (see also **Figs. 11.3**, **11.7**). **C**, In a different 400 µm thick P7 Wistar rat slice loading with 1 µM SR-101 at 34 ^{o}C resulted in staining of presumptive astrocytes. Movies for **B**, **C** and **D** are shown in the *Supplemental Web Material*.

Fig. 2-9

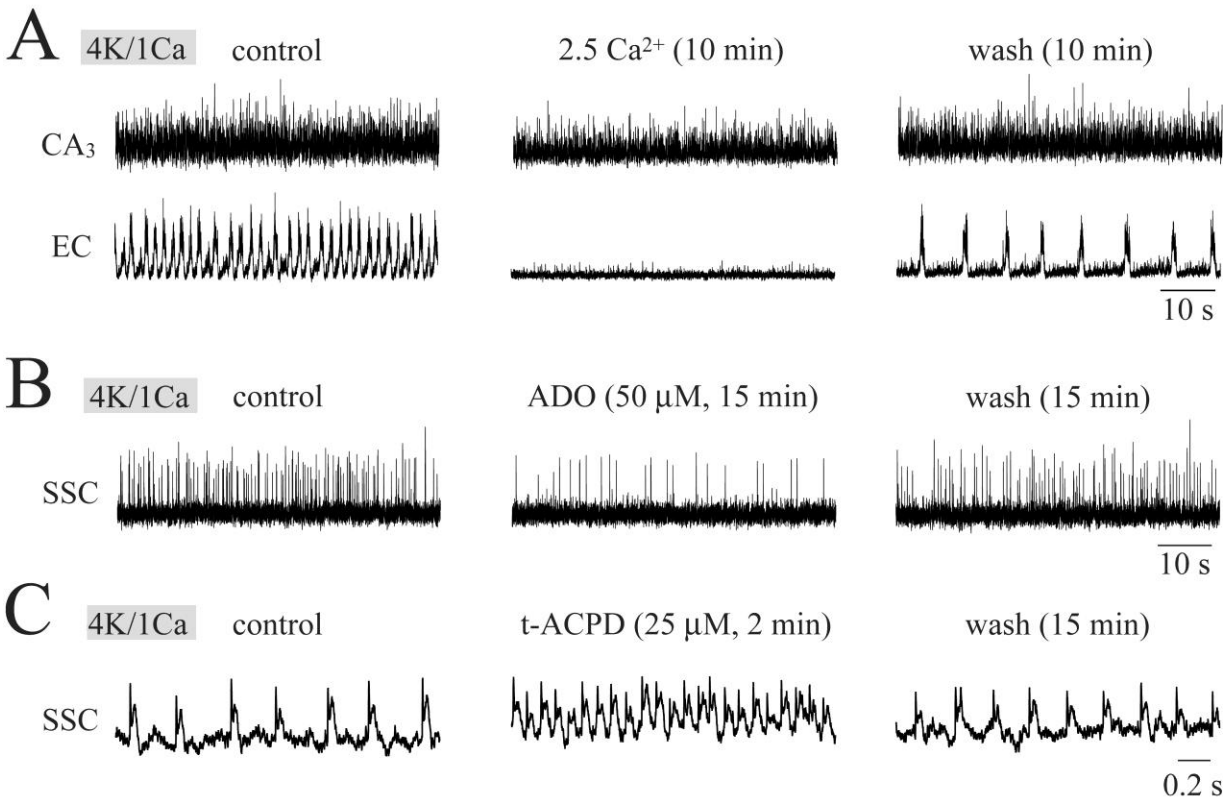

Fig. 2-9: ENOs in horizontal and coronal slices from newborn piglet. A, ENOs in 4K/1Ca superfusate with 10 mM glucose were simultaneously recorded with suction electrodes in the CA_3 and EC region of a 400 µm thick horizontal P4 piglet slice. Raising Ca^{2+} by 1.5 mM to a total of 2.5 mM reversibly abolished ENOs in the EC, whereas CA_3 bursting was only attenuated. **B**, ENOs in 4K/1Ca superfusate with 10 mM glucose in the somatosensory cortex (SSC) of a 300 µm thick coronal P4 piglet slice were reversibly attenuated by ADO. **C**, ENOs in 4K/1Ca solution with 20 mM glucose in the SSC region of 500 µm thick coronal P3 piglet slice were notably accelerated upon bath-application of the metabotropic glutamate receptor agonist trans-1-aminocyclopentane-1,3-dicarboxylic acid (t-ACPD).

Fig. 2-10

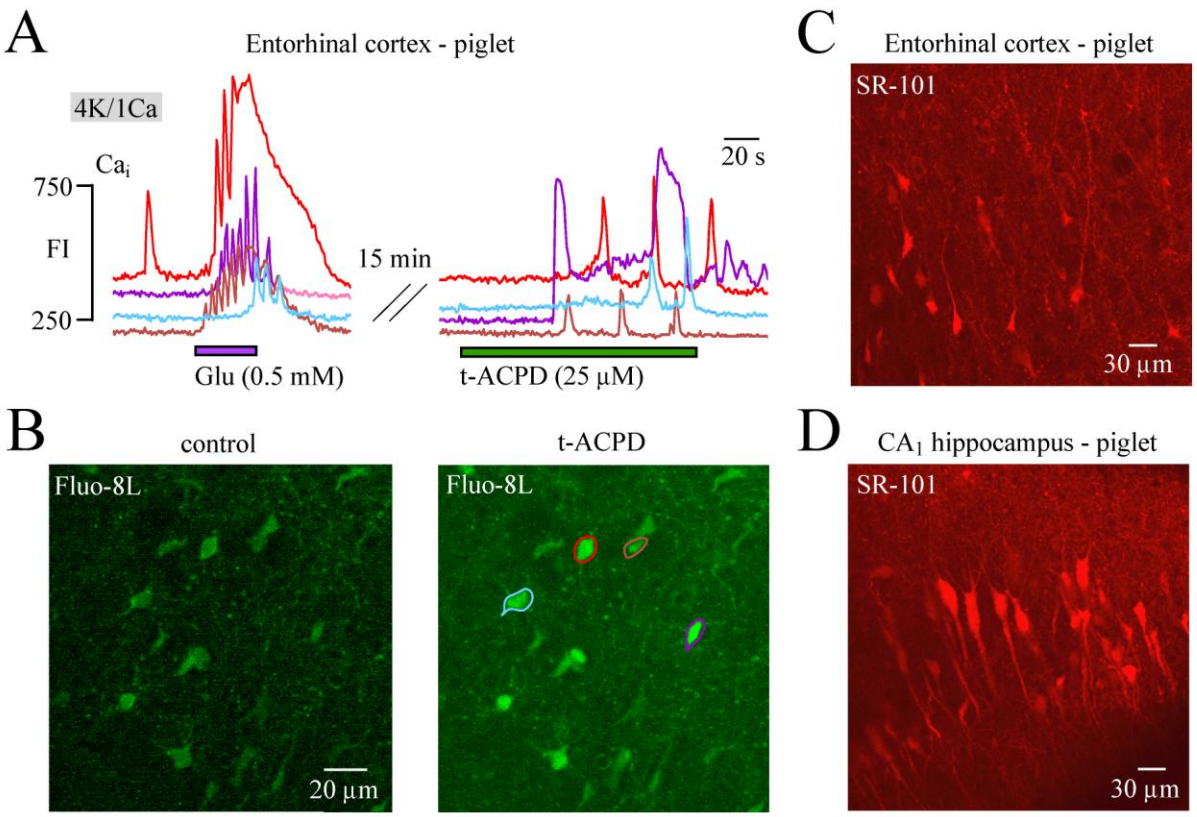

Fig. 2-10: Ca_i dynamics and morphological cellular features in horizontal newborn piglet slices. A, bath-application of glutamate (Glu) for 30s led to prominent Ca_i increase in cells in the EC region of a 500 µm thick horizontal P2 piglet slice loaded via incubation with 10 µM Fluo-8L. Exposure to 2 min of t-ACPD 15 min later evoked partly oscillatory Ca_i rises. **B**, shows in the right image the area imaged in **A** with ROIs around the somata of the cells whose Ca_i responses are shown in **A**. The image in the left shows baseline fluorescence in control, while the right image shows the summated image (over 100 s) during the peak of t-ACPD response. **C**, in a 500 µm thick horizontal P3 piglet slice incubation with 165 µM SR-101 at 22 ^{o}C revealed the morphology of neurons in the EC region. **D**, in a 500 µm thick horizontal P3 piglet slice corresponding incubation with SR-101 results in staining of neurons in the CA_1 area. Movies for **B**, **C** and **D** are shown in the *Supplemental Web Material*.

2.6 References

Agulhon C, Petravicz J, McMullen AB, Sweger EJ, Minton SK, Taves SR, Casper KB, Fiacco TA, McCarthy KD (2008) What is the role of astrocyte calcium in neurophysiology? Neuron 59, 932-946

Allene C, Cossart R (2010) Early NMDA receptor-driven waves of activity in the developing neocortex: physiological or pathological network oscillations? J Physiol 588, 83-91

Aston-Jones G, Cohen JD (2005) An integrative theory of locus coeruleus-norepinephrine function: adaptive gain and optimal performance. Annu Rev Neurosci 28, 403-450

Ballantyne D, Andrzejewski M, Mückenhoff K, Scheid P (2004) Rhythms, synchrony and electrical coupling in the Locus coeruleus. Respir Physiol Neurobiol 143, 199-214

Ballanyi K (1999) Isolated tissues: in vitro preparations. In: Windhorst U, Johansson H (eds) Modern Techniques in Neuroscience Research, Springer, Heidelberg, pp 307-326

Ballanyi K (2004a) Protective role of neuronal K_{ATP} channels in brain hypoxia. J Exp Biol 207, 3201-3212

Ballanyi K (2004b) Neuromodulation of the perinatal respiratory network. Curr Neuropharmacol 2, 221-243

Ballanyi K (2012) Isolated Central Nervous System Circuits. Neuromethods Series (Ed. W. Walz). Springer Science+Business Media, LLC, New York, NY (*in press*).

Ballanyi K, Grafe P (1985) An intracellular analysis of γ-aminobutyric-acid-associated ion movements in rat sympathetic neurones. J Physiol 365, 41-58

Ballanyi K, Ruangkittisakul A (2009a) Structure-function analysis of rhythmogenic inspiratory pre-Botzinger complex networks in "calibrated" newborn rat brainstem slices. Respir Physiol Neurobiol 168, 158-178

Ballanyi K, Ruangkittisakul A (2009b) Brain slices. In: Binder M, Hirokawa N, Windhorst U (eds). Encyclopedia of Neuroscience, Springer Verlag, Heidelberg, New York, Tokyo, pp. 483-490

Ballanyi K, Onimaru H, Homma I (1999) Respiratory network function in the isolated brainstem-spinal cord of newborn rats. Progr Neurobiol 59, 583-634

Ballanyi K, Panaitescu B, Ruangkittisakul A (2010) Control of breathing by nerve glue. Sci Signal 3, pe41

Ballanyi K, Ruangkittisakul A, Onimaru H (2009) Opioids increase and anoxia decreases delay of rhythmogenic pre-inspiratory (pFRG) and inspiratory (preBötC) network bursts in newborn rat brainstems. Eur J Physiol (Pflüger's Arch) 458, 571-587

Ben-Ari Y, Cherubini E, Corradetti R, Gaiarsa JL (1989) Giant synaptic potentials in immature rat CA3 hippocampal neurones. J Physiol 416, 303-325

Ben-Ari Y, Gaiarsa JL, Tyzio R, Khazipov R (2007) GABA: a pioneer transmitter that excites immature neurons and generates primitive oscillations. Physiol Rev 87, 1215-1284

Blaesse P, Airaksinen MS, Rivera C, Kaila K (2009) Cation-chloride cotransporters and neuronal function. Neuron 61, 820-838

Bonifazi P, Goldin M, Picardo MA, Jorquera I, Cattani A, Bianconi G, Represa A, Ben-Ari Y, Cossart R (2009) GABAergic hub neurons orchestrate synchrony in developing hippocampal networks. Science 326, 1419-1424

Brockmann MD, Pöschel B, Cichon C, Hanganu-Opatz IL (2011) Coupled Oscillations Mediate Directed Interactions between Prefrontal Cortex and Hippocampus of the Neonatal Rat. Neuron 71, 332-347

Broicher T, Speckmann EJ (2012) Living human brain slices: network analysis using voltage sensitive dyes. In: Isolated Central Nervous System Circuits (Ed K Ballanyi), Neuromethods Series (Ed W Walz). Springer Science+Business Media, LLC, New York, NY (*in press*)

Christie MJ, Williams JT, North RA (1989) Electrical coupling synchronizes subthreshold activity in locus coeruleus neurons in vitro from neonatal rats. J Neurosci 9, 3584-3589

Craner SL, Ray RH (1991) Somatosensory cortex of the neonatal pig: I. Topographic organization of the primary somatosensory cortex (SI). J Comp Neurol 306, 24-38

De Curtis M, Lilbrizzi L, Uva L, Gnatkovsky V (2012) Neuronal Networks in the in vitro Isolated Guinea Pig Brain. In: Isolated Central Nervous System Circuits (Ed K Ballanyi), Neuromethods Series (Ed W Walz). Springer Science+Business Media, LLC, New York, NY (*in press*)

Feldman JL, Del Negro CA (2006) Looking for inspiration: new perspectives on respiratory rhythm. Nat Rev Neurosci 7, 232-242

Fish KN, Gonzales-Burgos G, Zaitsev AV, Lewis DA (2012) Histological characterization of physiologically determined fast spiking interneurons in slices of the primate dorsolateral prefrontal cortex. In: Isolated Central Nervous System Circuits (Ed K Ballanyi), Neuromethods Series (Ed W Walz). Springer Science+Business Media, LLC, New York, NY (*in press*)

Garaschuk O, Linn J, Eilers J, Konnerth A (2000) Large-scale oscillatory calcium waves in the immature cortex. Nat Neurosci. 3, 452-459

Jantzie LL, Cheung PY, Johnson ST, Bigam DL, Todd KG (2010) Cerebral amino acid profiles after hypoxia-reoxygenation and N-acetylcysteine treatment in the newborn piglet. Neonatology 97, 195-203

Jefferys JG (1994) Experimental neurobiology of epilepsies. Curr Opin Neurol 7, 113-122

Kafitz KW, Meier SD, Stephan J, Rose CR (2008) Developmental profile and properties of sulforhodamine 101-Labeled glial cells in acute brain slices of rat hippocampus. J Neurosci Methods 169, 84-92

Kang J, Kang N, Yu Y, Zhang J, Petersen N, Tian GF, Nedergaard M (2010) Sulforhodamine 101 induces long-term potentiation of intrinsic excitability and synaptic efficacy in hippocampal CA1 pyramidal neurons. Neuroscience 169, 1601-1609

Keifer J, Vyas D, Houk JC (1992) Sulforhodamine labeling of neural circuits engaged in motor pattern generation in the in vitro turtle brainstem-cerebellum. J Neurosci 12, 3187-3199

Khazipov R, Luhmann HJ (2006) Early patterns of electrical activity in the developing cerebral cortex of humans and rodents. Trends Neurosci 29, 414-418

Kulik A, Nishimaru H, Ballanyi K (2000) Role of bicarbonate and chloride in GABA- and glycine-induced depolarization and $[Ca^{2+}]_i$ rise in fetal rat motoneurons in situ. J Neurosci 20, 7905-7913

Leinekugel X, Khazipov R, Cannon R, Hirase H, Ben-Ari Y, Buzsáki G (2002) Correlated bursts of activity in the neonatal hippocampus in vivo. Science 296, 2049-2052

Leinekugel X, Medina I, Khalilov I, Ben-Ari Y, Khazipov R (1997) Ca^{2+} oscillations mediated by the synergistic excitatory actions of $GABA_A$ and NMDA receptors in the neonatal hippocampus. Neuron 18, 243-255

Lind NM, Moustgaard A, Jelsing J, Vajta G, Cumming P, Hansen AK (2007) The use of pigs in neuroscience: Modeling brain disorders. Neurosci. Biobehavioral Rev 31, 728-751

Lingwood BE, Healy GN, Sullivan SM, Pow DV, Colditz PB (2008) MAP2 provides reliable early assessment of neural injury in the newborn piglet model of birth asphyxia. J Neurosci Methods 171, 140-146

Lombroso CT (2007) Neonatal seizures: gaps between the laboratory and the clinic. Epilepsia 48, 83-106

Mandal R, Anderson CW (2009) Anatomical organization of brainstem circuits mediating feeding motor programs in the marine toad, Bufo marinus. Brain Res 1298, 99-110

Martin LJ, Brambrink A, Koehler RC, Traystman RJ (1997) Primary sensory and forebrain motor systems in the newborn brain are preferentially damaged by hypoxic-ischemia. J Comp Neurol 377, 262-285

Metzger F, Klapproth N, Kulik A, Sendtner M, Ballanyi K (2005) Optical assessment of motoneuron function in a "twenty-four-hour" acute spinal cord slice model from fetal rats. J Neurosci Methods 141, 309-320

Milh M, Kaminska A, Huon C, Lapillonne A, Ben-Ari Y, Khazipov R (2007) Rapid cortical oscillations and early motor activity in premature human neonate. Cereb Cortex 17, 1582-1594

Moore AR, Zhou WL, Jakovcevski I, Zecevic N, Antic SD (2012) Physiological properties of human fetal cortex in vitro. In: Isolated Central Nervous System Circuits (Ed K Ballanyi), Neuromethods Series (Ed W Walz). Springer Science+Business Media, LLC, New York, NY (*in press*)

Moriceau S, Roth TL, Sullivan RM (2010) Rodent model of infant attachment learning and stress. Dev Psychobiol 52, 651-660

Nakamura S, Kimura F, Sakaguchi T (1987) Postnatal development of electrical activity in the locus coeruleus. J Neurophysiol 58, 510-524

Nakamura TJ, Michel S, Block GD, Colwell CS (2012) Neural circuits underlying circadian oscillations in mammals: clocks in a dish. In: Isolated Central Nervous System Circuits (Ed K Ballanyi), Neuromethods Series (Ed W Walz). Springer Science+Business Media, LLC, New York, NY (*in press*)

Neher E, Sakmann B (2009) Single-channel recording. 2nd ed. Springer, New York, Dordrecht, Heidelberg, London

Nimmerjahn A, Kirchhoff F, Kerr JN, Helmchen F (2004) Sulforhodamine 101 as a specific marker of astroglia in the neocortex in vivo. Nat Methods 1, 31-37

Ocaña M, Cendán CM, Cobos EJ, Entrena JM, Baeyens JM (2004) Potassium channels and pain: present realities and future opportunities. Eur J Pharmacol 500, 203-219

O'Donovan MJ, Bonnot A, Mentis GZ, Arai Y, Chub N, Shneider NA, Wenner P (2008) Imaging the spatiotemporal organization of neural activity in the developing spinal cord. Dev Neurobiol 68, 788-803

Panaitescu B, Ruangkittisakul A, Ballanyi K (2009) Silencing by raised extracellular Ca^{2+} of pre-Bötzinger complex neurons in newborn rat brainstem slices without change of membrane potential or input resistance. Neurosci Lett 456, 25-29

Ruangkittisakul A, Ballanyi K (2009) Neuron-glia-imaging. In: Binder M, Hirokawa N, Windhorst U (eds) Encyclopedia of Neuroscience. Springer Verlag, Heidelberg, New York, Tokyo, pp. 2756-2764

Ruangkittisakul A, Ballanyi K (2010) Methylxanthine reversal of opioid-evoked inspiratory depression via phosphodiesterase-4 blockade. Respir Physiol Neurobiol 172, 94-105

Ruangkittisakul A, Panaitescu B, Ballanyi K (2011) K^+ and Ca^{2+} dependence of inspiratory-related rhythm in novel "calibrated" mouse brainstem slices. Resp Physiol Neurobiol 175, 37-48

Ruangkittisakul A, Okada Y, Oku Y, Koshiya N, Ballanyi K (2009) Fluorescence imaging of active respiratory networks, Respir Physiol Neurobiol 168, 26-38

Ruangkittisakul A, Secchia L, Bornes TD, Palathinkal DM, Ballanyi K (2007) Dependence on extracellular Ca^{2+}/K^+ antagonism of inspiratory centre rhythms in slices and en bloc preparations of newborn rat brainstem. J Physiol 584, 489-508

Ruangkittisakul A, Schwarzacher SW, Secchia L, Poon BY, Ma Y, Funk GD, Ballanyi K (2006) High sensitivity to neuromodulator-activated signaling pathways at physiological $[K^+]$ of confocally imaged respiratory center neurons in on-line-calibrated newborn rat brainstem slices. J Neurosci 26, 11870-11880

Ruangkittisakul A, Schwarzacher SW, Secchia L, Ma Y, Bobocea N, Poon BY, Funk GD, Ballanyi K (2008) Generation of eupnea and sighs by a spatiochemically organized inspiratory network. J Neurosci 28, 2447-2458

Ruangkittisakul A, Secchia-Ballanyi L, Panaitescu B, Bobocea N, Kuribayashi J, Iizuka M, Kantor C, Ballanyi K (2012) Anatomically ‘calibrated‘ isolated respiratory networks from newborn rodents. In: Isolated Central Nervous System Circuits (Ed K Ballanyi), Neuromethods Series (Ed W Walz). Springer Science+Business Media, LLC, New York, NY (*in press*)

Ruusuvuori E, Kirilkin I, Pandya N, Kaila K (2010) Spontaneous network events driven by depolarizing GABA action in neonatal hippocampal slices are not attributable to deficient mitochondrial energy metabolism. J Neurosci 30, 15638-15642

Safiulina VF, Kasyanov AM, Giniatullin R, Cherubini E (2005) Adenosine down-regulates giant depolarizing potentials in the developing rat hippocampus by exerting a negative control on glutamatergic inputs. J Neurophysiol 94, 2797-2804

Sanchez-Vives MV (2012) Spontaneous rhythmic activity in the adult cerebral cortex in vitro. In: Isolated Central Nervous System Circuits (Ed K Ballanyi), Neuromethods Series (Ed W Walz). Springer Science+Business Media, LLC, New York, NY (*in press*)

Sipilä ST, Kaila K (2008) GABAergic control of CA3-driven network events in the developing hippocampus. Results Probl Cell Differ 44, 99-121

Sipilä ST, Huttu K, Voipio J, Kaila K (2006) Intrinsic bursting of immature CA3 pyramidal neurons and consequent giant depolarizing potentials are driven by a persistent Na^+ current and terminated by a slow Ca^{2+} -activated K^+ current. Eur J Neurosci 23, 2330-2338

Sipilä ST, Huttu K, Soltesz I, Voipio J, Kaila K (2005) Depolarizing GABA acts on intrinsically bursting pyramidal neurons to drive giant depolarizing potentials in the immature hippocampus. J Neurosci 25, 5280-5289

Smith JC, Ellenberger HH, Ballanyi K, Richter DW, Feldman JL (1991) Pre-Bötzinger complex: a brainstem region that may generate respiratory rhythm in mammals. Science 254, 726-729

Somjen GG (2002) Ion Regulation in the brain: implications for pathophysiology. Neuroscientist 8, 254-267

Spitzer NC (2006) Electrical activity in early neuronal development. Nature 444, 707-712

Stosiek C, Garaschuk O, Holthoff K, Konnerth A (2003) In vivo two-photon calcium imaging of neuronal networks. Proc Natl Acad Sci USA 100, 7319-7324

Teppema LJ, Baby S (2011) Anesthetics and control of breathing. Respir Physiol Neurobiol 177, 80-92

Trapp S, Ballanyi K (2012) Autonomic nervous system in vitro: studying tonically active neurons controlling vagal outflow in rodent brainstem slices In: Isolated Central Nervous System Circuits (Ed K Ballanyi), Neuromethods Series (Ed W Walz). Springer Science+Business Media, LLC, New York, NY (*in press*)

Tyzio R, Allene C, Nardou R, Picardo MA, Yamamoto S, Sivakumaran S, Caiati MD, Rheims S, Minlebaev M, Milh M, Ferré P, Khazipov R, Romette JL, Lorquin J, Cossart R, Khalilov I, Nehlig A, Cherubini E, Ben-Ari Y (2011) Depolarizing actions of GABA in immature neurons depend neither on ketone bodies nor on pyrubate. J Neurosci 31, 34-45

Van Bockstaele EJ, Reyes BA, Valentino RJ (2010) The locus coeruleus: A key nucleus where stress and opioids intersect to mediate vulnerability to opiate abuse. Brain Res 1314, 162-174

Walz W (2009) Patch-Clamp Analysis: Advanced Techniques, 2nd ed., Humana, Totowa, New Jersey

Wang DD, Bordey A (2008) The astrocyte odyssey. Prog Neurobiol 86, 342-367

Yuste R, Konnerth A, Masters B (2006) Imaging in neuroscience and development, a laboratory manual. J Biomed Opt 11, 19902

Zilberter Y, Zilberter T, Bregestovski P (2010) Neuronal activity in vitro and the in vivo reality: the role of energy homeostasis. Trends Pharmacol Sci 31, 394-401

Chapter-3

Ca^{2+}/K^{+} Antagonism of Spontaneous Network Bursting in Hippocampus, Cortex and *Locus Coeruleus* of Newborn Rat Brain Slices

Chase M. Kantor, Araya Ruangkittisakul, Bogdan Panaitescu, Junya Kuribayashi, Klaus Ballanyi*

Department of Physiology, 750 MSB, University of Alberta, Edmonton, AB, Canada T6G 2S2

My contribution to this study consisted of the execution of >70% of both the electrophysiology and calcium imaging studies and 100% of the corresponding analysis on LC rhythm. Analysis of c- and hENOs was conducted in conjunction with Dr. A. Ruangkittisakul. Other electrophysiology experiments were performed by Dr. J. Kuribayashi and Dr. B. Panaitescu. Dr. K Ballanyi developed the concept for the work and revised the manuscript.

*Corresponding author: Klaus Ballanyi at the above address

3.1 Abstract

Modulation of 'early network oscillations' (ENOs) in immature neural networks by extracellular K^+ and Ca^{2+} has not been studied systematically yet. Here, this was investigated for CA_3 hippocampal and cortical ENOs (hENOs, cENOs) and ENO-like bursting in the more mature *locus coeruleus* (LC rhythm) in newborn rats. Field potentials were recorded in these areas and free cytosolic Ca^{2+} was imaged in CA_3 neurons of 400-600 µm thick horizontal brain slices in solution with close-to-physiological K^+ (4 mM) and Ca^{2+} (1 mM). LC rhythm was fast (0.5-3 Hz), while hENOs had an intermediate frequency (15-45 bursts/min) and cENOs comprised the slowest events (0.2-10 bursts/min). Lowering K^+ to 3 mM did not perturb LC rhythm, but depressed cENOs (in >70% of cases) and tended to destabilized hENOs (65%). 6-7 mM K^+ slowed LC rhythm but accelerated cENOs. hENOs were not changed by 6 mM K^+ whereas in 7 mM bursting was perturbed by seizure-like discharges. 2 mM Ca^{2+} slowed LC rhythm to <50% of control and abolished cENOs. In >70% of cases, this slowed hENOs to <30% of control, whereas their amplitude decreased by 20-40% in the remaining slices which stopped bursting at 2.5-3 mM Ca^{2+}. Ca^{2+} depression of both ENOs was fully countered by 5-7 mM K^+, whereas recovery of LC rhythm was less pronounced. Desynchronization of spontaneous Ca^{2+} rises in CA_3 neurons by high Ca^{2+} was countered by high K^+. In conclusion, spontaneous activity in hippocampal, cortical and medullary neural circuits depends critically on 'Ca^{2+}/K^+ antagonism' providing robust bursting at close-to-physiological extracellular levels of these cations.

3.2 Introduction

Neuronal excitability is strongly modulated by extracellular Ca^{2+} and K^+ whose concentrations range in mammalian brain tissues from 1-1.2 mM and 3-4 mM, respectively (Heinemann et al., 1977; Nicholson et al., 1978; Hansen, 1985; Nilsson et al., 1993; Puka-Sundvall et al., 1994; Stringer, 1998; Hille, 2001; Somjen, 2002; Brown et al., 2004). However, to boost activities notably higher Ca^{2+} and/or K^+ levels are often used in isolated nervous structures (Somjen, 2002; Ballanyi, 2012). As a basic mechanism for excitation by elevated K^+, the resulting depolarization brings neuronal membrane potential closer to the threshold for action potential discharge (Hille, 2001; Somjen, 2002). A corresponding basic mechanism for excitatory actions of raised Ca^{2+} is potentiation of neurotransmitter release at chemical synapses by enhancement of presynaptic Ca^{2+} influx (Del Castillo & Engbaek, 1954; Hille, 2001). For example, transmission is stimulated in hippocampal slices when Ca^{2+} is raised from 1.2 to 1.8 mM and, conversely, depressed when Ca^{2+} is $\leq$0.8 mM (Balestrino et al., 1986; Rausche et al., 1990). In mouse spinal cords, reflexes are maximal at 2.4-3.6 mM Ca^{2+}, but are depressed upon further elevation to 4.8 mM (Czéh & Somjen, 1989). On the other hand, inhibitory Ca^{2+} actions on neurons have been revealed *in vivo* when Ca^{2+} injection close to the location of medullary respiratory networks depressed breathing (Berndt et al., 1969; Leusen, 1972; Berkenbosch & Adan, 1974). These studies also showed that the inhibitory Ca^{2+} effect on breathing is countered by injection of K^+. This 'Ca^{2+}/K^+ antagonism' (Leusen, 1972) was analyzed further by our group using respiratory active newborn rat brainstem models (Ruangkittisakul et al., 2007; Ballanyi & Ruangkittisakul, 2009; Panaitescu et al., 2009). This showed that raising superfusate Ca^{2+} in 3 mM K^+ from 1.0 to 1.5 mM blocks fictive inspiratory rhythm while 7-9 mM K^+ counters this strong depression.

Extracellular Ca^{2+}/K^{+} antagonism may also determine neural network bursting in supramedullary brain regions. For example, reducing extracellular Ca^{2+} from 1.8-2 mM to 0.75-1.2 mM activated *in vivo*-like neuronal activities in hypothalamic slices (Pittman et al., 1981) and cortical slices from adult ferret (Sanchez-Vives & McCormick, 2000), newborn rat (Sheroziya et al., 2009) or fetal human tissue (Moore et al., 2012). Moreover, stimulation of spontaneous neural network activity by K^{+} was seen in slice studies on 'early network oscillations' (ENOs) that are considered as pivotal for manifestation of brain connectivity (Garaschuk et al., 2000; Ben-Ari et al., 2007; Sipilä & Kaila, 2007; Allene & Cossart, 2010). Specifically, raising K^{+} to 5-8 mM restored ENOs in newborn mouse cortex following inhibition by blockers of kainate/AMPA-type glutamate receptors (McCabe et al., 2007) and in newborn rat hippocampus after inhibition by γ-aminobutyric acid ($GABA_A$) receptor blockers (Sipilä et al., 2005).

It is yet unknown, how systematic variation of extracellular Ca^{2+} and/or K^{+} modulates ENOs in the immature neonatal hippocampus and cortex. This was studied here in horizontal newborn rat brain slices under *in vitro* conditions similar to our studies on Ca^{2+}/K^{+} antagonism in inspiratory networks (Kantor et al., 2012; Ruangkittisakul et al., 2012) **(Fig. 3-1)**. This novel slice type also contains the medullary *locus coeruleus* that seems to be more mature at this stage (Moriceau et al., 2010), and generates robust ENO-like field potentials (**§1.6, 2.3.1.1**) **(Fig. 2-1)** (Kantor et al., 2012). The present analysis used novel suction electrode-based field potential recording in these three active slice areas and Ca^{2+} imaging in CA_3 neurons to show that rhythmic bursting in these networks is determined by Ca^{2+}/K^{+} antagonism **(Fig. 3-1)**.

3.3 Methods

(see **§2**)

3.4 Results

Effects of systematic alteration of superfusate Ca^{2+} and K^+ concentrations were investigated in 400-600 µm thick horizontal brain slices from P0-9 days-old rats on ENOs in the CA_3 hippocampal (hENOs) or entorhinal/perirhinal cortical regions (cENOs) and ENO-like rhythm in the medullary area of the *locus coeruleus*. For this, suction electrode-based field potentials were recorded in these areas while multiphoton/confocal Ca^{2+} imaging was performed in CA_3 neurons. All reported values are based on analysis of effects during steady state at the end of a 20 min application period.

3.4.1 Hippocampal and Cortical ENOs

The capability of hippocampal and cortical networks to generate ENOs for several hours appears to depend on a recovery time period of at least 1 h on a net in a specific storage container (**§2.1.2.1**) (Kantor et al., 2012). hENOs occurred at a mean rate of 12.2 ± 1.9 bursts/min (n= 10) and mean burst duration of 0.8 ± 0.13 s (n= 10), while cENOs were slower (2.2 ± 0.5 bursts/min, n= 9) with a single burst duration of 0.83 ± 0.12 s (n= 9) **(Figs. 3-2)**.

In a first series of experiments, effects of variation of superfusate Ca^{2+} between 0.5, 1, 1.5, 2 and 2.5 mM were investigated. Lowering Ca^{2+} to 0.5 mM perturbed hENOs by occurrence of large amplitude seizure-like events that turned into small amplitude irregular discharges after 5-10

min. The latter events persisted until the end of the 20 min application period and could not be analyzed statistically. hENOs recovered to control values within 10-20 min after return to control solution **(Fig. 3-2)**. In contrast, cENOs were stable in 0.5 mM Ca^{2+} and their rate increased to 170.8 ± 35.3 % of control, whereas both amplitude and duration showed a non-significant trend for an increase **(Fig. 3-2)**. Raising Ca^{2+} from 1 mM to 2 and 2.5 mM depressed the rate of hENOs to 25.7 ± 9.7 and 9.7 ± 5.3 % of control, respectively **(Fig. 3-2)**. This was accompanied by reduction of single burst duration to 85.5 ± 11.4 and 68.9 ± 7.3 % of control, respectively, whereas burst amplitude did not change **(Fig. 3-2)**. A clear trend for slowing of cENOS in 1.5 and 2 mM became only significant in 2.5 mM, where bursting was abolished in all 5 slices **(Fig. 3-2)**. At neither 1.5 nor 2 mM, did Ca^{2+} affect the amplitude or duration of cENOs.

In ~20% of slices, hENOs did not show the typical 'burst' pattern but instead of show 'spike' activity pattern comprised of quite regular rhythmic events with mean rate of 46.4 ± 14.6 bursts/min (n= 4) and shorter single burst duration of 0.397 ± 0.08 s **(Fig. 3-3)**. The rate of these spike pattern hENOs decreased to 53.9 ± 12.6 and 53.5 ± 9.9 % of control ($P< 0.05$) in response to 2 and 2.5 mM Ca^{2+}, respectively, and their amplitude showed a similar reduction that was significant for 1, 2 and 2.5 mM **(Fig. 3-3)**. In contrast, burst duration was affected neither by 1.5, 2 nor 2.5 mM Ca^{2+} **(Fig. 3-3)**.

Because of the low incidence of this hENO pattern, effects of K^+ variation and Ca^{2+}/K^+ antagonism could not be analyzed further.

In the next series of experiments, effects of variation of superfusate K^+ were investigated. The results revealed that lowering of K^+ from 4 to 3 mM did not affect the rate, amplitude or duration of hENOs, as evident from the sample recordings and statistical analysis in **Fig. 3-4**. Raising K^+ to 5 or 6 mM revealed, however, a trend for stimulation of hENO rate. Responses of hENOS to 7 mM K^+ could not be quantified because of occurrence of large amplitude seizure-like discharges in 1 of 6 slices or due to the presence of small amplitude 'chaotic' activity in the remaining slices within the first few minutes of application **(Fig. 3-4)**. Lowering K^+ from 4 to 3 mM had no significant effect on either burst rate, amplitude or duration of cENOs, but there was a trend for depression of burst rate to <50 % of control **(Fig. 3-4)**. Conversely, raised K^+ appeared to stimulate burst rate and this effect became significant for 6 and 7 mM, whereas high K^+ did not change burst amplitude and duration **(Fig. 3-4)**.

While effects of variation of K^+ between 3-5 mM on hENOs and cENOs were not significant, it appeared that 4 or 5 mM K^+ had a reversible long-term stabilizing effect, as in the cases where bursting was not regular in 3 mM K^+ used in initial series of experiments in the control solution. For these reasons, we changed to 4 mM K^+ in the control solution for the quantitative part of this study.

For studying whether Ca^{2+}/K^+ antagonism determines the robustness of hENOs and cENOs, a series of experiments was performed in which bursting was depressed in 4 mM K^+ by raising Ca^{2+} to 2.5 mM. Subsequently, K^+ was elevated consecutively to 5, 6 and 7 mM in 2.5 mM Ca^{2+} to test for recovery of bursting. As evident from the sample recordings and statistical analysis in **Fig. 3-5**, high Ca^{2+} reduced the rate of hENOs in 5 slices to 18.2 ± 10.6 % of control, but this

apparently strong effect was not significant, while burst amplitude did not change. In contrast, burst duration was significantly reduced in high Ca^{2+} to ~60 % (0.78 ± 0.21 s) of control **(Fig. 3-4)**. Raised K^+ appeared to restore burst rate at all concentrations beyond control values, but this was significant only for 7 mM, where burst rate reached >200 % (13.3 ± 2.6 bursts/min) of control **(Fig. 3-5)**. The amplitude of hENO bursts was not affected by high K^+ in high Ca^{2+}, whereas burst duration remained depressed at values of ~60 % below control **(Fig. 3-5)**. On the other hand, cENO bursting in 5 slices was abolished in 2.5 mM Ca^{2+} and reoccurred in all cases upon raising K^+ to 5, 6, or 7 mM. Neither the amplitude, nor duration of cENO bursts differed from control values in high K^+ plus high Ca^{2+}.

3.4.2 ENO-like LC Rhythm

The neonatal rodent *locus coeruleus* shows a bilateral organization and spans 200-400 μm in all dimensions (Ballantyne et al., 2004). Thus, this structure is typically contained in only 1 horizontal slice per animal. The amplitude of *locus coeruleus* population oscillations reached steady-state within 0.5-1 h after start of recording in slices that were incubated in recovery solution for 1 h prior to transfer to the submerged-type experimental chamber (**§2.2.1.1**) (Kantor et al., 2012). Both *locus coeruleus* aspects are not synaptically coupled in these slices and therefore do not show synchronous discharges. In control solution, *locus coeruleus* rhythm occurred at a mean rate of 106.7 ± 3.4 bursts/min (n= 23) and had a single burst duration of 0.175 ± 0.018 s.

Firstly, it was investigated whether variation of superfusate Ca^{2+} has similar effects on *locus coeruleus* rhythm as on ENOs. Because effects in initial experiments seemed more modest, a

larger spectrum of Ca^{2+} concentrations was tested, specifically 0, 0.25, 0.5, 2, 2.5 and 3 mM. As evident from the sample recordings and statistical analysis in **Fig. 3-6**, both high and low Ca^{2+} depressed the rate of *locus coeruleus* rhythm notably over the entire range, whereas nominally 0 mM Ca^{2+} abolished bursting in all 10 slices tested. For all concentrations except 0 and 0.25 Ca^{2+}, burst amplitude remained close to control values, whereas its duration increased substantially as Ca^{2+} concentration deviated from 1 mM. Specifically, high Ca^{2+} prolonged burst duration to ~180 % of control, whereas 0.5 and 0.25 mM Ca^{2+} prolonged them to >800 and 1200 % of control, respectively **(Fig. 3-6)**.

Testing for variation of superfusate K^+ in a different set of experiments revealed that 3-5 mM did not affect burst rate, amplitude or duration of *locus coeruleus* rhythm **(Fig. 3-7)**. While 6, 7 and 8 mM K^+ did not change burst amplitude, they depressed burst rate substantially, to 58.1 ± 10.9, 33.5 ± 8.2 and 21.0 ± 2.5 % of control, whereas burst duration increased profoundly, to 270 ± 55.9, 687 ± 118 and 709 ± 99.0 % of control, respectively **(Fig. 3-7)**.

These findings on partly substantial modulation of both Ca^{2+} and K^+ on *locus coeruleus* rhythm suggested that bursting within this neural network is greatly determined by a Ca^{2+}/K^+ antagonism as revealed for both types of ENOs. Indeed, as evident from the sample recordings and statistical analysis in **Fig. 3-8**, elevation of K^+ clearly reversed Ca^{2+} depression. However, while recovery of bursting from significant depression by 3 mM Ca^{2+} was significant for 7 and 8 mM K^+, rhythm even at 8 mM recovered only to 53.8 ± 3.8 % (51.5 ± 2.2 bursts/min) of control **(Fig. 3-8)**.

3.4.3 Effects of $GABA_A$ Receptor blockade ENOs and ENO-like *locus coeruleus* rhythm

It has been suspected (Sanchez-Vives & McCormick, 2000; Brumberg et al., 2000; Sheroziya et al., 2009) that activity in brain slices in 'low' superfusate Ca^{2+}, i.e. around 1 mM compared to unphysiologically high 2-2.5 mM, may correspond to seizure-like hyperexcitability as induced by <0.5 mM Ca^{2+} which is an established *in vitro* epilepsy model (Heinemann et al., 1977; Konnerth et al., 1986; Jeffereys, 1995; Kilb et al., 2007).

To test this possibility, we have investigated effects of pharmacological blockade of $GABA_A$ receptors as an established seizure model (Jeffereys, 1995; Kilb et al., 2007). As evident from the sample recordings and statistical analysis in **Fig. 3-9**, the $GABA_A$ receptor blocker gabazine (1 μM) transformed 'burst-type' hENOs (n= 4) and 'spike-type' hENOs (n= 3) into large amplitude events that occurred at a regular rate, although the effect was not significant for the slices with spike ENOs, despite a seemingly >500 % amplitude increase **(Fig. 3-9).** Blockade of GABAA receptors did not affect the rate of burst-type hENOs but increased their duration, whereas the rate of spike-type hENOs was significantly depressed while spike duration was unaffected. Similar to burst-type hENOs, gabazine augmented cENO burst amplitude (n= 6), while showed a tendency to increase burst rate and duration **(Fig. 3-9)**. In contrast, gabazine did not affect *locus coeruleus* rhythm as analyzed in 7 further slices **(Fig. 3-9)**.

3.4.4 Consequences of Ca^{2+}/K^+ Antagonism for Ca^{2+} Dynamics in CA3 Neurons

For the present study, multiphoton/confocal Ca^{2+} imaging was performed in the CA3 region in 13 slices. Slices were loaded with the Ca^{2+}-sensitive dye Fluo-8L-AM via bath-application which resulted in apparently uniform staining of both CA3 neurons and presumptive astrocytes located

in the *stratum radiatum* and *stratum oriens* with a soma diameter of ~10 μm. In 13 slices, imaging revealed sometimes synchronous, but more often asynchronous, spontaneous cytosolic Ca^{2+} (Ca_i) rises at a rate of 14-20 events/min in somata and primary dendrites of CA3 neurons that were imaged between 30-50 μm below the upper slice surface. The incidence for synchronous activity appeared to be larger in identified neurons at recording depths of 50-80 μm. Rhythmic Ca_i rises in cells of deeper layers seemed to show more synchronicity as indicated by rhythmic increases in 'background' fluorescence because of lack of cellular resolution at this depth. In a single imaging plane, typically 15-20 cells with a soma diameter of 15-25 μm showed rhythmic increases of Ca_i. As exemplified in **Fig. 3-10**, Ca_i rises were slowed upon elevating superfusate Ca^{2+} from 1 mM to initially 2.5 mM and then 3 mM, and this depression was reversed upon returned to 1 mM Ca^{2+}. Very similar findings were obtained in one additional slice. In another series of 11 experiments, superfusate Ca^{2+} was raised to 2 mM (n= 2), 2.5 mM (n= 7) or 3 mM (n= 2) and K^+ was raised to 7-8 mM which (partially) recovered synchronous Ca_i rises **(Fig. 3-11)**. In 2 slices, recovery of Ca_i rate by high K^+ was accompanied by an increase in synchronicity of Ca_i increases in superficial (between 30-50 μm below the surface) CA3 neurons **(Fig. 3-12)**. Contrary to these dynamic changes of neuronal Ca_i, presumptive astrocytes were mainly silent except for occasional 'Ca_i spikes' occurring at rates <1 event/min and neither high Ca^{2+} nor high K^+ in high Ca^{2+} had a notable effect **(Fig. 3-12)**. After these experiments, glutamate (Glu; 1 mM) and trans-1-aminocyclopentane-1,3-dicarboxylic acid (t-ACPD; 25 mM) were bath-applied to show morphological features of principal neurons and presumptive astrocytes for 30 s and 2 min, respectively **(Fig. 3-12)**. Glu application resulted in an augmentation of both neuronal and glial Ca_i baseline by ~200% and 300-500%, respectively, though neuronal increases in fluorescence intensity (FI) lasted longer than that of astrocytes. t-

ACPD similarly increased glial Cai baseline by ~400% (~400 FI units), while neuronal responses were more modest, <100% augmentation.

3.5 Discussion

In the present study, suction electrode-based field potential recording was performed in novel brain slices that show robust spontaneous bursting in at least three areas. Focus was on developmentally-related ENOs in the hippocampal CA_3 region and cortex, and on fast ENO-like rhythm in *locus coeruleus* networks which appear to be more mature at that stage. It was revealed that population bursting in all these networks depends critically on Ca^{2+}/ K^+ antagonism. This view is supported by the finding that high Ca^{2+} depressed rhythmic Ca^{2+} rises in CA_3 neurons and that this was countered by high K^+. These results suggest that superfusate with close-to-physiological Ca^{2+} (1 mM) and K^+ (4 mM) is optimal for studying these networks.

3.5.1 Mechanisms of Ca^{2+}/ K^+ Antagonism in Active Neural Networks

The rationale for our study was to analyze whether neuronal bursting not only in rhythmogenic inspiratory networks, but also in other spontaneously active neural networks in newborn mammals is depressed by supraphysiological extracellular Ca^{2+} and if this is countered by also raising K^+ above normal *in vivo* levels. As indicated above (**§3.2**), such Ca^{2+}/ K^+ antagonism of neural network activity was discovered when Ca^{2+} application to the vicinity of medullary respiratory networks depressed breathing (Leusen, 1972). These findings on anesthetized adult animals apply also to newborns as demonstrated in brainstem-spinal cord preparations from newborn rats (Kuwana et al., 1998; Okada et al., 2005). These reports showed that raised superfusate Ca^{2+} (and Mg^{2+}) depress inspiratory-related bursting of spinal motoneurons and that

high K^+ accelerates this rhythm. Our group used this *en bloc* model and also inspiratory active newborn rat and mouse brainstem slices for quantifying these antagonistic respiratory Ca^{2+} and K^+ effects (Ruangkittisakul et al., 2007, 2011; Ballanyi & Ruangkittisakul, 2009; Panaitescu et al., 2009). This analysis presented evidence that Ca^{2+} depression of breathing originates from direct actions on rhythmogenic neurons within the pre-Bötzinger complex which initiates and controls normal breathing. In the latter studies from Okada's team and our group on the *in vitro* respiratory networks, the following potential mechanisms for depression of neural respiratory control by raised extracellular Ca^{2+} were discussed. Ca^{2+} depression may result from (*i*) neutralization of negative surface charges at the outside of the neuronal plasma membrane, resulting in an increase in transmembrane potential difference, thus exerting a hyperpolarizing effect (Hille, 2001), (*ii*) decreased neuronal input resistance (Jefferys, 1995; Hille, 2001; Somjen, 2002), (*iii*) modulation of the activity of ion channels such as (presynaptic) non-selective cation channel or Ca^{2+}-activated K^+ channels (Xiong et al., 1997; Hille, 2001; Chen et al., 2010), (*iv*) modulation of the latter and other types of ion channels by a Ca^{2+}-sensing receptor that shows structural similarity with metabotropic $GABA_B$ or group-I glutamate receptors (Brown & MacLeod, 2001), and (*v*) a relatively stronger excitatory effect on inhibitory than excitatory synapses (Jefferys, 1995). These mechanisms are not discussed in more detail here because neither in the previous studies on Ca^{2+}/ K^+ antagonism nor the present study were experiments conducted to provide data in support of one of these mechanisms. A further mechanism that was not considered previously by us, but by others (Su et al., 2001; Sheroziya et al., 2009) is depression by raised Ca^{2+} of intrinsic neuronal bursting mediated by persistent Na^+ channels. This mechanism may indeed be important because, firstly, this slowly inactivating sub-type of voltage-activated Na^+ channels is a characteristic feature of pre-Bötzinger complex neurons

(Feldman & Del Negro, 2006; Ruangkittisakul et al., 2009). Secondly, these channels also seem to be important for intrinsic bursting in both hippocampal and cortical circuits (Su et al., 2001; Sipilä et al., 2005; Sipilä & Kaila, 2007; Sheroziya et al., 2009). Evidence for this hypothesis in the latter studies by Kaila's group (Sipilä et al., 2005; Sipilä & Kaila, 2007) is partly based on the finding that the (not very specific) persistent Na^+ channel blocker riluzole abolished hENOs at 30 µM in newborn rat slices. Also in our hands, 5-20 µM riluzole abolished both hENOs and cENOs, whereas even 50 µM of the agent did not fully block *locus coeruleus* rhythm in the same type of newborn rat slices as used here **(Fig. 2-5)** (**§2.3.1.1**) (Kantor et al., 2012). Correspondingly, the rate of *locus coeruleus* rhythm was less depressed than both types of ENOs by high Ca^{2+} in the present study. This suggests that a less pronounced role of persistent Na^+ channels in synchronized bursting of *locus coeruleus* neurons (De Oliveira et al., 2011) may be causally related to more modest effects of high Ca^{2+} on this network.

3.5.2 Ca^{2+} Depression of Network Bursting in Supramedullary Brain Slices

A variety of findings on slices from supramedullary brain structures are similar to our previous observation on isolated pre-Bötzinger complex inspiratory networks that supraphysiological Ca^{2+} strongly inhibits spontaneous neural network bursting in mammals. In most of these studies, the superfusate for generating (and storing) such brain slices contained 2-2.5 mM Ca^{2+} and they often report that these slices are silent in this solution, but become active when Ca^{2+} is lowered. As an early example for studies using brain slices from adult mammals, *in vivo*-like neuronal activities were evoked in hypothalamic slices upon lowering of superfusate Ca^{2+} from 1.26 mM to 0.75 mM (Pittman et al., 1981). Similarly, in adult rat hippocampal slices 'fast ripples' developed mainly when superfusate Ca^{2+} was lowered from 2 to 1 mM while at the same time

increasing K^+ from 3 mM to 4 mM (Foffani et al., 2007). Moreover, reduction of Ca^{2+} from 2 mM to 1-1.2 mM evoked *in vivo*-like bursting in slices from neocortex and piriform cortex of adult ferrets (Sanchez-Vives & McCormick, 2000; Sanchez-Vives et al., 2008). In 2 mM Ca^{2+} solution, neurons in slices of human fetal cortex principally show rhythmic sustained plateau depolarizations and concomitant action potential firing that resembles up and down states in the adult neocortex (Moore et al., 2012). However, the rate and incidence of these events is notably increased when superfusate Ca^{2+} is lowered to 1.2 mM (Moore et al., 2012). Similarly, reduction of extracellular Ca^{2+} from 2 mM to 1 mM increased the fraction of neurons with prolonged bursting by inducing intrinsic bursts in regularly firing neurons in newborn rat slices of the developing entorhinal cortex (Sheroziya et al., 2009). Based on the intracellular recordings in the latter study from a large number of different classes of developing entorhinal cortex neurons, the authors hypothesized that the cellular effects should be reflected by effects on field potentials representing the summated response of populations of neurons. Indeed, we found here that high Ca^{2+} had a very pronounced depressing effect on synchronous neuronal bursting in the entorhinal cortex. However, we did not find evidence that rhythmic bursting is transformed into tonic firing in a major number of neurons. This is based on lack of an increase in the baseline of the integrated suction electrode signal which was a clear measure for non-synchronized tonic firing in our studies on the isolated pre-Bötzinger complex (Panaitescu et al., 2009; Ballanyi & Ruangkittisdakul, 2009). In addition to strong inhibition of cENOs by supraphysiological Ca^{2+}, also hENOs and *locus coeruleus* rhythm were depressed in the present study. As an additional, albeit unexpected, finding it was revealed that spike-type hENOs are less sensitive to high Ca^{2+}. Whether this new type of rhythm represents a 'missing link' between relatively slow bursting of immature CA_3 neurons and fast, e.g. theta, oscillations typically seen in the mature hippocampus,

or is rather due to desynchronization of subpopulations of hippocampal neurons (Foffani et al., 2007; Bonifazi et al., 2009) remains to be studied.

These findings indicate that high Ca^{2+} exerts a strong inhibitory effect on neural network bursting despite its established augmenting effect on synaptic transmission (**§3.2**) (Del Castillo & Engbaek, 1954; Balestrino et al., 1986; Rausche et al., 1990; Hille, 2001; Somjen, 2002). Based on the above discussion (**§3.5.1**), it is possible that a depressing effect of high Ca^{2+} on persistent Na^{+} channels outweighs the stimulatory effect on synaptic transmission, if neural network bursting depends greatly on such channels.

3.5.3 Lack of Similarity with Seizures of Neonatal Network Bursting in Physiological Ca^{2+}

The above study (**§3.5.2**) by Foffani et al. (2007) was cited as an example that lowering of superfusate Ca^{2+} promotes spontaneous activity in adult rat hippocampal slices, in this case fast ripples. Moreover, they showed in that report that bath-application of 10 μM gabazine does not affect these events in line with their assumption that fast ripples in slices resemble those in the epileptic hippocampus. As a further example in that regard, it has been demonstrated in adult rat hippocampal slices that lowering of Ca^{2+} from 1.5 mM to 1 mM made them considerably more prone to epileptiform activity (Stringer & Lothman, 1988). This raises the possibility that reducing superfusate Ca^{2+} from commonly used 2-2.5 mM to physiological values of 1-1.2 mM promotes seizure-like activity in brain slices, possibly because the strength of (tonic) $GABA_A$ (and glycine receptor) mediated inhibition, which may endogenously depress seizures *in vivo* (Jeffreys, 1995), is weak *in vitro*. This may particularly be the case for the neonatal hippocampus and cortex, where GABA acts in depolarizing fashion on $GABA_A$ receptors to promote giant

depolarizing potentials (GDPs) and/or ENOs (Ben-Ari et al., 1989, 2007; Sipilä et al., 2005, 2006; Sipilä & Kaila, 2007; Allene et al., 2008). However, using the common *in vitro* epilepsy model gabazine (Jeffreys, 1995; Foffani et al., 2007; Kilb et al., 2007), we found here that large amplitude seizure-like discharge developed in both CA3 and cortical slice regions, while ENOs disappeared. This argues against the view that robust ENOs in 1 mM Ca^{2+} are an expression of artificial hyperexcitability in these isolated circuits. In support of this, 0.5 mM Ca^{2+} blocked hENOs and did not change the amplitude or duration of cENO bursts while raising Ca^{2+} did not change the amplitude or duration of single hENO or cENO bursts. These findings argue against the possibility that these activities in 1 mM Ca^{2+} correspond to seizure-like discharge evoked by low Ca^{2+} or Mg^{2+} (typically <0.5 mM) that are further *in vitro* epilepsy models (Heinemann et al., 1977; Konnerth et al., 1986; Jeffreys, 1995; Foffani et al., 2007; Kilb et al., 2007).

Contrary to gabazine-evoked occurrence in hippocampus and cortex of seizure-like discharge resembling IAs **(Fig. 1-7)** (Kilb et al., 2007), bursting in *locus coeruleus* was not affected by the agent which is in line with previous studies indicating a minor role of GABAergic neurons in this network (Olpe et al., 1988). However, 0.25-0.5 mM Ca^{2+} transformed the fast oscillations into longer-lasting bursts of lower rate whereas increasing Ca^{2+} depressed burst rate and amplitude, but did not profoundly change the discharge pattern or single burst duration.

3.5.4 Ca^{2+}/K^{+} Antagonism of ENOs and ENO-like Bursting in Newborn Rat Slices

Previous studies showed that K^{+} can stimulate neonatal ENOs in slices from newborn rodent cortex and hippocampus (Khazipov et al., 2004; Sipilä et al., 2005; Ben-Ari et al., 2007; Sipilä & Kaila, 2007; Sheroziya et al., 2009; McCabe et al., 2007). In one of the latter reports (Khazipov

et al., 2004), 8.5 mM K^+ evoked seizure-like discharge in newborn rat hippocampal slices, similar to our finding here that already 7 mM K^+ profoundly perturbed hENOs and could evoke epileptiform discharges. In contrast, particularly the rate of cENOs was stimulated in the present study, similar to observations in a related study on spontaneously active neurons in the entorhinal cortex of newborn rat slices (Sheroziya et al., 2009). Moreover, it was demonstrated that raised superfusate K^+ counters depression of hENOs in newborn rat slices by blocking $GABA_A$ receptors (Sipilä et al., 2005) and of cENOs in mouse neocortical slices by blocking AMPA/kainate-type glutamate receptors (McCabe et al., 2007).

Here, it was shwon that K^+ also effectively counters depression on both types of ENOs by supraphysiological extracellular Ca^{2+} levels similar to Ca^{2+}/K^+ antagonism of rhythmogenic pre-Bötzinger complex inspiratory networks as discussed above. While Ca^{2+}/K^+ antagonism was very effective in these three active neonatal neural networks, even 8 mM K^+ did not recover bursting that was depressed by high Ca^{2+} back to control values. Nevertheless, it caused a significant recovery from this depression. As studied in CA_3 neurons, Ca^{2+}/K^+ antagonism at the neuronal population level was reflected by depression of more or less synchronous cytosolic Ca^{2+} rises in individual neurons in control solution. Application of high K^+ in high Ca^{2+} was capable of reactivating (or enhancing persistent depressed) rhythmic Ca^{2+} rises in individual neurons. In fact, the combination of high Ca^{2+} and high K^+ could result in very regular Ca^{2+} rises with enhanced synchronicity compared to Ca^{2+} oscillations in control. This behavior could be reflected at the network level by boosted and/or more regular hENOs or cENOs **(Fig. 3-5)**.

3.6 Conclusions

In summary of our present and previous findings and taken published data from others into account, is seems that superfusate with close-to physiological content of Ca^{2+} (1-1.2 mM) and K^{+} (3-4 mM) provides robust spontaneous neural network bursting in both (more or less immature) neonatal and adult medullary and supramedullary nervous structures. Ca^{2+}/K^{+} antagonism seems to be a general feature of such networks, meaning that depression of network bursting by supraphysiological Ca^{2+} is countrered by supraphysiological K^{+}. Because combined high Ca^{2+} and K^{+} can enhance the strength and/or synchronicity of cellular and network bursting, use of such conditions may be advantageous though for some aspects of the analysis of such networks.

Figures

Fig. 3-1

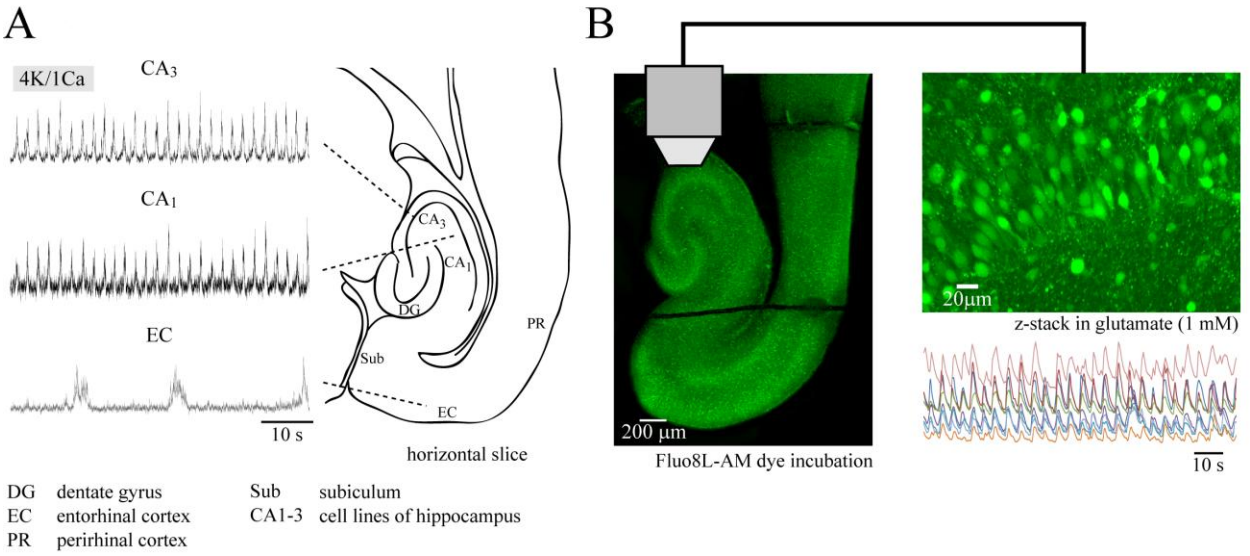

Fig. 3-1: Generation of rhythmically active newborn rat horizontal brain slices. A, schematic of a hemisected brain slice from a postnatal day (P) 7 Wistar rat showing simultaneous suction electrode recordings (left) positioned over the CA3 and CA1 hippocampal areas (CA3; CA1) as well as in the entorhinal cortex (EC). The slice was kept in superfusate containing (among other components) 4 mM K^+ and 1 mM Ca^{2+} (4K/1Ca) plus 10 mM glucose. Signals represent integrated extracellular neural population discharges representing 'early network oscillations' (ENOs). Note that ENOs in the hippocampus are synchronized between the CA_3 and CA_1 subfields. **B**, (left) horizontal slice that had been incubated with the fluorescent Ca^{2+}-sensitve dye Fluo-8L-AM; (right) rhythmic inctracellular Ca^{2+} rises associated with ENOs are reflected by an increase in fluorescence intensity measured with an Olympus-based confocal or multiphoton laserscanning microscope from regions of interest (ROIs; color traces) corresponding to individual CA3 neurons. Visualization of cell morphology improves upon bath-application of glutamate due to strong neuronal (and glial) Ca^{2+} rises (top right).

Fig. 3-2

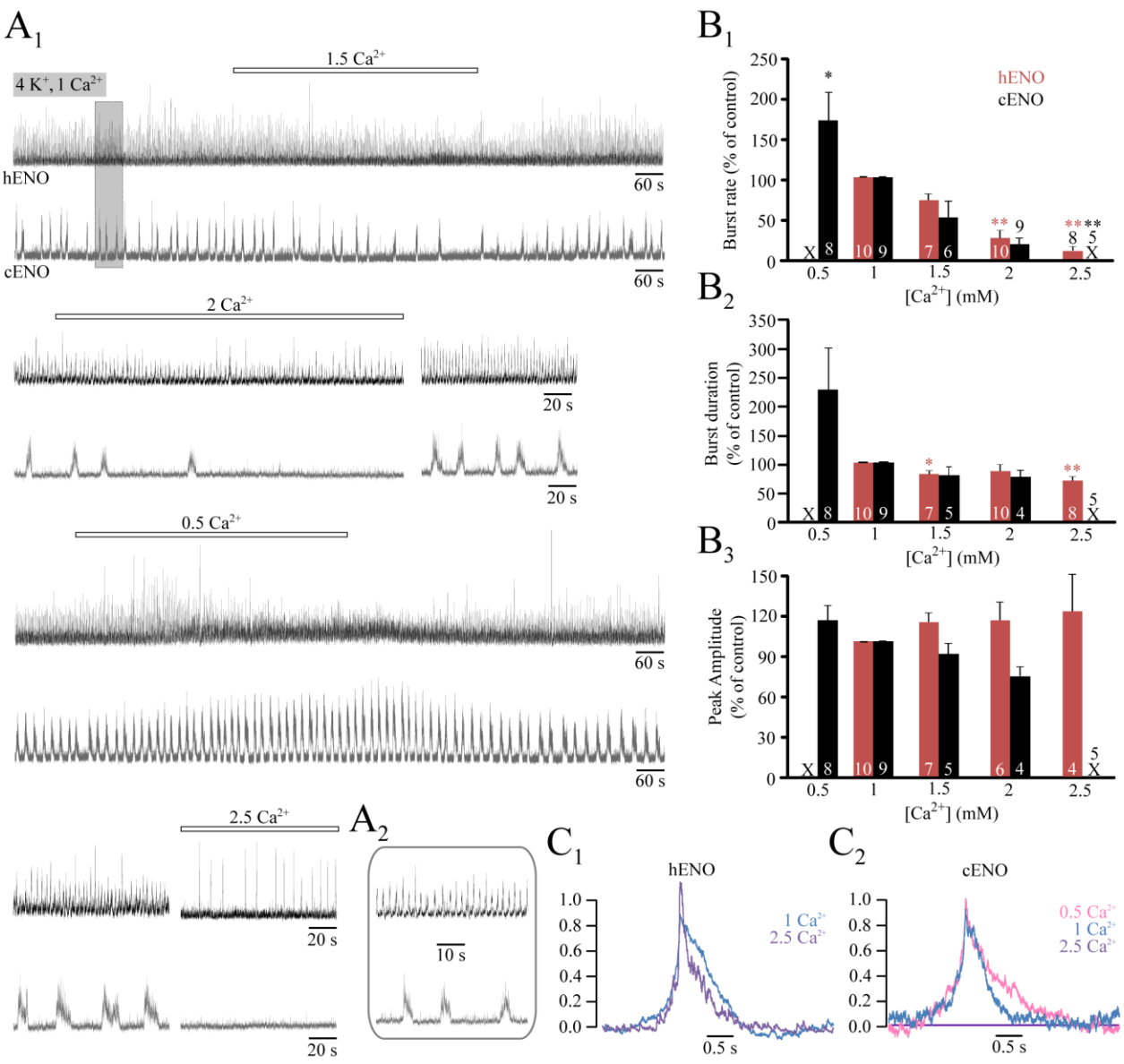

Fig. 3-2: Modulation of ENOs by extracellular Ca^{2+}. A, continuation of simultaneous recordings of cortical and hippocampal ENOs (cENOs, hENOs) from **Fig. 3-1A**. Elevating superfusate Ca^{2+} from 1 mM to 1.5 and 2 mM partially depressed amplitude and rate of hENOs and cENOs. Contrary, lowering Ca^{2+} from 1 to 0.5 mM evoked a transient stimulation that transformed into high amplitude/long duration cENO bursting while depressing hENOs. Following recovery in 1 mM Ca^{2+}, further application of 2.5 mM Ca^{2+} abolished cENOs and

slowed hENOs from 25 bursts/min to 2-3 bursts/min. Note that 2.5 mM Ca^{2+} does not abolish fast 'spike' hENO discharge (duration <0.5 s). Both, cENO and hENO rates recovered to levels similar to control upon returning to 1 mM Ca^{2+} (not shown). **B_1-B_3**, effects of Ca^{2+} on mean value with SEM for ENO rate, burst duration, and burst amplitude, respectively. Digits in bars indicate number of slices tested. **C**, average bursts of hENOs (**C_1**) and cENOs (**C_2**) seem to become shorter in duration with increasing superfusate Ca^{2+}. (* P< 0.05, ** P< 0.01)

Fig. 3-3

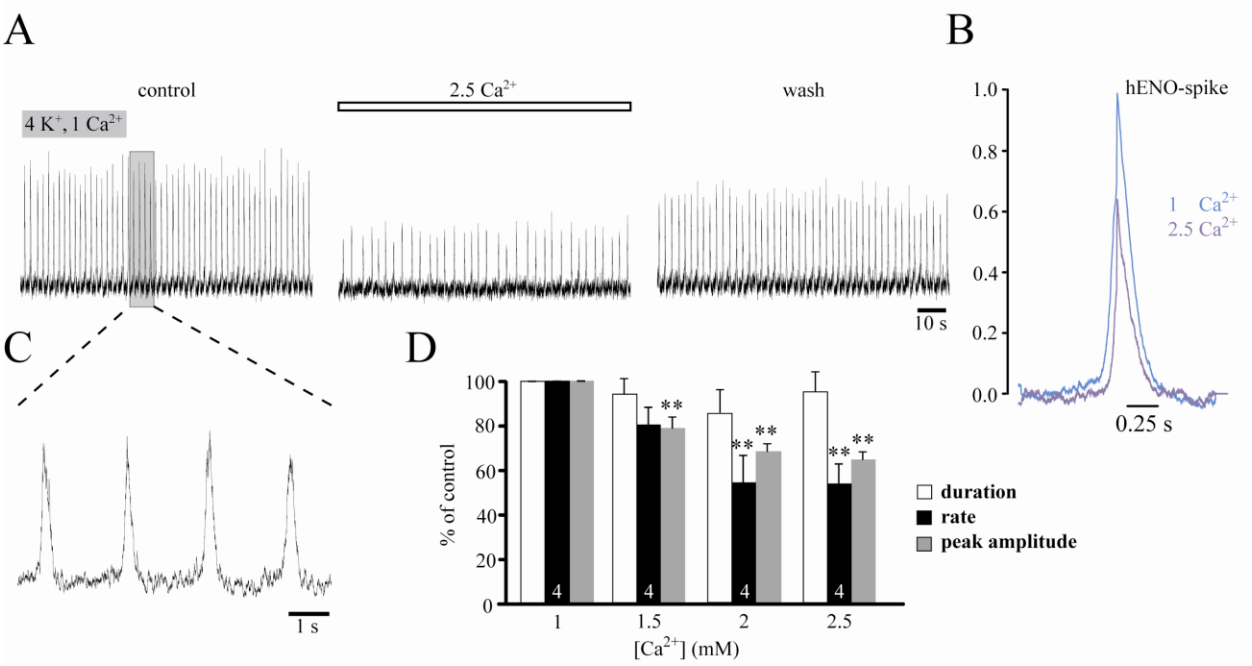

Fig. 3-3: Less prominent Ca^{2+} depression of spike-type hENOs. In a subset of slices, activity recorded from the CA_3 area comprised fast-rising, short duration spikes with a rate of 46.4 ± 15.6 bursts/min in 4 mM K^+. **A**, effect of high Ca^{2+} on typical spike hENOs. Raising Ca^{2+} to 2.5 mM depressed its rate to 31.5 ± 15.6 bursts/min and suppressed its amplitude by ~40%. **B**, average bursts of hENO-spike rhythm in control and high Ca^{2+}. **C**, inset of control hENO spike rhythm as seen in $\mathbf{A_1}$. **D**, bar graph showing spike duration, rate and peak amplitude, respectively, at incrementing increases in extracellular Ca^{2+}. (** P< 0.01)

Fig. 3-4

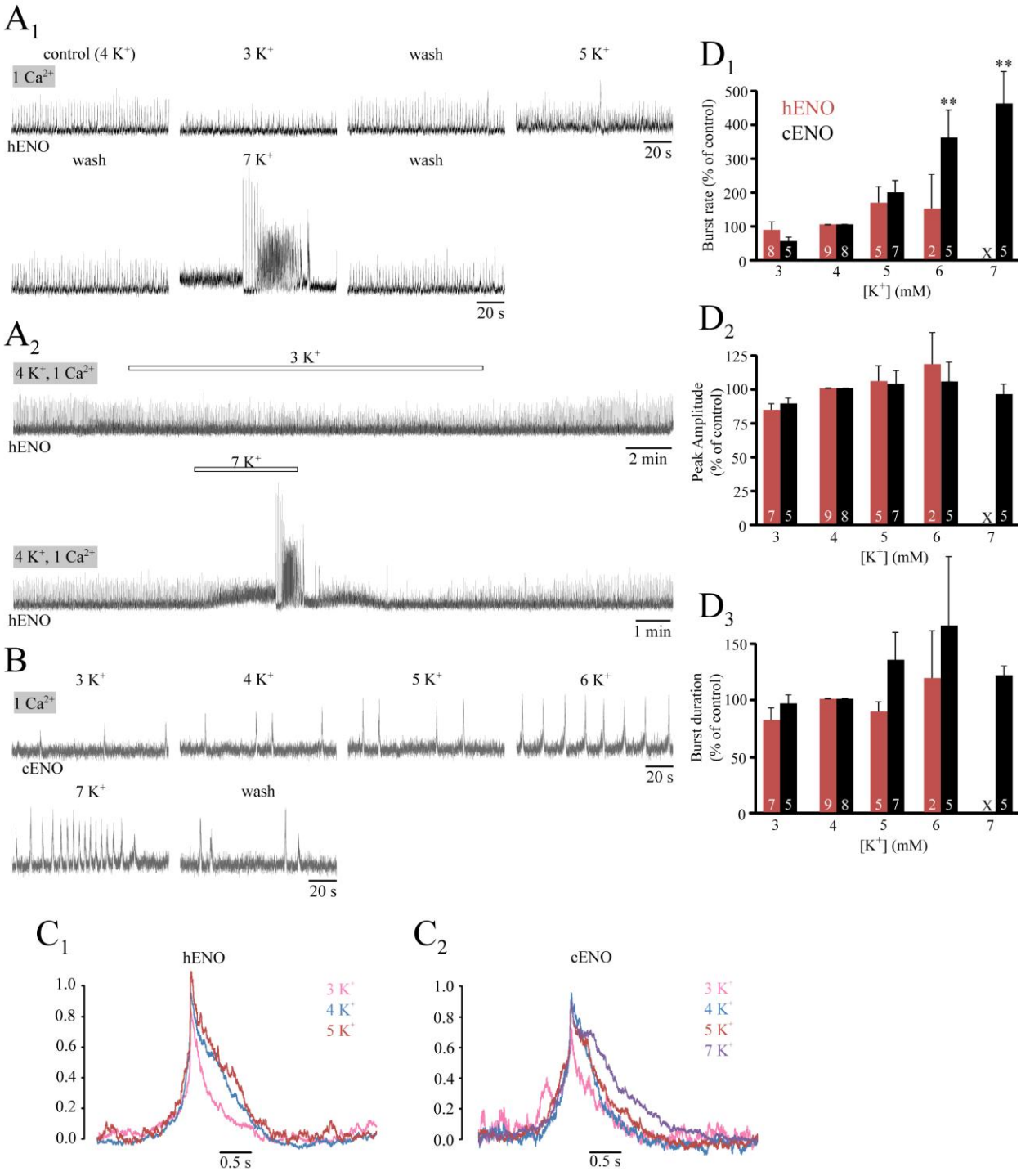

Fig. 3-4: Extracellular K^+ increases burst rates of ENOs. A_1, raising K^+ increased hENO rate, while reduction to 3 mM K^+ appeared to depress bursting. However, K^+ did not exert a major effect of hENOs. **A_2**, effects of varying K^+ as shown in **A_1** on extended time scale. Elevating K^+ from 4-7 mM evoked transient hyperexcitation in the CA3 region in the form of high amplitude,

interictal activity (IA) paired with ictal-like events (ILEs). **B**, Increasing K^+ to 5-7 mM increased the rate of cENOs from 4 bursts/min to 11-18 bursts/min while reducing K^+ to 3 mM slowed cENO rate to 1.5 bursts/min. K^+ did not seem to affect the pattern of average bursts (**C_1-C_2**). **D_1-D_3**, bar graphs showing mean ENO rates, burst amplitude, and burst duration, respectively. (** $P< 0.01$)

Fig. 3-5

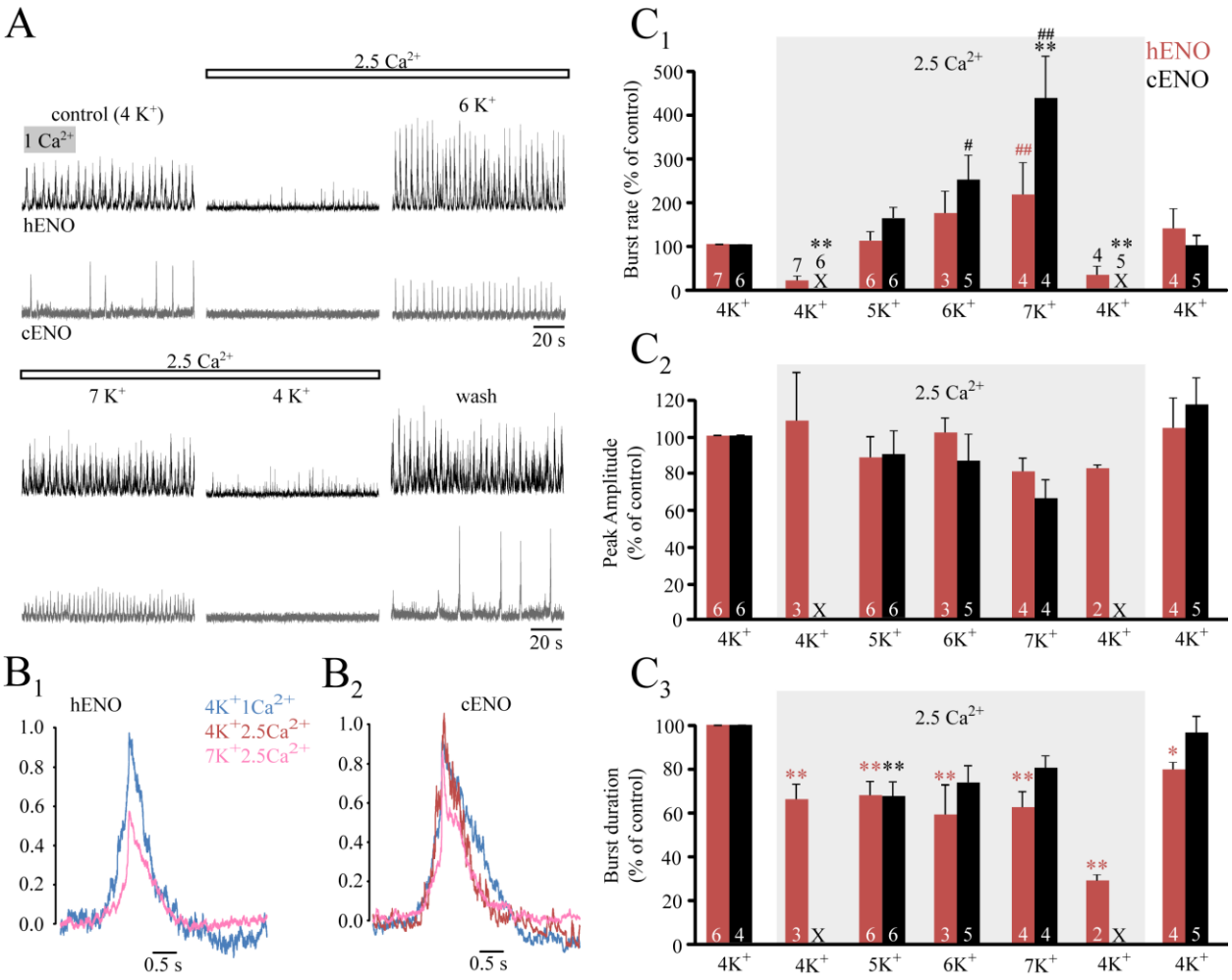

Fig. 3-5: Ca^{2+}/K^{+} antagonism of ENOs. A, simultaneous recordings of hENOs and cENOs were depressed upon increasing Ca^{2+} from 1 to 2.5 mM. Note that persistent small CA_3 activity in 2.5 mM Ca^{2+} comprised rhythmic short duration (0.5 s) spikes. Subsequently increasing K^{+} antagonized Ca^{2+} depression of ENO rates in dose-dependent manner. However, 7 mM K^{+} typically induced fast irregular hENOs. Subsequent return to 4 K^{+}/2.5 Ca^{2+} depressed both ENOs. Upon returning to control superfusate, spontaneous ENOs were restored. Average bursts (**B_1-B_2**) and analyses of ENO rates, amplitude, and duration (**C_1-C_3**) suggested strong modulation of Ca^{2+}/K^{+} on ENO rate, while burst durations were shorten by raised Ca^{2+}. Contrary, Ca^{2+}/K^{+} did not exert major effects on ENO amplitude. (* P< 0.05, ** P< 0.01)

Fig. 3-6

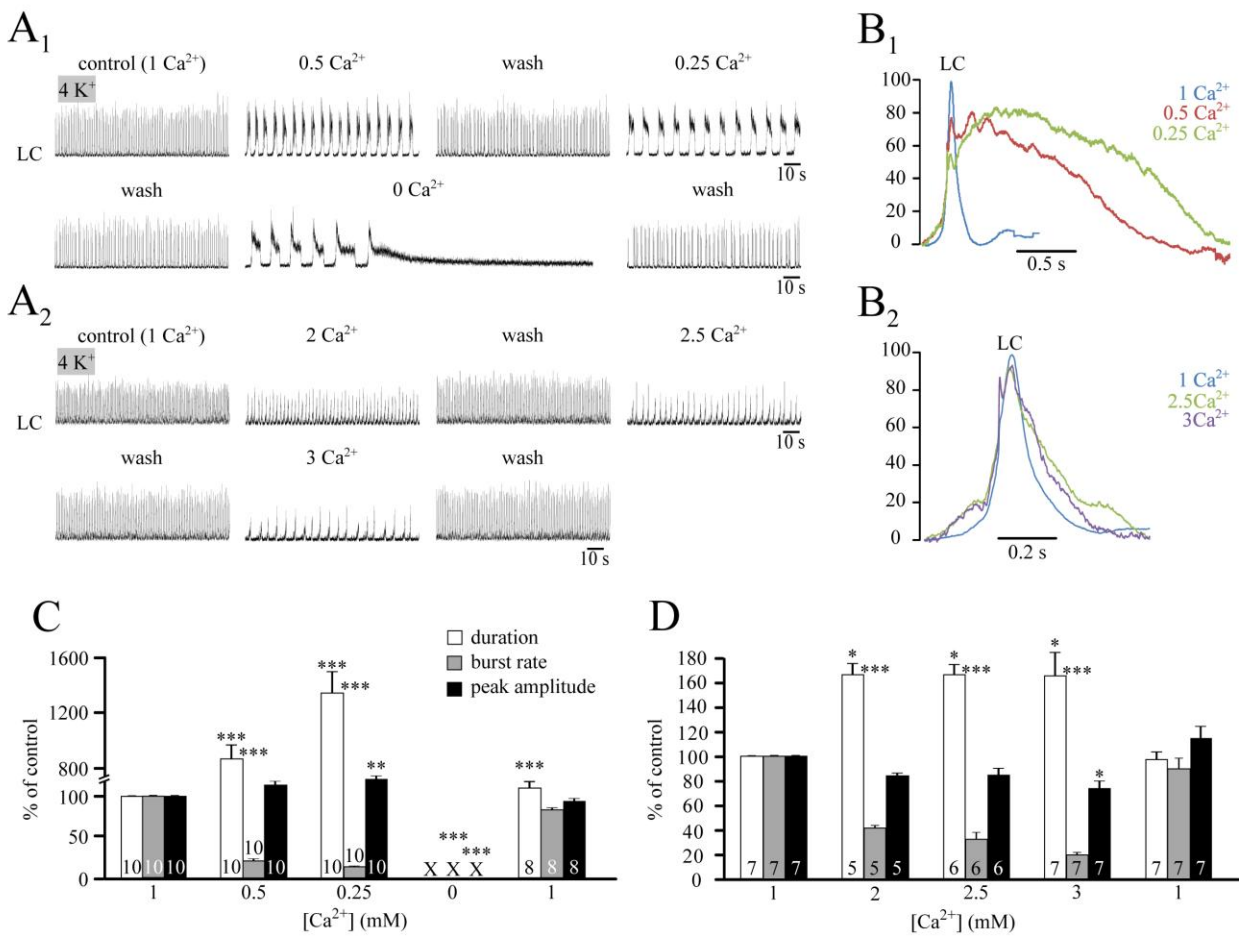

Fig. 3-6: Modulation of LC rhythm by extracellular Ca^{2+}. A, recording of *locus coeruleus* (LC) neurons in horizontal slice. **A_1**, decreasing Ca^{2+} to 0.25-0.5 mM decreased burst rate from 108 bursts/min to 14-22 bursts/min. LC rates recovered to levels similar to control upon returning to 1 mM Ca^{2+}. Within 5 min after start of removing Ca^{2+} from the superfusate, LC rhythm transformed into long duration, multi-peak bursts and then would be abolished. Returning to 1 mM Ca^{2+} recovered LC rhythm to levels similar to control. **A_2**, raising Ca^{2+} from 1 to 3 mM depressed the rate of LC bursts from 114 bursts/min to 22 bursts/min. **B_1-B_2**, average LC burst properties in low and high Ca^{2+}, respectively. Average bursts become longer in duration with supra- and subphysiological Ca^{2+}. **C**, **D**, effects of Ca^{2+} on mean LC duration, rate and burst amplitude, respectively. (* P< 0.05, ** P< 0.01, *** P<0.001)

Fig. 3-7

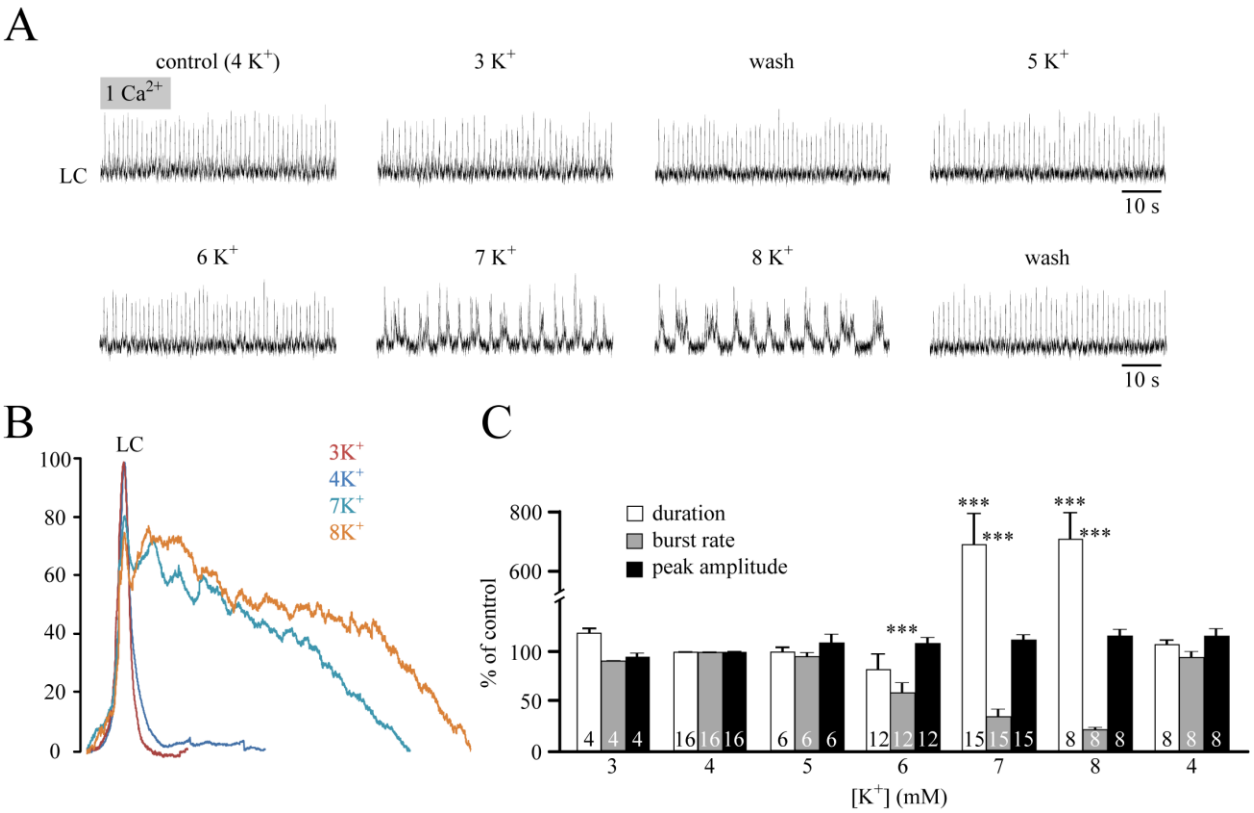

Fig. 3-7: Perturbation of LC rhythm by extracellular K^+. A, electrophysiological recording of the LC. Raising K^+ between 6-8 mM decreased LC burst rate to 58-21% and increased duration to 270-700% of control values, while lowering K^+ to 3 mM had little effect on burst dynamics. **B**, average LC bursts in varying extracellular K^+. **C**, bar graphs showing mean LC burst duration, rates, and peak amplitude, respectively, in varying K^+ concentrations. (*** P< 0.001)

Fig. 3-8

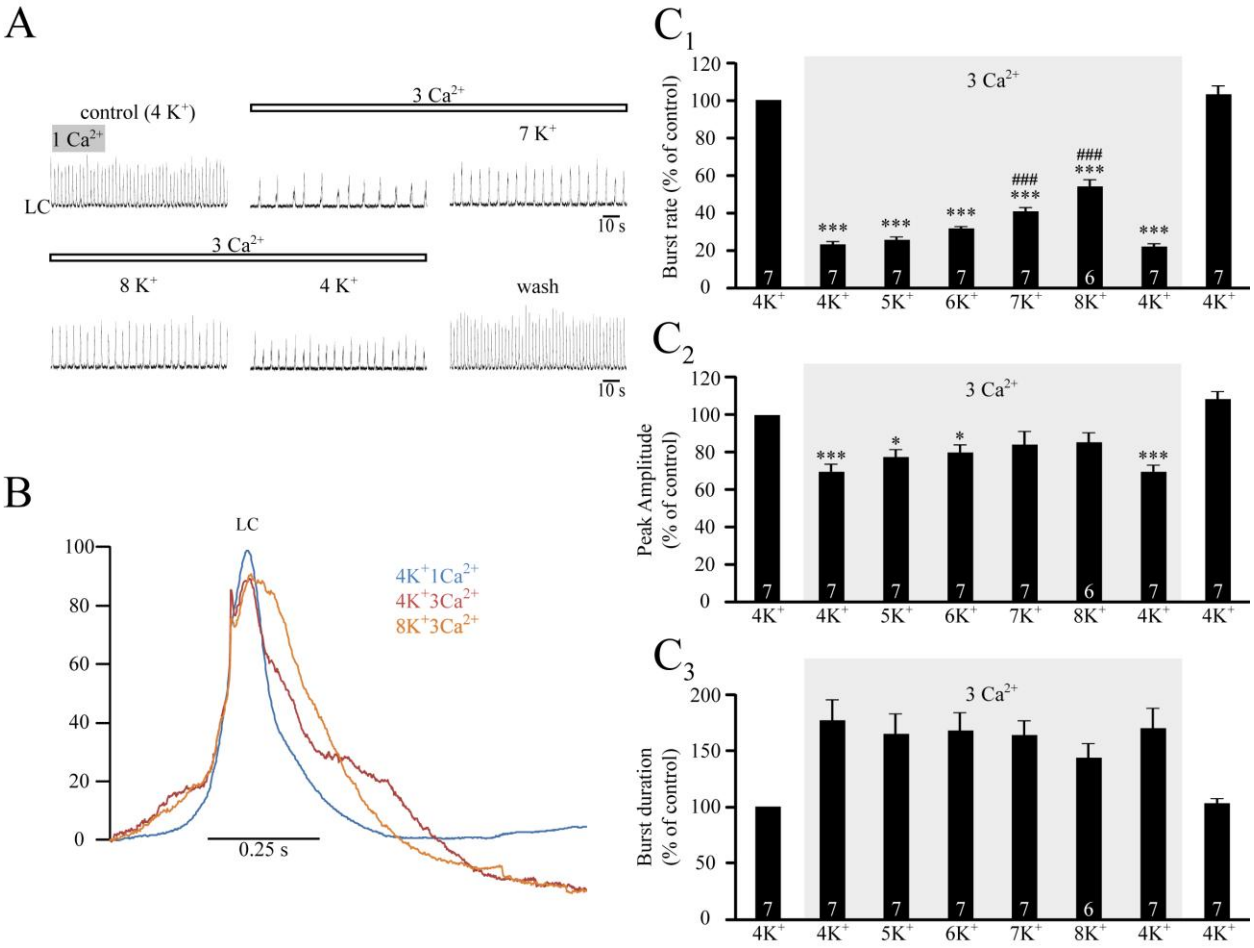

Fig. 3-8: Ca^{2+}/K^{+} antagonism of LC rhythm. A, LC burst rate and amplitude were depressed upon increasing Ca^{2+} from 1 to 3 mM. Concomitant increase in K^{+} antagonized Ca^{2+} depression of both LC burst rate and amplitude in dose-dependent manner with 7-8 mM K^{+} being the most effective at recovering close to control values. Subsequent return to 4K/3Ca solution depressed LC rhythm. Upon returning to control superfusate, spontaneous LC bursts were restored. Average LC bursts (**B**) in Ca^{2+}-depressed and concomitant K^{+}-evoked stimulation. **C_1-C_3,** bar graphs showing Ca^{2+}/K^{+} antagonism of mean LC burst rates, amplitude, and duration. (* P< 0.05, *** P< 0.001, ### *vs* values in 4 K^{+}/3 Ca^{2+})

Fig. 3-9

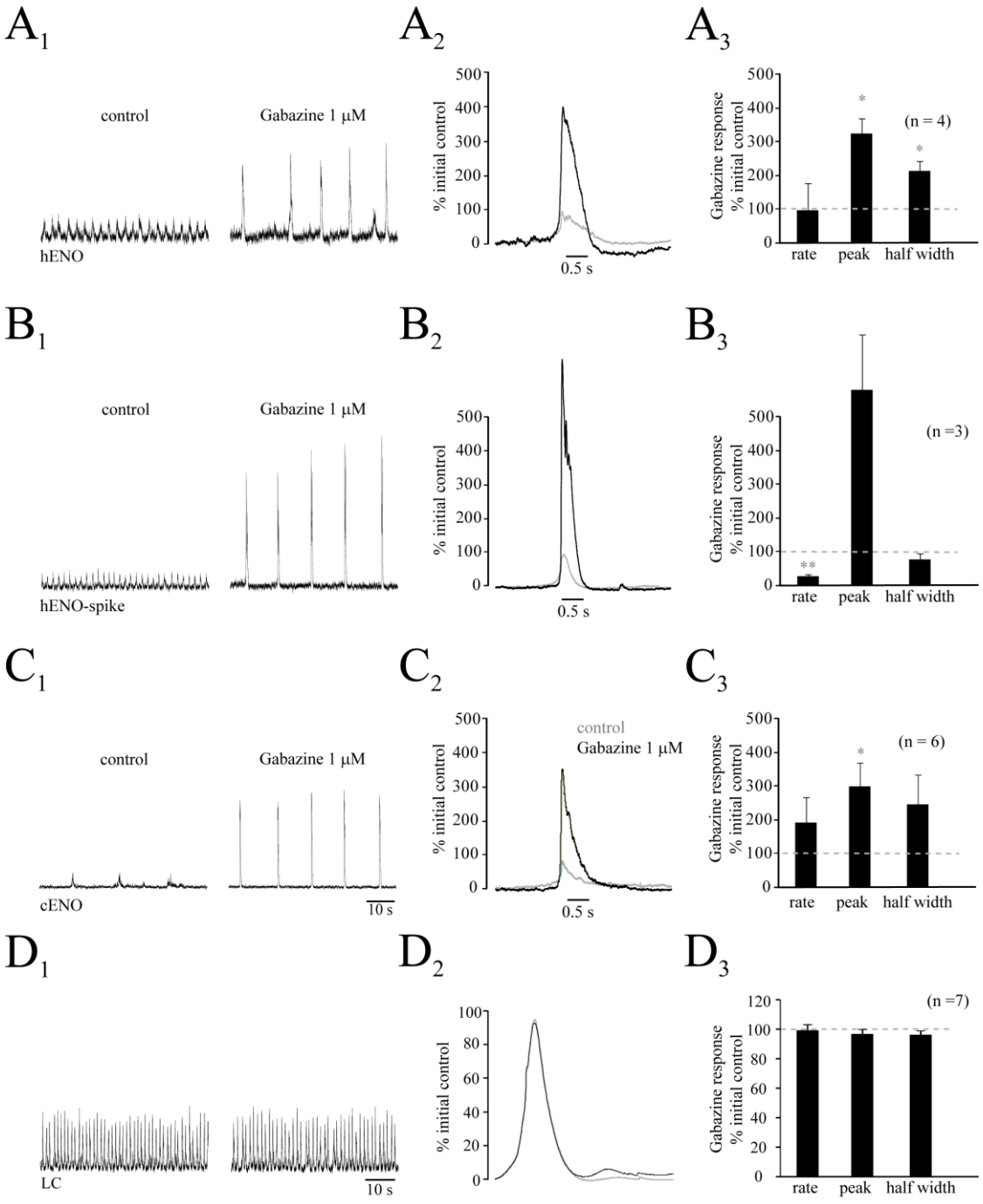

Fig. 3-9: Differential modulation by (anti)convulsant agents of bursting in CA3, EC and LC regions of horizontal newborn rat slices. A1-C1 , bath-application in 4 K^+/1 Ca^{2+} solution with 10 mM glucose of the pharmacological 'seizure model' gabazine (1 µM), an antagonist of A-type γ-aminobutyric acid ($GABA_A$) receptors, caused transformation of cENOs and hENOs

(bursts and spikes) into large amplitude bursts, reminiscent of interictal activity (IA) with representative average bursts shown in **A2-C2**. **A3-C3**, effects of gabazine on ENO rate, amplitude, and half-width, of hENOs, spike-hENOs, and cENOs, respectively. **D1**, Contrarily, application of 1 μM gabazine did not affect LC bursting as shown in average bursts (**D2**) and analyses of LC burst rate, peak, and half-width (**D3**). (* $P< 0.05$, ** $P<0.01$)

Fig. 3-10

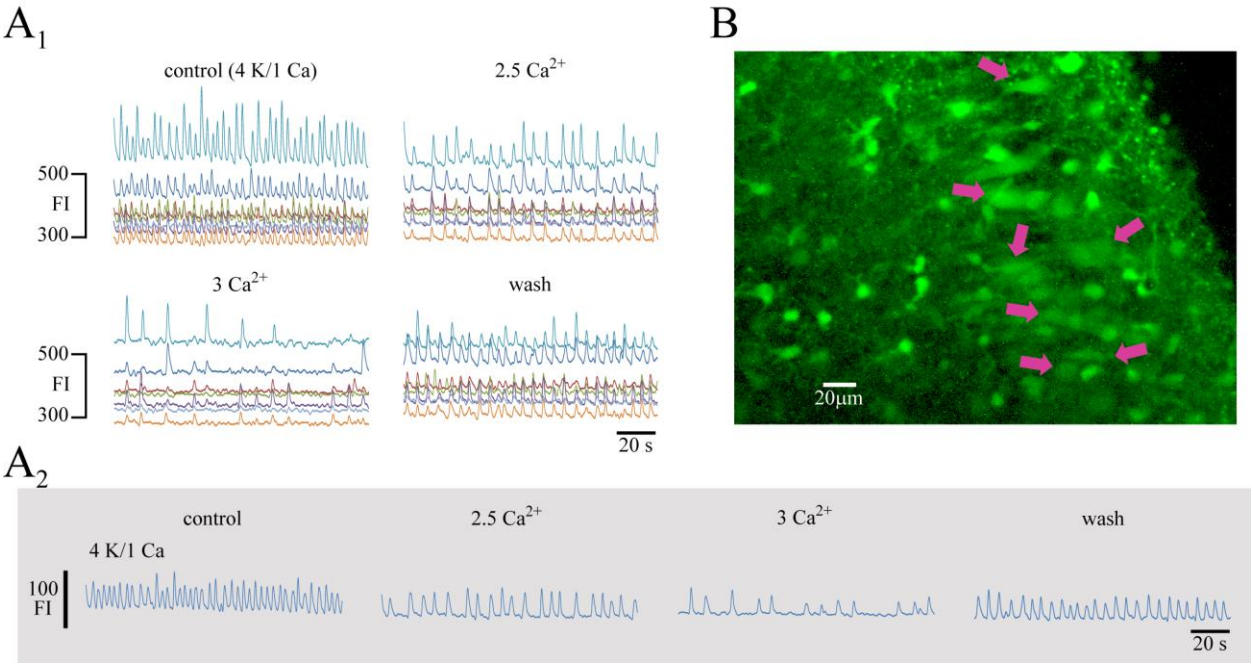

Fig. 3-10: Ca^{2+} rises in CA_3 neurons are depressed by supraphysiological Ca^{2+}. A-B, in a 400 mm thick hippocampal slice, CA_3 neurons (purple arrows, **B**) showed spontaneous and synchronous rises in intracellular Ca^{2+}. The frequency and synchronicity of these Ca^{2+} transients were depressed upon raising superfusate Ca^{2+} content to 2.5 and 3 mM (**A_1**) and recovered after returning to control. **A_2**, average traces (in grey box) of 7 spontaneously active CA_3 neurons show high degree of synchronicity between pyramidal neurons at physiologically relevant Ca^{2+} concentrations.

Fig. 3-11

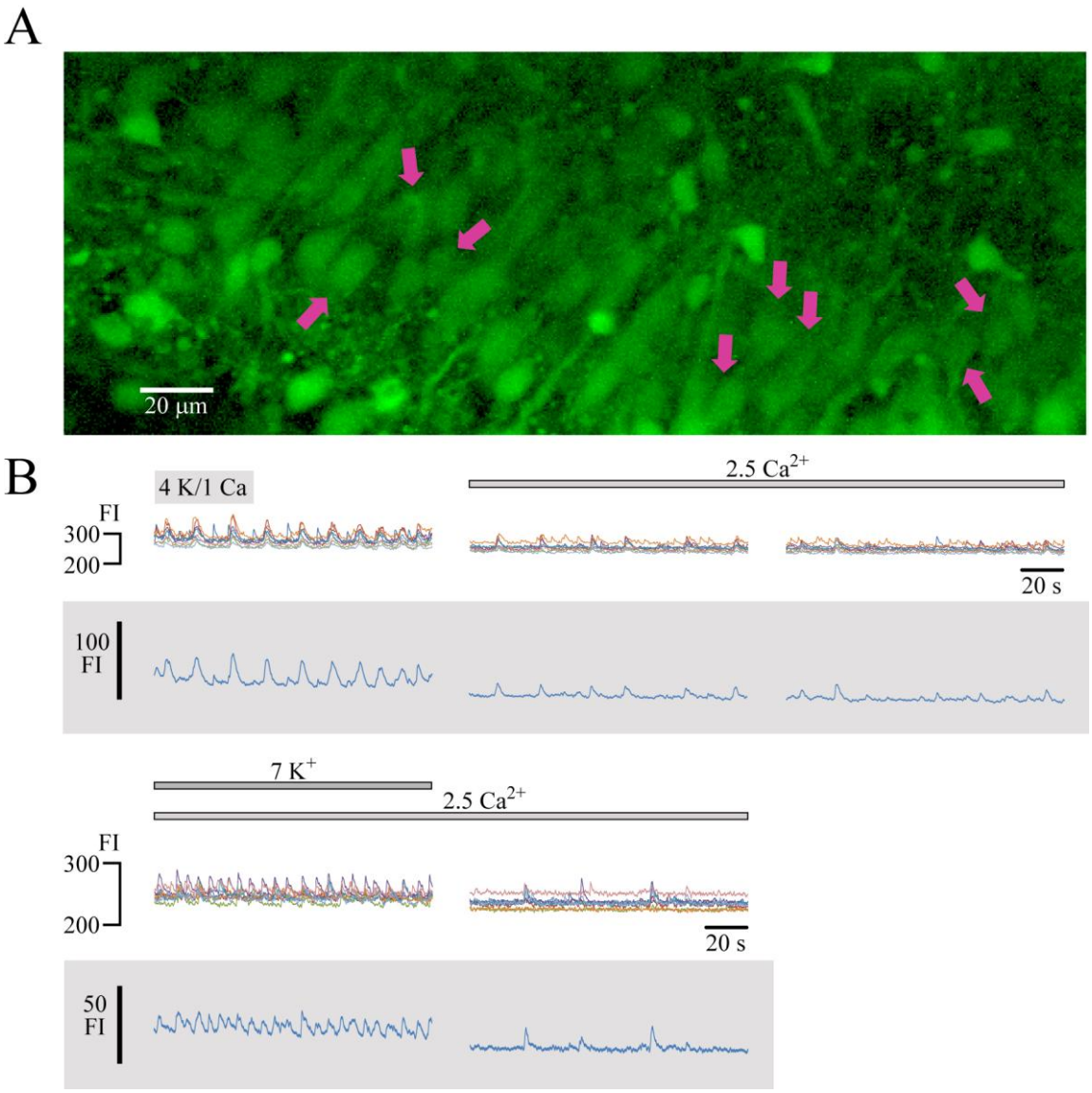

Fig. 3-11: Ca^{2+} rises in CA_3 neurons show typical Ca^{2+}/K^+ antagonism. In a 400 µm thick hippocampal slice from a P2 newborn rat, eight CA_3 neurons (**A**) showed spontaneous and synchronous Ca^{2+} rises, which were depressed with elevated Ca^{2+} (2.5 mM) (**B**). Concomitantly raising K^+ to 7 mM partially recovered frequency of oscillations similar to results shown in **Fig. 3-5.** Average traces of these eight CA_3 neurons are shown in grey boxes below individual neuronal traces.

Fig. 3-12

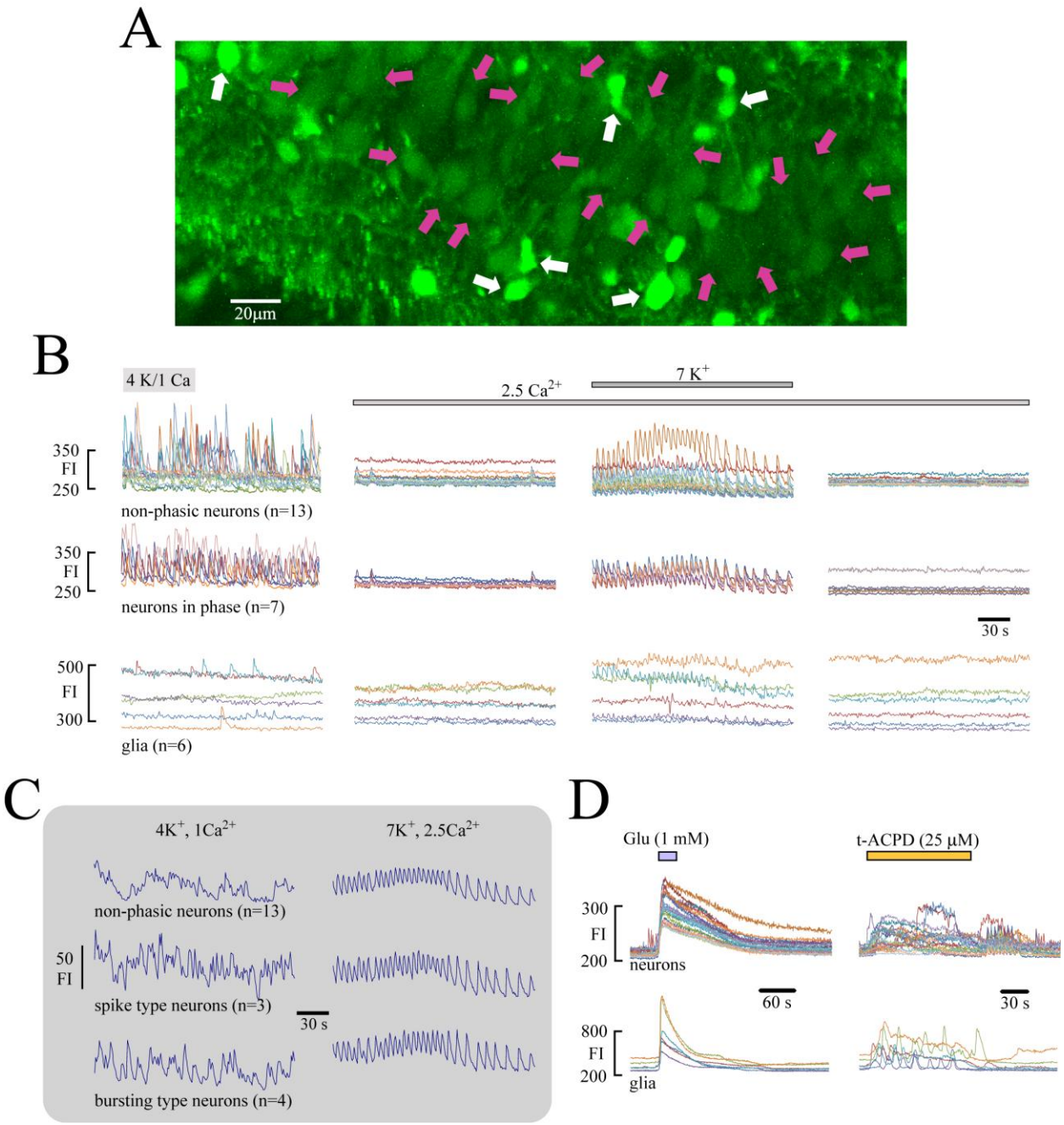

Fig. 3-12: K^+ improves synchronicity between CA_3 neurons in elevated Ca^{2+}. In a P3 hippocampal slice, suppression of Ca_i rises in CA_3 neurons (purple arrows, **A**) by high Ca^{2+} was antagonized by raising K^+ to 7 mM (**B**). Small cells outside the pyramidal layer roughly 8-10 µm in diameter, presumably glial cells, showed minor Ca_i rises in control superfusate, which were

similarly depressed with supraphysiological Ca^{2+}. Fast glial Ca_i rises were evoked after concomitant elevation of K^+ to 7 mM. **C**, Ca^{2+} rises in CA_3 neurons were divided into three groups based on firing properties: chaotic Ca^{2+} rises out of phase (non-phasic neurons), fast Ca^{2+} oscillations in phase (spike-type neurons), and slower rhythmic Ca^{2+} rises (bursting-type neurons). Traces represent averages of "n" number of cells in control and in supraphysiological Ca^{2+} and K^+. High K^+ in elevated Ca^{2+} improves the synchronicity of all three groups. All neurons studied (n=20) were recruited into a uniform burst that encompassed the entire CA3 region. **D**, bath-application of glutamate (Glu) for 30 s led to a prominent Ca_i increase in both CA3 neurons and presumptive glia. Exposure to 2 min of t-ACPD roughly 20 min later evoked partly oscillatory Ca_i rises in both cell types.

3.7 References

Allene C, Cossart R (2010) Early NMDA receptor-driven waves of activity in the developing neocortex: physiological or pathological network oscillations? J Physiol 588.1, 83-91

Allène C, Cattani A, Ackman JB, Bonifazi P, Aniksztejn L, Ben-Ari Y, Cossart R (2008) Sequential generation of two distinct synapse-driven network patterns in developing neocortex. J Neurosci 28, 12851-12863

Balestrino M, Aitken PG, Somjen GG (1986) The effects of moderate changes of extracellular K+ and Ca2+ on synaptic and neural function in the CA1 region of the hippocampal slice. Brain Red 377, 229-239

Ballantyne D, Andrzejewski M, Muckenhoff K, Scheid P (2004) Rhythms, synchrony and electrical coupling in the locus coeruleus. Resp Physiol Neurobiol 143, 199-214

Ballanyi K (2012) Isolated Central Nervous System Circuits. Neuromethods Series (Walz W, ed.) Springer Science+Business Media, LLC, New York, NY (*in press*)

Ballanyi K, Ruangkittisakul A (2009) Structure-function analysis of rhythmogenic inspiratory pre-Botzinger complex networks in 'calibrated' newborn rat brainstem slices. Respir Physiol Neurobiol 168, 158-178

Ben-Ari Y, Cherubini E, Corradetti R, Caiarsa JL (1989) Giant synaptic potentials in immature rat CA3 hippocampal neurones. J Physiol 416, 303-325

Ben-Ari Y, Gaiarsa JL, Tyzio R, Khazipov R (2007) GABA: a pioneer transmitter that excites immature neurons and generates primitive oscillations. Physiol Rev 87, 1215-1284

Berkenbosch A, Adan AJ (1974) Influence of CSF calcium concentration on the ventilator response to CO_2 and O_2. Eur J Physiol (Pflüger's Arch) *348, 33-50*

Berndt J, Fenner A, Berger K. (1969) Influence of calcium and magnesium on the respiratory response to changes in CSF pH. Respir Physiol Neurobiol 7, 216-229

Brown PD, Davies SL, Speake T, Millar ID (2004) Molecular mechanisms of cerebrospinal fluid production. Neuroscience 129, 957-970

Browm EM, MacLeod RJ (2001) Extracellular calcium sensing and extracellular calcium signalling. Physiol Rev 81, 239-297

Bonifazi P, Goldin M, Picardo MA, Jorquera I, Cattani A, Bianconi G, Represa A, Ben-Ari Y, Cossart R. (2009) GABAergic hub neurons orchestrate synchrony in developing hippocampal networks. Science 326, 1419-1424

Brumberg JC, Nowak LG, McCormick DA (2000) Ionic mechanisms underlying repetitive high-frequency burst firing in supragranular cortical neurons. J Neurosci 20, 4829-4843

Chen W, Bergsman JB, Wang X, Gilkey G, Pierpoint CR, Daniel EA, Awumey EM, Dauban P, Dodd RH, Ruat M, Smith SM (2010) Presynaptic external calcium signaling involves the calcium-sensing receptor in neocortical nerve terminals. PLoS One 5, e8563

Czeh G & Somjen GG (1989) Changes of extracellular calcium and magnesium and synaptic transmission in isolated mouse spinal cord. Brain Res 486, 274-285

De Oliveira RB, Howlett MC, Gravina FS, Imtiaz MS, Callister RJ, Van Helden DF (2011) Developmental changes in pacemaker currents in mouse locus coeruleus neurons. Brain research 1425, 27-36

Del Castillo J, Engbaek L (1954) The nature of the neuromuscular block produced by magnesium. J Physiol 124, 370-384

Feldman JL, Del Negro CA (2006) Looking for inspiration: new perspectives on respiratory rhythm. Nat Rev Neurosci 7, 232-242

Foffani G, Uzcategui YG, Gal B, Menendez de la Prida L (2007) Reduced spike-timing reliability correlates with the emergence of fast ripples in the rat epileptic hippocampus. Neuron 55, 930-941

Garaschuk O, Linn J, Eilers J, Konnerth A (2000) Large-scale oscillatory calcium waves in the immature cortex. Nature 3(5), 452-459

Hansen AJ (1985) Effect of anoxia on ion distribution in the brain. Physiol Rev 65, 101-148

Heinemann U, Stabel J, Rausche G (1990) Activity-dependent ionic changes and neuronal plasticity in rat hippocampus. Progr Brain Res 83, 197-214

Heinemann U, Lux HD, Gutnick MJ (1977) Extracellular free calcium and potassium during paroxsmal activity in the cerebral cortex of the cat. Exp Brain Res 27, 237-243

Hille B (2001) Ion channels of excitable membranes. Sunderland, MA: Sinauer Associates

Jefferys JG (1995) Nonsynaptic modulation of neuronal activity in the brain: electric currents and extracellular ions. Physiol Rev 75, 689-723

Kantor CM, Panaitescu B, Kuribayashi J, Ruangkittisakul A, Jovanovic I, Leung V, Lee TF, MacTavish D, Jhamandas JH, Cheung PY, Ballanyi K (2012) Spontaneous neural network oscillations in hippocampus, cortex, and locus coeruleus of newborn rat and piglet brain slices. In: Isolated CNS circuits. (Ballanyi K, ed.) Humana-Springer (in press)

Khazipov R, Khalilov I, Tyzio R, Morozova E, Ben-Ari Y, Holmes GL (2004) Developmental changes in GABAergic actions and seizure susceptibility in the rat hippocampus. Eur J Neurosci 19, 590-600

Kilb W, Sinning A, Luhmann HJ (2007) Model-specific effects of bumetanide on epileptiform activity in the in-vitro intact hippocampus of the newborn mouse. Neuropharmacol 53, 524-533

Konnerth A, Heinemann U, Yaari Y (1986) Nonsynaptic epileptogenesis in the mammalian hippocampus in vitro. I. Development of seizurelike activity in low extracellular calcium. J Neurophysiol 56, 409-423

Kuwana S, Okada Y, Natsui T (1998) Effects of extracellular calcium and magnesium on central respiratory control in the brainstem-spinal cord of neonatal rat. Brain Res 786, 194-204

Leusen I. (1972) Regulation of cerebrospinal fluid composition with reference to breathing. Physiol Rev 52, 1-56

McCabe AK, Easton CR, Lischalk JW, Moody WJ (2007) Roles of glutamate and GABA receptors in setting the developmental timing of spontaneous synchronized activity in the developing mouse cortex. Dev Neurobiol 67, 1574-1588

Moore AR, Zhou WL, Jakovcevski I, Zecevic N, Antic SD (2012) Physiological properties of human fetal cortex in vitro. In: Isolated Central Nervous System Circuits (Ed K Ballanyi), Neuromethods Series (Ed W Walz). Springer Science+Business Media, LLC, New York, NY (*in press*)

Moriceau S, Roth TL, Sullivan RM (2010) Rodent model of infant attachment learning and stress. Dev Psychobiol 52, 651-660

Nicholson C, ten Bruggencate G, Stockle H & Steinberg R (1978) Calcium and potassium changes in extracellular microenvironment of cat cerebellar cortex. J Neurophysiol 41, 1026-1039

Nilsson P, Hillered L, Olsson Y, Sheardown MJ & Hansen AJ (1993) Regional changes in interstitial K^+ and Ca^{2+} levels following cortical compression contusion trauma in rats. J Cereb Blood Flow Metab 13, 183-192

Okada Y, Kuwana S, Kawai A, Mückenhoff K, Scheid P (2005) Significance of extracellular potassium in central respiratory control studied in the isolated brainstem-spinal cord preparation of the neonatal rat. Respir Physiol Neurobiol 146, 21-32

Olpe HR, Steinmann MW, Hall RG, Brugger F, Pozza MF (1988) $GABA_A$ and $GABA_B$ receptors in locus coeruleus: effects of blockers. Eur J Pharmacol 149, 183-185

Panaitescu B, Ruangkittisakul A, Ballanyi K (2009) Silencing by raised extracellular Ca2+ of pre-Botzinger complex neurons in newborn rat brainstem slices without change of membrane potential or input resistance. Neuosci Lett 456, 25-29

Pittman QJ, Hatton JD & Bloom FE (1981). Spontaneous activity in perfused hypothalamic slices: dependence on calcium content of perfusate. Exp Brain Res 42, 49-52

Puka-Sundvall M, Hagberg H, Andine P (1994) Changes in extracellular calcium concentration in the immature rat cerebral cortex during anoxia are not influenced by MK-801. Brain Res Dev Brain Res 77, 146-150

Rausche G, Ingelmund P, Heinemann U (1990) Effects of changes in extracellular potassium, magnesium, and calcium concentration on synaptic transmission in CA1 and the dentate gyrus of rat hippocampal slices. Pflugers Arch 415, 588-593

Ruangkittisakul A, Panaitescu B, Ballanyi K (2011) K^+ and Ca^{2+} dependence of inspiratory-related rhythm in novel "calibrated" mouse brainstem slices. Resp Physiol Neurobiol 175, 37-48

Ruangkittisakul A, Secchia L, Bornes TD, Palathinkal DM, Ballanyi K (2007) Dependence on extracellular Ca^{2+}/K^+ antagonism of inspiratory centre rhythms in slices and en bloc preparations of newborn rat brainstem. J Physiol 584, 489-508

Ruangkittisakul A, Secchia-Ballanyi L, Panaitescu B, Bobocea N, Kuribayashi J, Iizuka M, Kantor C, Ballanyi K (2012) Anatomically 'calibrated' isolated respiratory networks from newborn rodents. In: Isolated Central Nervous System Circuits (Ed K Ballanyi), Neuromethods Series (Ed W Walz). Springer Science+Business Media, LLC, New York, NY (*in press*)

Sanchez-Vives MV, McCormick DA (2000) Cellular and network mechanisms of rhythmic recurrent activity in neocortex. Nat Neurosci 3, 1027-1034

Sanchez-Vives MV, Descalzo VF, Reig R, Figueroa NA, Compte A, Gallego R (2008) Rhythmic spontaneous activity in the piriform cortex. Cereb Cortex 18, 1179-1192

Sheroziya MG, von Bohlen und Halbach O, Unsicker K, Egorov AV (2009) Spontaneous bursting activity in the developing entorhinal cortex. J Neurosci 29, 12131-12144

Sipilä ST, Huttu K, Soltesz I, Voipio J, and Kaila K (2005) Depolarizing GABA acts on intrinsically bursting pyramidal neurons to drive giant depolarizing potentials in the immature hippocampus. J Neurosci 25, 5280-5289

Sipila ST, Kaila K (2007) GABAergic control of CA3-driven network events in the developing hippocampus. *Results* Probl Cell Differ 44, 99-121

Somjen GG (2002) Ion regulation in the brain: implications for pathophysiology. Neuroscientist 8, 254-267

Stringer JL (1998) Regulation of extracellular potassium in the developing hippocampus. Brain Res Dev Brain Res 110, 97-103

Stringer JL, Lothman EW (1988) In vitro effects of extracellular calcium concentrations on hippocampal pyramidal cell responses. Exp Neurol 101, 132-46

Su H, Alroy G, Kirson ED, Yaari Y (2001) Extracellular calcium modulates persistent sodium current-dependent burst-firing in hippocampal pyramidal neurons. J Neurosci 21, 4173-4182

Xiong Z, Lu W, MacDonald JF (1997) Extracellular calcium sensed by a novel cation channel in hippocampal neurons. Proc Natl Acad Sci *USA.* 94, 7012-7017

Chapter-4

Methylxanthine-evoked Seizure-like Perturbation of Spontaneous Bursting in Hippocampal and Cortical Networks of Newborn Rat Brain Slices

Chase M. Kantor, Araya Ruangkittisakul, Junya Kuribayashi, Klaus Ballanyi*

Department of Physiology, 750 MSB, University of Alberta, Edmonton, AB, Canada T6G 2S2

My contribution to this study consisted of the planning, execution, and analysis of the electrophysiology studies for both age groups. Calcium imaging of horizontal slices was conducted in conjunction with Dr. A. Ruangkittisakul. Other electrophysiology experiments were performed by Dr. J. Kuribayashi. Dr. K Ballanyi developed the concept for the work and revised the manuscript.

*Corresponding author: Klaus Ballanyi at the above address

4.1 Abstract

Caffeine and theophylline counter apneas in (preterm) infants by stimulating active medullary neural respiratory networks. It is not known whether these methylxanthines influence 'Early Network Oscillations' in the neonatal hippocampal CA3 area (hENOs) and ento/perirhinal cortex (cENOs). Here, we studied this in newborn rat brain slices upon bath-application of 0.1-10 mM theophylline or caffeine. At 0.25-2.5 mM, theophylline tended to increase the rate and/or amplitude of both types of electrophysiologically recorded ENOs. Starting at 0.25 mM, theophylline perturbed both events by inducing seizure-like discharges that comprise either complex ictal-like events (ILEs) or interictal activities (IAs). During theophylline-evoked ILEs and IAs, rises of cytosolic Ca^{2+} (Ca_i) in CA_3 and cortical neurons were more synchronized and augmented in amplitude without occurrence of perturbation of Ca^{2+} homeostasis. In both networks, responses to caffeine were similar, but typically required higher doses while ILEs occurred less frequently. Slices from postnatal day (P) 8-10 rats appeared to be more prone to methylxanthine-evoked ILEs and IAs than the P1-4 slices. In both CA_3 and cortical areas, $GABA_A$ receptor blockade with gabazine (1-5 µM) evoked ILEs and IAs similar to methylxanthines. Phosphodiesterase-4 inhibition with rolipram (5-10 µM) did not mimic methylxanthine effects as tested for hENOs. The findings indicate that 0.25-2.5 mM methylxanthine can stimulate hippocampal and cortical ENOs. However, the threshold for severe seizure-like perturbation of these events by methylxanthines is only slightly higher, with theophylline being more effective and the older age group being more susceptible. Underlying mechanisms likely involve neither blockade of store-mediated Ca^{2+} release nor phosphodiesterase-4, while $GABA_A$ receptor blockade contributes partially.

4.2 Introduction

Methylxanthines like caffeine or theophylline stabilize irregular breathing in (preterm) human infants (Comer et al., 2001; Schmidt et al., 2006; Daly, 2007). This excitatory methylxanthine action appears to target primarily neuron-glia networks in the inspiratory active pre-Bötzinger complex (preBötC) that initiates and controls normal breathing movements (Ballanyi et al., 1999; Ballanyi, 2004a; Feldman & Del Negro, 2006). According to the latter reports, rhythmic preBötC bursting depends on the interaction of intrinsic cellular bursting properties such as persistent Na^+ channels with (recurrent glutamatergic) excitatory synaptic processes. In the early postnatal period, also neural networks in the hippocampus and entorhinal cortex show spontaneous rhythmic bursting comprising 'early network oscillations' (ENOs) based on 'giant depolarizing potentials' (GDPs) in individual neurons (Ben-Ari et al., 1989, 2007; Garaschuk et al., 2000; Khazipov & Luhmann, 2006; Sipilä & Kaila, 2007; Allene & Cossart, 2010). While respiratory networks must function already at birth, cortical networks are yet immature and ENOs may promote connectivity particularly via depolarization-related rises of neuronal Ca^{2+} (Leinekugel et al., 1997; Garaschuk et al., 2000; Spitzer, 2006). It has not been studied yet, whether therapeutic methylxanthine concentrations modulate these ENOs and if higher doses cause hyperexcitability in these circuits. In fact, it is known that methylxanthine doses above therapeutic plasma levels of 100-200 µM can evoke seizures in addition to other systemic side effects such as nausea, hyperglycemia, tachycardia or tachypnea (Dzalha et al., 1997; Delanty et al., 1998; Comer et al., 2001; Korematsu et al., 2008; El-Bitar & Boustany, 2009). The latter clinical reports and studies on respiratory control (Eldridge et al., 1985; Hedner et al., 1985; Herlenius et al., 2002; Montandon et al., 2008) established the idea that therapeutic methylxanthine primarily blocks A_1-type adenosine receptors which presumably tonically inhibit respiratory networks. This view

contrasts with our previous *in vitro* findings on isolated newborn rat slice and *en bloc* brainstem preparations. Specifically, we showed that adenosine does not affect fictive inspiratory-related preBötC bursting and that >1 mM methylxanthine is necessary to stimulate the preBötC and evoke seizure-like discharges in spinal motor networks (Brockhaus & Ballanyi, 2000; Ballanyi, 2004a,b; Ruangkittisakul et al., 2010; Ruangkittisakul & Ballanyi, 2010). This suggests that other mechanisms than adenosine receptor blockade can excite or cause seizures in (active) neural networks. Specifically, these mechanisms are blockade of (*i*) degradation of cyclic-adenosine monophosphate (cAMP) by phosphodiesterase-4 (PDE4), (*ii*) A-type γ-aminobutyric acid ($GABA_A$) receptors, or (*iii*) cellular Ca^{2+} homeostasis (Ukena et al., 1993; Fredholm et al., 1999; Daly, 2007).

Here, horizontal newborn rat brain slices were used to study modulatory methylxanthine effects on hippocampal and cortical ENOs (hENOs, cENOs) assessed in the CA_3 region and the entorhinal/perirhinal cortex, respectively. For this, neuronal population activity underlying these ENOs was electrophysiological assessed with suction electrodes to determine dose-response relationships for bath-applied theophylline and caffeine to study whether possible epileptogenic effects of low millimolar methylxanthine involve blockade of PDE4 or $GABA_A$ receptors. To explore whether such methylxanthine doses perturb (store-mediated) Ca^{2+} signaling, free cytosolic Ca^{2+} concentration (Ca_i) was monitored in CA_3 hippocampal and entorhinal/perirhinal cortex neurons as well as neighboring astrocytes using a multiphoton/confocal imaging approach that we have established for studying preBötC cells (Ruangkittisakul et al., 2006, 2008, 2009).

4.3 Methods

(see **§2**)

4.4 Results

A three-pronged strategy was applied here for studying methylxanthine effects on isolated newborn rat hippocampal (CA3) and cortical (entorhinal/perirhinal) circuits. Specifically, horizontal brain slices were used for (*i*) dose-response analysis of their effects on hENOs and cENOs and assessment of effects of blockade of PDE4 and $GABA_A$ receptors, (*ii*) Ca_i imaging in CA3 and cortical neurons and astrocytes, (*iii*) experiments were done on slices from P1-4 and P8-10 rats serving as a model for nervous processes in preterm and term human infants, respectively.

It was revealed here that low millimolar methylxanthine evoked two types of seizure-like discharges. Because these activities closely resembled those described for bumetanide-evoked epileptiform activity in intact newborn mouse hippocampi (Kilb et al., 2007), we refer to them as 'ictal-like events' (ILEs) or 'interictal activities' (IAs). In the latter study, ILEs comprised a series of >1 min long bursts occurring about once every 5 min **(Fig. 1-7)**. Each burst consisted of initially large amplitude short discharge at ~20 Hz which turned after about 10 s into smaller amplitude discharge at ~5-10 Hz with longer burst duration while it ended with large amplitude bursts at a rate of 11-14 bursts/min. In contrast, IAs had a simpler pattern and consisted of large amplitude regular bursts occurring at a rate of ~1-3 bursts/min.

4.4.1 Methylxanthine Effects on hENOs

It was one major aim of the present study to determine methylxanthine effects on hENOs and cENOs based on suction electrode recording of their synchronized extracellular field potentials. For this, we firstly established dose-response relationships for both theophylline and caffeine in either age group. However, methylxanthine effects on hENOs were quite variable, particularly in the submillimolar range. This was partly due to the fact that hENOs showed 4 different patterns in control solution **(Fig. 4-1)**. The predominant activity (~60% of cases) was a regular 'burst' pattern whereas a 'spike' pattern occurred in about 20% of cases. The mixed 'burst/spike' and the 'plateau burst' patterns, which comprised about 15% and 5% of activities, respectively, were at times stable for time periods <1 h needed to test different doses of theophylline or caffeine. Because of this variability, this section of the results is partly descriptive while several parameters, such as the incidence of occurrence of IAs and ILEs and the augmentation of their amplitude compared to that of control hENOs, could be quantified.

Submillimolar methylxanthine: At 0.1, 0.25 and 0.5 mM, both theophylline and caffeine showed a trend in ~30% of cases at P1-4 and ~60% of cases at P8-10 to increase burst amplitude and/or burst rate, in both cases by 20-100% **(Fig. 4-2A**, **B, 4-3A)**. Moreover, the agents could raise the baseline of the integrated suction electrode signal resembling findings from our group on preBötC slices which indicates activity of tonic neurons (Panaitescu et al., 2009). The percentage of occurrence for such baseline increase was up to 50% of P1-4 (n= 8-13) slices and 60-85% of P8-10 (n= 11-13) slices for theophylline, compared to 10-30% of P1-4 (n= 10) and 100% at P8-10 (n= 6) with caffeine **(Fig. 4-2B, 4-4)**. Neither methylxanthine evoked IAs or ILEs at P1-4 or P8-10 (each 6-10 slices), except in one P9 slice **(Tab. 1)**.

Low millimolar methylxanthine: At 1, 2.5, 5 and 10 mM, both methylxanthines could exert similar stimulatory effects on hENO burst amplitude, rate, and electrode signal baseline at P8-10 as submillimolar doses. Caffeine seemed to better stimulate P1-4 hENOs as a higher percentage (~60%) of slices showed increases in amplitude and rate during caffeine. Both methylxanthines increased baseline in 40-80% of cases at P1-4 **(Fig. 4-2, 4-4A)** and could also evoke wave-like baseline oscillations in this age group, with caffeine effects being more prominent (20-60% *versus* 8-13%) than those of theophylline **(Fig. 4-2, 4-4A)**. However, such wave-like baseline oscillations were not a typical response of methylxanthines at P8-10, except in one slice during caffeine. In addition to stimulation of burst amplitude and rate, low millimolar methylxanthines characteristically evoked seizure-like discharges displayed as ILEs or IAs that perturbed or blocked normal hENOs **(Figs. 4-2B, 4-3B**, **4-4A)**. ILEs or IAs were observed at increased incidence when raising methylxanthine dose toward 10 mM **(Tab. 1)**. On the other hand, additional synaptic, non-correlated spikes were present between repetitive IA's or between IAs and ILEs. Specifically, IAs occurred in 5 or 10 mM theophylline in 58% and 60% of P1-4 slices, respectively. Quantitative analysis, performed for methylxanthine response at 10 mM, revealed a mean rate of 6.58 ± 0.66 bursts/min (n= 9) and amplitude augmentation to 391 ± 109% ($P< 0.05$) of control hENOs. At P8-10, IAs occurred in 6-50% of slices in response to 1-10 mM theophylline **(Tab. 1)**. For 10 mM, mean IA frequency was 12.53 ± 1.83 bursts/min (n= 8) while amplitude increased to 778 ± 225% of control ($P< 0.05$). On the other hand, 10 mM caffeine evoked IAs in 50% of cases at P8-10 (n= 3/6), but in 30% of cases at P1-4 (n= 3/10) **(Tab. 1)**. Caffeine-evoked IAs had a rate of 10.0 ± 1.53 bursts/min (n=6) and their amplitude reached 450 ± 126% of control ($P< 0.05$) in P1-4 slices. At P8-10, 44% (n= 7/16) and 33% (n= 2/6) of slices with theophylline-evoked and caffeine-evoked IAs also showed a ramp-like increase in (tonic)

activity prior to a discharge of an IA burst **(Fig. 4-4B)**, whereas this phenomenon did not occur at P1-4. ILEs mostly occurred at P8-10 (in 18-40% of slices during 1-10 mM theophylline and in 17-33% of cases during 5-10 mM caffeine), with an exception of two (of ten) P1-4 slices, which showed ILEs upon bath application of 2.5-10 mM caffeine **(Tab. 1)**. In ~50% of cases ILEs dynamics showed a tendency to initiate with a ramp-like baseline rise, accompanied by an increase in burst amplitude to 533 ± 198% of control during 10 mM theophylline (6 of 16 slices), while caffeine augmented ILE amplitudes to 850 ± 350 % of control (2 of 6 slices).

In summary, submillimolar methyxanthine did not evoke seizure-like perturbation of hENOs, but exerted a modest (reversible) stimulation of these spontaneous activities in <50% of slices. At low millimolar doses, 5 or 10 mM theophylline was required to elicit IAs in P1-4 slices while lower doses (starting at 1 mM) were sufficient at P8-10. Caffeine evoked IAs only in P8-10 slices and only at 10 mM. On the other hand, ILEs were more commonly evoked at P8-10 by 1-10 mM theophylline, while 5 or 10 mM caffeine was needed to elicit ILEs.

4.4.2 Methylxanthine Effects on cENOs

Like hENOs, cortical rhythms in control solution showed different patterns, particularly in the P1-4 group. These patterns include small amplitude bursts in 5 slices, concomitant small and large amplitude bursts in 8 slices, small bursts with long bursts in 2 slices, and spikes with long bursts in 2 slices. Burst pattern in the P8-10 group was more consistent, with the majority of slices (10 of 22) showing long duration bursts **(Fig. 4-5**). Because of this high degree of variability, results in this section are mostly descriptive.

Submillimolar methylxanthine: At 0.1, 0.25 and 0.5 mM, theophylline accelerated cortical bursts with no effect on the amplitude (n= 8/22), increased the duration of long bursts (n= 3/10) and increased rate of bursts with minor increases in amplitude of cortical bursts or spikes (n=12/22) (**Fig. 4-6A**). In the remaining slices, no detectable change in amplitude or frequency was apparent. Caffeine only slightly increased rate and/or amplitude of rhythm and increased duration of long bursts (6-15 s) up to 60 s long with short quiescence phase in 5 of 6 slices at 0.1-0.25 mM. Increasing doses to 0.25-2.5 mM induced faster rates of episodic bursting with gradual decrease in amplitude in 6 of 10 slices (**Fig. 4-7A**). The remaining slice only showed an increase in rate of small amplitude bursts. Integrated electrode signals did not show an increase in baseline or baseline oscillations in response to either methylxanthine **(Figs. 4-6, 4-7**). Submillimolar theophylline or caffeine did not typically evoke IAs or ILEs in either age group, except in three total slices (P3, P8, and P10) in which theophylline perturbed cENOs **(Tab. 2)**

Low millimolar methylxanthine: At 1, 2.5, and 5 mM, theophylline evoked ILEs in 21%, 50% and 56% of slices, respectively, at P8-10, while the remaining slices showed IAs **(Tab. 2)** (**Fig. 4-6B**). At 10 mM, theophylline evoked ILEs in 6 of 15 slices with a concomitant increase in burst amplitude to 150-800% of control. The remaining 9 slices exhibited regular or episodic IAs at a rate of 3-20 bursts/min with amplitude of 200-1300% of control. Theophylline did not elicit ILE in P1-4 slices and only induced IAs in 9-14% of cases. Similarly, only 20% of P1-4 slices displayed IAs upon administering 5 and 10 mM caffeine. Caffeine increased frequency and regularity of cENOs in 5 of 10 slices while gradual amplitude decay was observed in 8 of 10 slices. At P8-10, 5-10 mM caffeine was needed to evoke IAs with the same incidence as 1 mM theophylline **(Tab. 2)** (**Fig. 4-7B**). At these doses, caffeine evoked ILEs in 4 of 6 slices with

firing rates and amplitude augmentation similar to those in theophylline, whereas the other 2 slices showed IAs at 14-20 bursts/min that were 200-300% larger than control cENOs.

In summary, cENOs comprised a range of activity patterns similar to hENOs. At P1-4, methylxanthines produced a more robust and regular rhythm without evoking seizure-like discharges that perturbed normal ENOs. Such hyperexcitability, manifested as ILEs or IAs, was induced by 1-10 mM theophylline or 5-10 mM caffeine at P8-10, indicating a higher potency of theophylline and a higher susceptibility of P8-10 slices to seizure induction. Such transformation of spontaneous h- and cENOs into IA or ILEs is summarized in **Fig. 4-8**.

4.4.3 Effects of $GABA_A$ Receptor and PDE4 Blockade on ENOs

Next, we used the $GABA_A$ receptor blocker gabazine to study whether methylxanthine-evoked ILEs and IAs are mimicked by inhibition of these receptors as indication of involvement of this mechanism. In 20 of 22 slices at P1-4, bath-application gabazine (1 μM) perturbed hENOs by eliciting IAs that had a rate of 0.5-6 bursts/min (2.25 ± 0.41) with amplitude that was between 200-1100% (429 ± 71 %, $P< 0.01$) larger than in control hENOs **(Fig. 4-9A)**. In 2 of these 22 slices, IA bursts started with a ramp-like baseline increase, similar to effects of methylxanthines **(Fig. 4-9A)**. Only one incidence of ILEs was evoked by gabazine at P1-4, whereas they developed in 7 of 22 slices at P8-10 with characteristics very similar to those induced by theophylline including an amplitude increase to 825 ± 132 % ($P< 0.05$) of control **(Fig. 4-9B, C)**. In the remaining 15 slices, gabazine evoked either regular (n= 11) or episodic (n= 5) IAs at a rate of 7.30 ± 1.17 bursts/min while amplitude was augmented to 628 ± 136 % ($P< 0.01$) of control and bursts started with a ramp in 5 cases.

In seven P1-4 slices and eight P8-10 slices, the PDE4 blocker rolipram was used to investigate whether the resulting increase in cellular cAMP stimulated ENOs or perturbed their activity through induction of ILEs or IAs. Bath-application of rolipram at 5 and then 10 µM followed by a wash period of at least 30 min neither substantially affected hENOs (n= 6) nor cENOs (n= 8), except in one P8 slice where hENO rate increased by ~100%. In all cases, rolipram did not evoked seizure-like activities.

4.4.4 Ca^{2+} Imaging

To investigate whether methylxanthines affect cellular Ca^{2+} homeostasis, particularly during IAs and ILEs, Ca_i was monitored with our established multiphoton/confocal microscopy approach (Ruangkittisakul et al., 2006, 2008, 2009). For an initial series of experiments, slices were loaded with the Ca^{2+}-sensitive dye Fluo-8L-AM via bath-application which resulted in staining of both neurons and neighboring glial cells, likely comprising mostly astrocytes, in the CA3 area **(Figs. 4-10, 4-11, 4-12)** and entorhinal/perirhinal cortex **(Fig. 4-13)**.

In six P1-4 slices and five P8-10 slices, sometimes synchronous, but more often asynchronous, spontaneous rhythmic Ca_i rises occurred at a rate of 15-20 events/min in somata and primary dendrites of CA_3 neurons imaged 30-50 µm below the slice surface. Additionally, imaging in four of five P8-10 slices revealed highly synchronous, spontaneous Ca_i rises of comparable frequencies of neurons in the entorhinal/perirhinal cortices. The incidence for synchronous activity appeared to be larger in identified neurons at recording depths of 50-80 µm. Rhythmic Ca rises in cells of deeper layers seemed to show more synchronicity as indicated by rhythmic increases in 'background' fluorescence because of lack of cellular resolution at this depth.

Presumptive astrocytes with a soma diameter of ~10 µm were located, though sparsely, within the CA_3 principal neuron layer while they were located at notably higher density in *stratum radiatum* and *stratum oriens*. Because of lack of a principal neuron layer in cortex and the fact that cortical neurons are smaller than hippocampal pyramidal neurons, discrimination between neurons and astrocytes was more difficult for cortical areas. Presumptive astrocytes in both areas sometimes showed (non-synchronous) spontaneous 'Ca^{2+} spikes' lasting between 5-30 s at an interval of ~1 event/min **(Fig. 4-10, 4-13)**.

At 0.1-0.5 mM, theophylline had no major effect neither on synchronous or asynchronous rhythmic Ca_i rises in 6-10 recorded CA_3 neurons in each slice studied (n= 5) in the P1-4 group and similar number of neurons in 3 slices of the P8-10 group despite modest enhancement of their burst rate in 6 cases. Contrary, at both P1-4 (n= 4/5) and P8-10 (n= 3/4) 1-10 mM theophylline enhanced existing (modest) synchronicity for Ca_i rises in CA3 neurons, or induced synchronous activity, whereas neither the synchronicity nor rate of glial Ca^{2+} spikes increased notably (n= 5) **(Fig. 4-10B, top, middle)**. At no dose, including 10 mM, did theophylline affect Ca_i baseline in either cell type. In all 5 slices tested, gabazine (1 µM) evoked slow and large amplitude Ca_i rises that were synchronous across the CA_3 region **(Fig. 4-10B, bottom)**. The often several-fold increase in amplitude of electrophysiologically recorded methylxanthine- or gabazine-evoked seizure-like discharges compared to CA_3-ENOs was reflected in <50% of cases by an enhanced amplitude of the synchronized neuronal Ca_i rises in slices loaded via bath-application with Fluo-8L. This was due to a steady decrease in signal strength, probably reflecting loss of this Ca^{2+} dye from the cells due to photobleaching. This attenuating effect of long-term Ca^{2+} imaging was notably less pronounced in slices in which Fluo4-AM was focally

injected into the CA_3 pyramidal layer **(Fig. 4-11)**. In 3 slices at P1-4 and 5 slices at P8-10, spontaneous Ca_i rises in somata and primary dendrites of CA_3 neurons were imaged 40-70 μm below the slice surface. Bath-application of 10 mM theophylline induced rhythmic Ca_i rises that resembled IAs with concomitant enhanced synchronicity with a tendency to increase amplitude by ~200-400%. In 2 of 3 slices at P1-4, the synchronous optical activities in individual neurons occurred simultaneously with 'background Ca_i rises'. In one of these slices, IAs evoked in CA_3 neurons were transformed into slow rhythmic Ca^{2+} oscillations that may reflect the baseline oscillations in the electrophysiological recording, typically observed at P1-4 (**§4.4.1**, **4.4.2**). Gabazine (1 μM) elicited IAs with an amplitude increase by ~200% in both of the latter slices while 'background Ca_i rises' were observed in 1 slice. One remaining slice only showed nonsynchronous irregular slow Ca_i oscillations in control and was affected by neither 10 mM theophylline nor gabazine (1 μM). At P8-10, 10 mM theophylline evoked ILE-like Ca_i rises in 2 slices while the remaining 3 slices showed IAs-like Ca_i rises with a transient (plateau-like) baseline Ca_i increase. The amplitude of the latter Ca_i rises tended to be augmented by 300-500% of control while all slices showed boosted synchronicity. Subsequent application of gabazine evoked ILEs in 1 slice while the remaining 4 slices displayed IA-like Ca_i rises with a tendency for augmented amplitude in the order of 200-700% of control. Both theophylline and gabazine evoked a reversible 'background Ca_i rise' in 3 of 5 slices. In both slice groups, t-ACPD (25 μM) increased neuronal Ca_i baseline by ~200%. In 4 of 8 slices at both age groups, astrocytes showed spontaneous random Ca_i rises in control (**Fig. 4-12**). Theophylline showed a tendency to transiently increase the occurrence of such events in 6 slices while gabazine did not have a major effect. Astrocytes seemed to be more active in P8-10 slices compared to P1-4 group. Similar to neuronal responses, t-ACPD augmented astrocytic Ca_i rises by 200-300%.

The incidence of methylxanthine-evoked IAs or ILEs in cortical slices was highest at P8-10 **(§4.4.2**). At 10 mM theophylline, (partially) synchronous Ca_i rise of entorhinal/perirhinal cortical neurons of this group were transformed into slow, synchronous IA-like events with augmented (150-200%) fluorescence intensity in 4 cases (**Fig. 4-13**). In the remaining slice, nonsynchronous and irregular Ca_i rise in control was not affected by 10 mM theophylline. In this group, t-ACPD (25 μM) increased neuronal Ca_i baseline by ~175-200%. In these slices, presumptive astrocytes were inactive in control, although 10 mM theophylline induced often slow Ca^{2+} spikes in ~50% of presumptive cortical glia (n=4). Additionally, theophylline-induced glial Ca_i spikes consistently preceded cortical IA-like events by ~30-90 s. Similar to hippocampal responses, t-ACPD augmented Ca_i rise of both inactive and active astrocytes by 200-500% (**Fig. 4-13C**).

4.5 Discussion

As the major findings of the present study, theophylline could enhance hippocampal and cortical ENOs, particularly at doses between 0.25-2.5 mM, and typically evoked seizure-like discharges at low millimolar doses (**Fig. 4-14**). These epileptogenic theophylline effects had a tendency to be more pronounced in the P8-10 compared to the P1-4 age group. Caffeine exerted principally similar effects on both types of ENOs that were also apparently less pronounced in slices from younger rats. Moreover, caffeine appeared to act more modestly than theophylline, especially regarding induction of hyperexcitability. Ca_i imaging revealed that electrophysiological methylxanthine effects were reflected by changes in the pattern and amplitude of neuronal Ca_i rises. Ca_i signals in presumptive astrocytes were rather complex and differed between the CA_3 area and cortex.

4.5.1 Methylxanthine Effects on Electrophysiological Neural Network Properties

As indicated in the Introduction, one rationale for this study was related to recent findings from our group on methylxanthine effects on the isolated newborn rat preBötC and preBötC-driven cranial (hypoglossal) and spinal motor networks (Ballanyi, 2004a; Ruangkittisakul et al., 2010; Ruangkittisakul & Ballanyi, 2010). We reported in these studies that low millimolar methylxanthine is necessary to stimulate endogenously depressed rhythm and counter opioid-evoked slowing in the fetal and newborn preBötC, respectively, and to evoke spinal seizure-like bursting. Contrary, 20 µM aminophylline (the clinical form of theophylline) accelerated preBötC rhythm in P1-6 mouse slices and boosted inspiratory hypoglossal bursting at P7-13 (Wilken et al., 2000). Moreover, in newborn rat *en bloc* medullas 55 µM and 165 µM theophylline, respectively, reversed adenosine-evoked and hypoxic slowing of inspiratory rhythm (Kawai et al., 1995; Herlenius et al., 2002). This indicates that effective methylxanthine doses for 'physiological' stimulation or hyperexcitability in isolated inspiratory networks vary notably between studies. Similarly, hippocampal or cortical neurons in 'silent' mature rodent slices showed either (electrically-evoked) physiological responses or seizure-like discharge in response to low micromolar up to low millimolar methylxanthine (Greene et al., 1985; Ault et al., 1987; Moraidis & Bingmann, 1994; Dimpfel et al., 1994; Chesi & Stone, 1997; Thöne et al., 2008). Regarding their actions on neonatal hippocampal or cortical circuits, 1 mM caffeine was found to elicit long-lasting 'periodic inward currents' in newborn rat hippocampal slices (Cherubini et al., 1991) whereas 50 µM caffeine evoked seizures in the intact newborn rat hippocampal formation when applied in conjunction with brief episodes of anoxia (Dzahla et al., 1997). In the latter study, it is briefly mentioned that this caffeine dose increased the amplitude of evoked field postsynaptic potentials by 11% and accelerated GDP rate from 8 to 12 bursts/min in control

experiments. However, they did not provide evidence regarding whether these effects were significant.

We started our analysis at 0.1 mM because this methylxanthine dose should selectively block adenosine receptors whereas higher doses target additional process as dealt with below (Ukena et al., 1993; Fredholm et al., 1999; Dale, 2007). We found that this dose, and more effectively 0.25-2.5 mM, could indeed increase the rate and/or amplitude of both ENOs types. However, this effect could not be verified statistically because of the occurrence of different types of activity patterns in control solution and occasional lack of stability within one pattern of their rate and/or amplitude. It is discussed elsewhere (**§1.6**) (Kantor et al., 2012), to which extent these fluctuations reflect a variability of corresponding *in vivo* rhythmic network oscillations in the hippocampus and cortex, such as 'sharp waves' and associated ripples or spindle-bursts and human delta brushes, respectively. (Allene & Cossart, 2010; Maier et al., 2003; Vanhatalo et al., 2002, 2005). Possibly, also environmental conditions such as seasonal changes or slight differences in animal housing contribute to this variability (**§2.5**) (Kantor et al., 2012). Our latter report points out that we studied the horizontal slices under *in vitro* conditions that were very similar to those used by us for studying isolated preBötC (-driven) networks, in which we did not observe 'physiological' methylxanthine effects on inspiratory rhythms at doses <1 mM (Ruangkittisakul et al., 2012).

While spontaneous activity in both immature neonatal hippocampal and cortical networks showed a trend for enhancement by methylxanthines already at lower doses in our present study, particularly in the hippocampus, baseline fluctuations indicating recruitment of additional

neuronal circuits could partly obscure ENOs. Moreover, both types of ENOs were mostly blocked at the same time when either IAs or ILEs occurred in response to higher methylxanthine doses. As one possibility for this coincidence, it needs to be considered that hENOs depend on released GABA that acts in depolarizing fashion on $GABA_A$ receptors to promote neuronal bursting (Ben-Ari et al., 2007; Sipilä & Kaila, 2007). Thus, methylxanthine doses that block $GABA_A$ receptors would depress hENOs while they may, at the same time, disinhibit these or different hippocampal circuits to cause seizures. This scenario may not apply to cENOs that do not depend on depolarizing GABA but rather on glutamatergic excitation (Garaschuk et al., 2000).

The 'physiological' stimulatory methylxanthine effects on ENOs observed here started at doses that are still relatively selective for blockade of adenosine receptors as in the study, in which 50 µM caffeine already seemed to modestly stimulate hENOs (Dzalha et al., 1997). Contrary, seizure-like discharge had a higher incidence at low millimolar doses in the present study, similar to our preliminary findings on spinal hyperexcitability (Ruangkittisakul et al., 2010). The latter methylxanthine-evoked hyperexcitability resembled quite regular 'disinhibited rhythm' of spinal central pattern generators seen upon blockade of $GABA_A$ and/or glycine receptors (Bracci et al., 1996; Brockhaus & Ballanyi, 1998, 2000). Compared to that, IAs and ILEs in the hippocampal and cortical circuits in the present study had different patterns very much resembling such events in these and other brain regions based on rodent slice studies. Although some of these reports made use of the epileptogenic effect of methylxanthines, most applied established *in vitro* models for epilepsy such as high superfusate K^+ or low Ca^{2+}/Mg^{2+} and $GABA_A$ receptor blockers (Greene et al., 1985; Ault et al., 1987; Moraidis & Bingmann, 1994;

Dimpfel et al., 1994; Chesi & Stone, 1997; Dzahla et al., 1997; Kilb et al., 2007; Thöne et al., 2008). Also in the present study, $GABA_A$ receptor inhibition by gabazine appeared to mimic the epileptogenic effects of low millimolar methylxanthine quite well. Since that was not the case in all experiments, it is possible that additional mechanisms contribute to methylxanthine-evoked hyperexcitability in neonatal hippocampal and cortical networks. One of these mechanisms is blockade of cAMP-dependent PDE4, which causes a rise of cellular cAMP that in turn affects a variety of cellular processes (Ukena et al., 1993; Fredholm et al., 1999; Dale, 2007). Our above described findings on the isolated preBötC provided evidence for involvement of PDE4 inhibition because selective PDE4 blocker rolipram mimicked methylxanthine effects. Moreover, our group found that rolipram reactivates preBötC bursting after 'washout' of inspiratory rhythm after several hours of recording in solution with physiological K^+ and Ca^{2+} content (**§2.5.1**) (Ruangkittisakul et al., 2006, 2008). In contrast to respiratory network, PDE4 inhibition does not seem to be involved in stimulatory effects of 0.25-2.5 mM methylxanthine on hENOs or evoking seizure-like discharges because rolipram was ineffective. Also inhibition of Ca^{2+} uptake into cellular stores does not seem to play a major role in methylxantine-evoked seizure-like discharge as will be discussed in the next section.

4.5.2 Methylxanthine Effects on Ca_i in Neurons and Astrocytes

In contrast to the impression given in previous studies (Leinekugel et al., 1997; Canepari et al., 2000; Garaschuk et al., 2000; Takano et al., 2012), a major proportion (55%) of Ca_i recordings indicated lack of synchronous Ca_i oscillations in large arrays of hippocampal CA_3 neurons, despite the fact that most cells were spontaneously active. Also in the cortical areas, notable populations of neurons did not show obvious phase-locked Ca_i oscillation in line with previous

population Ca^{2+} imaging studies in these areas (Cossart et al., 2005; Nikolenko et al., 2007), while in most of the present slices, groups of 5-15 neurons were synchronously active. At submillimolar doses, methylxanthines did not exert a notable effect on neuronal Ca_i in either network. But, at doses that typically evoked electrophysiologically-recorded IAs or ILEs both theophylline and caffeine enhanced the synchronicity of neuronal Ca_i rises and transformed their pattern into those corresponding to one of these events. These effects were principally mimicked in the same slices by $GABA_A$ receptor blockade, except that theophylline caused in ~33% of cases an initial Ca_i rise that could principally be due to release from Ca^{2+} stores as shown for hippocampus and other tissues including the isolated preBötC (Fredholm et al., 1999; Blaustein & Golovina, 2001; Dale, 2007; Ruangkittisakul et al., 2009).

Presumptive astrocytes in the CA_3 area could show asynchronous spontaneous Ca_i spikes that become more pronounced upon methylxanthine application. In contrast, cortical astrocytes do not elicit spontaneous Ca_i spikes, but sporadic Ca_i rises can be evoked during application of 10 mM methylxanthine. It should be noted that the seemingly synchronous rhythmic Ca_i rises generated by hippocampal astrocytes evoked by theophylline or gabazine may reflect the background Ca_i rises rather than astrocyte activity per se. That astrocytes in both areas are capable of Ca^{2+} signaling via metabotropic release from the endoplasmatic reticulum (Agulhon et al., 2008; Ruangkittisakul et al., 2009) is indicated by the fact that they showed a robust Ca_i rise in response to t-ACPD. This metabotropic glutamate receptor agonist also raised Ca_i substantially in hippocampal neurons suggesting a role of Ca^{2+} store mediated signaling in these neurons, in line with an observation of Ca^{2+} release in response to the endoplasmic reticulum Ca^{2+} pump blocker thapsigargin (Koss et al., 2009), whereas cortical neurons were less affected.

In slices that were loaded with Ca^{2+} dye via incubation, the apparent electrophysiologically-recorded increase in burst amplitude during methylxanthine-evoked transition from ENOs to IAs or ILEs was not reflected by enhanced amplitudes of the now synchronized Ca_i rises. Moreover, the amplitude of these Ca^{2+} signals diminished progressively during long-term recording. Instead, amplitude increases during both high methylxanthine and $GABA_A$ receptor blockade were seen in slices loaded with Fluo-4 via pressure-injection, and imaging conditions tended to be stable for longer time periods. It is thus recommended for future studies to use the latter approach that has been applied previously to hippocampal, cortical and brainstem slices (Canepari et al., 2000; Stosiek et al., 2000; Ruangkittisakul et al., 2006, 2008, 2009). In line with this view, one of the latter studies showed that the $GABA_A$ receptor blocker bicuculline enhanced stimulus-evoked Ca_i rises in newborn rat hippocampal slices (Canepari et al., 2000). For the CA_3 area, it should be noted that methylxanthine-evoked baseline rises of the integrated electrode signals were not reflected in slow rhythmic neuronal Ca_i rises, whereas silent or sparsely active neurons were recruited to join the now synchronized population signals. In spite of this, these findings indicate that the same neurons contribute to IAs and ILEs and that these events are not generated by networks that are separate from those that show ENOs in control. The finding that methylxanthine-evoked Ca_i rises resembling IAs and ILEs were reversed upon washout and that subsequent gabazine application evoked robust and stable Ca_i rises argues against the view based on Ca_i imaging in hippocampal cultures exposed to 0 Mg^{2+} that seizure-like bursting causes acute (and subsequent long-lasting) disturbance of neuronal Ca^{2+} homeostasis (Pal et al., 2000).

4.5.3 Relevance to Brain Circuit Development and Clinical Methylxanthine Doses

Three further aspects of the present study deserve a short consideration. Firstly, there was a tendency for more pronounced disturbances of either methylxanthine in the P8-10 age group which seems to correspond to newborn humans regarding cortical development whereas the P1-4 group may be a model for the maturational state of cortical structures in the human fetus (Alling, 1985; Clancy et al., 2001). This finding may indicate that human fetuses and preterm infants are slightly less prone to seizure initiation upon acute exposure to methylxanthines than those at term, but may nevertheless share similarly severe long-term impairments in brain development due to perturbed spontaneous oscillations (Wang & Kriegstein, 2010). Secondly, in either age group theophylline effects seemed to be stronger than those of caffeine. This corresponds to our findings on isolated preBötC networks, which are more thoroughly stimulated by theophylline upon evoked-depression and also to clinical observations demonstrating that theophylline may be as much as "3 to 5 times more potent than caffeine" (Fredholm et al., 1999). Thirdly, seizure-like events were primarily evoked at low millimolar doses that are considerably higher than therapeutic levels, but correspond to doses that have a 'physiological' and epileptogenic effect on the isolated preBötC (Lowry et al., 2001; Ruangkittisakul & Ballanyi, 2010; Ruangkittisakul et al., 2010). It remains to be determined whether this relative insensitivity to these drugs is related to specific *in vitro* conditions in our studies and other reports demonstrating low sensitivity, compared to studies in which <100 µM of a methylxanthine has already major effects in both scenarios as discussed above (Dzhala et al., 1999; Moraidis et al., 1994).

Figures

Fig. 4-1

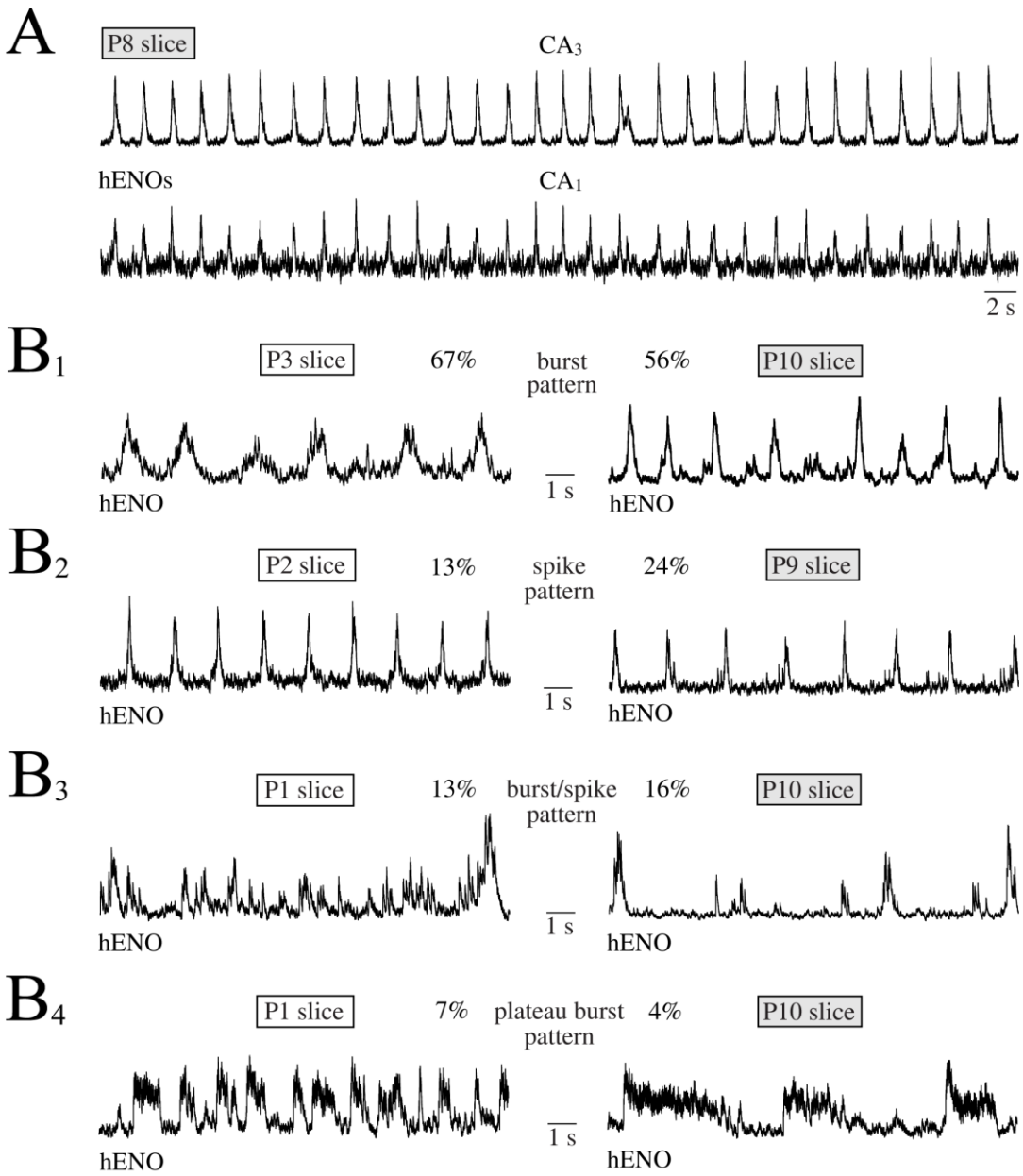

Fig. 4-1: Early network oscillation (ENOs) in the CA_3 region (hENOs) of newborn rat 400-500 µm thick horizontal slices. A, spontaneous CA_3-driven hENOs are synchronous in 4K/1.2 Ca solution, with the CA_1 subfield in this slice from a postnatal day (P) 8 animal. **B**, spontaneous CA_3 rhythm in 3-4K/1.2Ca in P1-4 slices (n= 25) showing a regular 'burst' pattern (0.5-3s single burst duration) that occurred in 67% of cases (**B_1**, left), while 13% of slices showed

predominantly a ‘spike’ pattern when single burst duration was <0.5 s. In an additional 13% of cases, hENOs exhibited a combination of ‘burst and spike’ pattern (**B_3**, left), while another 7% showed a prolonged ‘plateau burst’ pattern (**B_4**, left). Corresponding patterns with similar incidence were seen at P8-10 (n= 25, **B_1-B_4**, right).

Fig. 4-2

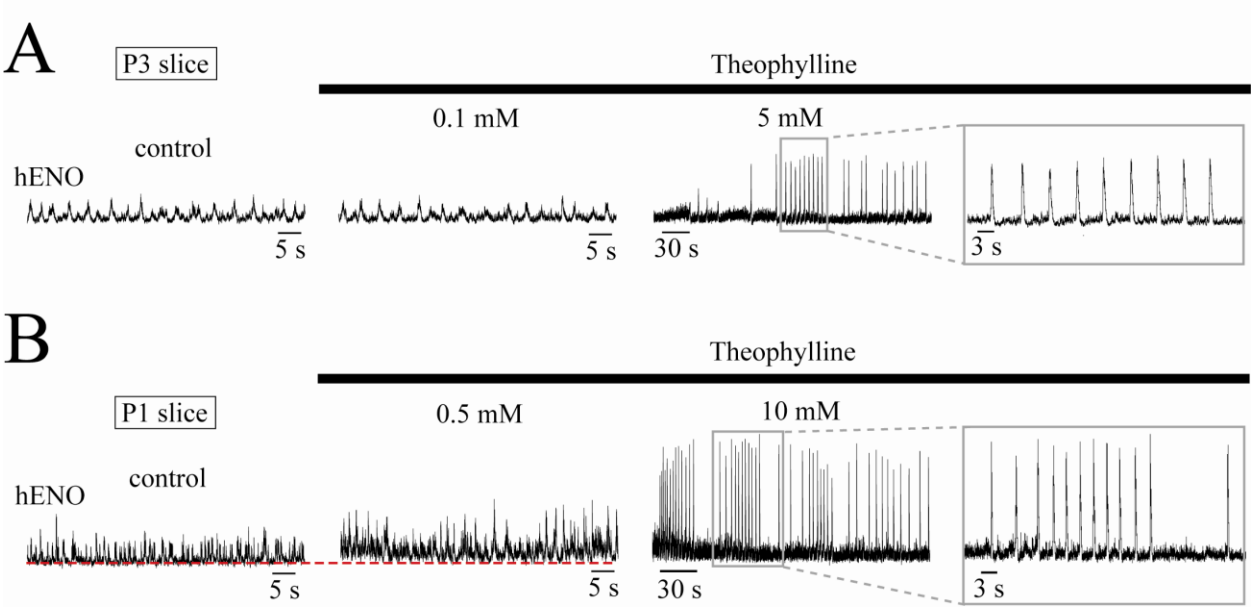

Fig. 4-2: Effects of bath-applied theophylline on hENOs of P1-4 newborn rats. A, hENOs of P1-4 age group. hENO recorded from a 500 μm horizontal slice of P3 rat consisted of small amplitude bursts with varying duration. At 0.1 mM, theophylline increased burst rate without apparent changes of burst amplitude. Subsequent increase to 5 mM evoked slow large amplitude bursts, or interictal activity (IA), with an incrementing ramp. **B**, hENO in another 500 μm P1 slice consisted of bursts and spikes, whose rate and amplitude were reversibly stimulated in 0.5 mM theophylline while integrated baseline signal slightly increased (see dotted line). Subsequent application of 10 mM theophylline evoked IAs.

Fig. 4-3

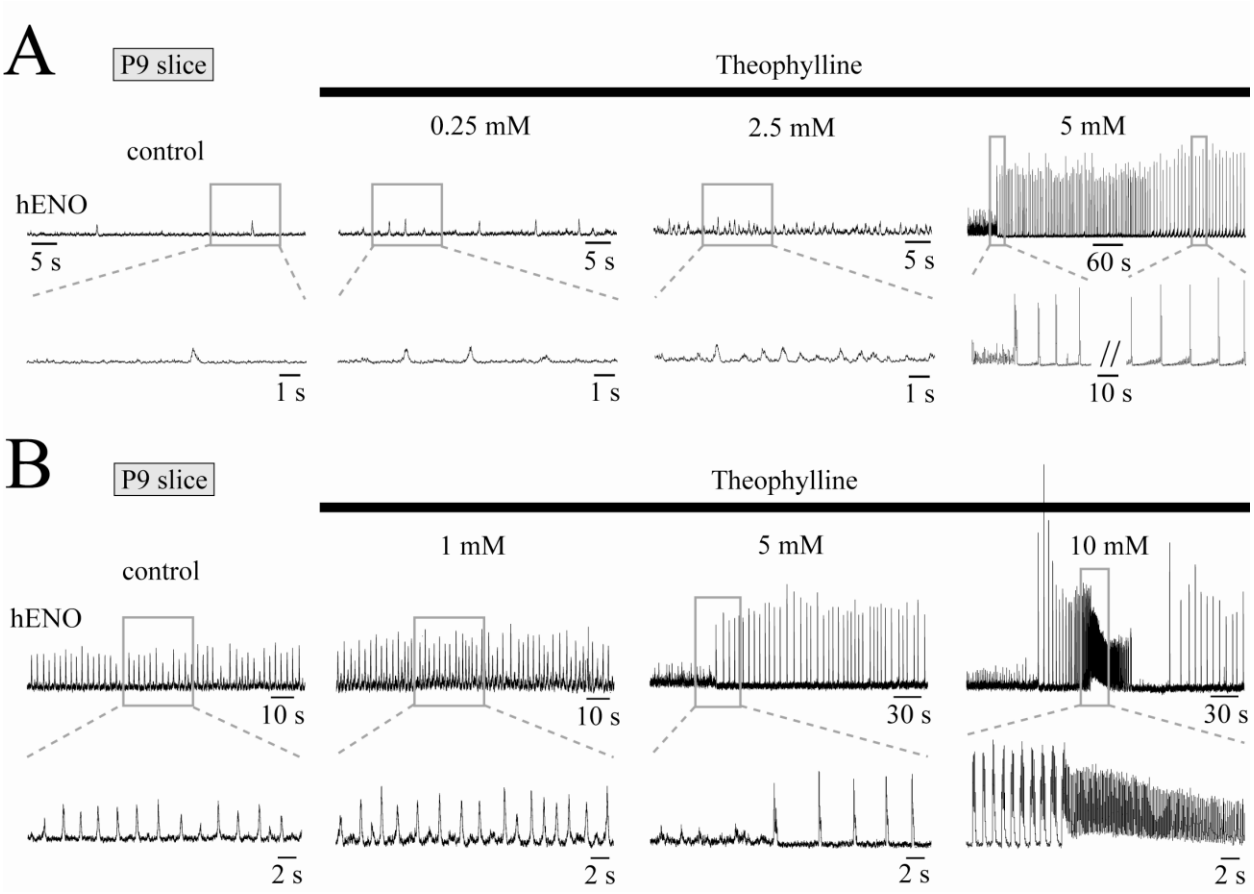

Fig. 4-3: Effects of bath-applied theophylline on hENOs of P8-10 newborn rats. A, hENOs of P8-10 age group. hENO in a P9 slice showed slow, small amplitude bursts in control that became faster in 0.25 and 2.5 mM theophylline. Further increasing the concentration to 5 mM induced an abrupt change to IAs. **B**, hENO of another 500 μm P9 rat slice exhibited regular bursts that became slightly faster and larger in amplitude in 1 mM theophylline. At 5 mM, the agent evoked IAs with amplitude increase by 200% compared to that in control 3K/1.2Ca solution. hENO returned to small burst pattern upon wash out. Subsequently, 10 mM theophylline evoked ictal-like events (ILEs) while hENOS were blocked. ILEs were characterized by a period of large amplitude bursts that became increasingly faster and longer in duration and transformed into small amplitude 7-10 Hz firing, followed by a quiescence phase and another period of regular large amplitude bursts.

Fig. 4-4

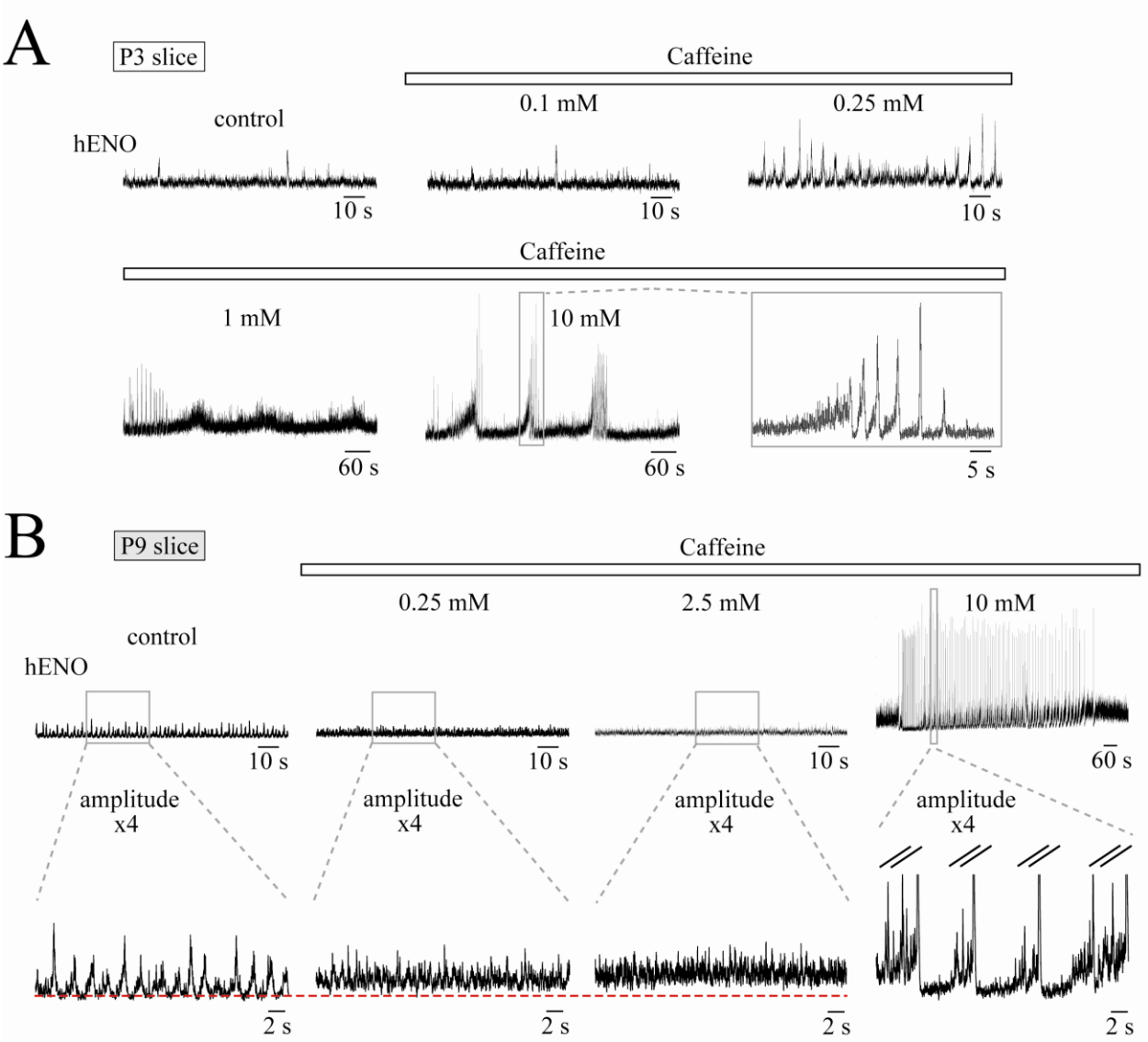

Fig. 4-4: Effects of bath-applied caffeine on hENOs. A, hENO recorded from a 500 μm horizontal P3 slice showed irregular small amplitude bursts that became faster and more robust upon application of 0.25 mM caffeine. Subsequent increase of caffeine to 1 mM evoked an initial transient period of bursting followed by integrated signal baseline oscillations intermingled with irregular small amplitude spikes. A similar pattern of baseline oscillations was evoked by 10 mM caffeine, but the events were accompanied by episodic firing of large amplitude bursts. **B**, in a 500 μm in P9 slice, 0.25 and 2.5 mM caffeine transformed regular hENOs into events with spike pattern without major effect on amplitude. Subsequent application

of 10 mM caffeine abruptly induced regular large amplitude (400-600% of control) bursts. **B** bottom traces: hENOs in boxes in upper panels in **B** at higher time resolution.

Fig. 4-5

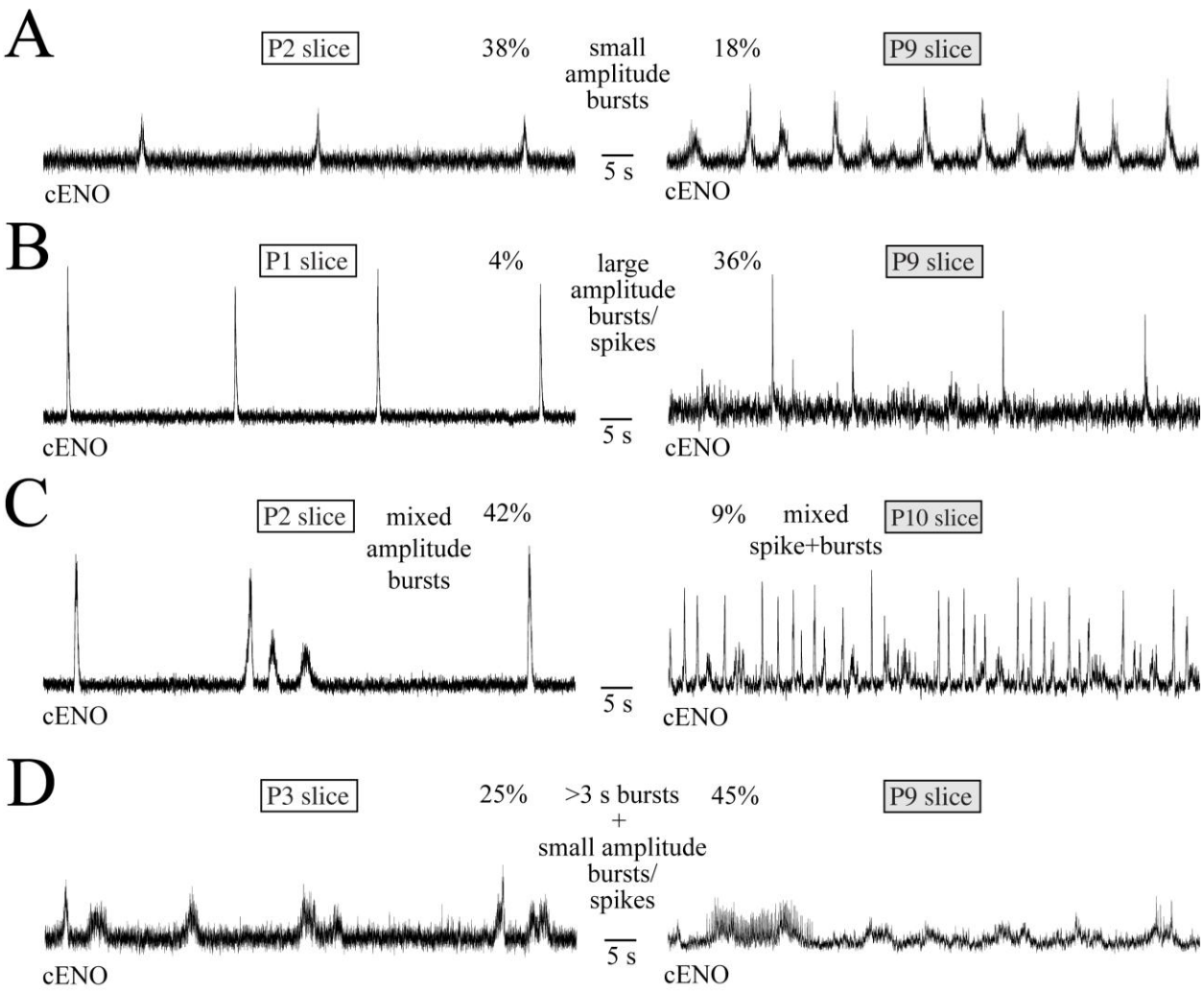

Fig. 4-5: ENOs burst patterns in entorhinal/perirhinal cortex region (cENOs) of newborn rat 400-500 µm thick horizontal slices. A-D, left panels show spontaneous cENOs in 3-4K/1.2Ca solution recorded from P1-4 slices showing different burst patterns as labeled with percentage values indicating the relative occurrence in 24 slices. Right panels show the corresponding patterns and incidences referred to a total of 22 P8-10 slices.

Fig. 4-6

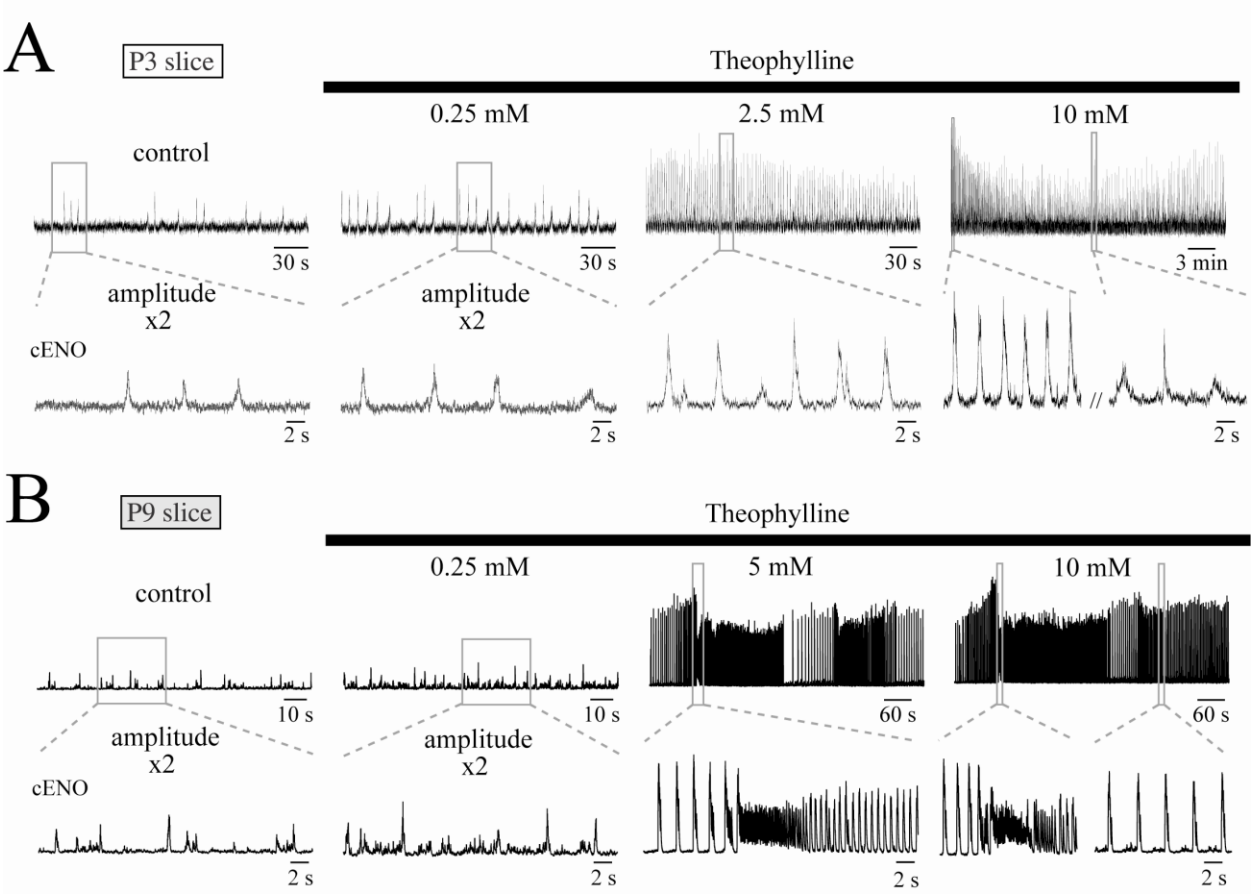

Fig. 4-6: Theophylline effects on cENOs. A, cortical-ENOs recorded from a 500 μm horizontal slice of P3 rat consisted of primarily small amplitude bursts. Bath application of 0.25 mM theophylline reversibly increased burst rate without major changes in burst amplitude. Subsequent increase to 2.5 mM evoked slow large amplitude bursts (IAs), which became faster and more regular upon 10 mM theophylline. **A** bottom trace, cortex rhythm in boxes in **A** at high time resolution. **B**, cortical-ENOs from a P9 rat 500 μm hippocampal slice exhibited regular small bursts and spikes that became slightly faster upon administration of 0.25 mM theophylline. Increasing concentration to 5 and 10 mM evoked periodic ILEs concomitant with IAs. Cortical-ENOs returned to small burst pattern upon wash out. **B** bottom trace, cENOs in boxes in **B** at high time resolution.

Fig. 4-7

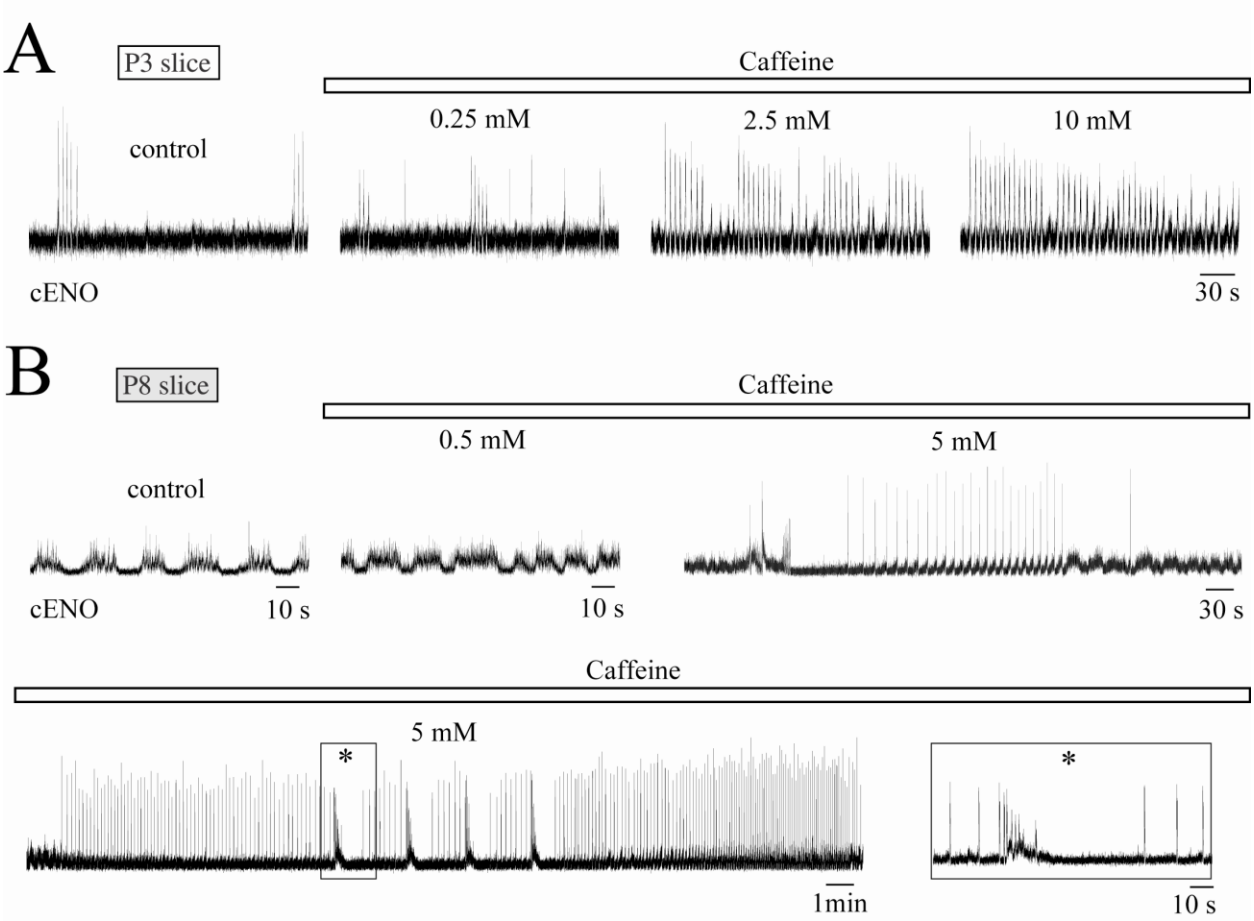

Fig. 4-7: Caffeine effects on cENOs. A, cortical-ENOs recorded from a P3 500 μm horizontal slice consisted of periodic high amplitude bursts that were partially reduced in amplitude by application of 0.25 mM caffeine. Subsequent increase to 2.5 and 10 mM increased rate of bursts and shortened latent period between bursts with concomitant progressive reductions in amplitude. **B**, In a P8 500 μm cortical slice, long duration bursts (>5 s) recorded in control were further broadened by 0.5 mM caffeine application. Increasing to 5 mM caffeine induced regular large amplitude discharges (IAs) and periodic ILEs. Inset shows box in **B** (bottom) at higher time scale.

Fig. 4-8

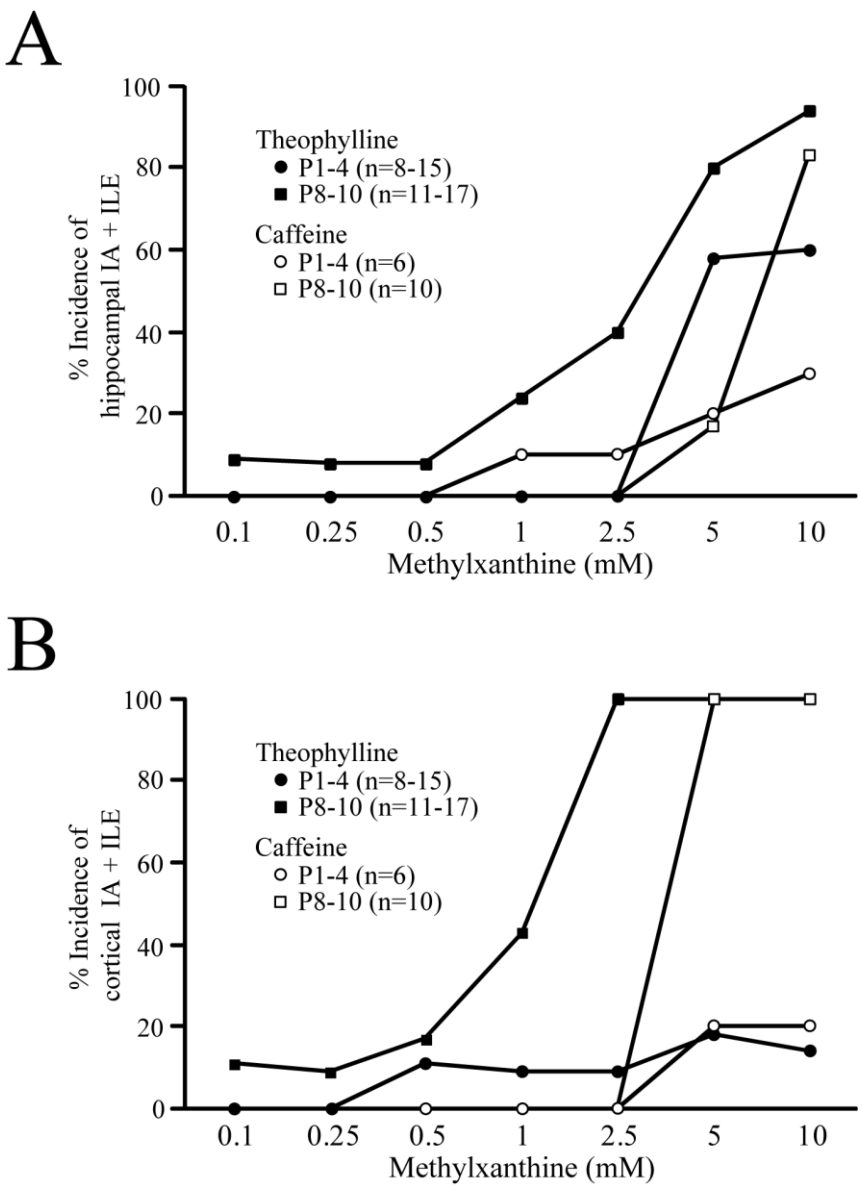

Fig. 4-8: Incidence of transformation of h- and c-ENOs into interictal activity and ictal-like events during methylxanthine application. Total % incidence of seizure formation in the form of interictal activity (IA) and ictal-like events (ILE) from h-ENOs (**A**), and c-ENOs (**B**) during sustained application of either theophylline (black squares and circles) or caffeine (open squares and circles). Higher concentrations of methylxanthines, (2.5-10 mM) theophylline and (5-10 mM) caffeine, were more effective in transforming spontaneous activity into seizure-like discharges and were more commonly seen in older animals: P8-10 (square) vs. P1-4 (circle). For more precise values of % incidence of IA and ILE, see **Tab. 1, 2.**

Fig. 4-9

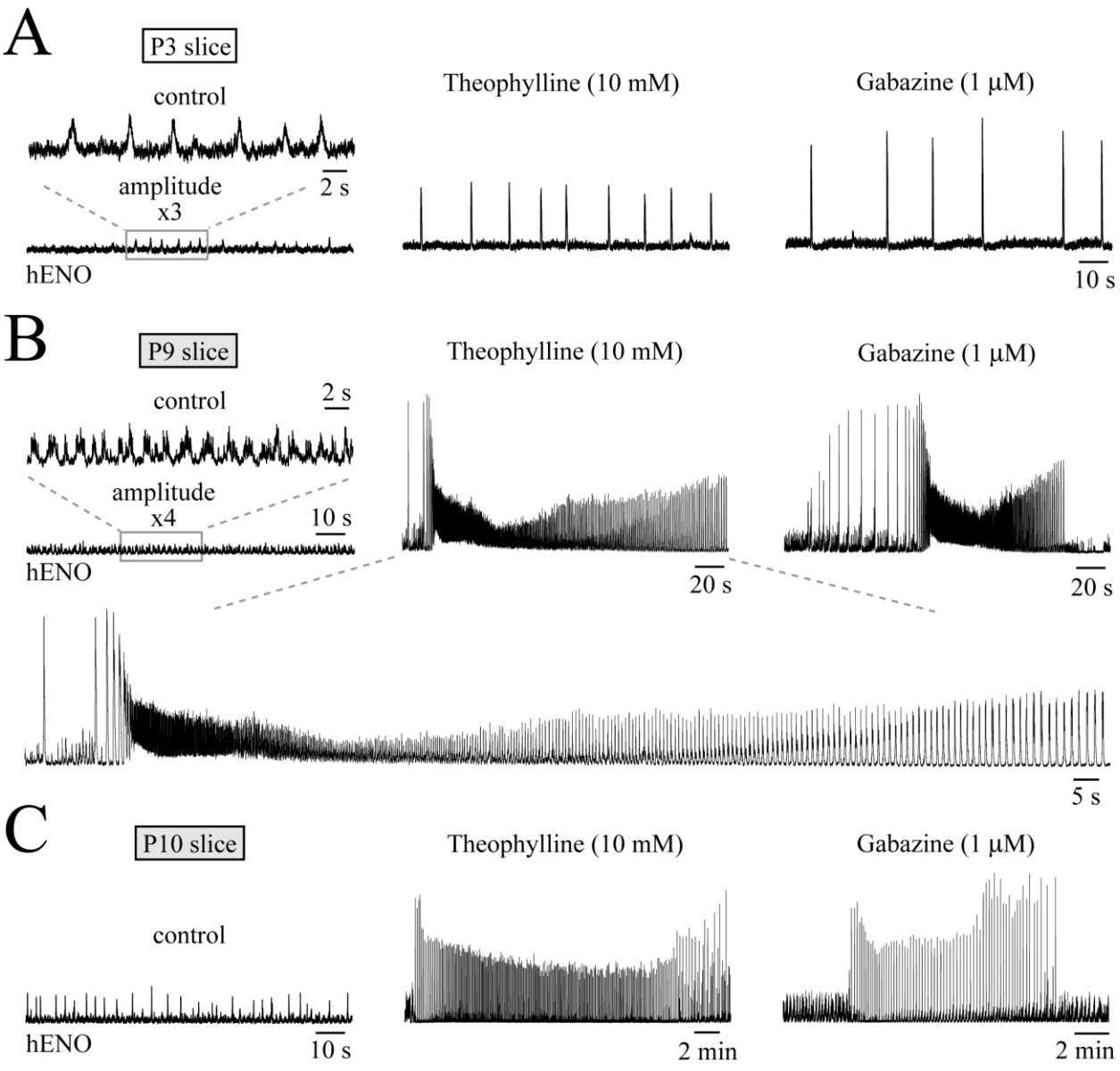

Fig. 4-9: Gabazine effects on hENOs. A, in a 500 μm thick P3 rat horizontal slice, 10 mM theophylline evoked IAs with amplitude augmentation by 400%, while gabazine induced a similar response with even larger amplitude (700% compared to control). **B**, Theophylline and gabazine evoked ILEs of CA_3 rhythm in a P9 slice while both drugs similarly induced regular large amplitude bursts in another P10 slice (**C**).

Fig. 4-10

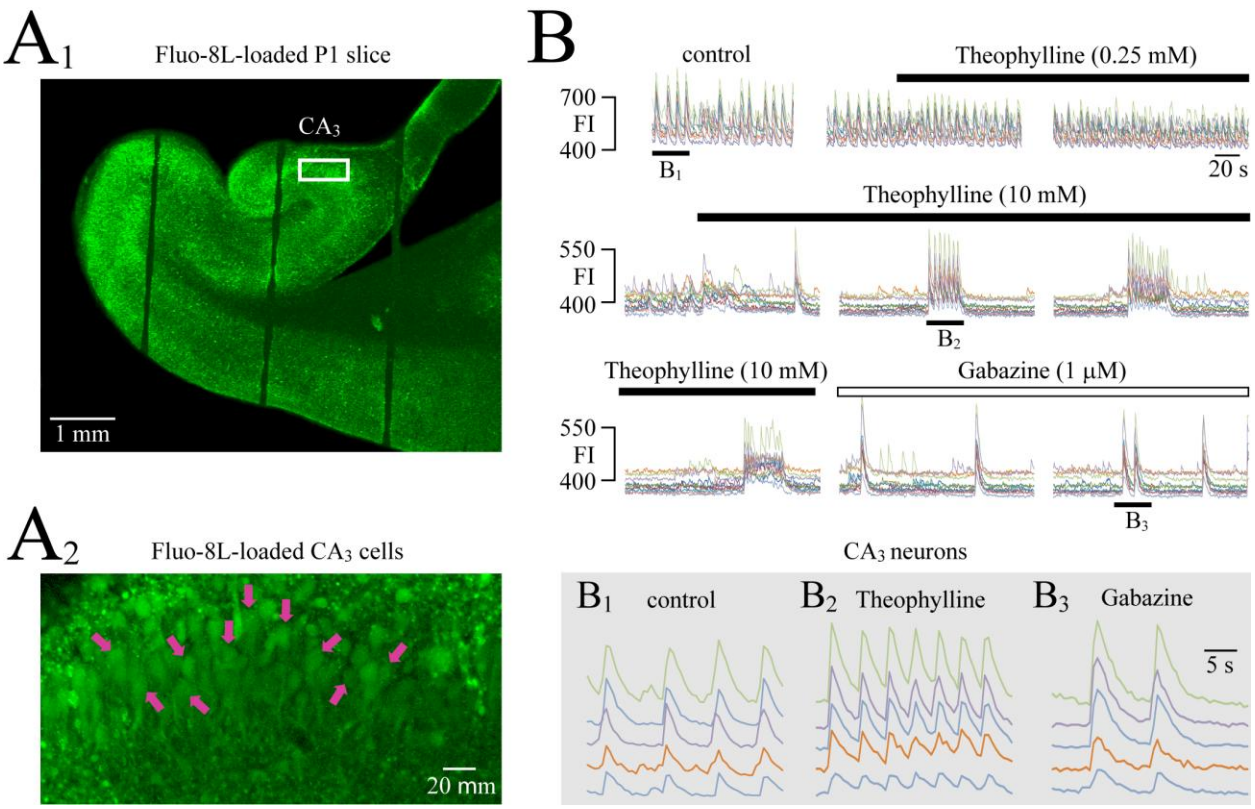

Fig. 4-10: Low millimolar theophylline evoked Ca^{2+} rises in hippocampus Confocal Ca^{2+} imaging in a newborn rat hippocampus. Each colored trace represents kinetic changes in fluorescence intensity (FI) measured in individual ROIs around cell somata as shown in the photograph representing a summated z-stack of images. (**A_1**) overview of a P1 horizontal slice incubated in the calcium-sensitive dye Fluo-8L-AM (10 μM) and selected CA_3 pyramidal neurons (purple arrows; **A_2**). **B**, CA_3 neurons (n=10) in a P1 hippocampus showed spontaneous and synchronous Ca^{2+} intensity (Ca_i) rises in control superfusate (4 K/1.2 Ca). Submillimolar (0.25 mM) concentrations of theophylline increased the rate of Ca_i rises and decreased overall fluorescence intensity (top row). Addition of high doses of Theo (middle row) substantially perturbed CA_3 oscillations and transformed uniform and synchronous Ca_i rises into episodic hyperexcitability, resembling ILE patterns as seen in **Fig.4-3B**. Theo-induced episodic ILEs are marked by brief (30-40 s) trains of synchronous Ca_i rises followed by neuronal quiescence. CA_3 neurons did not necessarily show a massive increase in amplitude in response to 10 mM Theo, which typically substantially augmented the amplitude of ENOs as show in **Figs. 4-2, 4-3**.

Application of the $GABA_A$ receptor antagonist, Gabazine (Gbz; 1 μM), transformed repetitive CA_3 activity into slow, large amplitude Ca_i discharges synchronous along the CA_3 region (bottom row). **B_1**, **B_2**, **B_3**, insets of selected CA_3 cell traces (n=5) under the three conditions at high resolution. Ca_i rises remain synchronous over the CA_3 region in control superfusate (left, **B_1**), during administration of 10 mM theophylline (middle, **B_2**), as well as during $GABA_A$ receptor antagonism (right, **B_3**).

Fig. 4-11

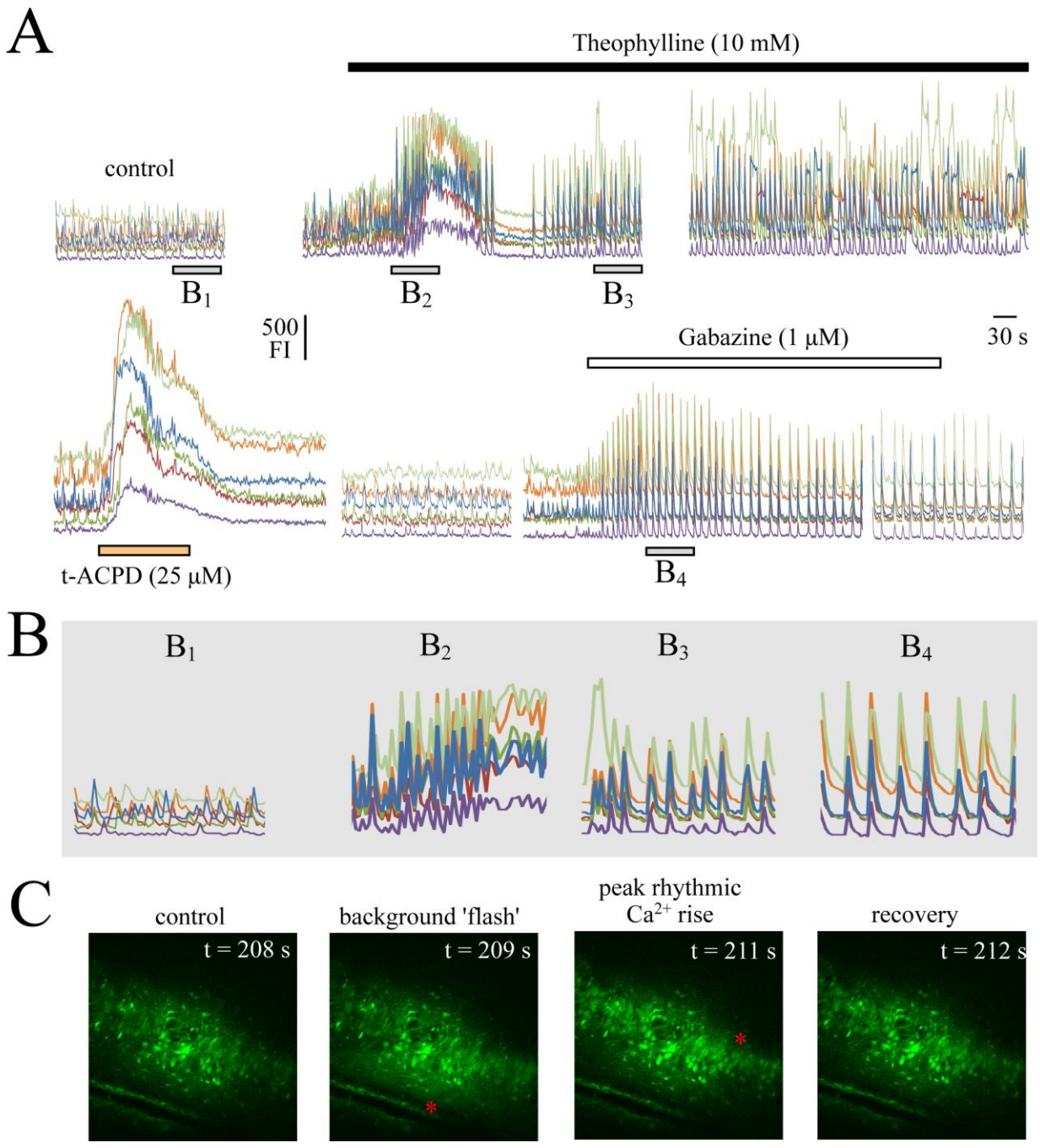

Fig. 4-11: Low millimolar theophylline does not increase neuronal intracellular Ca^{2+}. Confocal Ca^{2+} imaging in a P8 rat hippocampus**.** The Ca^{2+} sensitive dye, Fluo-4-AM was pressure injected directly into the CA_3 pyramidal cell line, yielding a more stable fluorescence signal. Each colored trace represents kinetic changes in fluorescence measured in individual

ROIs around cell somata taken at 72 μm below the slice surface. CA_3 neurons showed spontaneous, often synchronous Ca^{2+} rises in control (4 K/1.2 Ca) superfusate, which were transformed into uniform and synchronous high intensity Ca_i rises that resembled IAs upon 10 mM theophylline application (n=6 cells). Interestingly, while CA3 neurons responded with rhythmic discharges at augmented intensities, baseline Ca_i levels did not substantially deviate from control. Application of gabazine elicited IAs with an amplitude increase of ~200%. Both theophylline and gabazine evoked a reversible 'background Ca^{2+} rise' as shown in **C**. The metabotropic glutamate agonist, tACPD (25 μM), increased neuronal Ca^{2+} baseline by 200%, which returned to control upon washout of agent. **B_{1-4}**, boxes show fragments of fluorescence signal shown at higher time scale at various time points during experiment.

Fig. 4-12

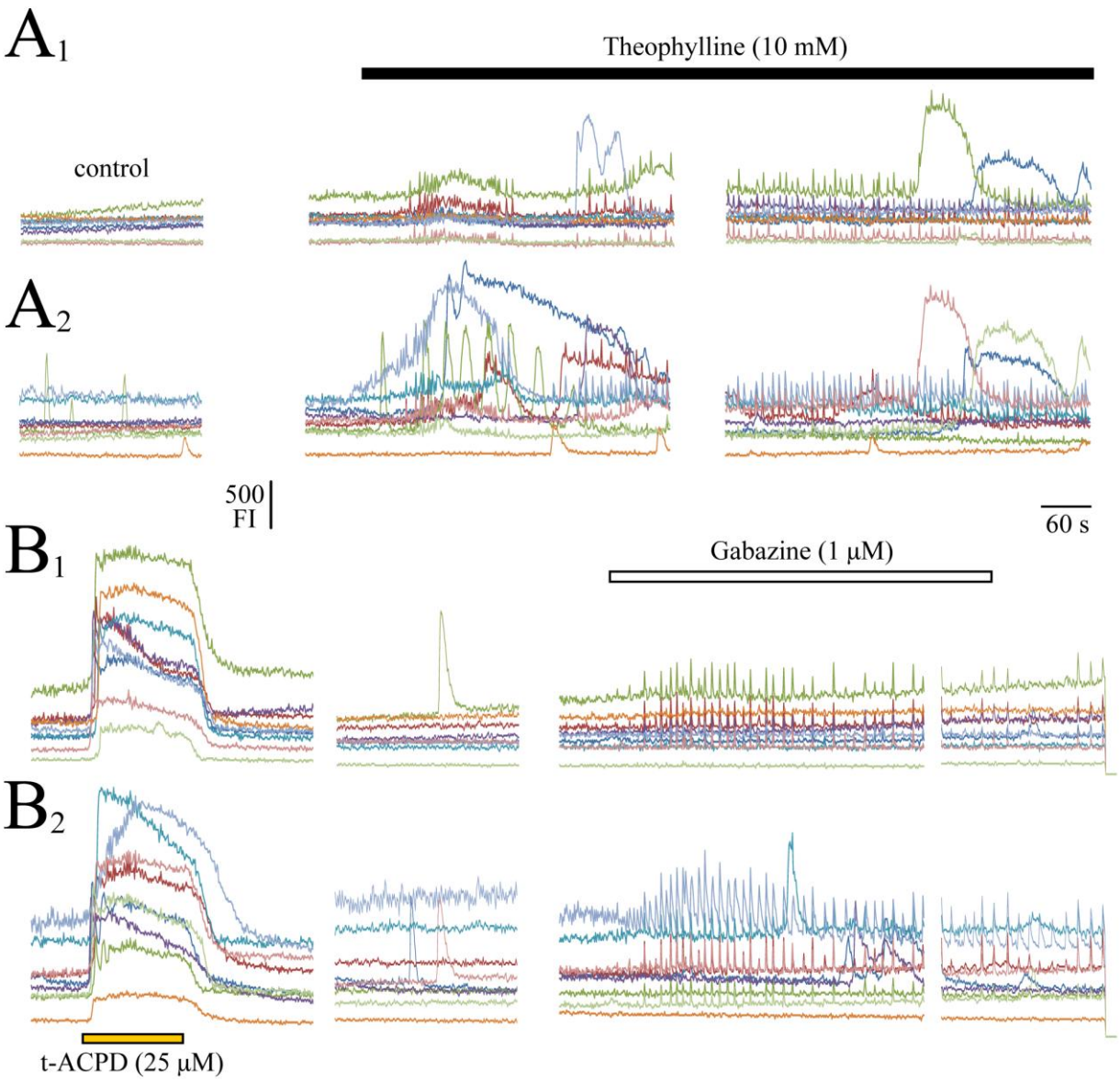

Fig. 4-12: Low millimolar theophylline effect on glial Ca^{2+}. Corresponding traces taken from neighbouring astrocytes in the same slice as **Fig. 4-11**. The Ca^{2+} sensitive dye, Fluo-4-AM was pressure injected directly into the CA_3 pyramidal layer at 72 μm depth, resulting in uniform staining of both pyramidal neurons and small, astrocytic glial cells. Here, glial signals are separated by degree of activity in control (4 K/1.2 Ca) superfusate. Inactive glial cells, **A_1**, oscillate at undefined frequencies upon 10 mM theophylline application with a similar time course of activity as theophylline evoked-neuronal oscillations. **A_2**, glial cells that showed

spontaneous Ca^{2+} rises in control were further activated by 10 mM theophylline, resulting in sometimes long duration Ca^{2+} transients. **B_{1-2},** Similar to neuronal responses, tACPD augmented glial Ca^{2+} rises by 200-300% in both groups, while gabazine did not seem to promote Ca^{2+} rises in contrast to theophylline. Note that the seemingly rhythmic Ca^{2+} rises in some glial cells during theophylline and gabazine application may reflect Ca^{2+} rises in the background and not glial activity per se.

Fig. 4-13

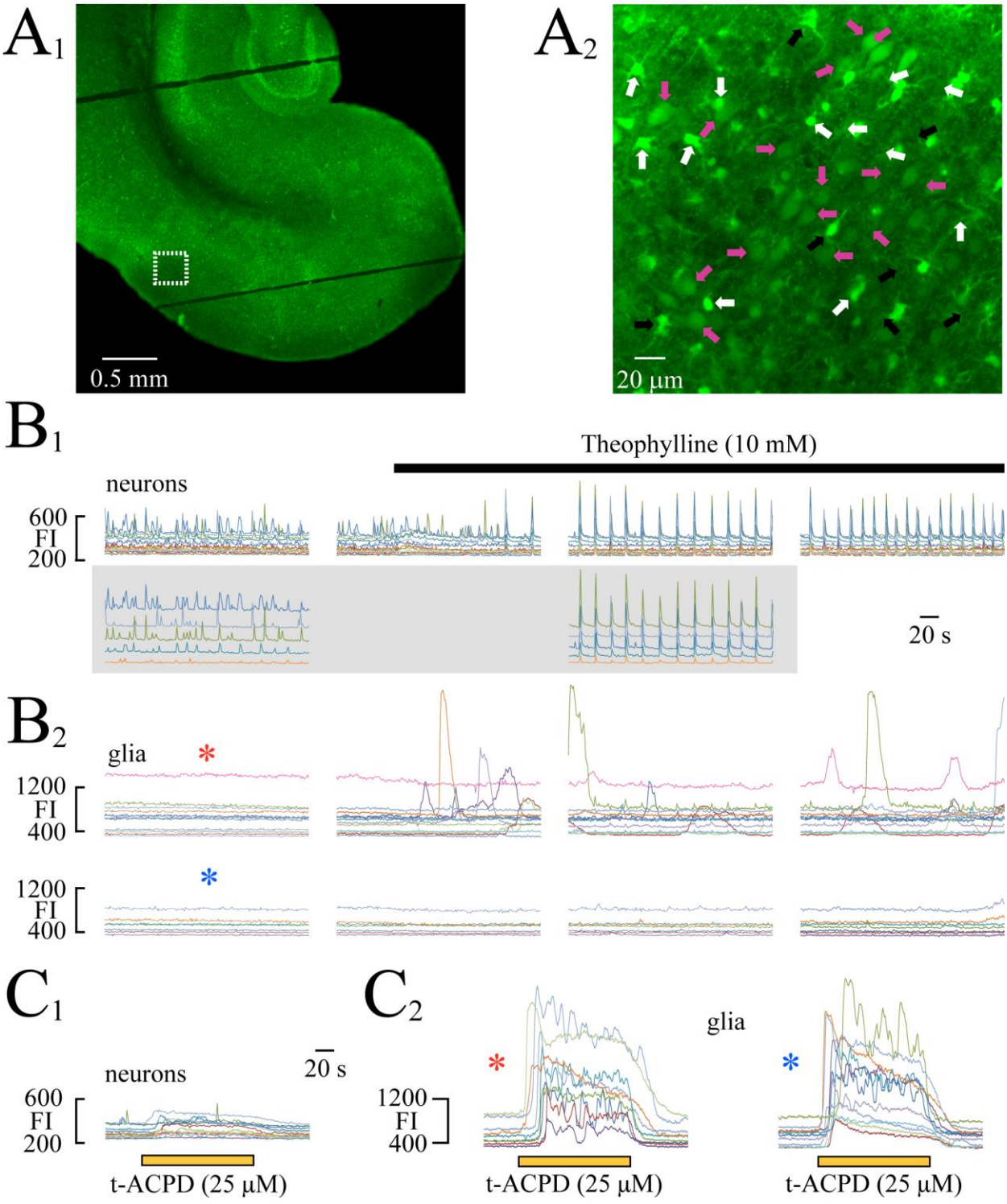

Fig. 4-13: Theophylline-evoked Ca^{2+} rises in cortical neurons. Confocal Ca^{2+} imaging in a P8 rat cortical slice. Spontaneous cortical Ca^{2+} rises in the perirhinal region were monitored via bath

application of Fluo-8L-AM. Activity in this region was mainly comprised of small Ca^{2+} rises at times synchronous with neighbouring cells, but more often asynchronous. (**A_1**) overview of a P8 horizontal slice incubated in Fluo-8L-AM and selected cortical neurons (purple arrows; **A_2**). Addition of 10 mM Theo (right, **B_1**) substantially perturbed cortical oscillations and transformed them into high amplitude, synchronous and uniform Ca^{2+} rises, resembling IA patterns as seen in **Fig. 4-6**. Neighbouring astrocytes (black and white arrows; **A_2**), separated into responsive and non-responsive groups (**B_2 top** and **bottom**, respectively) were inactive in control solution. In ~50% of recorded astrocytes, 10 mM theophylline induced large, intermittent and often long duration calcium transients, which preceded neuronal effects by ~90 s. **C**, t-ACPD application to the bath marginally increased neuronal Ca^{2+} baseline (**C_1**), while glial Ca^{2+} were augmented by 200-500% (**C_2**).

Fig. 4-14

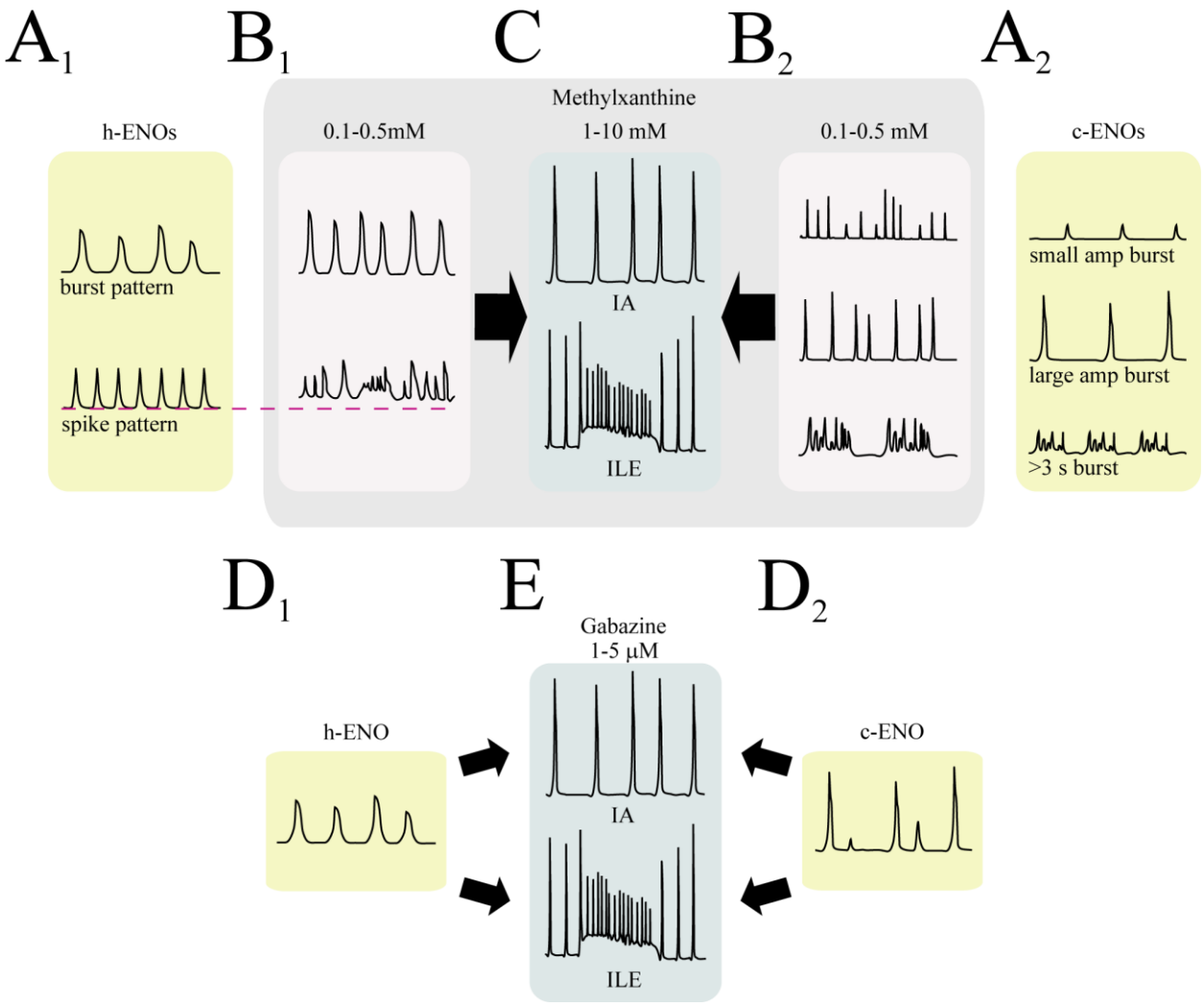

Fig. 4-14: Summary of methylxanthine-induced perturbation of c- and hENOs. Spontaneous h- (**A_1**) and cENOs (**A_2**) are more commonly stimulated (in burst rate and amplitude) by submillimolar (0.1-0.5 mM) concentrations of the methylxanthines caffeine and theophylline (**B_{1-2}**). **C**, at low millimolar concentrations (1-10 mM) methylxanthines transform either stimulated or endogenous ENOs into slow, large amplitude bursts, or interictal activity (IA) and ictal-like events, or (ILE), characterized by a period of large amplitude bursts that became increasingly faster and longer in duration and transformed into small amplitude 7-10 Hz firing, followed by a quiescence phase and another period of regular large amplitude bursts. **E**, application of the $GABA_A$ receptor antagonist, gabazine (1-5 μM), reliably transforms both h- (**D_1**) and cENOs (**D_2**) into either IA or ILE.

Table 4-1

Event	Drug age	0.1 mM	0.25 mM	0.5 mM	1.0 mM	2.5 mM	5.0 mM	10.0 mM
IA	Theophylline P1-4	0 % (0/8)	0 % (0/11)	0 % (0/10)	0 % (0/12)	0 % (0/12)	58% (7/12)	60% (9/15)
	Theophylline P8-10	9% (1/11)	0 % (0/13)	0 % (0/13)	6% (1/17)	7% (1/15)	40% (6/15)	50% (8/16)
	Caffeine P1-4	0 % (0/10)	0 % (0/10)	0 % (0/10)	10% (1/10)	0 % (0/10)	10% (1/10)	30% (3/10)
	Caffeine P8-10	0 % (0/6)	0 % (0/6)	0 % (0/6)	0 % (0/6)	0 % (0/6)	0 % (0/6)	50% (3/6)
ILE	Theophylline P1-4	0 % (0/8)	0 % (0/11)	0 % (0/10)	0 % (0/12)	0 % (0/12)	0% (0/12)	0% (0/15)
	Theophylline P8-10	0% (0/11)	0 % (0/13)	8% (1/13)	18% (3/17)	33% (3/15)	40% (6/15)	44% (7/16)
	Caffeine P1-4	0 % (0/10)	0 % (0/10)	0 % (0/10)	0 % (0/10)	10% (1/10)	10% (1/10)	0 % (0/10)
	Caffeine P8-10	0 % (0/6)	0 % (0/6)	0 % (0/6)	0 % (0/6)	0 % (0/6)	17% (1/6)	33% (2/6)
IA + ILE	Theophylline P1-4	0 % (0/8)	0 % (0/11)	0 % (0/10)	0 % (0/12)	0 % (0/12)	58% (7/12)	60% (9/15)
	Theophylline P8-10	9% (1/11)	8% (1/13)	8% (1/13)	24% (4/17)	40% (6/15)	80% (12/15)	94% (15/16)
	Caffeine P1-4	0 % (0/10)	0 % (0/10)	0 % (0/10)	10% (1/10)	10% (1/10)	20% (2/10)	30% (3/10)
	Caffeine P8-10	0 % (0/6)	0 % (0/6)	0 % (0/6)	0 % (0/6)	0 % (0/6)	17% (1/6)	83% (5/6)
		1 µM						
IA	Gabazine P1-4	91 % (20/22)						
	Gabazine P8-10	68% (15/22)						
ILE	Gabazine P1-4	4.5% (1/22)						
	Gabazine P8-10	32% (7/22)						

Table 4-1: Incidence of occurrence of seizure-like hyperexcitability in horizontal hippocampus slices of rats of postnatal day (P) 1-4 *versus* P8-10. % values are referred to numbers (in brackets) of tested slices.

Table 4-2

Event	Drug age	0.1 mM	0.25 mM	0.5 mM	1.0 mM	2.5 mM	5.0 mM	10.0 mM
IA	Theophylline P1-4	0% (0/7)	0% (0/10)	11% (1/9)	9% (1/11)	9% (1/11)	18% (2/11)	14% (2/14)
	Theophylline P8-10	11% (1/9)	9% (1/11)	8% (1/12)	21% (3/14)	50% (5/10)	44% (4/9)	56% (5/9)
	Caffeine P1-4	0% (0/10)	0% (0/10)	0% (0/10)	0% (0/10)	0% (0/10)	20% (2/10)	20% (2/10)
	Caffeine P8-10	0% (0/6)	0% (0/6)	0% (0/6)	0% (0/6)	0% (0/6)	33% (2/6)	33% (2/6)
ILE	Theophylline P1-4	0% (0/7)	0% (0/10)	0% (0/9)	0% (0/11)	0% (0/11)	0% (0/11)	10% (0/14)
	Theophylline P8-10	0% (0/9)	0% (0/11)	8% (1/12)	21% (3/14)	50% (5/10)	56% (5/9)	44% (4/9)
	Caffeine P1-4	0% (0/10)	0% (0/10)	0% (0/10)	0% (0/10)	0% (0/10)	0% (0/10)	0% (0/10)
	Caffeine P8-10	0% (0/6)	0% (0/6)	0% (0/6)	0% (0/6)	0% (0/6)	67% (4/6)	67% (4/6)
IA + ILE	Theophylline P1-4	0% (0/7)	0% (0/10)	11% (1/9)	9% (1/11)	9% (1/11)	18% (2/11)	14% (2/14)
	Theophylline P8-10	11% (1/9)	9% (1/11)	17% (2/12)	43% (6/14)	100% (10/10)	100% (9/9)	100% (10/10)
	Caffeine P1-4	0% (0/10)	0% (0/10)	0% (0/10)	0% (0/10)	0% (0/10)	20% (2/10)	20% (2/10)
	Caffeine P8-10	0% (0/6)	0% (0/6)	0% (0/6)	0% (0/6)	0% (0/6)	100% (6/6)	100% (6/6)
		1 µM						
IA	Gabazine P1-4	54% (7/13)						
	Gabazine P8-10	60% (6/10)						
ILE	Gabazine P1-4	0% (0/13)						
	Gabazine P8-10	40% (4/10)						

Table 4-2: Incidence of occurrence of seizure-like hyperexcitability in cortical slices of rats of P1-4 *versus* P8-10. % values are referred to numbers (in brackets) of tested slices.

4.6 References

Agulhon C, Petravicz J, McMullen A B, Sweger EJ, Minton SK, Taves SR, Casper KB, Fiacco TA, McCarthy KD (2008) What is the role of astrocyte calcium in neurophysiology? Neuron 59, 932-946

Allene C, Cossart R (2010) Early NMDA receptor-driven waves of activity in the developing neocortex: physiological or pathological network oscillations? J Physiol 588, 83-91

Alling C (1985) Biochemical maturation of the brain and the concept of vulnerable periods. In: Alcohol and the developing Brain. Eds: U. Rydberg et al., Raven Press, New York, p. 5-10

Ault B, Olney MA, Joyner JL, Boyer CE, Notrica MA, Soroko FE, Wang CM (1987) Pro-convulsant actions of theophylline and caffeine in the hippocampus: implications for the management of temporal lobe epilepsy. Brain Res 426, 93-102

Ballanyi K (2004a) Neuromodulation of the perinatal respiratory network. Curr Neuropharmacol 2, 221-243

Ballanyi K (2004b) Protective role of neuronal K_{ATP} channels in brain hypoxia. J Exp Biol 207, 3201-3212

Ballanyi K, Onimaru H, Homma I (1999) Respiratory network function in the isolated brainstem-spinal cord of newborn rats. Prog Neurobiol 59, 583-634

Ben-Ari Y, Cherubini E, Corradetti R, Gaiarsa J L (1989) Giant synaptic potentials in immature rat CA3 hippocampal neurones. J Physiol 416, 303-325

Ben-Ari Y, Gaiarsa JL, Tyzio R, Khazipov R (2007) GABA: a pioneer transmitter that excites immature neurons and generates primitive oscillations. Physiol Rev 87, 1215-1284

Blaustein MP, Golovina VA (2001) Structural complexity and functional diversity of endoplasmic reticulum Ca^{2+} stores. Trends Neurosci 24, 602-608

Bracci E, Ballerini L, Nistri A (1996) Localization of rhythmogenic networks responsible for spontaneous bursts induced by strychnine and bicuculline in the rat isolated spinal cord. J Neurosci 16: 7063-7076

Brockhaus J, Ballanyi K (1998) Synaptic inhibition in the isolated respiratory network of neonatal rats. Eur J Neurosci 10, 3823-3839

Brockhaus J, Ballanyi K (2000) Anticonvulsant adenosine A_1 receptor-mediated adenosine action on neuronal networks in the brainstem-spinal cord of newborn rats. Neuroscience 96, 359-371

Canepari M, Mammano F, Kachalsky SG, Rahamimoff R, Cherubini E (2000) GABA- and glutamate-mediated network activity in the hippocampus of neonatal and juvenile rats revealed by fast calcium imaging. Cell Calcium 27, 25-33

Cherubini E, Ben-Ari Y, Ito S, Krnjević K (1991) Persistent pulsatile release of glutamate induced by N-methyl-D-aspartate in neonatal rat hippocampal neurones. J Physiol 436, 531-547

Chesi AJ, Stone TW (1997) Alkylxanthine adenosine antagonists and epileptiform activity in rat hippocampal slices in vitro. Exp Brain Res 113, 303-310

Clancy B, Darlington RB, Finlay BL (2001) Translating developmental time across mammalian species. Neuroscience 105, 7-17

Comer AM, Perry CM, Figgitt DP (2001) Caffeine citrate: a review of its use in apnoea of prematurity. Paediatr Drugs 3, 61-79

Cossart R, Ikegaya Y, Yuste R (2005) Calcium imaging of cortical networks dynamics. Cell Calcium 37, 451-457

Daly JW (2007) Caffeine analogs: biomedical impact. Cell Mol Life Sci 64, 2153-2169

Delanty N, Vaughan CJ, French JA (1998) Medical causes of seizures. Lancet 352 (9125), 383-90

Dimpfel W, Dalhoff A, Hofmann W, Schülter G (1994) Electrically evoked potentials in the rat hippocampus slice in the presence of aminophylline alone and in combination with quinolones. Eur Neuropsychopharmacol 4(2), 151-156

Dzhala V, Desfreres L, Melyan Z, Ben-Ari Y, Khazipov R (1999) Epileptogenic action of caffeine during anoxia in the neonatal rat hippocampus. Ann Neurol 46, 95-102

El-Bitar MK, Boustany RM. Common causes of uncommon seizures. Pediatr Neurol. 2009 Aug;41(2):83-7.

Eldridge FL, Millhorn DE, Kiley JP (1985) Antagonism by theophylline of respiratory inhibition induced by adenosine. J Appl Physiol 59, 1428-1433

Feldman JL, Del Negro CA (2006) Looking for inspiration: new perspectives on respiratory rhythm. Nat Rev Neurosci 7, 232-242

Fredholm BB, Bättig K, Holmen J, Nehlig A, Zvartau EE (1999) Actions of caffeine in the brain with special reference to factors that contribute to its widespread use. Pharmacol Rev 51, 83-133

Garaschuk O, Linn J, Eilers J, Konnerth A (2000) Large-scale oscillatory calcium waves in the immature cortex. Nat Neurosci 3, 452-459

Greene RW, Haas HL, Hermann A (1985) Effects of caffeine on hippocampal pyramidal cells in vitro. Br J Pharmacol 85, 163-169

Hedner T, Hedner J, Bergman B, Mueller RA, Jonason J (1985) Characterization of adenosine-induced respiratory depression in the preterm rabbit. Biol Neonate 47, 323-332

Herlenius E, Adén U, Tang LQ, Lagercrantz H (2002) Perinatal respiratory control and its modulation by adenosine and caffeine in the rat. Pediatr Res 51, 4-12

Kantor C, Panaitescu B, Kuribayashi J, Ruangkittisakul A, Lee TF, Cheung PY, MacTavish D, Jhamandas J, Ballanyi K (2012) Electrophysiological imaging of early network oscillations in brain slices from newborn rats and piglets. In: Isolated Central Nervous System Circuits (Ed K Ballanyi), Neuromethods Series (Ed W Walz). Springer Science+Business Media, LLC, New York, NY (*in press*)

Kawai A, Okada Y, Mückenhoff K, Scheid P (1995) Theophylline and hypoxic ventilatory response in the rat isolated brainstem-spinal cord. Respir Physiol 100, 25-32

Khazipov R, Luhmann HJ (2006) Early patterns of electrical activity in the developing cerebral cortex of humans and rodents. Trends Neurosci 29, 414-418

Kilb W, Sinning A, Luhmann HJ (2007) Model-specific effects of bumetanide on epileptiform activity in the in-vitro intact hippocampus of the newborn mouse. Neuropharmacology 53, 524-533

Korematsu S, Miyahara H, Nagakura T, Suenobu S, Izumi T (2008) Theophylline-associated seizures and their clinical characterizations. Pediatr Int 50(1), 95-8

Koss DJ, Riedel G, Platt B (2009) Intracellular Ca^{2+} stores modulate SOCCs and NMDA receptors via tyrosine kinases in rat hippocampal neurons. Cell Calcium 46, 39-48

Leinekugel X, Medina I, Khalilov I, Ben-Ari Y, Khazipov R (1997) Ca^{2+} oscillations mediated by the synergistic excitatory actions of GABA(A) and NMDA receptors in the neonatal hippocampus. Neuron 18, 243-255

Lowry JA, Jarrett RV, Wasserman G, Pettett G, Kauffman RE (2001) Arch Pediatt Adolesc Med 155, 934-939

Maier N, Morris G, Johenning FW, Schmitz D (2009) An approach for reliably investigating hippocampal sharp wave-ripples in vitro. PLoS ONE 4, e6925 1-10

Montandon G, Kinkead R, Bairam A (2008) Adenosinergic modulation of respiratory activity: developmental plasticity induced by perinatal caffeine administration. Resp Physiol Neurobiol 164, 87-95

Moraidis I, Bingmann D (1994) Epileptogenic actions of xanthines in relation to their affinities for adenosine A1 receptors in CA3 neurons of hippocampal slices (guinea pig). Brain Res 640, 140-145

Nikolenko V, Poskanzer KE, Yuste R (2007) Two-photon photostimulation and imaging of neural circuits. Nat Methods 4, 943-950

Pal S, Limbrick DD Jr, Rafiq A, DeLorenzo RJ (2000) Induction of spontaneous recurrent epileptiform discharges causes long-term changes in intracellular calcium homeostatic mechanisms. Cell Calcium 28, 181-193

Panaitescu B, Ruangkittisakul A, Ballanyi K (2009) Silencing by raised extracellular Ca^{2+} of pre-Bötzinger complex neurons in newborn rat brainstem slices without change of membrane potential or input resistance. Neurosci Lett 456, 25-29

Ruangkittisakul A, Ballanyi K (2010) Methylxanthine reversal of opioid-evoked inspiratory depression via phosphodiesterase-4 blockade. Respir Physiol Neurobiol 172, 94-105

Ruangkittisakul A, Schwarzacher SW, Secchia L, Poon BY, Ma Y, Funk GD, Ballanyi K (2006) High sensitivity to neuromodulator-activated signaling pathways at physiological $[K^+]$ of confocally-imaged respiratory center neurons in online-calibrated newborn rat brainstem slices. J Neurosci 26, 11870-11880

Ruangkittisakul A, Panaitescu B, Kuribayashi J, Ballanyi K (2010) Caffeine reversal of opioid-evoked and endogenous inspiratory depression in perinatal rat en bloc medullas and slices. Adv Exp Med Biol 669, 123-127

Ruangkittisakul A, Secchia-Ballanyi L, Panaitescu B, Bobocea N, Kuribayashi J, Iizuka M, Kantor C, Ballanyi K (2012) Anatomically ‘calibrated‘ isolated respiratory networks from newborn rodents. In: Isolated Central Nervous System Circuits (Ed K Ballanyi), Neuromethods Series (Ed W Walz). Springer Science+Business Media, LLC, New York, NY (*in press*)

Ruangkittisakul A, Schwarzacher SW, Ma Y, Poon B, Secchia L, Bobocea N, Funk GD, Ballanyi K (2008) Generation of eupnea and sighs by a spatiochemically organized inspiratory network. J Neurosci 28, 2447-2458

Ruangkittisakul A, Okada Y, Oku Y, Koshiya N, Ballanyi K (2009) Fluorescence imaging of active respiratory networks, Respir Physiol Neurobiol 168, 26-38

Schmidt B, Roberts RS, Davis P, Doyle LW, Barrington KJ, Ohlsson A, Solimano A, Tin W, (2006) Caffeine therapy for apnea of prematurity. NEJM 354, 2112-2121

Sipilä ST, Kaila K (2007) GABAergic control of CA3-driven network events in the developing hippocampus. Results Probl Cell Differ 44, 99-121

Spitzer NC (2006) Electrical activity in early neuronal development. *Nature* 444, 707-712

Stosiek C, Garaschuk O, Holthoff K, Konnerth A (2003) In vivo two-photon calcium imaging of neuronal networks. Proc Natl Acad Sci USA 100, 7319-7324

Takano H, McCartney M, Ortinski PI, Yue C, Putt ME, Coulter DA (2012) Deterministic and stochastic neuronal contributions to distinct synchronous CA3 network bursts. J Neurosci 32, 4743-4754

Thöne J, Leniger T, Splettstösser F, Wiemann M (2008) Antiepileptic activity of zonisamide on hippocampal CA3 neurons does not depend on carbonic anhydrase inhibition. Epilepsy Res 79, 105-111

Vanhatalo S, Matias Palva J, Andersson S, Rivera C, Voipio J, Kaila K (2005) Slow endogenous activity transients and developmental expression of K^+-Cl^- cotransporter 2 in the immature human cortex. Eur J Neurosci 22, 2799-2804

Vanhatalo S, Tallgren P, Andersson S, Sainio K, Voipio J, Kaila K (2002) DC-EEG discloses prominent, very slow activity patterns during sleep in preterm infants. Clin Neuropharm 113, 1822-1825

Ukena D, Schudt C, Sybrecht GW (1993) Adenosine receptor-blocking xanthines as inhibitors of phosphodiesterase enzymes. Biochem Pharmacol 45, 847-851

Wang DD, Kriegstein AR (2010) Blocking early GABA depolarization with bumetanide results in permanent alterations in cortical circuits and sensorimotor gating deficits. Cereb Cort 21, 574-587

Wilken B, Ramirez JM, Hanefeld F, Richter DW (2000) Aminophylline modulation of the mouse respiratory network changes during postnatal maturation. J Appl Physiol 89, 2015-2022

Chapter-5

Perturbation of Hippocampal, but not Cortical ENOs by Opioids

Chase M. Kantor, Victoria Leung, Klaus Ballanyi*

Department of Physiology, 750 MSB, University of Alberta, Edmonton, AB, Canada T6G 2S2

My contribution to this study consisted of the execution of >80% of the electrophysiology and all of the calcium imaging studies and corresponding analysis. Dr. K Ballanyi developed the concept for the work and revised the manuscript.

*Corresponding author: Klaus Ballanyi at the above address

5.1 Abstract

Treatment of newborns with opioids for analgesia can depress breathing due to inhibition of medullary respiratory networks. It is not known whether opioids also affect immature neonatal hippocampal and cortical networks that show 'early network oscillations' (ENOs) to establish connectivity. This was studied here using field potential recording in both areas and Ca^{2+} imaging in CA_3 hippocampal neurons of newborn rat brain slices upon bath-application of the μ-opioid receptor agonist [D-Ala^2,N-Me-Phe^4,Gly^5-ol]-enkephalin (DAMGO). ≥10 nM DAMGO transformed regular hippocampal ENOs (burst rate 20/min, burst duration 0.73 s) into 10-60 s lasting periods of bursts of similar amplitude that were interrupted by 5-20 s periods of silence. ≥100 nM DAMGO either evoked large amplitude regular seizure-like discharges or ramp-like bursts that could trigger large amplitude 'spikes' followed by a period of inhibition. Cortical ENOs, which showed variable patterns in control, were not substantially perturbed by DAMGO except for a trend at ≥10 nM for increased burst duration. DAMGO effects were reversed by the opioid receptor blocker naloxone (1 μM) which, in control, did not affect cortical ENOs in control, but tended to deregulate hippocampal ENOs. DAMGO-evoked transformation of hippocampal ENOs was reflected by corresponding changes of Ca^{2+} rises in CA_3 neurons, whereas neighboring astrocytes, identified by the morphological dye SR-101, remained silent except for a subpopulation of ~30% of cells showing slow Ca^{2+} rises in >100 nM DAMGO. The findings show that opioid effects on cortical ENOs are modest, whereas hippocampal ENOs in the CA_3 area are profoundly perturbed which may hamper their maturation.

5.2 Introduction

Administration of opioids is common clinical practice for pain management in newborn human infants, but can be accompanied by depression of breathing (Santiago & Edelman, 1985; Gutstein, 2001; Anand et al., 2001; Simons & Anand, 2006; Geppetti & Benemei, 2009). Such opioid-evoked respiratory depression is presumably due to a direct inhibitory effect of μ-opioid receptor activation on rhythmogenic preBötzinger complex (preBötC) neurons that initiate and control normal breathing (Feldman & Del Negro, 2006; Ballanyi et al., 2009). Right from the first breath, the preBötC must be functional and adapt to various behaviors such as swallowing, coughing or phonation (Jansen & Chernick, 1983; Ballanyi, 2004; Greer et al., 2006). In contrast, most supramedullary brain structures are immature in newborn mammals. This is established for neural networks in the hippocampus and cortex that show spontaneous 'giant depolarizing potentials' (GDPs) which are often reflected by synchronous 'early network oscillations' (ENOs). Analysis of GDPs and ENOs in numerous studies led to the view that these events are pivotal for maturation of hippocampal and cortical circuits, e.g. by initiating and stabilizing synaptic connectivity between different populations of (glutamatergic) principal neurons and inhibitory interneurons acting via γ-aminobutyric acid (GABA) (Ben-Ari et al., 1989, 2007; Garaschuk et al., 2000; Sipilä & Kaila, 2007; Khazipov & Luhmann, 2006; Allene & Cossart, 2010). It is not yet studied, whether opioid treatment of newborns perturbs such ENOs in addition to their established inhibitory effects on inspiratory active preBötC networks and on spontaneous bursting in a further brainstem structure, the *locus coeruleus*, that is capable of modulating other brain structures already at birth through its extensive noradrenergic innervations (Dreyfuss et al., 1983; North & Williams, 1984; Nakamura et al., 1987; Marshall et al., 1991; Alreja & Aghajanian, 1993; Ballantyne et al., 2004).

It was the main objective of the present study to analyze whether opioids exert their most common inhibitory action on ENOs in the CA_3 area of the hippocampus (hENOs) and the entorhinal/perirhinal cortex (cENOs) or rather have a stimulatory effect in line with the finding that they enhanced spontaneous Ca^{2+} rises in cultured hippocampal neurons (Przewlocki et al., 1999). For this, field potential recording of hENOs and cENOs plus Ca^{2+} imaging in CA_3 neurons and neighboring presumptive astrocytes was performed on 400-500 μm thick horizontal newborn rat brain slices that also contained spontaneously active *locus coeruleus* networks as a reference to test for inhibitory opioid effects (**§1.9, 2.3.1.1**) **(Figs. 2-1, 2-4)** (Kantor et al., 2012).

5.3 Methods

(see **§2**)

5.4 Results

With reference to the occurrence of different ENO patterns in the preceding chapters **(§3**, **4**), it is important to note that hENOs in the present study were quite regular in 30 slices from P0-10 rats. In 12 of these slices, hENOs showed solely a burst pattern, whereas bursts were intermingled with spikes in the remaining cases. In contrast cENOs showed a large variability of patterns, similar to those described in **§4 (Fig. 4-5)**. For testing effects of opioids on these events, DAMGO was bath-applied for 20 min at increasing doses ranging from 1 nM to 10 μM.

5.4.1 Major DAMGO-evoked Perturbation of Hippocampal ENOs

At 1 or 10 nM, DAMGO either depressed (n= 10) or increased (n= 3) burst amplitude of hENOs (by <30%), or did not affect their amplitude nor rate (n= 7) **(Fig. 5-1)**. Also, while these effects appeared to be reversible upon washout of DAMGO in ~50% of cases, this may also reflect time-dependent fluctuations of the amplitude of hENOs in control. As a main finding for effects of 10 nM DAMGO, reversible small amplitude fluctuations of the baseline of the integrated suction electrode signal were observed in 10 of 30 slices. Both, the probability of occurrence and the amplitude of these 'slow wave oscillations' (SWOs) increased notably at 100 nM DAMGO. Specifically, in 14 of 21 slices, previously regular hENOs were now clustered, with 3-30 single bursts occurring for a time period of 10-60 s while activity was interrupted for 5-20 s time periods **(Fig. 5-1)**. During the silent periods, integrated signal baseline recovered to values observed between single hENO bursts in control. Also bath-application of 1 μM DAMGO induced SWOs in 8 of 13 slices whereas in 5 different slices regular hENOs were transformed into (or replaced by) regular large amplitude discharge**s**. The latter activities, which resembled IA-type seizure-like discharges **(Fig. 1-7, §4)** (Kilb et al., 2007), persisted for 3-12 min after start of exposure to DAMGO and then changed into smaller amplitude SWOs **(Fig. 5-1)**. While the onset of DAMGO-evoked IAs was rapid in 2 slices, it developed following a large amplitude ramp-like increase in integrated electrode signal baseline in the other 3 cases **(Fig. 5-1)**. A corresponding transformation of hENOs into IA-type seizure-like discharges was revealed in 3 slices in response to 10 μM DAMGO. Such activity would subsequently disappear after <10 min at such time SWOs would appear and persist for the remainder of the application (n= 10).

5.4.2 Modest DAMGO Effects on Cortical ENOs

DAMGO effects on cortical bursting varied between and within slices of different cENO types **(Fig 5-2)**. At 1 nM DAMGO, there did not appear to be a notable change in 7 of 16 slices, while other slices displayed bursts of either increased amplitude (by <10 %, n= 3), depressed amplitude (by <10 %, n= 3), longer burst duration (by <20 %, n= 1), bursts with multiple peaks (n= 1), or increased frequency (by <50 %, n= 1) **(Fig. 5-2)**. At 10 nM DAMGO, 7 of 18 slices did not show a notable change of cENO characteristics, whereas the remaining slices exhibited either depressed amplitude (by <8 %, n= 4), increased amplitude (by <8 %, n= 3), episodic bursting (n= 2) defined as groups of 2-4 bursts separated by sometimes several tens of seconds, or bursts with multiple peaks (n= 2) **(Fig. 5-2)**. At 100 nM, DAMGO had no apparent effects on cENOs in 5 of 19 slices, but attenuated burst amplitude in 5 cases (by <15%). In the remaining 9 slices, it either increased burst amplitude (by <15 %, n= 4) or duration (by ~11%, n= 1), or evoked episodic bursting (n= 3) *versus* multiple peak bursts (n= 1). Finally, there was a trend for a decrease in burst rate (by <30 %, n= 2) in 100 nM DAMGO **(Fig. 5-2)**. Because of the overall variability in control rhythms, these changes were not significant and quantification of bursting properties was deemed unreliable. However, at 1 μM DAMGO a trend for a reversible increase in burst duration (188.2 ± 21.1% of control, n= 7) regardless of cENO burst type and likewise decreases in rate (74.6 ± 9.4% of control) was more obvious **(Fig. 5-2)**.

5.4.3 Naloxone Reverses DAMGO-Induced Perturbation of ENOs

To investigate potential involvement of endogenous opioids in the generation of ENOS, the opioid receptor antagonist naloxone was bath-applied 30-40 min after stable control rhythm developed. In 8 of 11 slices, both regular burst (n= 4) and mixed burst-spike hENOs (n= 4) appeared less regular in naloxone, starting at 100 nM **(Fig. 5-3)**. In 2 of these slices, burst rate

appeared to increase **(Fig. 5-3)**. In the remaining cases, burst rate decreased and episodic doublet bursting occurred (n= 1) or no effect was seen, even at up to 1 µM naloxone (n= 2). In 9 different slices, 0.1-1 µM naloxone had no apparent effect on cENOs in 5 cases **(Fig. 5-3)**. In the other 4 slices, the drug increased (by <10 %, n= 1) or decreased (by <20 %, n= 1) burst amplitude, or transformed single bursts into couplets or multi-peak bursts (n= 2). To test whether DAMGO was acting on opioid receptors, naloxone was added to DAMGO-containing solution following 20-30 min of steady-state DAMGO application. In 10 slices, in which ≥100 nM DAMGO perturbed hENOs by occurrence of SWOs in CA_3 neurons, naloxone (1 µM) reversed such activity and restored hENOs in 9 cases **(Fig. 5-3)**. DAMGO-induced apparent prolongation of cENO bursts was reversed in 6 cases by naloxone addition to DAMGO-containing solution (≥100 nM) **(Fig. 5-3)**. In the remaining slices, naloxone in DAMGO either evoked episodic bursting (n= 2) or increased burst rate (by <50 %, n= 2).

5.4.4 Opioids depress ENO-like LC rhythm

The above described results on hENOs and cENOs did not present evidence for the most common inhibitory action of activation of µ-opioid receptors. To investigate if this may be due to experimental conditions of the present study, established inhibitory DAMGO effects were tested on spontaneously active *locus coeruleus* neurons (Williams & North, 1984; North & Williams, 1983; Alreja & Aghajanian, 1993). As recently reported by us, the *locus coeruleus* is contained in the slices used for the present study and its synchronous bursting generates an ENO-like robust rhythmic field potential (Kantor et al., 2012).

In 4 slices, the mean rate of *locus coeruleus* rhythm was 86.8 ± 5.3 bursts/min. This rhythm was reversibly blocked by 100-250 nM DAMGO which recovered within 10-15 min after start of DAMGO washout to 86 ± 5.7% of control (n= 3). In these slices, blockade of *locus coeruleus* bursting by a further exposure to DAMGO was countered by 1 µM naloxone (burst rate in control 78 ± 2.6 bursts/min *versus* 112 ± 11.2 bursts/min, n= 3). Simultaneously recorded cENOs were unaffected by DAMGO nor naloxone in DAMGO **(Fig. 5-4)**.

5.4.5 Opioid Response of CA3 Neurons and Astrocytes

For assessment of opioid effects at the cellular level, Ca^{2+} imaging was performed in the hippocampal CA_3 region of 10 slices. In a single focal imaging plane, typically 10-20 pyramidal neurons with a soma diameter of 15-25 µm showed spontaneous, more or less synchronous, rises of cytosolic Ca^{2+} (Ca_i) in the soma and primary dendrites which occurred at a rate of 12-20 bursts/min **(Fig. 5-5)**. The probability for synchronous Ca^{2+} rises seemed to be higher for cells located at greater tissue depths as indicated by rhythmic increases in background fluorescence. Smaller cells with a soma diameter of ~10 µm, likely comprising astrocytes, were predominantly located outside the pyramidal cell layer in the *stratum radiatum* and *stratum oriens*. These cells showed spontaneous Ca_i rises in <10 % of cases, and such transients were slower than those in the neurons. In previous studies from our group, pharmacological tools were established for a discrimination of such astrocytes from comparably small interneurons. Specifically, presumptive astrocytes responded to bath-applied glutamate in a similar fashion as neurons, whereas a major (oscillatory) rise of glial Ca_i was revealed in response to the metabotropic glutamate receptor agonist trans-1-aminocyclopentane-1,3-dicarboxylic acid (t-ACPD), contrary to modest responses in neurons (Ruangkittisakul et al., 2009, 2012; Ballanyi et al., 2010). Astrocytes were

further tagged by simultaneous loading of the slices with the morphological red fluorescent dye sulforhodamine-101 (at 34 ^{o}C, 1 μM) and the green fluorescent Ca^{2+} dye Fluo-8L-AM **(Fig. 5-5)** (**§2.2.3**) (Kantor et al., 2012).

Application of DAMGO (250 nM) transformed neuronal Ca_i rises either into events that resembled the suction electrode-recorded SWOs (n= 4) **(Fig. 5-5)** or synchronous and repetitive large amplitude events (n= 4) **(Fig. 5-6)**. Repetitive large amplitude events evoked in 250 nM DAMGO, resembling IAs, which were eventually transformed into or replaced by lower amplitude Ca_i rises (n= 4). These effects were reversed within <10 min after start of application of naloxone (1 μM) in DAMGO **(Fig. 5-6)**. In the remaining 2 slices, DAMGO evoked irregular and non-synchronous neuronal Ca_i rises that were insensitive to naloxone. In these slices (n= 10), t-ACPD (25 μM) increased neuronal Ca_i baseline by ~150%, while a brief (30 s) application of glutamate (Glu) augmented Ca_i baseline by ~200% **(Fig. 5-6)**.

In presumptive astrocytes (white arrows, **Fig. 5-5, 5-6**) DAMGO evoked Ca_i rises in only 25% of cells and in ~50% of preparations. These glial Ca_i increases typically comprised of long-lasting (~30-120 s) high amplitude Ca_i rises or fast small amplitude transients which appeared to coincide with DAMGO-evoked IAs in CA_3 neurons (**Fig. 5-6**). In ~50% of cases, naloxone (1 μM) did not abolish DAMGO-evoked glial Ca_i rises. Similar to neuronal responses, t-ACPD augmented astrocytic Ca_i rises by 200-300% with further similar augmentations seen during brief Glu application **(Fig. 5-6)**.

5.5 Discussion

As the main finding of the present study on newborn rat brain slices, activation of μ-opioid receptors had no major effect on cortical ENOs whereas it transformed the ENO pattern in the hippocampal CA_3 region into slow oscillating waves and IA-type seizure-like bursting at close to micromolar doses (**Fig. 5-7**). While this seems to contradict an already established inhibitory action of opioids on most nervous structures, the following discussion will point out that there is also published evidence for excitatory opioid actions on neural circuits, particularly in the hippocampus.

5.5.1 Modulation of Medullary Neural Networks by Opioids

Numerous studies on *locus coeruleus* neurons in rodent brain slices have provided valuable information on the signaling cascade involved in opioid-evoked inhibition via activation of postsynaptic G protein-coupled K^+ channels (Pepper & Henderson, 1980; Williams & North, 1983; North & Williams, 1984; Alreja & Aghajanian, 1993). Our preliminary findings on the same type of horizontal newborn rat brain slices used here indicated that DAMGO not only inhibits some of these neurons, but also abolishes synchronized neuronal population bursting in this structure (Kantor et al., 2012). These effects are similar to strong inhibition of preBötC inspiratory center bursting in both newborns and adult mammals (Gray et al., 1999; Feldman & Del Negro, 2006; Ballanyi et al., 2009; Montadon et al., 2012). While inhibition of preBötC bursting is responsible for the depressing action of opioids on breathing, there is evidence that functionally expiratory parafacial respiratory group neurons are rather stimulated by them (Ballanyi et al., 2009). Using newborn rat brainstem-spinal cord preparations, it was shown that opioids depress inspiratory-related spinal motor output in such preparations without pons,

whereas inspiratory rhythm is enhanced when the pons is intact (Tanabe et al., 2005). It was thus hypothesized that during birth, associated surge of endorphins stimulation of (pontine) parafacial respiratory group neurons by these agents is transmitted to preBötC neurons for maintaining their endorphin-depressed activity (Jaquin et al., 1996; Feldman & Del Negro, 2006). While this exemplifies an excitatory μ-receptor effect on a pivotal neural network function in newborns, the cellular mechanism of this stimulation of parafacial respiratory group neurons is not yet analyzed. Similarly, it is unknown by which mechanism morphine acts on postsynaptic opioid receptors to directly excite medial vestibular neurons in juvenile rat brainstem slices (Lin & Carpenter, 1994). Some possible mechanisms are discussed in the next section.

5.5.2 Excitation of Hippocampal Neurons by Opioids

While the latter study provided experimental evidence that excitation of medial vestibular neurons by opioids is not indirectly caused by disinhibition via hyperpolarization of GABAergic neurons, this mechanism explains their excitatory effects on supramedullary structures including the periaqueductual grey (Chiou & Huang, 1999) and hippocampus. Two thorough review articles (Drake et al., 2007; Henderson, 1983) point out that excitatory opioid actions on hippocampal circuits are well-studied since the mid-seventies. For example, it was proposed that the epileptogenic action of μ-receptor activation is secondary to inhibition of GABAergic transmission to CA_1 and CA_3 neurons (Nicoll et al., 1980; Siggins & Zieglgänsberger, 1981). In that regard, it has been proposed that inhibition of non-action potential-dependent GABA release contributes to reducing action potential-evoked GABA release, thereby decreasing synaptic inhibition (Cohen et al., 1992). In fact, μ-opioid receptor-containing CA_1 cells appear to form a neurochemically and functionally hetereogeneous subset of hippocampal GABAergic

interneurons that are specialized to inhibit pyramidal principal neurons (Drake & Milner, 2002; Stumm et al., 2004). The manifold electrophysiological evidence for opioid effects on hippocampal neural networks is supported by various studies that provided (immuno-histochemical) evidence for expression of different types of opioid receptors in the hippocampus. This revealed that μ-receptors are widely expressed in the hippocampus, on both presynaptic interneurons and postsynaptic CA_3 pyramidal bursters, and are already functional at birth (Leslie et al., 1982; Pickel et al., 1982; Meilandt et al., 2004). Moreover, there is an abundance of opioid-containing nerve fibres innervating CA_3 neurons (Gall et al., 1981; Chavkin et al., 1983).

As noted in several of the above studies, blocking effect of opioids on inhibitory interneurons not only promotes hyperexcitability causing epileptogenesis, but also promotes excitation-dependent processes such as those involved in long-term potentiation. However, as pointed out by Henderson (1983), mechanisms other than disinhibition can contribute to opioid-evoked enhancement of hippocampal excitability. Of particular relevance in that regard are presynaptic facilitation of release of excitatory neurotransmitter and increased efficacy of coupling between neurons. Moreover, opioids can directly stimulate neurons by blocking different types of K^+ channels (Crain & Shen, 1990; Moore et al., 1994) or enhancing current flow through NMDA-type ionotropic glutamate receptors (Chen & Huang, 1991; Martin et al., 1997). The above findings of excitatory opioid actions on hippocampal neurons are mainly based on electrophysiological studies testing 'simple' (electrically) evoked synaptic responses. Though, one study on adult rat hippocampal slices showed that complex electrically evoked gamma oscillations are desynchronized by a morphine-induced decrease in $GABA_A$ receptor-mediated

inhibition of both excitatory pyramidal cells and inhibitory interneurons (Whittington et al., 1998).

5.5.3 Opioid Effects on Spontaneous Hippocampal and Cortical Bursting

According to our knowledge, effects of μ-opioid receptor activation on spontaneous hippocampal or cortical bursting have been studied so far only in two cases. Firstly, it was found that 'periodic oscillatory activity' in the entorhinal and perirhinal cortex plus basolateral/lateral nuclei of the amygdala of juvenile rat parahippocampal slices is slowed in naloxone-sensitive fashion by DAMGO (Kano et al., 2005). As the underlying mechanism, the authors proposed that μ-opioid receptors hyperpolarize interneurons thus decreasing their ability to release GABA. Altenatively, DAMGO depression could involve presynaptic inhibition of glutamatergic excitation as suggested by findings from a study on excitatory postsynaptic currents in adult rat neocortical slices (Ostermeier et al., 2000). While both latter reports show clear effects of μ-agonists on spontaneous and evoked cortical responses, respectively, DAMGO effects did not significantly change cENOs in the present study. But, close-to-micromolar DAMGO doses showed a clear trend for slowing of cENOs and concomitant prolongation of single cENO bursts. The finding that also naloxone did not affect the different cENO burst patterns indicates a lack of a 'tonic' effect of endorphines that are spontaneously released into the slices.

Another report analyzed opioid actions on spontaneous hippocampal bursting by combining neuronal population Ca^{2+} imaging with cellular patch-clamp recording in organotypic slices from newborn rats (Przewlocki et al., 1999). The authors found that both the amplitude and synchronicity of spontaneous Ca^{2+} oscillations are increased by 1 μM DAMGO via boosting of

synaptically-driven NMDA receptor-mediated burst events, leading to depolarizing responses to exogenous NMDA and current-evoked Ca^{2+} spikes. They concluded that activation of naloxone-sensitive opioid receptors augments several components of neuronal Ca^{2+} signaling pathways and enhances Ca^{2+} signals as a consequence. Moreover, they claimed that these results provided evidence for a novel neuronal mechanism of opioid actions on central neural networks that may contribute to both short- and long-term effects of opioids. We have not analyzed the role of NMDA receptors and voltage-activated Ca^{2+} channels in opioid augmentation of hENOs in the present study. But, this mechanim seems possible considering that these processes are involved in the generation of hippocampal GDPs and ENOs (Ben-Ari et al., 1989; Bolea et al., 1999; Khazipov et al., 2001; Sipilä et al., 2005). Accordingly, our observation here that DAMGO stimulated spontaneous cytosolic Ca_i rises associated with hENOs in CA_3 neurons of acute slices supports the notion by Przewlocki et al. (1999) that opioids increase cytosolic Ca^{2+} in native neurons as well as neuron-derived cell lines (Jin et al., 1992; Fields et al., 1995; Connor & Henderson, 1996). While our present findings resemble those in the above study on organotypic hippocampal cultures (Przewlocki et al., 1999), they did not report that the pattern of Ca^{2+} oscillations is notably transformed by DAMGO. This indicates that the hippocampal circuitry differs between acute newborn rat slices and cultures (Przewlocki et al., 1999).

The opioid-evoked transformation from control hENOs to SWOs started at 10 nM DAMGO, whereas doses >250 nM revealed seizure-like events. The latter discharges resembled IAs seen by us in response to either blockade of $GABA_A$ receptors or (low millimolar) methylxanthine (**§4.3**) and by others using different types of pharmacological *in vitro* seizure models **(Fig. 1.7)** (Jefferys, 1995; Kilb et al., 2007). While it is unclear why no ILE-like seizure-like activities

were revealed here contrary to our findings using methylxanthines or $GABA_A$ receptor blockers in these slices (**§4.3**), our present data suggest that development of IAs is, at least partly, due to inhibition of $GABA_A$ receptors at DAMGO doses >250 nM. Whether the SWOs are due to partial inhibition of these receptors or rather the expression of a different effect of μ-opioid receptor activation in the immature hippocampal networks generating the hENOs remains to be studied.

5.5.4 Role of Astrocyte Ca^{2+} Signaling

For elucidating mechanisms of the opioid-evoked transformation of hENO patterns, it may be important to study the role of hippocampal astrocytes. Our present findings indicated that long-lasting Ca^{2+} transients occurred in a (minor) subpopulation of presumptive astrocytes in control and that these events were stimulated by DAMGO. Similarly, DAMGO could also activate astrocytes that were silent in control. While this was not a highly consistent finding, it raises the possibility that opioid-evoked Ca^{2+} release from glial stores may be part of the signaling cascade by which opioids transform hENO activity patterns. Indeed, findings in neuron-derived cell lines showed that opioids cause indeed store-mediated Ca^{2+} release (Jin et al., 1992; Fields et al., 1995; Connor & Henderson, 1996). That astrocytes in the present study are capable of pronounced signaling via Ca^{2+} release is indicated by the fact that t-ACPD caused a major Ca^{2+} rise in the small cells in the CA_3 area and only a modest response in neurons, similar to our findings based on Ca^{2+} imaging in the isolated inspiratory center (Ruangkittisakul et al., 2009; Ballanyi et al., 2010). Based on these considerations, future analyses of opioid effects on neonatal hippocampal networks should consider to elucidate the role of neuronal Ca^{2+} influx via different sorts of ion channels including NMDA receptors and voltage-activated Ca^{2+} channels *versus* neuronal and

glial Ca^{2+} release that is possibly related to activation of metabotropic receptors in the astrocytes. In that regard, it was found that glial cell activation by opioids works to oppose opioid-induced analgesia through activation of 'Toll-like receptors' (Watkins et al., 2009). In certain pathological states, e.g. proinflammation, astrocytes as well as microglia can either release neuroexcitatory substances (Liu et al., 2007; Binshtok et al., 2008), downregulate GABA receptors, upregulate the number and conductance of Ca^{2+}-permeable AMPA and NMDA receptors (Zhang et al., 2008) or potentiate inward currents through Na^{+} channels (Jin & Gereau, 2006). However, unlike methylxanthine-induced glial Ca^{2+} transients (**see §4**) activation of astrocytic glial cells by DAMGO did not precede epileptiform discharges of CA_3 neurons. Whether activation of glial cells is involved in opioid-induced hyperexcitation of hippocampal networks, or if glial cells rather work to oppose or attenuate this, remains unclear.

Figures

Fig. 5-1

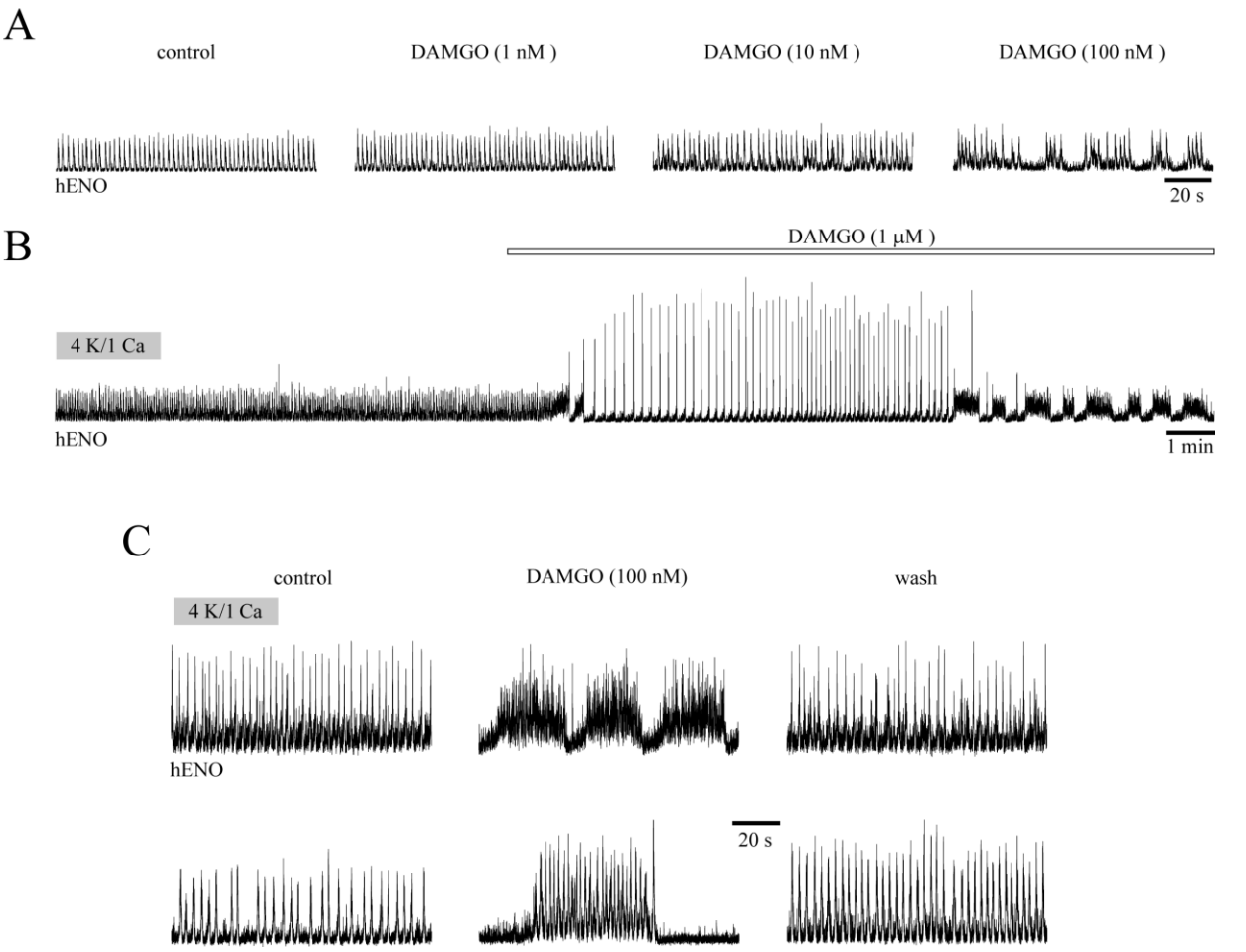

Fig. 5-1: DAMGO-evoked perturbation of hENOs. Amplified (10k), bandpass-filtered (0.3-3kHz) and integrated (τ: 50 ms) h-ENO signals were monitored during bath-application of [D-Ala^2, N-Me-Phe^4, Gly^5-ol]-enkephalin (DAMGO), a μ-opioid receptor agonist. **A**, DAMGO was applied at different concentrations with intermittent (20-30 min) 'wash' periods. At 1-10 nM, DAMGO caused minor perturbation of hENOs, whereas 100 nM evoked slow wave-like oscillations (SWOs) lasting between 10-60 s. **B**, Application of 1 μM DAMGO transformed single bursts into high amplitude, slow interictal-like activity (IA) reminiscent of hyperexcitability evoked by selective blockers of $GABA_A$ receptors (**Fig. 1-7)** (Kilb et al., 2007) which turn after several minutes into SWOs. **C**, DAMGO-induced SWOs would either oscillate

with a ramp-like increase in baseline (top) or begin with a sharp rise (bottom). Such activities disappeared after DAMGO was ‘washed’ from the solution.

Fig. 5-2

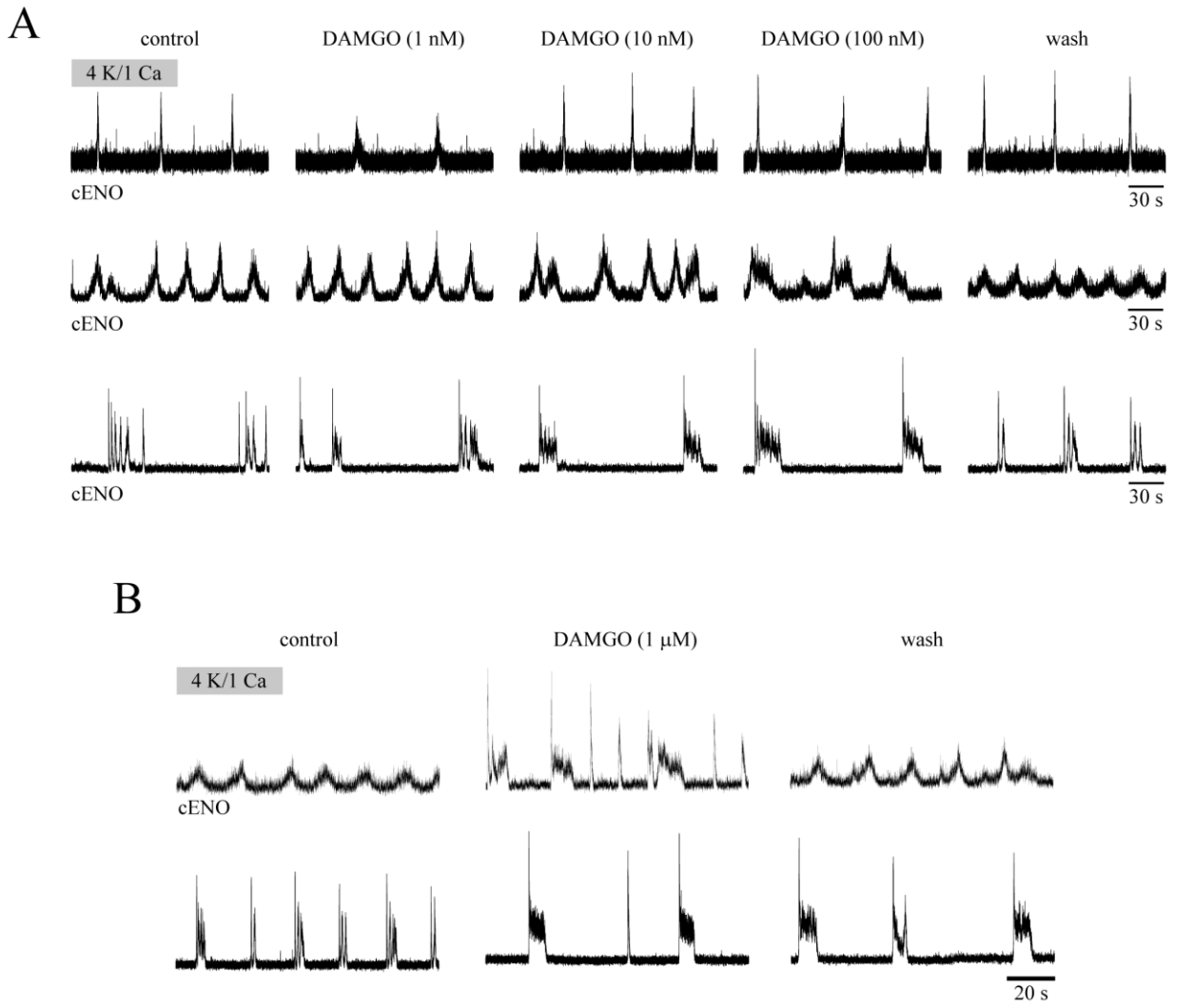

Fig. 5-2: Minor effects of DAMGO on cENOs. cENO burst patterns varied between slices. Here, DAMGO was tested on 4 major cENO patterns which consisted of either brief (burst duration ~2-3 s), high amplitude bursts discharging at low frequencies, slightly longer, lasting ~4 s, higher frequency discharges, low amplitude bursts lasting ~5-10 s or ~20-30 s, or sharp-rising multi-peak bursts. It was not uncommon to record mixed patterns of spontaneous activity simultaneously with one suction electrode. **A**, 1-10 nM DAMGO did not consistently depress nor stimulate cortical bursts, while 100 nM DAMGO slightly increased burst duration. **B**, during 1 μM DAMGO treatment, all preparations showed modest perturbation of cENOs with a tendency for increased cENO burst duration. Such perturbations subsequently disappeared following 'washing' DAMGO from the solution.

Fig. 5-3

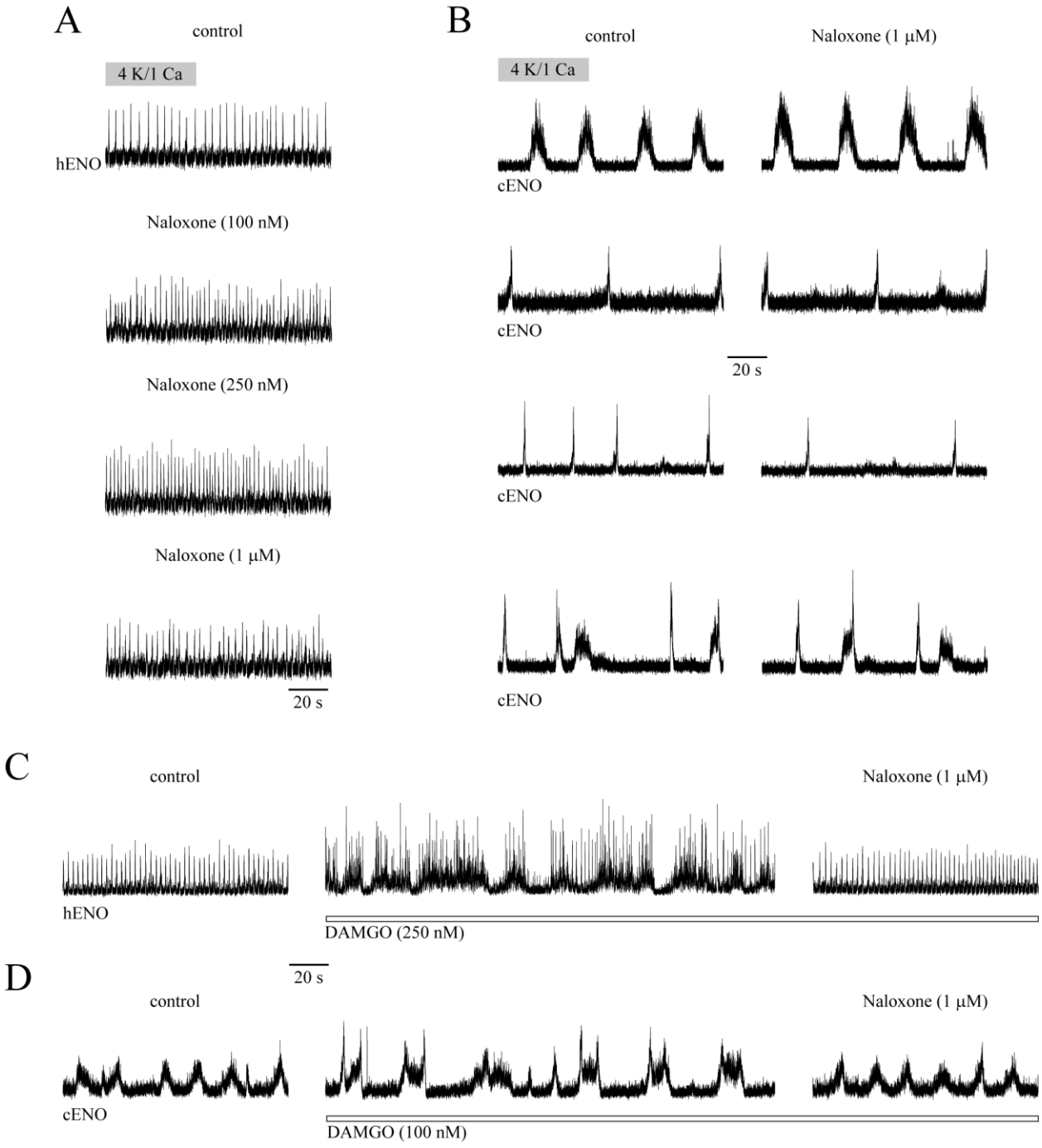

Fig. 5-3: Naloxone reverses DAMGO-induced perturbation of h- and cENOs. The opioid receptor antagonist naloxone was bath-applied for 18-20 min. **A**, In most cases (n=8/11), regular and irregular hENO bursts became more irregular after application of naloxone, starting at 100 nM. **B**, naloxone induced no observable effect on cortical bursts in the majority of 4 different

slices shown here, while a transformation of burst type was seen in a small proportion of slices. **C**, DAMGO transformed regular single hENOs into SWOs, which was countered by naloxone (right columns) in 9 cases (n=10). **D**, the duration of small amplitude cENOs was modestly increased by DAMGO and this was reversed by naloxone.

Fig. 5-4

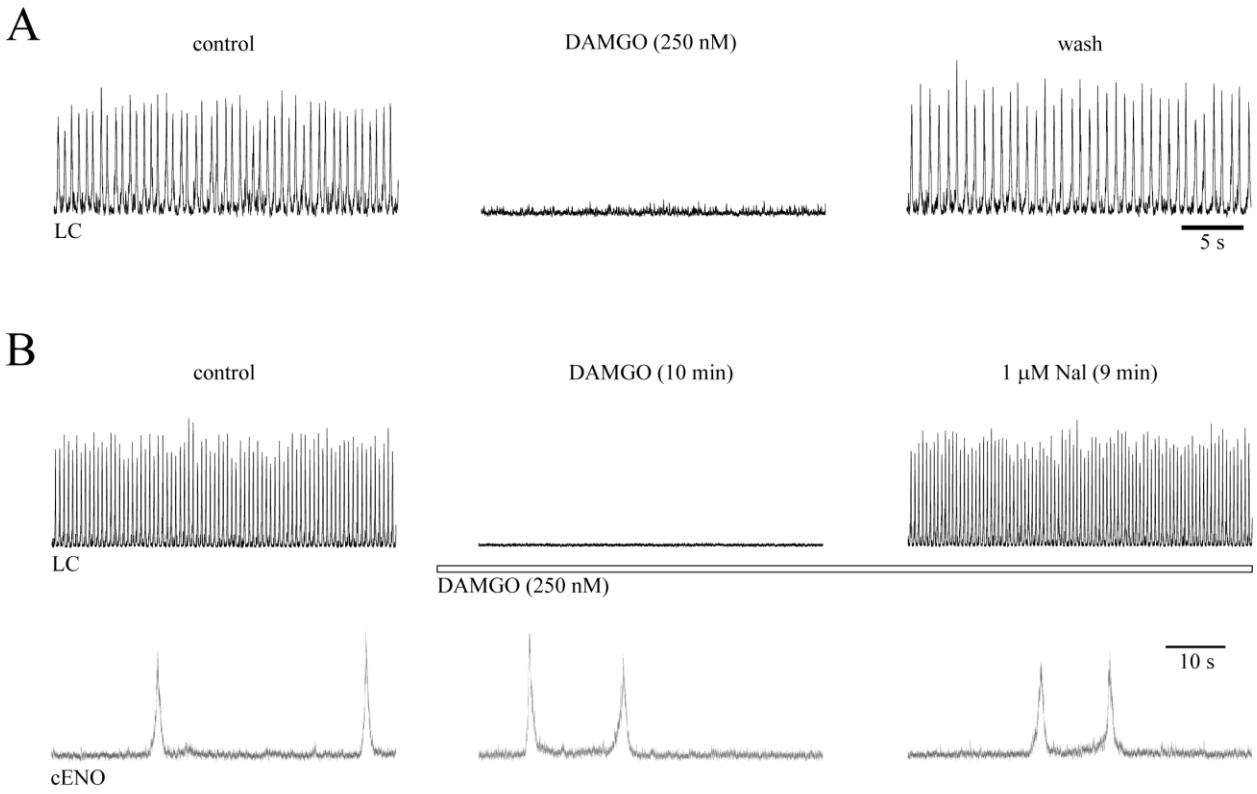

Fig. 5-4: DAMGO depresses ENO- like *locus coeruleus* rhythm. A, bath application of DAMGO reversibly blocked fast bursting in *locus coeruleus* contained in the same slice type showing the hENOs and cENO. **B**, In a different slice, DAMGO abolished *locus coeruleus* rhythm while having no effect on simultaneously recorded cENOs. Addition of naloxone reversed DAMGO-induced depression of *locus coeruleus* rhythm within 9-12 min.

Fig. 5-5

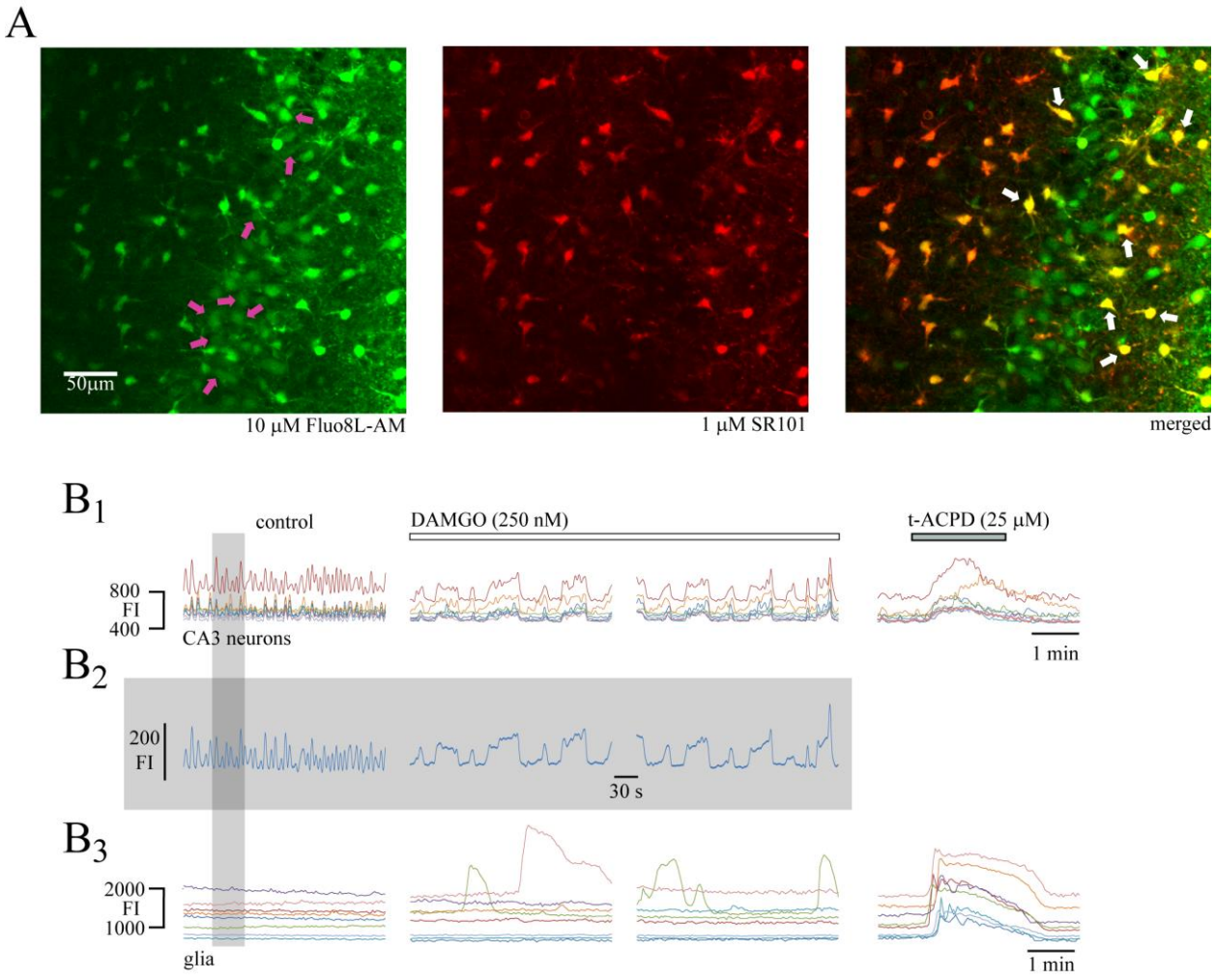

Fig. 5-5: DAMGO perturbs Ca_i rises in hippocampal slices. Fluorescence imaging was done using an Olympus FV300 laser-scanning confocal microscope or a multiphoton system based on a FV300 connected to an infrared ti:sa laser system. **A**, co-incubation of the Ca^{2+}-sensitive dye Fluo-8L-AM with the morphological indicator sulforhodamine 101 (SR101) at 34 ^{o}C revealed Fluo-labeled CA_3 neurons and dual-labeled small, presumably astrocytic cells. Selected regions of interest (ROIs) around neuronal cell somata (purple arrows) show spontaneous Ca_i rises as depicted in **B_1**. **B_2**, ROIs from individual CA_3 neurons were averaged (n= 8) (grey box) depicting overall synchronicity between cells and, thus, a quasi-integrated recording. DAMGO transformed single Ca_i rises into long duration (~20-40 s) oscillations whereas the degree of synchronicity between cells did not change. ROIs around somata of presumptive astrocytes (white arrows; **A**, right) revealed lack of spontaneous Ca_i rises which were activated in ~50% of

cases by DAMGO (**B_3**). Further differentiation between cell types was achieved pharmacologically through application of the metabotropic glutamate receptor agonist t-ACPD (25 μM). Neuronal Ca_i was increased by ~300 fluorescence intensity (FI) units during t-ACPD, whereas glial Ca_i baseline was boosted by ~1000 FI units.

Fig. 5-6

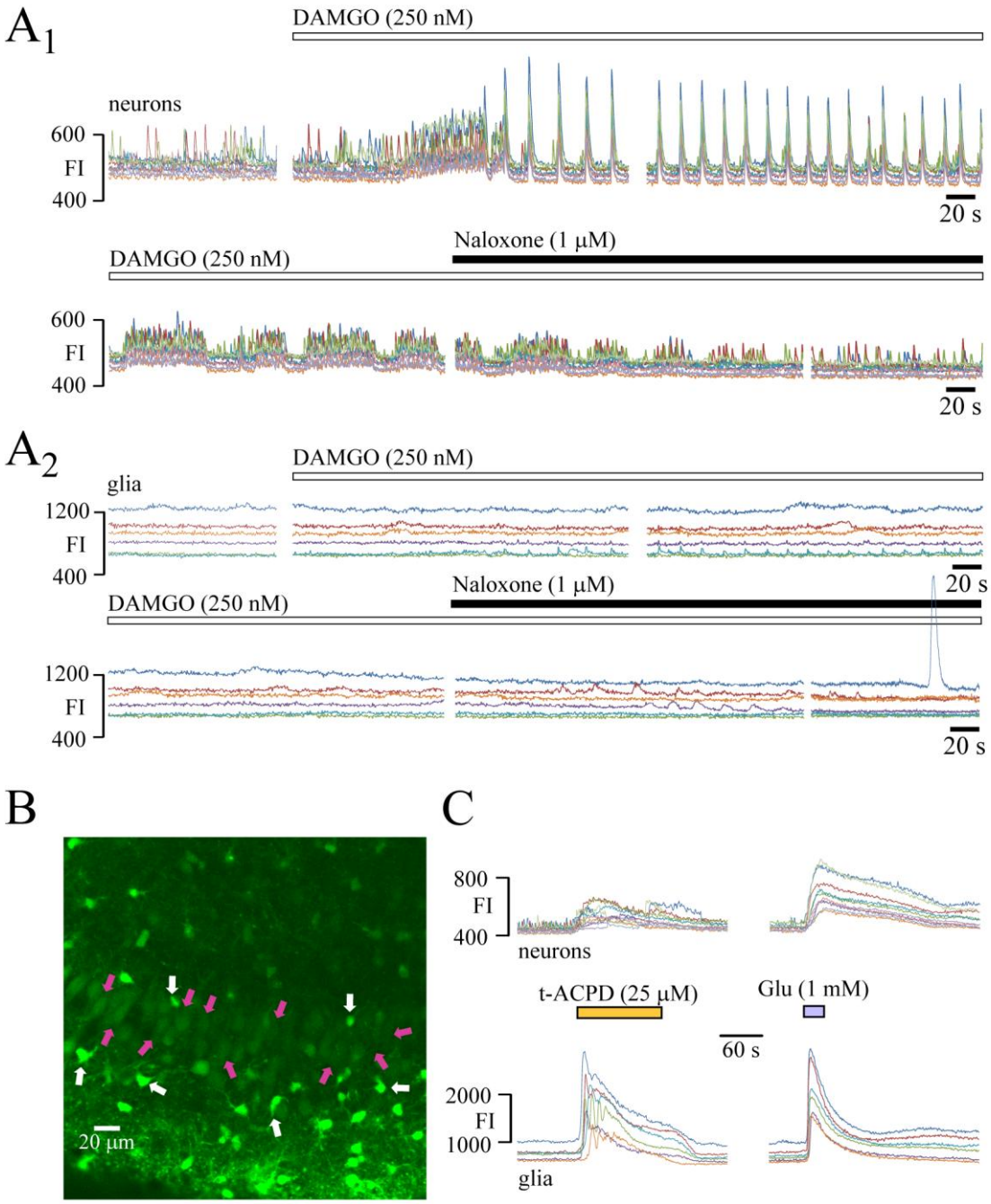

Fig. 5-6: DAMGO-induced perturbation of Ca_i rises is reversed by naloxone. A_1, spontaneous Ca_i rises in CA_3 neurons (purple arrows, **B**) were transformed by DAMGO into high-amplitude, synchronous Ca_i rises, resembling suction electrode recordings of DAMGO-induced IAs. Also similar to suction electrode recording, such hyperexcitation transformed into or was replaced with long duration (20-60 s) oscillations that were reversed by naloxone. **A_2,**

simultaneous monitoring of presumptive astrocytic Ca_i rises (white arrows, **B**) showed lack of spontaneous oscillations in control (4K/1Ca) solution. DAMGO evoked fast, small amplitude Ca_i rises in ~33% of recorded astrocytes that appeared to coincide with neuronal Ca_i rises. Naloxone abolished such activities within 5 min of start of application. **C**, neuronal and glial Ca_i responses to t-ACPD and glutamate (Glu) differed notably. Specifically, neuronal Ca_i baseline was increased by ~150 FI units in response to t-ACPD while glial Ca_i baseline was raised by ~1000 FI. Application for 30 s of Glu produced a prolonged (~4 min) increase in neuronal Ca_i baseline (~200 FI) as opposed to that of glial cells, which showed a brief augmentation (60 s) with amplitude increases by 200-300 FI.

Fig. 5-7

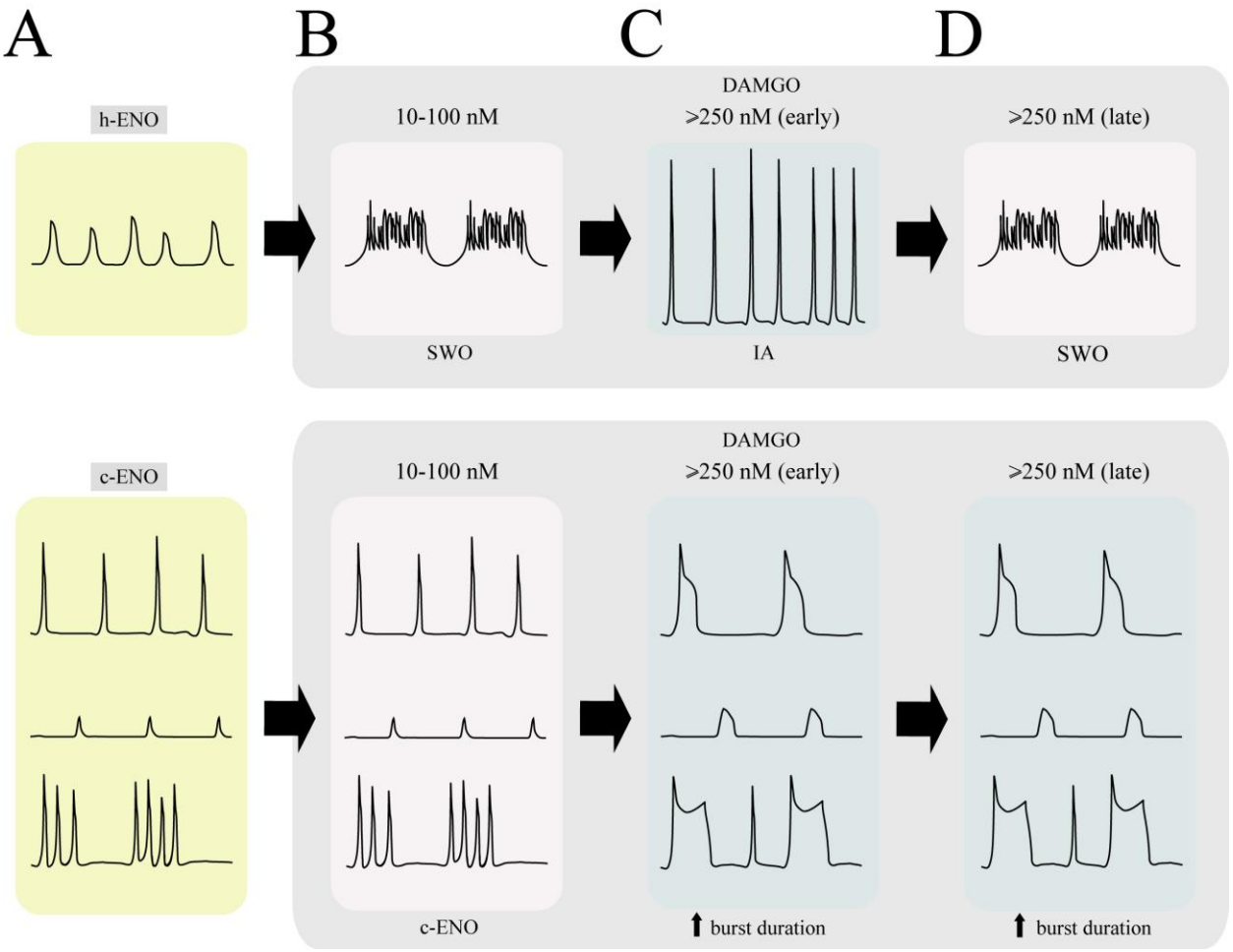

Fig. 5-7: Summary of DAMGO-induced perturbation of c- and hENOs. A top, spontaneous hENOs were transformed by DAMGO at modest nanomolar concentrations (10-100 nM) into slow wave-like oscillations (SWOs) (**B, top**) lasting between 10-60 s. **C top**, Application of higher concentrations (≥ 250 nM) of DAMGO would transform single bursts into high amplitude, slow interictal-like activity (IA) reminiscent of hyperexcitability evoked by selective blockers of $GABA_A$ receptors (**Fig. 1-7)** (Kilb et al., 2007). DAMGO-evoked hyperexcitation was transient and IAs would transform into SWOs towards the end of application. **A bottom**, selected forms of unique spontaneous cENOs were largely unaffected by sub-micromolar concentrations of DAMGO (**B, bottom**). cENOs responded with a tendency for increased burst duration and depressed rate of bursting in response to DAMGO ≥ 250 nM (**C-D, bottom**). These bursting characteristics of cENOs persisted for the entirety of the application of the drug.

5.6 References

Allene C, Cossart R (2010) Early NMDA receptor-driven waves of activity in the developing neocortex: physiological or pathological network oscillations? J Physiol 588, 83-91

Alreja M, Aghajanian GK (1993) Opiates suppress a resting sodium-dependent inward current and activate an outward potassium current in locus coeruleus neurons. J Neurosci 13, 3525-3532

Alvarez-Maubecin V, Garcia-Hernandez F, Williams JT, Van Bockstaele EJ (2000) Functional coupling between neurons and glia. J Neurosci 20, 4091-4098

Anand KJS, Hopkins SE, Wright JA, Ricketts RR, Flanders DW (2001) Statistical models to predict the need for postoperative intensive care and hospitalization in pediatric surgical patients. Neonat Pediatr Intens Care 27, 873-883

Ballantyne D, Andrzejewski M, Mückenhoff K, Scheid P (2004) Rhythms, synchrony and electrical coupling in the locus coeruleus. Resp Physiol Neurobiol 143, 199-214

Ballanyi K (2004) Neuromodulation of the perinatal respiratory network. Curr Neuropharmacol 2, 221-243

Ballanyi K, Panaitescu B, and Ruangkittisakul A (2010) Control of breathing by nerve glue. Sci Signal 3, pe41

Ballanyi K, Ruangkittiskul (2009) Structure-function analysis of rhythmogenic inspiratory pre-Botzinger complex networks in "calibrated" newborn rat brainstem slices. Respir Physiol Neurobiol 168, 158-178

Ballanyi K, Ruangkittisakul A, Onimaru H (2009) Opioids prolong and anoxia shortens delay between onset of pre-inspiratory (pFRG) and inspiratory (preBotC) network bursting in newborn rat brainstems. Eur J Physiol (Pfuger's Archiv) 458, 571-587

Ben-Ari Y (2002) Excitatory actions of GABA during development: the nature of the nurture. Nature 3, 728-739

Ben-Ari Y, Cherubini E, Corradetti R, Caiarsa JL (1989) Giant synaptic potentials in immature rat CA3 hippocampal neurones. J Physiol 416, 303-325

Ben-Ari Y, Gaiarsa JL, Tyzio R, Khazipov R (2007) GABA: a pioneer transmitter that excites immature neurons and generates primitive oscillations. Physiol Rev 87, 1215-1284

Berridge CW, Waterhouse BD (2003) The locus coeruleus-noradrenergic system: modulation of behavioral state and state-dependent cognitive processes. Brain Res Rev 42, 33-84

Binshtok AM, Wang H, Zimmerman K, Amaya F, Vardeh D, Shi L, Brenner GJ, Ji R-R, Bean BP, Woolf CJ, Samad TA (2008) Nociceptors are interleukin-1beta sensors. J Neurosci 28, 14062-14073

Bolea S, Avignone E, Berretta N, Sanchez-Andres JV, Cherubini E (1999) Glutamate controls the induction of GABA-mediated giant depolarizing potentials through AMPA receptors in neonatal rat hippocampal slices. J Neurophysiol 81, 2095-2102

Chavkin C, Bakhit C, Weber E, Bloom FE (1983) Relative contents and comitant release of prodynorphin/neoendorphin-derived peptides in rat hippocampus. Proc Natl Acad Sci USA. 80, 7669-7673

Chen L, Huang LY (1991) Sustained potentiation of NMDA receptor- mediated glutamate responses through activation of protein kinase C by a μ-opioid. Neuron 7, 319-326

Chiou LC, Huang LY (1999) Mechanism underlying increased neuronal activity in the rat ventrolateral periaqueductal grey by a mu-opioid. J Physiol 518, 551-559

Cohen GA, Doze VA, Madison DV (1992) Opioid inhibition of GABA release from presynaptic terminals of rat hippocampal interneurons. Neuron 9, 325-335

Connor MA, Keir MJ, Henderson G (1997) δ-Opioid receptor mobilization of intracellular calcium in SH-SY5Y cells: lack of evidence for δ-receptor subtypes. Neuropharmacol 36, 125-133

Crain SM, Shen KF (1990) Opioids can evoke direct receptor-mediated excitatory effects on sensory neurons. Trends Pharmacol Sci 11, 77-81

Drake CT, Chavkin C, Milner TA (2007) Opioid systems in the dentate gyrus. Prog Brain Res 163, 245-263

Dreyfus CF, Markey KA, Goldstein M, Black IB (1983) Development of catecholaminergic phenotypic characters in the mouse locus coeruleus in vivo and in culture. Dev Biol 97, 48-58

Feldman JL, Del Negro, C.A (2006) Looking for inspiration: new perspectives on respiratory rhythm. *Nat Rev Neurosci* 7, 232-242

Fields A, Gafni M, Oron Y, Sarne Y (1995) Multiple effects of opiates on intracellular calcium level and on calcium uptake in three neuronal cell lines. Brain Res 687, 94-102

Gall CM, Brecha HJ, Karten H, Chang H (1981) Localization of enkephalin-like immunoreactivity to identified axonal and neuronal populations of the rat hippocampus. J Comp Neurol 198, 335-350

Garaschuk O, Hanse E, Konnerth A (1998) Developmental profile and synaptic origin of early network oscillations in the CA1 region of rat neonatal hippocampus. J Physiol Lond 507, 219-236

Garaschuk O, Linn J, Eilers J, Konnerth A (2000) Large-scale oscillatory calcium waves in the immature cortex. Nature 3(5), 452-459

Geppetti P, Benemei S (2009) Pain treatment with opioids: achieving the minimal effective and the minimal interacting dose. Clin Drug Invest 29, 3-16

Gray PA, Rekling JC, Bocchiaro CM, Feldman JL (1999) Modulation of respiratory frequency by peptidergic input to rhythmogenic neurons in the preBotzinger complex. Science 286, 1566-1568

Gutstein HB (2001) Opioid analgesics. In: Goodman and Gilmans‘s the pharmacological basis for therapeutics (Hardman, J.G., Limbird, L.E., Gilman, A.G., eds). New-York: McGraw-Hill. 569–618

Henderson G (1983) Electrophysiological analysis of opioid action in the central nervous system. Br Med Bull 39, 59-64

Jacquin TD, Borday V, Schneider-Maunoury S, Topilko P, Ghilini G, Kato F, Charnay P, Champagnat J (1996) Reorganization of pontine rhythmogenic neuronal networks in Krox-20 knockout mice. Neuron 17, 747-758

Jansen AH, Chernick V (1983) Development of respiratory control. Physiol Rev 63, 437-483

Jin W, Lee NM, Loh HH, Thayer SA (1992) Dual excitatory and inhibitory effects of opioids on intracellular calcium in neuroblastoma X glioma hybrid NG108-15 cells. Mol Pharmacol 42, 1083-1089

Jin X, Gereau RWt (2006) Acute p38-mediated modulation of tetrodotoxin-resistant sodium channels in mouse sensory neurons by tumor necrosis factor-alpha. J Neurosci 26, 246-255

Kano T, Inaba Y, Avoli M (2005) Periodic oscillatory activity in parahippocampal slices maintained in vitro. Neuroscience 130, 1041-1053

Kantor CM, Panaitescu B, Kuribayashi J, Ruangkittisakul A, Jovanovic I, Leung V, Lee TF, MacTavish D, Jhamandas JH, Cheung PY, Ballanyi K (2012) Spontaneous neural network oscillations in hippocampus, cortex, and locus coeruleus of newborn rat and piglet brain slices. In: Isolated CNS circuits. (Ballanyi K, ed.) Humana-Springer (in press)

Khazipov R, Escalpez M, Caillard O, Bernard C, Khalilov I, Tyzio R, Hirsch J, Dzhala V, Berger B, Ben-Ari Y (2001) Early development of neuronal activity in the primate hippocampus in utero. J Neurosci 21(24), 9770-9781

Khazipov R, Luhmann HJ (2006) Early patterns of electrical activity in the developing cerebral cortex of humans and rodents. Trends Neurosci 29, 414-418

Komuro H, Rakic R (1992) Selective role of N-type calcium channels in neuronal migration. Science 257, 806-809

Lin Y, Carpenter DO (1994) Direct excitatory opiate effects mediated by non-synaptic actions on rat medial vestibular neurons. Eur J Pharmacol 262, 99-106

Liu Y-L, Zhou L-J, Hi N-W, Xu C-Y, Zhang T, Li Y-Y, Liu X-G (2007) Tumor necrosis factor-alpha induces long-term potentiation of C-fiber evoked field potentials in spinal dorsal horn in rats with nerve injury: the role of NF-kappa B, JNK and p38 MAPK. Neuropharmacol 52, 708-715

Marshall KC, Christie MJ, Finlayson PG, Williams JT (1991) Developmental aspects of the locus coeruleus-noradrenaline system. Progr Brain Res 88, 173-185

Martin G, Nie Z, Siggins GR (1997) mu-Opioid receptors modulate NMDA receptor-mediated responses in nucleus accumbens neurons. J Neurosci 17, 11-22

Montadon G, Kinkead R, Bairam A (2008) Adenosinergic modulation of respiratory activity: developmental plasticity induced by perinatal caffeine administration. Respir Physiol Neurobiol 164, 87-95

Moore SD, Madamba SG, Schweitzer P, Siggins GR (1994) Voltage dependent effects of opioid peptides on hippocampal CA3 pyramidal neurons in vitro. J Neurosci 14, 809–820

Nakamura S, Kimura F, Sakaguchi T (1987) Postnatal development of electrical activity in the locus ceruleus. J Neurophysiol 58, 510-524

Nicoll RA, Alger BE, Yahr CE (1980) Enkephalin blocks inhibitory pathways in the vertebrate CNS. Nature 287, 22-25

North R, Lovinger D (1993) Presynaptic actions of opioids. In: Presynaptic receptors in the mammalian brain (Dunwiddie, T., ed). Birkenhauser, Boston. 71–76

North RA, Williams JT (1983) Opiate activation of potassium conductance inhibits calcium action potentials in rat locus coeruleus neurones. Brit J Pharmacol 80, 225-228

Pepper CM, Henderson G (1980) Opiates and opioid peptides hyperpolarize locus coeruleus neurons in vitro. Science 209, 394-395

Przewlocki R, Parsons KL, Sweeney DD, Trotter C, Netzeband JG, Siggins GR, Gruol DL (1999) Opioid enhancement of calcium oscillations and burst events involving NMDA receptors and L-type calcium channels in cultured hippocampal neurons. J Neurosci 19(22), 9705-9715

Ruangkittisakul A, Ballanyi K (2010) Methylxanthine reversal of opioid-evoked inspiratory depression via phosphodiesterase-4 blockade. Resp Physiol Neurobiol 172, 94-105

Samuels ER, Szabadi E (2008) Functional neuroanatomy of the noradrenergic locus coeruleus: its roles in the regulation of arousal and autonomic function part II: physiological and pharmacological manipulations and pathological alterations of locus coeruleus activity in humans. Curr Neuropharmacol 6, 254-285

Simons SHP, Anand KJS (2006) Pain control: opioid dosing, population kinetics and side-effects. Sem Fetal Neonat Med 11(4), 260-267

Siggins GR, Zieglgänsberger W (1981) Morphine and opioid peptides reduced inhibitory synaptic potentials in hippocampal pyramidal cells in vitro without alteration of membrane potential. Proc Natl Acad Sci USA 78, 5235-5239

Simons SHP, Anand KJS (2006) Pain control: opioid dosing, population kinetics and side-effects. Sem Fetal Neonat Med 11(4), 260-267

Sipilä S T, Huttu K, Soltesz I, Voipio J, and Kaila K (2005) Depolarizing GABA acts on intrinsically bursting pyramidal neurons to drive giant depolarizing potentials in the immature hippocampus. J Neurosci 25, 5280-5289

Sipilä ST, Kaila K (2007) GABAergic control of CA3-driven network events in the developing hippocampus. Results Probl Cell Differ 44, 99-121

Stumm RK, Zhou C, Schulz S, Höllt V (2004) Neuronal types expressing mu- and delta-opioid receptor mRNA in the rat hippocampal formation. J Comp Neurol 469, 107-118

Tanabe A, Fujii T, Onimaru H (2005) Facilitation of respiratory rhythm by a mu-opioid agonist in newborn rat pons-medulla-spinal cord preparations. Neurosci Lett 375, 19-22

Whittington MA, Traub RD, Faulkner HJ, Jefferys JG, Chettiar K (1998) Morphine disrupts long-range synchrony of gamma oscillations in hippocampal slices. Proc Natl Acad Sci USA 95, 5807-5811

Williams JT, North RA (1984) Opiate-receptor interactions on single locus coeruleus neurones. Mol Pharmacol 26, 489-497

Wimpey TL, Chavkin C (1991) Opioids activate both an inward rectifier and a novel voltage-gated potassium conductance in the hippocampal formation. Neuron 6, 281–289

Zhang R-X, Li A, Liu B, Wang L, Ren K, Zhang H, Berman BM, Lao L (2008) IL-1ra alleviates inflammatory hyperalgesia through preventing phosphorylation of NMDA receptor NR-1 subunit in rats. Pain 135, 232-239

Chapter 6

General Summary and Conclusions

6.1 Summary of Findings

This work examined methylxanthines and opioids affect spontaneous electrical activities in the hippocampus and neocortex that are important for brain maturation. In addition, consideration was given to experimental approaches used to study them. Three projects revealed the following major findings which supported the proposed hypotheses in two out of three projects.

Project-1: Ca^{2+}/K^{+} Antagonism of ENOs and ENO-like Locus Coeruleus rhythm

The electrolytes Ca^{2+} and K^{+} are fundamental to neuronal excitability. Thus, slices of newborn mammalian brains which show rhythmic bursts of neurons are greatly affected if discrepancies exist between ionic composition of recording solution and of interstitial brain fluid. Here, these effects were studied in horizontal brain slices of neonatal rats containing rhythmic hippocampus (hENOs), neocortex (cENOs), and *locus coeruleus*. Increasing Ca^{2+} in the superfusate from 1 to 2, 2.5, or 3 mM greatly depressed ENOs and *locus coeruleus* bursts. While the precise mechanism for Ca^{2+}-induced depression of rhythms was not explored in this study, others have suggested a wide range of actions from membrane surface screening, presynaptic stimulation of tonic (inhibitory) interneurons, modulation of postsynaptic K^{+} channels, to interaction with a class of G protein-coupled Ca^{2+} sensing receptors and modulation of Na^{+} channels required to generate them. Consistently, increasing K^{+} in the superfusate (6-8 mM), well beyond physiological concentrations and concurrently with elevated Ca^{2+}, 'rescued' depressed h- and cENOs and bursts in *locus coeruleus*. Such a 'Ca/K antagonism' first reported for inspiratory-related preBötC activity in brainstem slices (Leusen, 1992; Ruangkittisakul et al., 2009) is also a

fundamental property of emerging network activity in cortex and hippocampus as well as *locus coeruleus*.

Project-2: Methylxanthine-evoked Perturbation of ENOs

The methylxanthines theophylline and caffeine used to combat apneas of prematurity in human infants were shown in this section to greatly perturb h- and cENOs and transform their activity patterns into seizure-like discharges. These drugs were tested in two groups of neonatal rats, P1-4 and P8-10, representing preterm and term human infant, respectively (Alling, 1985; Clancy et al., 2001). At submillimolar concentrations, methylxanthines antagonize adenosine ($A_{1\text{-}2}$) receptors either pre- or postsynaptically to increase the excitability of neurons. At these levels, theophylline and caffeine appeared to augment spontaneous c- and hENOs or induce irregularity. Importantly however, theophylline- or caffeine-associated seizures were evoked at concentrations in the low millimolar range, at such concentrations where their primary action is not at adenosine receptors. This effect also does not appear to be mediated by PDE-4 inhibition or depletion of Ca^{2+} stores, as rolipram was ineffective at affecting either h- or cENOs and baseline intracellular Ca^{2+} levels, as indicated by Fluo8L-AM or Fluo-4 treatment, did not change drastically. Methylxanthines are known to antagonize A-type GABA receptors, and blockade of these receptors with gabazine mirrored effects seen during methylxanthine application. While already occurring in the P1-4 age group, methylxanthine-associated seizures were more common in slices from older animals. Additionally, theophylline appeared to be a more potent convulsant than caffeine as generally higher concentrations of caffeine were necessary to evoke seizure-like perturbations. These findings may indicate that human fetuses

and preterm infants are slightly less prone to seizure initiation upon acute exposure to methylxanthines than those at term, but may nevertheless share similarly severe long-term impairments in brain development due to perturbed spontaneous oscillations or may further prime the brain for certain epilepsies (Wang & Kriegstein, 2010).

Project-3: Opioid effects on ENOs

Opioid use for pain management or recreation is known to depress breathing and if measures are not taken to reverse these effects, brain tissues can quickly become hypoxic and death can occur in severe cases. Such depression is apparent in newborn brainstem preBötC neurons which generate inspiratory rhythm and *locus coeruleus* neurons that release neurotransmitters important for development of brain areas. Thus, it was examined in this chapter whether opioid-induced depression might also be a characteristic of developing cortical and hippocampal networks. Here, however, it was found that μ-opioid receptor activation transforms hENOs into slow waves of activity, sometimes 30-40 s in length, at submicromolar concentrations, which is reversed after the drug is washed out. Alternatively, above 250 nM, the μ-opioid agonist DAMGO induces high-amplitude seizure-like discharges, consistent with previous *in vitro* findings in mature CA_3 hippocampal neurons. These effects were reversed when the selective μ-opioid antagonist naloxone was added to the solution, whereas cENOs were only slightly affected (i.e. increased burst duration and sometimes amplitude) by DAMGO. Taken together, the data suggest that opioid application, which may persist for several weeks in the neonate, might have neurological consequences in certain cortical/hippocampal areas besides those caused by respiratory-depression derived brain hypoxia.

6.2 Limitations

The following makes note of some potential and minor limitations of studying ENOs in newborn rat brain slices. The focus of this discussion is thus on factors that may be important for long-term stability of ENOs in the hippocampus and cortex, our ability to differentiate between cell types, and the apparent variability of spontaneous activities that occur in the neonate.

6.2.1 Stability and Variability of ENOs

For studying spontaneous hippocampal and cortical ENOs in brain slices, experimental conditions among research groups vary notably (Ben-Ari et al., 1989, 2007; Garaschuk et al., 2000; Khazipov & Luhmann, 2006; Sipilä et al., 2005, 2006; Sipilä & Kaila, 2007; Kafitz et al., 2008; Bonifazi et al., 2009; Allene & Cossart, 2010; Ruusuvuori et al., 2010; Tyzio et al., 2010; Zilberter et al., 2010). Importantly, (*i*) the immediate use of slices after cutting *versus* storing them (on a net) in 'recovery solution' of particular composition and (*ii*) use of different types of 'cerebrospinal' superfusates, specifically concentrations for superfusate Ca^{2+}, K^{+} and glucose, should be discussed (**§2.1.2.1, 3.5**). A systematic investigation of the efficacy of storing slices in regards to stability or robustness of ENOs was not performed as of yet, though it was apparent that spontaneous activity in horizontal slices was very much depressed immediately following generation. Such slices would require perhaps upwards of 1 h before typical spontaneous activities would appear. In that regard, other groups have demonstrated the benefit of storing similar slices in 'recovery solution' for a defined period before recording from them, e.g. sharp waves in hippocampal slices are more pronounced following 'recovery' on a net (Maier et al., 2009). In reference to the latter aspect (*ii*), both, Ca^{2+} and K^{+} have a major influence on neuronal

excitability (Somjen, 2002; Ballanyi & Ruangkittisakul, 2009a,b) and our findings of pronounced Ca^{2+}/K^{+} antagonism for all three types of ENOs strongly support this view. While h- and cENOs were recorded here for time periods up to 5 h in 3K/1Ca solution, elevation of K^{+} to 4-5 mM seemed to have a stabilizing effect on weak bursting in these areas. In contrast, ENO-like bursting in *locus coeruleus* is extremely robust in 3K/1Ca solution regardless of whether slices are stored or recorded from immediately following generation.

Additionally, slices that have been stored for several hours can still generate all types of ENOs in the recording chamber, indicating that isolated neural circuits from newborn mammals remain functional for >10 h, in contrast to (adult) brain slices, which are believed to be used within 5 h due to limited viability of neurons (Ballanyi, 1999; Ballanyi & Ruangkittisakul, 2009a). In fact, it is possible that the neonatal ENOs persist for >24 h in acute slices in our conditions as reported also in the study on their discovery (Ben-Ari et al., 1989); thus, 'slow' neuromodulators such as neurotrophic factors, e.g. BDNF, could be principally applied to such slices to monitor their effects on spontaneous bursting. Furthermore, responses of these networks to long-lasting application of opioids or methylxanthines to test whether this clinical scenario affects h- or cENOs could also be investigated. Our preliminary findings using a 're-perfusion' apparatus that recycles superfusate demonstrate that these rhythms continue to be stable for >5 h. Thus, the above mentioned drugs could also be recirculated to better mimic *in vivo* accumulation of these potentially dangerous stimulants. However, it needs to be considered that some properties of neural circuits in slices may reconfigure within several hours after their isolation as evident of preBötC rhythm in transverse medullary slices (Ballanyi, 1999; Ballanyi & Ruangkittisakul, 2009).

Glucose content in the superfusate may be vital to the robustness and stability of ENOs. Hippocampal ENOs are possibly more robust in 20 *versus* 10 mM glucose, though glucose in brain interstitial space ranges between 0.1-2 mM (Zilberter et al., 2010). Accordingly, it has been proposed that brain slices of newborn mammals should be studied in close-to-physiological glucose, i.e. ~1-2 mM, and/or in solution in which glucose is supplemented or fully substituted by energy substrates that are more relevant for newborns, specifically ketone bodies, lactate and pyruvate (Zilberter et al., 2010). In that article, the authors refer to their work showing that hENOs and cENOs are blocked in close-to-physiological energy substrate levels in the superfusate. However, findings from other recent studies suggest that (10 mM) glucose provides an appropriate metabolic fuel for (newborn rodent) slices (Ruusuvuori et al., 2010; Tyzio et al., 2010).

6.2.2 Cell discrimination using morphological indicator dyes

A common limitation of imaging with Ca^{2+}-indicator dyes to investigate spontaneous neuronal and glial activities in the horizontal brain slice has been the non-specific morphological staining of a variety of cell types. For discriminating between neurons and glia, it has been proposed based on both *in vivo* (Nimmerjahn et al., 2004) and *in vitro* findings (Kafitz et al., 2008) that the fluorescence dye SR-101 selectively stains glia. However, according to other reports the same dye selectively stains neurons (Keifer et al., 1992; Mandal & Anderson, 2009). We have reported preliminary evidence that the capability SR-101 to stain either astrocytes or neurons in the hippocampus and cortex of newborn rat slices depends on the loading protocol (**§2.2.3**) (Kantor et al., 2012). While the fact that neurons and glia in various types of brain slices from (neonatal)

mammals are stained at the same time by Ca^{2+} dyes is a limitation of the method, it is at the same time an advantage. This is because there is steadily increasing evidence that neurons and glial cells interact in a way that can even influence behaviors, such as sleep (Halassa & Haydon, 2010) or the (chemical) control of breathing (Ballanyi et al., 2010; Gourine et al., 2010). Previous chapters have shown that both methylxanthines (**§4.4**) and opioids (**§5.4**) may induce Ca_i transients in presumptive astrocytes, while simultaneously evoking hyperexcitation in CA_3 neurons. Interestingly, methylxanthine-evoked excitation in entorhinal areas appears to be consistently preceded (sometimes by up to 2 min) by evoked-glial transients. It may be possible to study whether hampered interactions between these brain cell types are causally-related to perturbation of ENOs by methylxanthines and opioids. As a further limitation, SR-101 imaging using either low or high concentrations of this dye does not seem to discriminate between neurons and astrocytes in *locus coeruleus*, whereas Ca_i imaging of responses to particular 'gliomodulators' such as t-ACPD or ATP seems to be more useful in that regard.

There is some evidence that SR-101 induces hyperexcitability in isolated (hippocampal) neural networks (Kang et al., 2010), and my preliminary findings related to this thesis (not shown) have shown similar effects on hENOs. However for the purposes of this study, SR-101 loading was limited to brief (20 min) incubations of relatively low (1 μM) concentrations of the morphological dye (**§2.1.8, 2.2.3, 2.3.2.1**). Using such a protocol, SR-101 evoked perturbations in hENOs were not detected using suction electrodes or Ca^{2+} imaging tools.

To elucidate the roles of glia and how they contribute to network-driven activities that occur during development, further optical tools, e.g. optogenetics, or more specific indicator dyes, need to be applied for specifically discriminating astrocytes from oligodendrocytic glia and similarly small microglia of non-neural origin (Agulhon et al., 2008; Wang & Bordey, 2008; Ruangkittisakul et al., 2009; Ballanyi et al., 2010).

6.2.3 Practicality of Electrophysiological Imaging

One limitation that is common to the analysis of ENOs in all regions described above refers to simultaneous electrophysiological imaging. This approach has proven fundamental for studying inspiratory networks in newborn rodent brainstem slices because population activity can be recorded with suction electrodes in one lateral aspect of the bilaterally-organized preBötC networks while the contralateral aspect or inspiratory active XII motor nucleus can be loaded with Ca^{2+} and/or morphological dyes for imaging (Ballanyi & Ruangkittisakul, 2009a; Ruangkittisakul & Ballanyi, 2010; Ruangkittisakul et al., 2009).

Simultaneous electrophysiological imaging is principally also possible for analyzing ENOs occurring in cortical areas and the hippocampus. However, our ability to monitor hENOs and GDPs simultaneously with both electrophysiological equipment and sometimes quite large objectives for imaging is restricted due to the size of the hippocampus. As both ventral and dorsal surfaces of the horizontal slice should be rhythmically active, it may be beneficial to use inverted confocal/multiphoton microscopes to image one surface while positioning suction/patch-clamp electrodes on the opposite surface. It may be the case, however, that the

surface of the slice which is in direct contact with the glass surface of the recording chamber is not sufficiently perfused with oxygenated solution, thus, this surface could potentially become hypoxic and recorded activity may not be indicative of endogenous ENOs. It would be more beneficial, therefore, to monitor ENOs that occur synchronously across both hippocampi and on the same surface (Ben-Ari, 2001). In hemi-sected preparations in which commissural connections are cut between bilateral hippocampi, simultaneous positioning of suctions electrodes in one aspect and imaging and/or intracellular patch-clamp recording in the contralateral aspect is not technically feasible. Furthermore, at depths at which hENOs are most robust, the fornix commissure is usually absent, impairing synchronous hENOs from both hippocampi **(Figs. 1-1, 2-1, 3-1)**. However, as hENOs tend to spread throughout the hippocampus, notably from the CA_3 subregion to the neighbouring CA_1 (Menendez de la Prida et al., 1998; Ben-Ari, 2001), it may be possible to monitor hENOs within one hippocampus with both suction electrodes placed in the CA_1 regions and imaging and/or patch-clamp techniques in the CA_3 region or vice versa.

In cortical areas, cENOs propagate the entire rostral-caudal extent of the neocortex (Garaschuk et al., 2000), thus similar simultaneous techniques would also be beneficial in correlating electrophysiological events with cENOs. Though care must be taken that recorded events originate from the same lamina, as it is possible that burst dynamics vary between neighbouring cell layers. This is unlike the *locus coeruleus* that does not generate synchronized activity in the *in vitro* horizontal slice and does not allow activity phase analyses between extracellular recording via suction electrode in one aspect and imaging and/or intracellular patch-clamp recording in the contralateral aspect. As a major limiting factor, Ca_i imaging in *locus coeruleus* is

mostly not feasible in superfusate of close-to-physiological ion content. This is because bursts occur at a rate of >1 Hz while recovery from a single burst-related Ca_i increase in cortical structures or the isolated preBötC lasts typically >1 s using conventional Ca^{2+} dyes like Fluo-4 or Fluo-8L-AM (Leinekugel et al., 2002; Garaschuk et al., 2000; Ballanyi & Ruangkittisakul, 2009a; Ruangkittisakul & Ballanyi, 2010; Ruangkittisakul et al., 2009). Accordingly, *locus coeruleus* rhythm needs to be slowed down for Ca_i imaging, e.g. by raising superfusate K^+ or Ca^{2+} (**§2.3.1.1, 3.4.2**). As it is established that loading of cells with Ca^{2+}-sensitive dyes affects their intrinsic buffering capability (Yuste et al., 2006), other Ca^{2+}-sensitive dyes with much faster kinetics than those of Fluo-4-AM or Fluo8L-AM could be utilized to capture spontaneous *locus coeruleus* rhythm in control solution.

6.3 Conclusions and Future Perspectives

This thesis for the first time using simultaneously positioned suction electrodes revealed spontaneous ENOs that occur in the hippocampus and neocortex in addition to *locus coeruleus* and are stable for several hours in superfusate of physiologically relevant ionic content. There has been increasing evidence that the hippocampus and neocortex generate an incredibly varied collection of network activities, indicative of the variety of tools used to study them, different animal species in which they are studied, or perhaps a sequential developmental programme (Allene & Cosart, 2010). Over the past 20 years, GDPs, ENOs, spontaneous electrical/bursting activity, and even SPAs have all been reported to occur endogenously in the immature brain, either *in vivo* or *in vitro*. Here we have focused on h- and cENOs which were shown to occur spontaneously even in more mature (P10) animals. This is in disagreement with other reported

times of termination for both hENOs and cENOs, which disappear after the first postnatal week and after P6, respectively (Ben-Ari, 1989; Sipilä & Kaila, 2007; Allene et al., 2008), and additionally display further variability of spontaneous activity **(Figs. 4-1, 4-5)**. It has become increasingly important to adopt a standardized nomenclature to reliably investigate these activities.

A detailed analysis of the relationship between Ca^{2+} and K^{+} was performed for the first time here using systematically varied concentrations of the two ionic species in all three brain areas (**§3.4**). These findings indicated that ENOs and more mature *locus coeruleus* activity that occur at birth depend critically on a balance between these two species. Though it was not the focus of this thesis, it would be important to identify the specific mechanism of this Ca^{2+}-dependent inhibition in the future. Initial targets for such research should determine whether Ca^{2+} sensing metabotropic or ionotropic receptors exist in CA_3 and cortical neurons during this time period or, alternatively, whether Ca^{2+} acts to facilitate persistent Na^{+} currents that drive intrinsic bursting in the hippocampus (Su et al., 2001; Sipilä & Kaila, 2007; Sheroziya et al., 2009). The latter mechanism may indeed be important because this slowly inactivating sub-type of voltage-activated Na^{+} channels is also a characteristic of pre-BötC neurons (Feldman & Del Negro, 2006; Ruangkittisakul et al., 2009). Though this would also suggest a less pronounced role of persistent Na^{+} channels in synchronized bursting of *locus coeruleus* neurons (De Oliveira et al., 2011) as they are only partially depressed by raised Ca^{2+} (**§3.4**) **(Figs. 3-6, 3-8)** and the non-specific persitant Na^{+} channel blocker, riluzole (**§2.3.1.1**) **(Fig 2-5)**.

It was further revealed that the methylxanthines caffeine and theophylline induce ictal-like events and interictal discharges in the hippocampus and neocortex and that hENOs and cENOs are not detectable while these agents are applied (**§4.4**). Whether this represents a scenario where methylxanthines abolish c- and hENO generation, or transform their activities into seizure patterns is unclear. Furthermore, we have shown that these events are not mediated by intracellular increases in cAMP by inhibition of phosphodiesterase-4, as rolipram has no effect on these rhythms. Using confocal/multiphoton Ca^{2+} imaging, we have also shown that sustained increases in Ca_i from stores likely do not contribute to methylxanthine-associated seizures, despite the fact that theophylline caused in ~33% of cases an initial Ca_i rise that could principally be due to release from Ca^{2+} stores as shown for hippocampus and other tissues including the isolated preBötC (Fredholm et al., 1999; Blaustein & Golovina, 2001; Daly, 2007; Ruangkittisakul et al., 2009). An area of future research would be to determine the extent of stimulation provided by certain inhibitors of Ca^{2+}-sequestering pumps, for example thapsigargin or cyclopiazonic acid, which raise Ca_i levels and prevents them from entering the stores. As methylxanthine-associated seizures often become intractable in infants with delayed respiratory capabilities, the need for fast and selective antagonists to counter these effects are of the utmost importance to the survivability of these patients (Angehagen et al., 2003; Korematsu, 2008; Aden, 2011). Certain studies like those conducted by Schmidt and colleagues (2006, 2007) which examined the long-term gross neurological consequences, such as incidence of cerebral palsy and deafness, in infants exposed to methylxanthines to combat apneas of prematurity, showed no correlation between neurological deficits and caffeine/theophylline use. However, it would be pertinent to broaden such a definition of 'neurodevelopmental disabilities' to test for

subtle perturbations and behavioral disorders, such as learning disabilities, attention deficit disorders, or other cognitive delays.

Anecdotally it is well known that caffeine and other methylxanthines evoke seizures. The inability to correlate serum levels of the agent to onset of methylxanthine-associated seizures is a major setback in describing its proconvulsive role. Moreover, other factors such as developmental age, weight, functionality of hepatic enzymes all determine the efficacy of methylxanthines to induce seizures. It would be crucial to utilize *in vivo* techniques to demonstrate a correlation between serum concentrations methylxanthines and derived seizures. An additional area of research would involve Ca^{2+} imaging *in vivo* to monitor methylxanthine effects on spontaneous ENOs in freely moving unanesthetized newborn rats, similar to studies conducted by the groups of Garaschuk and Konnerth (Adelsberger et al., 2005).

Also shown for the first time in this thesis was the discovery that *in vitro* c- and hENOs are altered during μ-opioid receptor activation which additionally induces hyperexcitation in the hippocampus (**§5.4**). These seizures mirror effects seen during methylxanthine application and gabazine antagonization of $GABA_A$ receptors. However, similar perturbations were not seen in cENOs. As noted in several previously mentioned studies (**§5.5**), the blocking effect of opioids on inhibitory interneurons is the likely cause of hippocampal hyperexcitation (Nicoll et al., 1980; Siggins & Zieglgänsberger, 1981; Cohen et al., 1992; Drake & Milner, 2002; Stumm et al., 2004), even though μ-receptors are widely expressed in the hippocampus, on both presynaptic interneurons and postsynaptic CA3 pyramidal bursters, and are already functional at birth (Leslie

et al., 1982; Pickel, 1982; Meilandt et al., 2004). Whether such opioid-induced hyperexcitation originates pre- or postsynaptically was not the focus of this thesis. In future directions, whole cell/patch clamp techniques should be utilized to determine the target of opioid-induced perturbations. Additionally, slow waves of activity evoked by nanomolar concentration of DAMGO (**§5.4.1**) are very similar in dynamics to hypoxia-induced slow network oscillations (Allene et al., 2008) and excitotoxic oscillations evoked by glutamate transporter blockers in the neocortex (Demarque et al., 2004). Accordingly, it would be important to determine if opioids affect glutamate concentrations in interstitial space in the neonate. For such studies, electrophysiological or imaging techniques should ultimately be done in conjunction with probes/sensors that monitor glutamate levels.

Infants in intensive care can receive more than 10 different drugs simultaneously and the potential for adverse drug reactions is high (Du et al., 2006; Black et al., 2008). While opioid-induced respiratory depression is readily reversed by naloxone and naltrexone, any analgesic benefit is likewise reversed. Thus there is growing need for other respiratory stimulants that do not antagonize the analgesic qualities of opioids. Methylxanthines are regarded as a current option for these reasons (Schmidt et al., 2006, 2007). As low millimolar and close-to micromolar concentrations of methylxanthines and opioids, respectively, have an overall stimulatory (and proconvulsive) effect on the developing hippocampus (**§4.4, 5.4**), it may be the case that combined administration of these two drugs may lower the threshold for seizure generation. My preliminary findings in that regard, however, do not indicate that opioids lower the threshold for methylxanthine-evoked seizures *in vitro*. On the other hand, during intermittent or sustained brain hypoxia it was shown that methylxanthines, at submillimolar concentrations, can elicit

seizures (Dzhala et al., 1999). While this may at first seem to contradict reported findings (**§4.4, 4.5**), it may be the case that hypoxic episodes lower the threshold for methylxanthine-associated seizures. Opioids such as morphine acting on respiratory centres in the brainstem can depress breathing, potentially resulting in brain hypoxia. Thus, opioids may indirectly lower the threshold for methylxanthine-associated seizures. The central action of opioids and how they interact with methylxanthines is unclear, though recent evidence has shown that simultaneous administration of these two drugs can impair astrogenesis and increase neuronal death (Black et al., 2008). Based on these findings, it would be important to study these interactions further *in vivo*.

In conclusion, standardization of solution with physiological ion content and novel use of respirogenic drugs on newborn rat brain slices has provided new findings on the susceptibility of the developing brain to seizures. These findings may stimulate further research to utilize such experimental approaches to discover more effective therapeutic pharmacology for the treatment of respiratory-related difficulties and associated pain.

6.4 References

Adelsberger H, Garaschuk O, Konnerth A (2005) Cortical calcium waves in resting newborn mice. Nat Neurosci 8, 988-990

Aden U (2011) Methylxanthines during pregnancy and early postnatal life. Handb Exp Pharmacol 200, 373-389

Agulhon C, Petravicz J, McMullen AB, Sweger EJ, Minton SK, Taves SR, Casper KB, Fiacco TA, McCarthy KD (2008) What is the role of astrocyte calcium in neurophysiology? Neuron 59, 932-946

Allene C, Cattani A, Ackman JB, Bonifazi P, Aniksztejn L, Ben-Ari Y, Cossart R (2008) Sequential generation of two distinct synapse-driven network patterns in developing neocortex. J Neurosci 28, 12851-63

Allene C, Cossart R (2010) Early NMDA receptor-driven waves of activity in the developing neocortex: physiological or pathological network oscillations? J Physiol 588, 83-91

Angehagen M, Margineanu DG, Ben-Menachem E, Rönnbäck L, Hansson E, Klitgaard H (2003) Levetiracetam reduces caffeine-induced Ca2+ transients and epileptiform potentials in hippocampal neurons. Neurorep 14, 471-475

Ballanyi K (1999) Isolated tissues: in vitro preparations. In: Windhorst U, Johansson H (eds) Modern Techniques in Neuroscience Research, Springer, Heidelberg, pp 307-326

Ballanyi K, Ruangkittisakul A (2009a) Structure-function analysis of rhythmogenic inspiratory pre-Botzinger complex networks in "calibrated" newborn rat brainstem slices. Respir Physiol Neurobiol 168, 158-178

Ballanyi K, Ruangkittisakul A (2009b) Brain slices. In: Binder M, Hirokawa N, Windhorst U (eds). Encyclopedia of Neuroscience, Springer Verlag, Heidelberg, New York, Tokyo, pp. 483-490

Ballanyi K, Panaitescu B, and Ruangkittisakul A (2010) Control of breathing by nerve glue. Sci Signal 3, pe41

Ben-Ari Y (2001) Developing networks play a similar melody. TRENDS Neurosci 24(6), 353-360

Ben-Ari Y, Cherubini E, Corradetti R, Caiarsa JL (1989) Giant synaptic potentials in immature rat CA3 hippocampal neurones. J Physiol 416, 303-325

Ben-Ari Y, Gaiarsa JL, Tyzio R, Khazipov R (2007) GABA: a pioneer transmitter that excites immature neurons and generates primitive oscillations. Physiol Rev 87, 1215-1284

Black AM, Pandya S, Clark D, Armstrong EA, Yager JY (2008) Effect of caffeine and morphine on the developing pre-mature brain. Brain Res 1219, 136-142

Blaustein MP, Golovina VA (2001) Structural complexity and functional diversity of endoplasmic reticulum Ca^{2+} stores. Trends Neurosci 24, 602-608

Bonifazi P, Goldin M, Picardo MA, Jorquera I, Cattani A, Bianconi G, Represa A, Ben-Ari Y, and Cossart R (2009) GABAergic hub neurons orchestrate synchrony in developing hippocampal networks. Science 326, 1419-1424

Cohen GA, Doze VA, Madison DV (1992) Opioid inhibition of GABA release from presynaptic terminals of rat hippocampal interneurons. Neuron 9, 325-335

Daly JW (2007) Caffeine analogs: biomedical impact. Cell Mol Life Sci 64, 2153-2169

Du W, Warrier I, Tuag Lehr V, Salari V, Ostrea E, Aranda JV (2006) Changing patterns of drug utilization in a neonatal intensive care population. Am J Perinatol 23, 279-285

Demarque M, Villeneuve N, Manent JB, Becq H, Represa A, Ben-Ari Y, Anikstejn L (2004) Glutamate transporters prevent the generation of seizures in the developing rat neocortex. J Neurosci 24, 3289-3294

De Oliveira RB, Howlett MC, Gravina FS, Imtiaz MS, Callister RJ, Van Helden DF (2011) Developmental changes in pacemaker currents in mouse locus coeruleus neurons. Brain research 1425, 27-36

Drake CT, Milner TA (2002) Mu opioid receptors are in discrete hippocampal interneuron subpopulations. Hippocampus 12, 119-136

Dzhala V, Desfreres L, Melyan Z, Ben-Ari Y, Khazipov R (1999) Epileptogenic action of caffeine during anoxia in the neonatal rat hippocampus. Ann Neurol 46, 95-102

Feldman JL, Del Negro CA (2006) Looking for inspiration: new perspectives on respiratory rhythm. Nat Rev Neurosci 7, 232-242

Fredholm BB, Battig K, Holmen J, Nehlig A, Zvartau EE (1999) Actions of caffeine in the brain with special reference to factors that contribute to its widespread use. Pharmacol Rev 51, 83-133

Garaschuk O, Linn J, Eilers J, Konnerth A (2000) Large-scale oscillatory calcium waves in the immature cortex. Nature 3(5), 452-459

Gourine AV, Kasymov V, Marina N, Tang F, Figueiredo MF, Lane S, Teschemacher AG, Spyer KM, Deisseroth K, Kasparov S (2010) Astrocytes control breathing through pH-dependent release of ATP. Science 329, 571-575

Halassa MM, Haydon PG (2010) Integrated brain circuits: astrocytic networks modulate neuronal activity and behavior. Annu Rev Physiol 72, 335-355

Kafitz KW, Meier SD, Stephan J, Rose CR (2008) Developmental profile and properties of sulforhodamine 101-Labeled glial cells in acute brain slices of rat hippocampus. J Neurosci Methods 169, 84-92

Kang SH, Lee YA, Won SJ, Rhee KH, Gwag BJ (2002) Caffine-induced neuronal death in neonatal rat brain and cortical cell cultures. Neruoreport 13, 1945-1950

Kantor CM, Panaitescu B, Kuribayashi J, Ruangkittisakul A, Jovanovic I, Leung V, Lee TF, MacTavish D, Jhamandas JH, Cheung PY, Ballanyi K (2012) Spontaneous neural network oscillations in hippocampus, cortex, and locus coeruleus of newborn rat and piglet brain slices. In: Isolated CNS circuits. (Ballanyi K, ed.) Humana-Springer (in press)

Keifer J, Vyas D, Houk JC (1992) Sulforhodamine labeling of neural circuits engaged in motor pattern generation in the in vitro turtle brainstem-cerebellum. J Neurosci 12, 3187-3199

Khazipov R, Luhmann HJ (2006) Early patterns of electrical activity in the developing cerebral cortex of humans and rodents. Trends Neurosci 29, 414-418

Korematsu S, Miyahara H, Nagakura T, Suenobu S, Izumi T (2008) Theophylline-associated seizures and their clinical characterizations. Pediatr Int 50, 95-98

Leinekugel X, Khazipov R, Cannon R, Hirase H, Ben-Ari Y, Buzsáki G (2002) Correlated bursts of activity in the neonatal hippocampus in vivo. Science 296, 2049-2052

Leslie FM, Tso S, Hurlbut E (1982) Differential appearance of opiate receptors subtypes in neonatal rat brain. Life Sciences 31, 1393-1396

Maier N, Morris G, Johenning FW, Schmitz D (2009) An approach for reliably investigating hippocampal sharp wave-ripples in vitro. PLoS ONE 4, e6925 1-10

Mandal R, Anderson CW (2009) Anatomical organization of brainstem circuits mediating feeding motor programs in the marine toad, Bufo marinus. Brain Res 1298, 99-110

Meilandt WJ, Barea-Rodriguez E, Harvey SAK, Martinez JL Jr (2004) Role of hippocampal CA3 μ-opioid receptors in spatial learning and memory. J Neurosci 24, 2953-2962

Menendez de la Prida L, Bolea S, Sanchez-Andres JV (1998) Origin of the synchronized network activity in the rabbit developing hippocampus. Eur J Neurosci 10, 899–906

Nicoll RA, Alger BE, Yahr CE (1980) Enkephalin blocks inhibitory pathways in the vertebrate CNS. Nature 287, 22-25

Nimmerjahn A, Kirchhoff F, Kerr JN, Helmchen F (2004) Sulforhodamine 101 as a specific marker of astroglia in the neocortex in vivo. Nat Methods 1, 31-37

Pickel V (1982) Central noradrenergic neurons: Identification, distribution, and synaptic interactions with axons containing morphine-like peptides. J Clin Psychiatry 43, 13-16

Ruangkittisakul A, Ballanyi K (2010) Methylxanthine reversal of opioid-evoked inspiratory depression via phosphodiesterase-4 blockade. Respir Physiol Neurobiol 172, 94-105

Ruangkittisakul A, Okada Y, Oku Y, Koshiya N, Ballanyi K (2009) Fluorescence imaging of active respiratory networks, Respir Physiol Neurobiol 168, 26-38

Ruusuvuori E, Kirilkin I, Pandya N, Kaila K (2010) Spontaneous network events driven by depolarizing GABA action in neonatal hippocampal slices are not attributable to deficient mitochondrial energy metabolism. J Neurosci 30, 15638-15642

Schmidt B, Roberts RS, Davis P, Doyle LW, Barrington KJ, Ohlsson A, Solimano A, Tin W (2006) Caffeine therapy for apnea of prematurity. N Engl J Med 354, 2112-2121

Schmidt B, Roberts RS, Davis P, Doyle LW, Barrington KJ, Ohlsson A, Solimano A, Tin W (2007) Long-term effects of caffeine therapy for apnea of prematurity. N Engl J Med 357, 1893-1902

Sheroziya MG, von Bohlen und Halbach O, Unsicker K, Egorov AV (2009) Spontaneous bursting activity in the developing entorhinal cortex. J Neurosci 29, 12131-12144

Siggins GR, Zieglgänsberger W (1981) Morphine and opioid peptides reduced inhibitory synaptic potentials in hippocampal pyramidal cells in vitro without alteration of membrane potential. Proc Natl Acad Sci USA 78, 5235-5239

Sipilä S T, Huttu K, Soltesz I, Voipio J, and Kaila K (2005) Depolarizing GABA acts on intrinsically bursting pyramidal neurons to drive giant depolarizing potentials in the immature hippocampus. J Neurosci 25, 5280-5289

Sipilä ST, Huttu K, Voipio J, Kaila K (2006) Intrinsic bursting of immature CA3 pyramidal neurons and consequent giant depolarizing potentials are driven by a persistent Na current and terminated by a slow Ca-activated K current. Eur J Neurosci 23, 2330-2338

Sipilä ST, Kaila K (2007) GABAergic control of CA3-driven network events in the developing hippocampus. Results Probl Cell Differ 44, 99-121

Somjen GG (2002) Ion regulation in the brain: implications for pathophysiology. Neuroscientist 8, 254-267

Stumm RK, Zhou C, Schultz S, Holit V (2004) Neuronal types expressing μ- and δ-opioid receptor mRNA in the rat hippocampal formation. J Compar Neurol 469, 107-118

Su H, Alroy G, Kirson ED, Yaari Y (2001) Extracellular calcium modulates persistent sodium current-dependent burst-firing in hippocampal pyramidal neurons. J Neurosci 21, 4173-4182

Tyzio R, Allene C, Nardou R, Picardo MA, Yamamoto S, Sivakumaran S, Caiati MD, Rheims S, Minlebaev M, Milh M, Ferré P, Khazipov R, Romette JL, Lorquin J, Cossart R, Khalilov I,

Wang DD, Bordey A (2008) The astrocyte odyssey. Prog Neurobiol 86, 342-367

Yuste R, Konnerth A, Masters B (2006) Imaging in neuroscience and development, a laboratory manual. J Biomed Opt 11, 19902

Zilberter Y, Zilberter T, Bregestovski P (2010) Neuronal activity in vitro and the in vivo reality: the role of energy homeostasis. Trends Pharmacol Sci 31, 394-401